

# Interfacing mechanical resonators with excited atoms

Dissertation  
zur Erlangung des akademischen Grades  
Doctor rerum naturalium

vorgelegt von  
Adrián Sanz Mora  
geboren am 13. Januar 1989 in Madrid, Spanien

Fakultät Physik  
Technische Universität Dresden

Max-Planck-Institut für Physik komplexer Systeme



MAX-PLANCK-GESellschaft



Eingereicht am 30.01.2018

Erste Gutachter: Prof. Dr. Jan-Michael Rost

Zweite Gutachter: Prof. Dr. Walter Strunz

Dritte Gutachter: Dr. Sebastian Wüster

Verteidigt am 10.07.2018



*A mis padres,*

*A mi tía Rosa*



# Acknowledgements

With these lines I want to express my gratitude to all individuals and groups that consciously or unconsciously have helped me to chart my course towards the culmination of this work. Although vibrant, it has also been an arduous task, specially during its writing stage. The ones close to me know it very well, specially my supervisor. For putting up with my stubbornness on such writing process, I want to thank you Jan-Michael. Thank you for your patience. Thank you for your tolerance. Likewise, thanks for having offered me a doctoral position within the framework of the initial training network COHERENCE. Equally gratifying is that you have entrusted the monitoring of my work to Sebastian Wüster. Sebastian, thanks for being such a magnanimous mentor and keep teaching and supporting me until the end. I highly appreciate you have always been predisposed to explain me up to the easiest physical concepts ever, as well as to listen up to the craziest ideas of mine. I hope that those many discussions could provide you something valuable; luckily they may have served me to learn a bit of the excellent level of physical intuition you have.

A *Finite* person I am truly grateful to is my former office mate, Gerhard Ritschel. I owe you all my programming skills in *Python*. Besides, those fun chess discussions of us were always a balsam to smother whichever research related annoyance I had. I wish you and your family all the best! It was also very rewarding to work next to every other *Finite* member, both former ones and present ones. In particular, next to Wildan. You are such a great soul! Thank you for your constant and true care. I also want to express a special thanks to you Abraham, for your genius sense of humor, for being able to turn a bad day into a good one. Particularly joyful were those lunches that we used to have with the rest of *los menseros*, Ángel, Mónica, *los Diegos*, *los Jorges*, Yaniel, Silvia, Enrique, Joan, David, Manolo *Jumilla*, Ginés, Eva, María, *las Anas*, and many more ... You made the lunch time a sought after event everyday. Specially you Eugenio, *the master*, who, with your eloquence, were capable to get a smile out of the sorriest face. (N.B. *The knight of the sorry face* would like to thank Sándalo, to whom he owes such a fantastic nickname. Thanks for the careful proofread of the introduction too.) Thanks also to the rest of the *camaradas*, Daniel Aguilar, Édgar, Judit, for your continued support. For helping me on thesis submission related stuff I am thankful to Daniel Vorberg and Alan. Crucial for the realization of this work has also been the institute in which I have been hosted, the Max Planck Institute for the Physics of Complex Systems (MPIPKS), as well as the Max Planck Society. Many thanks. In this respect I also want to thank Hubert and its entire department of information technology (IT) at the MPIPKS. It is thanks to you that our computer calculations can be carried out smoothly.

Other scientists beyond the walls of the MPIPKS to whom I want to acknowledge are Klemens Hammerer and Kai Stannigel. Although our discussions were little, they were very didactic. Thank you also Charles Adams for those excellent lectures (and notes) on nonlinear optics. I also want to thank Henning Labuhn for his hospitality and help with that crazy poster printout in Paris. For the always stimulating lectures in my undergraduate days I

want to thank Daniel Alonso, Javier Rojas, José Llorente, José Pascual, Santiago Brouard, Andrés, Silvana, Basilio ...

There are also my friends who enrich my life beside science. I am very fortunate to have friends like Jorge (*pues, you are all heart!*), Max (*el niño prodigio*), Andro (*jugón!*), Amparo, Abraham, Wildan, Omar, Talía (thanks T&O for those tasty *tamales*), Izaak, Younes, Karsten, Alan, Jorge Rehn, Manos, ... And of course, those from *las Islas Afortunadas* Raúl *el amigazo*, Alba, Juan, Nuria, Amós. My basketball mates, specially Eugenio and Álvaro, with whom I enjoyed every single match we played in the Dresden summer and winter leagues. Kamila, *dziękuję*. You invited me to a journey of delightful experiences completely unknown to me. My most sincere gratitude also to the Dittmann family, who has always welcomed my brother and I with open arms.

Manuel, what would I do without such a great brother you are? Everyday I learn something joyful and interesting next to you, from cook tricks to magnificent comedians; our discussions always help me to develop a better critical thinking; your generosity is unvaluable. Together with your lively Laura, I have felt to be part of a very fraternal community in our home. Thanks to you too, Laura. You got into our grey house and make it colorful, besides, you help us *a cenar como Dios manda*. Finally, there are my parents, the two most incredible human beings I know. Thanks for being always supportive, for all your love, for helping me to assuage my sorrows. Without you I would not have reached this far.

I gratefully acknowledge funding from the European Research Council (ERC) under the European Union's Seventh Framework Programme (FP7/2007-2013)/ ERC grant agreement no 265031.



# Abstract

We investigate two different coupling schemes between a nano-scale mechanical resonator and one-electron atoms. In these schemes, classical electromagnetic radiation mediates a mutual communication between the mechanical resonator and the atoms. In the process it generates atomic coherences, quantum superpositions of excited electronic levels of the atoms. An atomic coherence is highly responsive to subtle variations in the relative frequencies of the levels participating in such superposition state. By exposing the atoms to electromagnetic radiation modulated by the motion of the mechanical resonator, we show how the response of an atomic coherence can, under appropriate conditions, be used to affect on demand the dynamical state of the mechanical resonator.

The first scheme realizes a long range interface between a mechanical resonator and an ensemble of three-level atoms. Here, mechanically modulated electromagnetic radiation comes from a laser beam reflected off an oscillating mirror, the mechanical resonator. This light beam drives the transition between an excited level and a hyperfine sublevel of the atoms with a certain detuning. A weaker light beam resonantly couples to the transition between the excited level and another hyperfine sublevel. On full resonance, the atoms evolve into a stationary coherence of the above (non-absorbing) hyperfine sublevels only. The atoms then become transparent to the weaker light beam, in a phenomenon called *electromagnetically induced transparency*. Off resonance, we find that this transparency is modulated at the mirror frequency with some phase shift, which allows the weaker beam to cause resonant backaction onto the moving mirror. The strength of this backaction is enhanced near atomic resonances and its character can be switched between amplification or damping of mirror vibrations by adjusting the detuning.

In contrast, the second scheme accomplishes a closer range interface between a torsion pendulum and guided two level Rydberg atoms. Attaching a point electric dipole to the torsion pendulum allows electromagnetic coupling to two Rydberg levels of a passing atom. This coupling modifies the eigenfrequencies of the Rydberg levels such that they become dependent on the phonon number of the torsion pendulum. Via Ramsey interferometry, we may readout this effect and thus measure the phonon number. We show that, by subjecting several atoms, one by one, to a Ramsey measurement, a quantum non-demolition detection of the phonon number is feasible. Likewise, we show coherent oscillator displacements possible, by driving the atoms with external fields while they interact with the torsion pendulum. We propose a protocol to reconstruct the quantum state of motion of the torsion pendulum, combining these two techniques, Ramsey measurements and oscillator displacements.

Our interfaces between a mechanical resonator and atoms provide alternative routes for the control of the state of motion, ultimately quantum mechanical, of a mechanical resonator, in which the latter is not restricted to be part of a cavity. We will thus ease quantum dynamical manipulations of mechanical resonators of sub micron scales, for which an efficient design of cavity opto- and electro-mechanical systems is hard.



# Contents

<b>1</b>	<b>Prolegomenon</b>	<b>1</b>
<b>2</b>	<b>A glimpse into excited atoms, mechanical resonators and their interaction with light</b>	<b>7</b>
2.1	Excited state atoms: Rydberg atoms . . . . .	7
2.1.1	Rydberg states of alkali metal atoms . . . . .	10
2.2	Driving atomic transitions with electromagnetic waves . . . . .	13
2.2.1	Optically induced atomic dipoles . . . . .	13
2.2.2	Dielectric susceptibility . . . . .	16
2.3	Mechanical resonators . . . . .	19
2.3.1	Quantum motion from the mechanics of miniature solids . . . . .	20
2.3.2	Forced mechanical oscillations, friction and noise . . . . .	23
2.3.3	Cooling and amplification of mechanical harmonic motion with a viscous force . . . . .	30
2.3.4	An example: radiation pressure force and optomechanics . . . . .	32
<b>3</b>	<b>A nanomechanical resonator remotely coupled to an ultracold atomic gas</b>	<b>41</b>
3.1	Atom-optomechanical setup . . . . .	42
3.1.1	Electromagnetically induced transparency . . . . .	45
3.2	Coupled dynamics of atomic gas, light waves and nanomechanical mirror . .	48
3.3	Interaction between multiple monochromatic light waves and atomic gas . .	51
3.3.1	Linearly oscillating nanomirror coupled to atomic gas . . . . .	51
3.3.2	Time periodic model . . . . .	51
3.3.3	Linear response in the presence of optomechanical sidebands . . . . .	52
3.4	Optomechanical interface between atomic gas and oscillating nanomirror . .	55
3.4.1	Dynamics of oscillating nanomirror driven by a viscous like radiation pressure force . . . . .	55
3.4.2	Range of applicability . . . . .	56
3.5	Conclusions . . . . .	57
<b>4</b>	<b><i>In situ</i> monitoring of the quantum state of a nano-scale torsion pendulum with Rydberg atoms</b>	<b>59</b>
4.1	Hybrid platform of nano-torsional oscillator and Rydberg atom . . . . .	59
4.2	Dynamics of a Rydberg atom and a torsion pendulum interacting electrostatically . . . . .	61
4.2.1	The Jaynes-Cummings Hamiltonian . . . . .	62
4.2.2	Time evolution in the dispersive regime . . . . .	64
4.2.3	Adiabatic evolution . . . . .	65

4.3	Quantum non demolition measurement of torsional mechanical excitation quanta . . . . .	67
4.3.1	Ramsey interferometry . . . . .	67
4.3.2	Projecting the quantum state of motion of a torsion pendulum onto a phonon number eigenstate . . . . .	70
4.4	Simulation of Ramsey measurement series subject to decoherence and statistical noise . . . . .	72
4.4.1	Decoherence . . . . .	72
4.4.2	Guided atomic motion with initial position and momentum spreads. Statistical averages . . . . .	74
4.4.3	Averaged atomic probabilities $P_{\pm}$ and phonon statistics . . . . .	75
4.4.4	System design and parameter choices . . . . .	77
4.5	Direct sampling of the Wigner function of a torsion pendulum . . . . .	79
4.5.1	Phase space representation of the quantum state of motion of a torsion pendulum . . . . .	80
4.5.2	Sampling the phase space of a torsion pendulum. Wigner function reconstruction . . . . .	82
4.6	Conclusions . . . . .	85
<b>5</b>	<b>Summary and outlook</b>	<b>87</b>
<b>A</b>	<b>Supplement: optical absorption of an ultracold gas of three-level atoms</b>	<b>91</b>
A.1	Linear polarization and electromagnetic wave propagation inside the atomic gas . . . . .	91
A.2	Dynamics of the optically driven atoms . . . . .	94
A.2.1	Linear susceptibility. Free radiation . . . . .	94
A.2.2	Linear susceptibility. Mechanically modulated radiation . . . . .	96
A.3	Radiation damping of mirror's oscillation amplitude . . . . .	99
<b>B</b>	<b>Supplement: parameters, electromagnetic coupling and joint evolution of a torsion pendulum and a Rydberg atom</b>	<b>101</b>
B.1	Mechanical frequency of torsion pendulum . . . . .	101
B.2	Coupling a two-level atom and a torsion pendulum . . . . .	101
B.2.1	Electromagnetic radiation of a point electric dipole attached to a torsion pendulum . . . . .	102
B.2.2	Frequency spectrum of the radiated signal. The <i>near zone</i> limit . . . . .	103
B.2.3	Interaction between a two level atom and a mechanically modulated point electric dipole . . . . .	104
B.3	Hamiltonian of torsion pendulum and driven atom . . . . .	106
B.4	Unitary evolution of joint atom-oscillator system during a Ramsey sequence .	107
B.5	Numerical test of the mechanical oscillator state collapse . . . . .	110
B.6	Effective coherent driving of mechanical oscillator . . . . .	112

**References**

**115**



# 1 Prolegomenon

Let us adventure for a moment into a human ear. Pressure (sound) waves excite the tympanic membrane. The entire membrane reverberates. Eventually, in the ear's cochlea, these reverberations become audible. Thus, hearing reduces to the perception of the tympanum reverberations. Just like the reverberations of the tympanic membrane in the ear enable a proper hearing of sound waves, the swing of the suspended mirrors that are part of a gravitational wave observatory allow for hearing the wobbling of the spacetime of our Universe. Essentially, both the reverberating tympanic membrane and the swinging mirrors of a gravitational wave observatory, are examples of the type of mechanical resonators of concern in this thesis: solids in which its entire body vibrates, meaning that the characteristic wavelength of such vibrations is of the order of the size of the solid itself.

Mechanical resonators work in many respects as a primordial element of a very sensitive *ear*. Mechanical oscillations of the suspended mirrors that form part of the Advanced Laser Interferometer Gravitational-Wave Observatory (LIGO) laboratories [1, 2, 3] have already manifested in five occasions as a direct reproduction of a ripple in spacetime, a.k.a. gravitational wave. The first detection of a gravitational wave by the LIGO laboratories took place in the fall of 2015, and it was later reported by its team in [4]. A LIGO laboratory lines up two cavities in L-shape. Each of the cavities is made of two suspended mirrors placed in front of each other enclosing a distance of 4 km long. The ear sensitivity, figuratively speaking, of Advanced LIGO amounts then to the detection of mechanical oscillations of the mirrors that entail a length variation of the cavities as small as a ten-thousandth part of the size of a proton. The colossal effort devoted to the development of the LIGO project until achieving its current status, enabling the observation of gravitational waves, has earned the 2017 Nobel prize in physics to its original promoters [5].

Besides of playing a key role in LIGO detectors, the utility of the mechanical resonators is also ubiquitous in many of our everyday use appliances (e.g., in all those that integrate a microphone: an elastic diaphragm connected to an electrical circuit). Notably, the *modus operandi* of mechanical resonators in these technological devices, from a smartphone, to a pressure sensor, to an airbag, etc., is based on a phenomenology describable in the framework of classical mechanics. However, during the last fifty years scientists have applied themselves to the task of understanding and developing functional mechanical resonators, the behavior of which may instead be ruled by the laws of quantum theory. There exist strong motives for conducting research in this direction. From a practical point of view, mechanical resonators operating at will with a displacement sensitivity down to the limit imposed by its zero point motion (displacement fluctuations arising from the Heisenberg uncertainty principle [6]) promises true advances in high precision metrology, specially in the realm of mechanical biosensing (concerned with the detection of forces, masses and displacements in biological systems) [7, 8], as well as a means for the communication between other quantum systems, thus turning them into excellent candidates for information processing architectures [9]. At

the same time, probing the quantum behavior of mechanical resonators may provide itself with the means to test fundamental aspects of the theory related with the manifestation and inhibition of its genuine properties at both length and mass scales yet unexplored [10, 11, 12, 13, 14, 15]. These types of tests may then serve to gain a better understanding on the quantum-classical transition [16]. Under a long-term and more industry-oriented endeavor, the challenge also seems to be worth a try. The spectacular success of other technological products, the functionality of which is grounded on quantum principles, like e. g. the laser [17] or the transistor [18], are evidence of it. Nowadays, approximately one third of the world economy is based on such products [19].

Theoretical studies on mechanical devices under conditions in which physical phenomena may manifest according to the laws of quantum theory, were originally stir to enable laser interferometry detectors (such as the ones of the LIGO project) to operate at the ultimate level of precision set by quantum fluctuations of the physical components of such detectors [20, 21, 22]. These studies ushered in a brand-new research field: optomechanics. It is in the context of optomechanics, which deals with the interaction between an electromagnetic field and the motion of a mechanical resonator [23, 24], wherein scientists have developed most of today's known concepts and techniques that facilitate the preparation, measurement and coherent control of the dynamical state of a mechanical resonator in the quantum domain. These three steps –preparing, measuring, and controlling coherently (a physical observable)– are arguably crucial for a successful performance of a mechanical resonator operating in the quantum regime [25]. Until the early 21st century, the majority of this work could only be realized in theoretical terms. The improvement of the fabrication techniques in the material industry have finally enabled the development of numerous solid-state structures quite diverse in their shape, size and weight, capable to accommodate mechanical resonances within a wide range of frequencies [26]. An important breakthrough in this respect has been the consolidation of functional mechanical systems at the micro- and nano-scales. Solids of this size are generally lightweight and support collective mechanical vibration modes (those in which the entire solid vibrates) of considerably short wavelengths or, equivalently, of high frequencies (from a few MHz up to the GHz range). These two features are favorable to access more easily the quantum dynamics of a given collective mechanical vibration mode of a solid-state structure [27, 28]. As we will discuss in more detail in the following chapter 2, a high resonance frequency makes it easier for the mechanical system to approach the displacement limit set by its zero point fluctuations, and at the same time a smaller mass enhances this zero point motion of the vibration mode, thus facilitating its possible observation. For these reasons, tabletop experiments involving this new generation of miniature mechanical resonators have proven possible the preparation of collective mechanical vibration modes very near to its quantum ground state of motion [29], the detection of the zero point fluctuations of such state [30, 31], the realization of quantum information transfer between rather dissimilar spectral realms [32, 33, 34, 35, 36] and to squeeze states of motion of a mechanical resonator [37, 38, 39, 40], just to mention a few among other achievements. See references [41, 42, 43] for a more detailed account on recent milestones related to quantum opto- and



electro-mechanical systems.

An important hallmark of these miniature mechanical systems is their capability of coupling to electromagnetic radiation over a wide range of the spectrum. Along with their extreme sensitivity to the action of any external force, they appear as an excellent means for interfacing with quantum systems as diverse as optical cavities [41], Josephson circuits [44] or quantum dots [45] in pursuit of operational hybrid setups [46, 47]. Hybrid systems are comprised of several physically different components each of which may execute a distinct but complementary technological task. When operated in the quantum regime, hybrid systems could then be targeted to process, store and transfer quantum information all at once, which would be a real milestone in quantum technology [48]. An increasingly emerging group of hybrid devices comprises atomic or molecular systems [49, 50, 51, 52, 53, 54, 55, 56, 57, 58, 59, 60].

This thesis pursues the realization of different interfacing schemes between a nanoscale mechanical resonator and an atomic system from a theoretical perspective. We particularly aim for strategies in which the mechanical resonator of concern is not coupled to the radiation field inside of a finite cavity, as a complementary route to the majority of the proposals cited above. The actual trend to miniaturize the mechanical structures, naturally concurs with this approach of divesting the mechanical element of a coupling to an electromagnetic cavity. On the one hand, even for optical wavelengths, which fall in the micro-scale, engineering a cavity that may both incorporate a nanoscale mechanical system and possess low optical losses is challenging [42]. Furthermore, the tiniest mechanical resonators, such as carbon nanotubes (CNT), which are built from a *bottom-up* approach, i. e. realizing a solid structure by gathering elemental molecular compounds, and are sound candidates to study solid-state mechanical motion deep in the quantum regime, are still lacking of reliable and efficient displacement detectors [61, 27]. On the other hand, mechanical resonances of nano-scale mechanical systems are closer to Bohr frequencies between hyperfine states or Rydberg states in atomic systems, which could open new doors to achieve a strong coupling between a quantum mechanical resonator and another quantum system both working at the level of single energy quanta. Likewise, interfacing mechanical resonators with electronic states of atoms may benefit from the extensive variety of techniques that allow an accurate quantum manipulation of these atomic states. As of today, atoms can be isolated and studied both collectively and individually, at temperatures as low as a few  $\mu\text{K}$ , and under a high level of control, mainly through laser light [62, 63, 64, 65, 66]. An important aspect for us in this regard is the possibility to easily handle coherent superpositions of electronic atomic levels (atomic coherences). Atomic coherences are very sensitive under the action of external fields and relatively long-lived in comparison with quantum coherences attained in other potential mechanical system's companions made up of solid-state superconducting materials. The longevity of atomic coherences persists even in the vicinity of chip surfaces, disregarding if the coherent superposition involves either hyperfine sublevels or Rydberg levels [67, 68]. In our endeavor to interface mechanical systems with atoms we subject atomic coherences to classical electromagnetic radiation that couples to and is modulated by the vibrations of a

mechanical resonator. By monitoring the response of the atomic coherences or using them to conveniently affect back the electromagnetic radiation, we are able to achieve certain level of control over the dynamics of the mechanical resonator of concern.

Another potential resource to intervene in the dynamics of a mechanical resonator are inter-atomic interactions. Interactions among a collection of atoms can be used to create strongly correlated (quantum entangled [69]) states among different atomic individuals [70, 71]. Particularly promising in this context are atoms excited to a high-lying electronic state, which are commonly known as Rydberg atoms [72]. Just as many other of its physical properties, the polarizability of a Rydberg atom is found to be abnormally magnified as compared to that of a ground state atom. As a result, Rydberg atoms can couple very strongly with one another, as well as to any other external electromagnetic perturbation. Either by selectively adjusting the Rydberg states of the atoms or by changing the distance that separates them, one can drastically modify the mutual interaction energy of such atoms, an effect that can then be harnessed to prepare atoms in entangled states deliberately [73, 74, 75], to enhance information technologies or to foster quantum nonlinear optics, among many other possibilities [76, 77, 78]. Mediating interactions between Rydberg atoms and mechanical resonators have just begun to be contemplated [79, 80]. Given that both, Rydberg atoms and miniature mechanical resonators, can significantly respond to feeble forces, their combination may pave the way towards full quantum control of mechanical motion of nano-scale solids by exploiting the robust control that we already have over atomic systems.

### Topical outline

In the following, we provide a summary of the topics that we address in the remaining of the thesis. Chapter 2 introduces the main physical elements that we use to develop our research. We start with a succinct overview on Rydberg atoms, their properties and their potential utilities for our undertaking. Likewise, we present how we can induce an atomic coherence with light and how its response may in turn affect light. Next, we briefly describe the oscillating mechanics of miniature solid structures and discuss under which conditions can quantum phenomena showcase a noticeable role. We analyze the response of a mechanical vibration mode under the action of an external drive and give an account of the ultimate limits of displacement resolution set by both thermal and quantum fluctuations, which arise due to the interactions of the mechanical structure with its environment. We also present a conventional strategy used to bring a mechanical vibration mode towards the quantum regime, and show how this is realized in the context of cavity optomechanics.

In Chapter 3 we examine an optomechanical interface between an ensemble of ultracold atoms and a nano-scale vibrating mirror. In this scheme we assess the influence that the dielectric response of the atomic ensemble exerts on the classical dynamics of a linearly vibrating mirror and vice versa, and discuss applications in optomechanical cooling in free space. The findings of the work explained in this chapter are published in reference [81].

The following Chapter 4 discusses a hybrid setting of Rydberg state atoms and a nano-scale mechanical torsional resonator. The hybrid setup is brought into being through electrostatic interactions between the atoms and a ferroelectric domain attached to the torsional resonator. A coherent interaction between atoms and torsional resonator enables the encoding of the quantum state of motion of a single mechanical torsion mode into the atomic coherence between two Rydberg levels.

Based on the detection of such atomic coherence we propose a quantum tomography protocol to reconstruct the quantum state of motion of the torsion pendulum. This chapter provides a detailed account of the work published in reference [82]. We close the thesis in Chapter 5, wherein we highlight the overall disclosure of our work and provide a survey of prospective research.



## 2 A glimpse into excited atoms, mechanical resonators and their interaction with light

### 2.1 Excited state atoms: Rydberg atoms

To a good approximation we speak of a ground state atom if its electronic energy, that is, the kinetic plus electrostatic interaction energies of the electrons and the nucleus comprising the atom, is lowest. Electrons bound to the atom may be excited to a state of very high and well defined energy, for example by irradiating the atom with electromagnetic waves. Consider an atom in a singly excited state and of very high energy, i.e., a bound state in which only one electron is highly excited. Most of the time the excited electron will likely be located far away from both the atomic nucleus and all the other electrons that surround the nucleus. The result is an *outer* electron that moves under the action of an approximately Coulomb type force due to a finite size ionic core which comprises the nucleus together with the remaining *inner* electrons to add up a total charge of  $+1$ . Atoms with such a highly excited bound electron receive the name of Rydberg atoms<sup>1</sup>. Probably the reason why they are known as Rydberg atoms is because they encompass a physical scenario that resembles very nearly that of a very excited electron bound to a hydrogen atom. And it was the spectroscopist Johannes Rydberg who provided, in 1888, a mathematical formula (a generalization of Balmer's one [83]) to describe the wavelengths of the discrete spectral lines of light emitted by hydrogen [84], which were regularly observed in laboratory experiments. The formula was proven to be useful not only for studying hydrogen but other types of atoms as well, in particular alkali metal atoms which we will introduce later on in section 2.1.1. Thus the physics of Rydberg atoms is in many respects very much like the physics of hydrogen.

Bohr's atomic model of 1913 [85] was the first theoretical work capable of providing a successful physical understanding of hydrogen's electron dynamics and thus of the aforementioned spectroscopic studies. Although Bohr's model was soon superseded by the quantum descriptions of Schrödinger [86, 87], and of Heisenberg, Born and Jordan [88, 89], it still constitutes a very useful tool to describe Rydberg atom physics. The model regards the motion of the outer electron around the ionic core as the motion of a planet around the sun. However, differently from a planetary motion, Bohr's model assumes that the revolving electron can only exist in certain stationary orbits of well defined energy in which the electron remains stable unless it is perturbed externally. Accordingly, the model predicts

---

1 Although we will restrict our discussion to the case of an atom with only one very excited electron, the term Rydberg atom can also be used to designate an atom in which more than one electron is brought into a very excited state.

## 2.1 Excited state atoms: Rydberg atoms

that the allowed binding energies of an electron bound to a hydrogen atom are

$$E_\nu = -hc \frac{R_\infty}{\nu^2}, \quad \nu \in \mathbb{N}^+. \quad (2.1)$$

The emission lines would arise from jumps of the electron from a higher energy orbit to a lower energy orbit, so that the excess of energy on passing from orbit to orbit is carried by the emitted electromagnetic radiation. The principal quantum number  $\nu$  in equation (2.1) labels the energy level of the electron's stationary orbit, whereas  $R_\infty = m_e e^4 / (8\epsilon_0^2 h^3 c)$  stands for the Rydberg constant where  $m_e$  is the rest mass of the electron,  $e$  the elementary charge,  $\epsilon_0$  the vacuum permittivity,  $c$  the speed of light in vacuum and  $h$  the Planck's constant. To demand that each level admits only a finite number of orbits Bohr postulated that the angular momentum or eccentricity of an orbit (its shape geometrically speaking) can only be quantified by discrete values  $l\hbar$ , where  $\hbar = h/(2\pi)$  and the orbital angular momentum quantum number can take the values  $l = 0, \dots, \nu - 1$ .

Bohr's planetary model is not only suitable to determine binding energies. It also allows us to find similar (large) power laws of  $\nu$  for many properties of Rydberg atoms based solely on classical arguments. The success of this so called correspondence principle [90] can be intuitively seen by recognizing that electron jumps from two nearby orbits of high  $\nu$  translate into a tiny energy change when compare it to a jump between low lying orbits of small  $\nu$ . And smooth or continuous like energy changes are usually a distinctive feature of classical systems. Perhaps the most obvious classical alike property of a Rydberg state is the emergence of an orbital radius, and thus of an electric dipole moment both proportional to  $\nu^2$ . A principal quantum number  $\nu = 100$  amounts then to a Rydberg state with an electric dipole six orders of magnitude larger than that of the ground state. Another remarkable property of Rydberg states is their long spontaneous radiative lifetimes compared to the ones of ordinary excited states. The inference of the longevity of Rydberg states against radiative emission using a classical picture is less obvious but it still provides a good numerical estimate. From the Larmor formula we estimate that the power  $W$  radiated by the orbiting electron is determined by the square of its acceleration  $|\mathbf{a}|$ ,  $W \simeq e^2 |\mathbf{a}|^2 / (6\pi\epsilon_0 c^3)$ . The radiative emission rate can be approximated as the ratio of the radiative power to the energy emitted during the lifetime of the initial Rydberg state. Differently from other physical properties, the lifetimes of Rydberg states are also sensitive upon  $l$ . As argued in [91], for large orbital angular momentum quantum numbers  $l \approx \nu - 1$ , the orbit of the excited (Rydberg) electron is nearly circular. The acceleration of the Rydberg electron is mostly centripetal, scaling as  $|\mathbf{a}_0| = \alpha_{\text{fs}}^2 c^2 a_0^{-1} \nu^{-4}$ , where we introduced the fine structure constant  $\alpha_{\text{fs}} = 4\pi a_0 R_\infty$ . Since the acceleration is uniform across the whole orbit, the Rydberg electron radiates continuously. Upon radiation the Rydberg electron jumps to a lower circular orbit, releasing light waves of frequency  $[E_{\nu+1} - E_\nu]/h \simeq 2cR_\infty \nu^{-3}$ . The radiated power is  $W_0 \simeq e^2 |\mathbf{a}_0|^2 / (6\pi\epsilon_0 c^3) = (4hc^2 R_\infty \alpha_{\text{fs}}^4 a_0 / 3) \nu^{-8}$ , and thus the emission rate scales as  $(W_0 / 2cR_\infty) \nu^3 = (2a_0^{-1} \alpha_{\text{fs}}^4 c / 3) \nu^{-5}$ . Circular Rydberg states have then a radiative lifetime proportional to  $\nu^5$ .

**Table 2.1** Scaling of different atomic properties with the principal quantum number  $\nu$ .

Physical property	(Magnitude)·Power law of $\nu$	At $\nu = 1$	At $\nu = 100$	Unit
Classical radius	$(a_0) \cdot \nu^2$	0.53	5300	Å
Maximum induced dipole moment	$(ea_0) \cdot \nu^2$	$8.48 \times 10^{-30}$	$8.48 \times 10^{-26}$	C m
Energy difference, $[E_{\nu+1} - E_\nu]/h$	$(2cR_\infty) \cdot \nu^{-3}$		$2.7 \times 10^{-5}$	eV
Polarizability	$\left(\frac{e^2 a_0^2}{2hcR_\infty}\right) \cdot \nu^7$	$1.65 \times 10^{-41}$	$1.65 \times 10^{-37}$	C <sup>2</sup> m <sup>2</sup> J <sup>-1</sup>
RMS velocity	$(\alpha_{fs} c) \cdot \nu^{-1}$	$2.2 \times 10^6$	$2.2 \times 10^4$	m s <sup>-1</sup>
Orbital period	$(cR_\infty)^{-1} \cdot \nu^3$	$3.0 \times 10^{-16}$	$3.0 \times 10^{-10}$	s
Lifetime: $l \ll \nu$	$(a_0^{-1} \alpha_{fs}^4 c) \cdot \nu^3$		$10^{-3}$	s
$l \approx \nu - 1$	$(a_0^{-1} \alpha_{fs}^4 c) \cdot \nu^5$		1	s

For the other limit case, that is  $l \ll \nu$ , the orbit of the excited (Rydberg) electron is very eccentric, so that its acceleration is considerably larger at the distance of maximum proximity to the nucleus, i.e. the perihelion of the orbit. Consequently, we may consider now that the Rydberg electron emits sporadically, basically each time it targets the perihelion. Since at the perihelion the acceleration is nearly independent from  $\nu$ , we then may assume that the lifetime of the Rydberg electron is determined by the orbital period. From third Kepler's law we know that the square of the orbital period is proportional to  $(\nu^2 a_0)^3$ , and so the lifetime of a Rydberg state with low orbital angular momentum scales with  $\nu^3$ . A more rigorous calculation of the lifetime of a Rydberg state atom using a classical formalism can be found in [92].

In table 2.1 we display a selection of physical properties of hydrogen and contrasts the magnitudes that result from considering a ground state  $\nu = 1$  and a Rydberg state with  $\nu = 100$ . Taking a close look at this table it is evident that the sensitive dependence of Rydberg states on  $\nu$  extrapolates to all of the properties shown therein. The enormous physical magnitudes of Rydberg state atoms, have caught more and more the attention and interest of atomic physicists during the last two decades. Probably the basic driving motivation underlying this interest lies on what Kleppner phrased already back in the 1980s [93]:

*“Rydberg atom research provides a means for changing the scale of atomic interactions by many orders of magnitude, and whenever such a change of scale occurs in physics one can look forward to new discoveries and unexpected phenomena”.*

The observation above manifests itself in the extraordinarily large dipole moments of atomic Rydberg states, which, e.g., enable a strong coupling between atoms and electromagnetic

radiation. Thus, together with their long lifetimes, Rydberg atoms have turned very useful in the development of cavity quantum electrodynamics (QED), see e.g. [94, 95]. In cavity QED, Rydberg atoms can serve, e.g., as an extremely sensitive probe for examining the quantum properties of a single electromagnetic field mode. Later on, in chapter 4, we shall investigate the use of that extreme sensitivity to electromagnetic radiation of a rubidium Rydberg atom for detecting the motion of a mechanical resonator in the quantum regime.

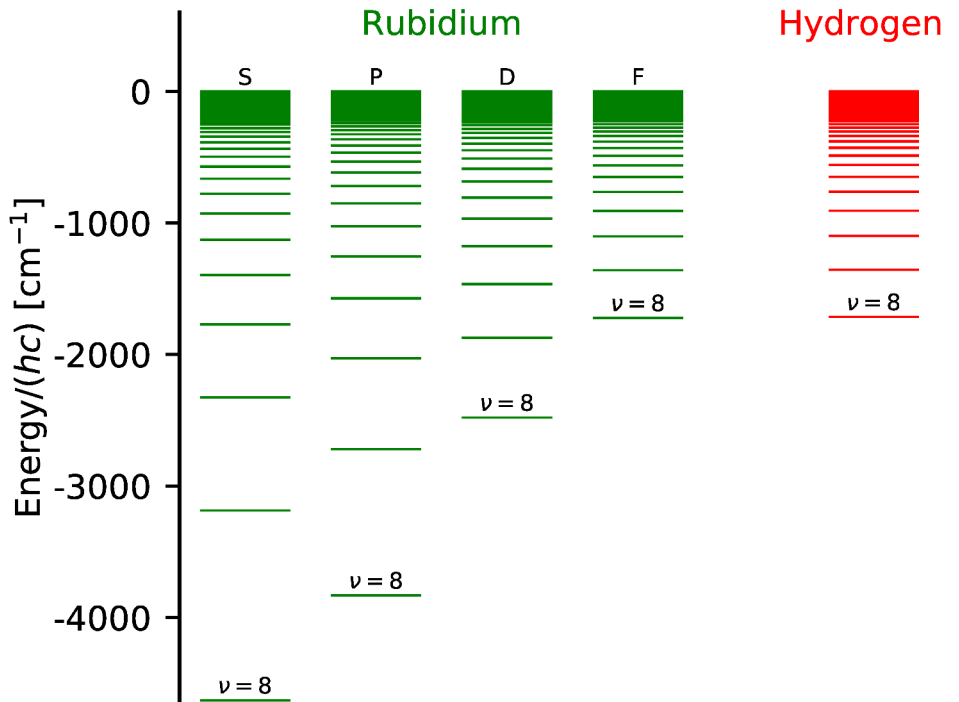


**Figure 2.1** Energy level diagram of hydrogen (red) and rubidium (green) plotted according to the Rydberg formulas (2.1) and (2.2) respectively. We use the standard spectroscopic notation to designate each energy term. Every value of the principal quantum number  $\nu$  accounts for an energy manifold. For hydrogen, each manifold contains  $l = \nu - 1$  angular momentum states all of them having the same energy. However, in the case of rubidium this degeneracy breaks down due to the non Coulombic character of the potential describing the interactions between the electrons and the ionic core in the atom. This is specially the case for the low angular momentum states, corresponding, in increasing order of  $l$  from 0 to 3, to the S, P, D and F terms depicted in the diagram. The core penetrating feature of these states results in energy shifts. These core penetration effects are captured in the Rydberg formula (2.2) by the quantum defects, which tend to lower the overall energy of a given electronic state as it is clearly seen in the diagram. The non Coulombic nature of the potential starts to be less relevant for increasing  $\nu$ . For  $\nu > 14$  all the energy terms are very much like the hydrogenic ones. The reason being that for increasing values of  $\nu$  the electronic states are each time found to be more localized further away from the ionic core.

### 2.1.1 Rydberg states of alkali metal atoms

Rubidium is an element of the periodic table belonging to the alkali metal group. A ground state alkali metal atom comprises a single valence electron revolving around a spherically symmetric ionic core (i.e. with total angular momentum equal to zero). The core electrons



are tightly bound, with a binding energy at least of  $\sim 20$  eV, in comparison with the valence electron, the binding energy of which is  $\sim 5$  eV [96]. Then, just like in hydrogen, the electronic structure of an alkali metal atom (within the first ionization limit) is essentially determined by a single electron (the valence electron). To account for the properties of the Rydberg states of an alkali atom one uses a modified principal quantum number  $\nu^* = \nu - \mu_l$ , where  $\mu_l$  is known as a quantum defect that is dependent majorly on the quantum number  $l$  as well as on the atomic species under consideration, see [96, 97]. Replacing  $\nu$  by  $\nu^*$  in the power laws displayed in table 2.1 allows us to estimate the magnitude of the physical properties of the Rydberg states of an alkali atom. The quantum defect  $\mu_l$  quantifies the relative difference in binding energy between a Rydberg state of an alkali atom and the counterpart state of hydrogen, thus capturing the perturbation effects of the ionic core onto the excited valence electron (the Rydberg electron) of the alkali atom [93]. For circular or nearly circular Rydberg states of an alkali atom the Rydberg electron is mostly separated from the ionic core and loosely bound to the atom via an approximately Coulomb type potential. Thus, for a given value of  $\nu$ , these nearly circular Rydberg states, which have a high a value of  $l$ , are subject, to a good approximation, to the same accidental degeneracy that undergo all the states of hydrogen, meaning that for high values of  $l$  the quantum defect  $\mu_l$  is essentially zero. As  $l$  is decreased, the Rydberg electron moves, on average, along a very eccentric orbit such that it may sit very close or even penetrate the ionic core. In that case the shielding of the nucleus by the inner electrons diminishes, and the Rydberg electron experiences a stronger attraction towards the nucleus than the one resulting from a purely Coulomb potential. As a result, the binding energy of a Rydberg state of an alkali atom with a low value of  $l$  is always higher than that of its equivalent in hydrogen, and therefore  $\mu_l > 0$  for low values of  $l$ . For example, the binding energies of the Rydberg states of  $^{87}\text{Rb}$  with  $\nu \geq 8$  show appreciably nonzero quantum defects  $\mu_l > 0$  only for  $l \leq 3$ , for  $l > 3$  the quantum defects are negligible. We can appreciate this in figure 2.1, which allows us to visualize the shifts in the binding energies of the Rydberg states of  $^{87}\text{Rb}$  relative to those of hydrogen. We calculate the binding energies for hydrogen according to the formula (2.1), whereas the binding energies for rubidium are obtained from the following expression

$$E_{\nu l} = -hc \frac{R_{m_I}}{(\nu - \mu_l)^2}, \quad \nu \in \mathbb{N}^+, \quad (2.2)$$

where  $R_{m_I} = R_\infty m_I / (m_I + m_e)$  denotes the Rydberg constant for an isotope of a given atomic species with mass  $m_I$ . Using the mass  $m_I = m(^{87}\text{Rb})$  and the quantum defects of  $^{87}\text{Rb}$  displayed in table 2.2, formula (2.2) yields the binding energies of  $^{87}\text{Rb}$  plotted in figure 2.1. Current experimental techniques employed in laboratories enable the preparation and study of Rydberg states with principal quantum numbers typically ranging from a few tens to a few hundreds.

These techniques are commonly based on laser excitation schemes carried out onto ground state atoms in, e.g., a beam or a gas cell [98]. When considering transitions between neighboring Rydberg states, having access to such a wide range of values for  $\nu$  translates

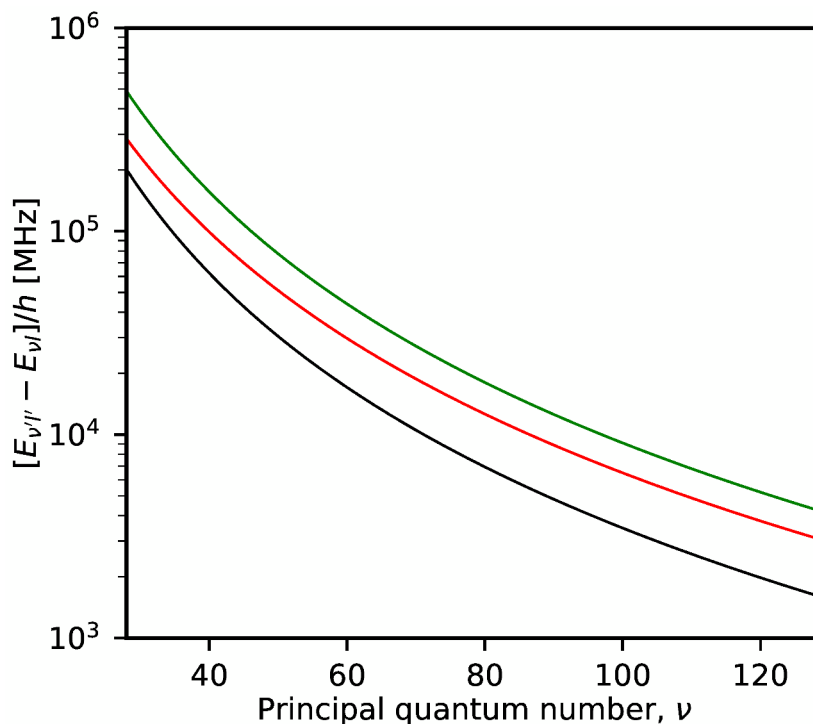


**Figure 2.2** Energy differences  $E_{\nu'l'} - E_{\nu l}$  between adjacent Rydberg levels of  $^{87}\text{Rb}$  as a function of the principal quantum number  $\nu$  as determined from equation (2.2). Energy differences between levels  $\nu\text{S}$  and  $\nu\text{P}$  are shown in black, and between levels  $\nu\text{P}$  and  $\nu\text{D}$  in green. The red line shows energies for transitions between circular Rydberg states  $\nu + 1l$  and  $\nu l - 1$ , with  $l = \nu$ , for which the quantum defects are negligible.

**Table 2.2** Parameters for the binding energies of the Rydberg states of  $^{87}\text{Rb}$ .

Mass, $m(^{87}\text{Rb})$	Quantum defects, $\mu_l$			
	$l = 0$	$l = 1$	$l = 2$	$l = 3$
kg				
$1.44 \times 10^{-25}$	3.13	2.65	1.35	0.016

into a broad band of transition frequencies available for being probed. Figure 2.2 shows this explicitly for a few electric dipole allowed transitions between nearby Rydberg levels in  $^{87}\text{Rb}$ .

Transitions induced by electromagnetic radiation between two different Rydberg states, labeled with  $\nu l$  and  $\nu' l'$ , are mostly mediated by the electric dipole moment of the atom. Therefore, to a good extent, the overlap with the electric dipole moment of the states involved in the transition, the so called electric dipole matrix element, determines the coupling strength of the atom to the radiation field. Transition selection rules demand  $l' - l = \pm 1$ . Of particular interest for us are also transitions for which  $\nu \sim \nu'$ , in which case the reduced dipole matrix element can be estimated as  $\sim 3ea_0\nu^2/2$  [93].

## 2.2 Driving atomic transitions with electromagnetic waves

An atomic gas interacting with an incoming electromagnetic wave may be subject to absorption and (stimulated) emission processes in which the electronic state of the atoms changes. Electromagnetically driven transitions between different atomic states give rise to oscillating dipoles in the gas that emit electromagnetic waves in all directions, which in turn can interfere with the incident wave. As a result, a fraction of the incoming wave is spatially redirected, a process known as scattering. Furthermore, the amplitude of the total (incident plus emitted) wave in the direction of the incident wave becomes attenuated. In this section we will characterize these phenomena in terms of the dielectric response of the atoms. The familiarization with the dielectric response on a quantitative basis will prove useful in the research work of the following chapter 3, in which we exploit the linear optical response of an atomic gas to affect the dynamics of a mechanical resonator. We adopt a so called semiclassical approach in which the electromagnetic waves are described by the laws of classical physics whereas the atoms are treated according to the laws of the quantum theory. For this description to be accurate it is necessary to consider electromagnetic fields sufficiently intense, in other words, fields with an average number of photons much larger than the number of atoms present in the gas [99], a condition that will be fulfilled in the systems that we study.

### 2.2.1 Optically induced atomic dipoles

Our analysis is concerned with the scattering of a monochromatic electromagnetic wave incident on an atomic medium of finite length  $L$ . The electric field  $\mathbf{E}$  of the wave at the spatial location  $\mathbf{r}$  and time  $t$  reads

$$\mathbf{E}(\mathbf{r}, t) = \frac{1}{2} \mathcal{E}_{\omega_\lambda}(\mathbf{r}) \exp(-i\omega_\lambda t) + \text{c.c.} \quad (2.3)$$

where  $\omega_\lambda$  is the carrier frequency of the wave and  $\mathcal{E}_{\omega_\lambda}(\mathbf{r}) = \mathbf{E}_{\omega_\lambda}(\mathbf{r}) \exp(i\mathbf{k}_\lambda \cdot \mathbf{r})$  its envelope with amplitude  $\mathbf{E}_{\omega_\lambda}$  and wavevector  $\mathbf{k}_\lambda$ . The frequency  $\omega_\lambda$  and the wavevector  $\mathbf{k}_\lambda$  relate to each other via a dispersion relation determined from the appropriate wave equation to describe the propagation of electromagnetic waves through the medium of concern. In vacuum, and before the arrival of the wave onto the medium, the frequency and wavevector fulfill the dispersion free relation  $|\mathbf{k}_\lambda| = \omega_\lambda/c$  and the amplitude  $\mathbf{E}_{\omega_\lambda}(\mathbf{r}) = \mathbf{E}_{0\omega_\lambda}$  is constant with a strength<sup>2</sup>  $|\mathbf{E}_{0\omega_\lambda}| = \sqrt{2\mathcal{W}_{0\omega_\lambda}/[\epsilon_0 c \mathcal{A}_{\omega_p}]}$  given by the input power  $\mathcal{W}_{0\omega_\lambda}$  and the cross sectional area  $\mathcal{A}_{\omega_\lambda}$  of the wave, here chosen to satisfy  $|\mathbf{k}_\lambda|^{-2} \ll \mathcal{A}_{\omega_\lambda} \lesssim L^2$ , thus minimizing any spatial variations of the wave transverse to its propagation direction. Inside the medium the wavevector is determined from the electromagnetic wave equation in the presence of the atoms, whereas the amplitude is found from the appropriate boundary conditions.

---

<sup>2</sup> We assume that the phase of the input envelope can be taken as a phase reference and thus we set it to zero without loss of generality.

We shall calculate the linear polarization or, equivalently, the linear dielectric susceptibility of a gas of atoms settled into some stationary state. Physically, the number of induced electric dipoles per unit volume defines the polarization of the gas. The dielectric susceptibility is identified with the strength of the polarization per unit electric field, and represents, to some extent, a quantifier of the average displacement of the atomic charges in medium. We start assuming a gas of  $N$  identical, neutrally charged and non-interacting one-electron atoms (e.g.  $^{87}\text{Rb}$  atoms). We further assume that the gas is kept at an ultracold temperature  $T \lesssim 1 \mu\text{K}$ , suggesting that we may ignore the Doppler motion of the atoms<sup>3</sup>. Then, in the absence of the incident wave, the Hamiltonian for the discrete electronic structure of atom  $n$  at location  $\mathbf{r}_n$  simply reads  $\hat{H}_0^{(n)} = \sum_{\mu} \hbar\omega_{\mu} \hat{\sigma}_{\mu\mu}^{(n)}$ , where  $\{\hbar\omega_{\mu}\}$  is the set of its eigenenergies (identical for every atom in the gas) and  $\hat{\sigma}_{\mu\mu'}^{(n)} = [|\mu\rangle\langle\mu'|]_n$  denotes the atomic transition operator between eigenstates  $|\mu\rangle_n$  and  $|\mu'\rangle_n$  acting on atom  $n$  only. For the sake of clarity, the frequency of the incident wave is chosen to be nearly resonant only with a single Bohr atomic frequency  $\omega_{\lambda} \approx \omega_{eg} = \omega_e - \omega_g > 0$  corresponding to an atomic transition between the electronic ground state  $|g\rangle$  and the excited state  $|e\rangle$ . In addition, we introduce the rate of spontaneous emission  $\Gamma_{eg}$  to account for the finite lifetime of the excited state  $|e\rangle$ . Although spontaneous emission arises due to the coupling of the atoms with the electromagnetic field vacuum, we are solely interested in the evolution of the atoms rather than in the correlated dynamics of atoms plus field vacuum. We then opt for a density operator formalism to describe the dynamical state of the atoms, whereby spontaneous decay appears as a dissipation mechanism for the atoms. Due to the non-interacting feature of the atoms, the density operator of the atomic gas takes on the form

$$\hat{\rho} = \hat{\rho}^{(1)} \otimes \hat{\rho}^{(2)} \otimes \dots \otimes \hat{\rho}^{(N)}, \quad (2.4)$$

where  $\hat{\rho}^{(n)}$  denotes the single-particle density operator for the  $n$ th atom. The unitary dynamics of  $\hat{\rho}$  are governed by the total Hamiltonian  $\hat{H} = \sum_n \hat{H}_0^{(n)} + \hat{H}_1$ , where  $\hat{H}_1$  describes the interaction of the atoms with the applied electromagnetic field and the sum runs over all the  $N$  atoms. For the physical scenarios of concern in this thesis, an electromagnetic field-atom coupling will be well described in the long-wavelength approximation, for which  $|\mathbf{k}_{\lambda}|^{-1}$  is way larger than the separation between the excited electron and the ionic core. In that case, the interaction  $\hat{H}_1$  is given by an electric dipole coupling<sup>4</sup>  $\hat{H}_1 = -\sum_n \sum_{\mu \neq \mu'} [\mathbf{d}_{\mu\mu'} \cdot \mathbf{E} \hat{\sigma}_{\mu\mu'}^{(n)} + \text{h. c.}]$ , with  $\mathbf{d}_{\mu\mu'} = \mathbf{d}_{\mu'\mu}^*$  the transition dipole moment between electronic states  $|\mu\rangle$  and  $|\mu'\rangle$ , fulfilling  $\mathbf{d}_{\mu\mu} = 0$ , and  $\mathbf{E}$  is the electric field defined in (2.3). Since the field is only quasi-resonant with the  $|e\rangle$ - $|g\rangle$  transition, it is convenient to work in a rotating frame that enables us to

3 For a  $^{87}\text{Rb}$  gas the thermal velocity of the atoms at  $T = 1 \mu\text{K}$  is  $\bar{v} = \sqrt{k_{\text{B}}T/m(^{87}\text{Rb})} \simeq 10^{-2} \text{ m s}^{-1}$  which, for a regular optical transition as we shall consider here with  $|\mathbf{k}_{\lambda}|^{-1} \approx 500 \text{ nm}$ , gives rise to a Doppler shift  $|\mathbf{k}_{\lambda}|\bar{v} \approx 20 \text{ kHz}$  much smaller than the natural width  $\sim 10 \text{ MHz}$  for the atomic dipole of such optical transition.

4 We have ignored any magnetic couplings since they are, at least, a factor  $\sim \alpha_{\text{fs}}^2$  smaller than the electric dipole coupling [96].

identify all the non-resonant contributions in the atomic Hamiltonian. This is achieved by applying a unitary transformation of the form  $\hat{U} = \exp(i\hat{\mathcal{H}}t/\hbar)$ , where

$$\hat{\mathcal{H}}/\hbar = \sum_{n=1}^N \sum_{\mu} v_{\mu} \hat{\sigma}_{\mu\mu}^{(n)}, \quad (2.5)$$

with  $v_e = \omega_g$  and  $v_{\mu} = \omega_{\mu}$  if  $\mu \neq e$ . In this manner, the Hamiltonian transforms into  $\hat{H} \mapsto \hat{U}\hat{H}\hat{U}^{\dagger} + i\hbar\dot{\hat{U}}\hat{U}^{\dagger} = \hat{H}_{\text{tla}}$  which, after using a rotating wave approximation (rwa), it effectively describes a gas of two level atoms (tla), i.e., after such rwa is

$$\hat{H}_{\text{tla}}(t) = \sum_{n=1}^N \left\{ \hat{H}_0^{(n)} + \hat{H}_1^{(n)}(\mathbf{r}_n, t) \right\} \simeq \hbar \sum_{n=1}^N \left\{ \omega_{eg} \hat{\sigma}_{ee}^{(n)} - \frac{1}{2} [\Omega_{\lambda}(\mathbf{r}_n) \hat{\sigma}_{eg}^{(n)} + \text{h. c.}] [e^{-i\omega_{\lambda}t} + \text{c. c.}] \right\}, \quad (2.6)$$

where  $\omega_{\mu'\mu} = \omega_{\mu'} - \omega_{\mu}$  stands for the Bohr frequency of the  $|\mu'\rangle$ - $|\mu\rangle$  transition and  $\Omega_{\lambda}(\mathbf{r}_n) = \mathbf{d}_{eg} \cdot \mathcal{E}_{\omega_{\lambda}}(\mathbf{r}_n)/\hbar$  is the Rabi frequency for atom  $n$ . The rwa above consisted in ignoring all non-resonant terms oscillating with large detunings  $|\omega_{\lambda} \pm v_{\mu\mu'}| \gg \{|\omega_{\lambda} - \omega_{eg}|, |\mathbf{d}_{\mu\mu'} \cdot \mathcal{E}_{\omega_{\lambda}}(\mathbf{r}_n)|/\hbar\}$ , where  $v_{\mu\mu'} = v_{\mu} - v_{\mu'} \neq 0$ . Likewise, the density operator of the atomic gas transforms into  $\hat{\rho} \mapsto \hat{U}\hat{\rho}\hat{U}^{\dagger} = \hat{\rho} = \hat{\rho}^{(1)} \otimes \hat{\rho}^{(2)} \otimes \dots \otimes \hat{\rho}^{(N)}$ . Taking into account that the atoms do not interact among each other and that the trace of every one-particle density operator  $\hat{\rho}^{(n)}$  is equal to one, it follows that the time evolution of  $\hat{\rho}$  yields a separate and identical equation of motion for each  $\hat{\rho}^{(n)}$ . Thus, the dynamics of the atomic gas is entirely given by a solution of the equation of motion for a single  $\hat{\rho}^{(n)}$ . With the rwa of (2.6) this evolution follows a Lindblad master equation of the form

$$\frac{\partial}{\partial t} \hat{\rho}^{(n)}(t) = -\frac{i}{\hbar} [\hat{H}_0^{(n)} + \hat{H}_1^{(n)}(t), \hat{\rho}^{(n)}(t)] + \mathcal{L}[\hat{\rho}^{(n)}(t)], \quad (2.7)$$

where the super-operator  $\mathcal{L}$  describes spontaneous decay of atom  $n$  from level  $|e\rangle$  to  $|g\rangle$  [100],  $\mathcal{L}[\hat{\rho}^{(n)}] = \hat{L}_n \hat{\rho}^{(n)} \hat{L}_n^{\dagger} - (\hat{L}_n^{\dagger} \hat{L}_n \hat{\rho}^{(n)} + \hat{\rho}^{(n)} \hat{L}_n^{\dagger} \hat{L}_n)/2$  with Lindblad operator  $\hat{L}_n = \sqrt{\Gamma_{\text{p}}} \hat{\sigma}_{ge}^{(n)}$ . Knowledge of the density operator  $\hat{\rho}$  allows for the evaluation of the induced atomic dipoles in the gas, and therefore of the polarization. By introducing the atomic density distribution  $\mathcal{N}(\mathbf{r}) = \sum_n \delta(\mathbf{r} - \mathbf{r}_n)$  where  $\delta(\mathbf{r})$  stands for the Dirac delta function, and remembering that we are in an interaction picture with respect to (2.5), the polarization  $\mathbf{P}$  reads

$$\mathbf{P}(\mathbf{r}, t) = \left\langle \sum_{n=1}^N \delta(\mathbf{r} - \mathbf{r}_n) \sum_{\mu, \mu'} e^{i\hat{\mathcal{H}}t/\hbar} \mathbf{d}_{\mu\mu'} \hat{\sigma}_{\mu\mu'}^{(n)} e^{-i\hat{\mathcal{H}}t/\hbar} \right\rangle = \sum_{\mu, \mu'} \mathcal{R}_{\mu'\mu}(\mathbf{r}, t) \mathbf{d}_{\mu\mu'} e^{-iv_{\mu'\mu}t}, \quad (2.8)$$

where we introduced collective atomic density matrix elements defined as [99]

$$\mathcal{R}_{\mu'\mu}(\mathbf{r}, t) = \sum_{n=1}^N \langle \hat{\sigma}_{\mu\mu'}^{(n)}(t) \rangle \delta(\mathbf{r} - \mathbf{r}_n) = \sum_{n=1}^N \rho_{\mu'\mu}^{(n)}(t) \delta(\mathbf{r} - \mathbf{r}_n). \quad (2.9)$$

In the last equality of equation (2.9) we used the fact that the trace of every one-particle density operator is equal to one. Restricting our study for the case of an equally distributed gas of atoms with a constant density  $\mathcal{N}(\mathbf{r}) = \mathcal{N}_0$ , the collective atomic density matrix simplifies

to  $\hat{\mathcal{R}}(\mathbf{r}, t) \equiv \mathcal{N}_0 \hat{\rho}(\mathbf{r}, t)$ , where  $\hat{\rho}(\mathbf{r}, t)$  is determined from the solution of equation (2.7) for a single atom standing representative for the entire atomic gas. Then, by virtue of the rwa of (2.6) we obtain

$$\mathbf{P}(\mathbf{r}, t) = \mathcal{N}_0 \rho_{eg}(\mathbf{r}, t) \mathbf{d}_{ge} + \text{c. c.} \quad (2.10)$$

At every point in the atomic gas the polarization is determined by a uniform collection of independent dipoles. Note that this independent (non-interacting) rather than cooperative behavior of the dipoles can only be satisfied for a sufficiently dilute gas, such that  $\mathcal{N}_0 |\mathbf{k}_\lambda|^{-3} < 1$ . To find an explicit expression for the polarization in the linear regime (meaning that the components of  $\mathbf{P}$  relate linearly with the components of  $\mathbf{E}$ ) we shall solve the master equation (2.7) using first order time dependent perturbation theory for the perturbation  $\hat{H}_1 \equiv \hat{H}_1^{(n)}$ .

### 2.2.2 Dielectric susceptibility

We seek a solution for the density operator based on perturbation theory and expressed in the basis of the eigenstates  $\{|g\rangle, |e\rangle\}$  of the unperturbed Hamiltonian  $\hat{H}_0 \equiv \hat{H}_0^{(n)}$ . First, we write the density operator in a series expansion  $\hat{\rho}(t) = \hat{\rho}_0 + \hat{\rho}_1(t) + \dots = \sum_k \hat{\rho}_k(t)$ , wherein each successive term in the series accounts for a higher order correction of the initial state due to the action of the time dependent perturbation  $\hat{H}_1(t)$ . Equivalently, we decompose the polarization into the series  $\mathbf{P}(t) = \mathbf{P}_0 + \mathbf{P}_1(t) + \dots = \sum_k \mathbf{P}_k(t)$ . Next, we assume that far in the past  $t = -\infty$  the atoms were all in the ground state before they were disturbed by the electromagnetic field, i.e. it was  $\hat{H}_1(-\infty) = 0$ , so that  $\hat{\rho}_k(-\infty) = 0$  for  $k > 0$  and  $\hat{\rho}_0 = \hat{\rho}(-\infty) = \hat{\sigma}_{gg}$ . Consequently, the density operator  $\hat{\rho}_0$  is diagonal in the energy basis  $\{|g\rangle, |e\rangle\}$  of the unperturbed atomic system, and since initially the atomic gas is neutrally charged, the zeroth order polarization is  $\mathbf{P}_0 = 0$ . First and higher order corrections to the density operator are obtained from the definition of the master equation (2.7). Making use of the series expansion of  $\hat{\rho}$  in the master equation (2.7) and matching terms of the same order, we obtain the evolution equation for arbitrary order  $k$  in a recursive manner,

$$\frac{\partial}{\partial t} \hat{\rho}_k(t) = -\frac{i}{\hbar} [\hat{H}_0, \hat{\rho}_k(t)] - \frac{i}{\hbar} [\hat{H}_1(t), \hat{\rho}_{k-1}(t)] + \mathcal{L}[\hat{\rho}_k(t)]. \quad (2.11)$$

We solve the time evolution up to the first order correction  $\hat{\rho}_1$  to obtain the linear polarization  $\mathbf{P}_1$ . Since  $\hat{H}_1$  is Hermitian and the zeroth order density operator is diagonal in  $\{|g\rangle, |e\rangle\}$ , it follows from the equation (2.11) above that the populations are  $\rho_{1,gg} = \rho_{1,ee} = 0$ . To compute the coherence  $\rho_{1,eg} = \rho_{1,ge}^*$  we formally integrate equation (2.11) for  $k = 1$  in the interval  $]-\infty, t]$ . Taking into account that  $\rho_{1,eg}(-\infty) = 0$ , the result is

$$\rho_{1,eg}(t) = \frac{\rho_{0,gg} - \rho_{0,ee}}{i\hbar} \int_{-\infty}^t dt' e^{-i(\omega_{eg} - i\Gamma_{eg}/2)(t-t')} \langle e | \hat{H}_1(t') | g \rangle. \quad (2.12)$$

Using the explicit expression  $\hat{H}_1(t) = -\hbar [\Omega_\lambda \hat{\sigma}_{eg} + \text{h. c.}] [\exp(-i\omega_\lambda t) + \text{c. c.}] / 2$ , the integral yields two terms, a resonant term proportional to  $[\omega_\lambda - \omega_{eg} + i\Gamma_{eg}/2]^{-1}$  and a non-resonant

term proportional to  $[\omega_\lambda + \omega_{eg} + i\Gamma_{eg}/2]^{-1}$ . Since we set  $\omega_\lambda \sim \omega_{eg}$  and used a weak coupling approach we advocate the rwa  $|\omega_\lambda + \omega_{eg}| \gg \{|\omega_\lambda - \omega_{eg}|, |\Omega_\lambda|\}$  to neglect the non-resonant term resulting from the integral (2.12) above. With this rwa and the initial condition  $\hat{\rho}_0 = \hat{\sigma}_{gg}$ , the linear response of the atomic gas reads

$$\rho_{1,eg}(\mathbf{r}, t) = -\frac{\Omega_\lambda(\mathbf{r})}{2} \frac{\exp(-i\omega_\lambda t)}{\omega_\lambda - \omega_{eg} + i\Gamma_{eg}/2}. \quad (2.13)$$

For an atomic gas of rubidium atoms the initial state  $\hat{\rho}_0 = \hat{\sigma}_{gg}$  is spherically symmetric (since the ground state of every alkali metal atom has spherical symmetry). If, in addition, we assume that the incident wave is linearly polarized, every dipole induced in the gas, and thus the atomic polarization  $\mathbf{P}$ , will orientate along the same direction of the incident field, i.e. we can conceive the atomic gas as an isotropic medium. Let us consider such an isotropic gas. Then, inserting the expression (2.13) for the coherence into the definition of  $\mathbf{P}$  in equation (2.10), writing  $\mathcal{E}_{\omega_\lambda} = \epsilon|\mathcal{E}_{\omega_\lambda}|$  with  $\epsilon$  a real unit-norm vector, and considering that both  $\mathbf{d}_{eg}$  and  $\epsilon$  lie along the same direction, we obtain the linear atomic polarization as

$$\mathbf{P}_1(\mathbf{r}, t) = -\frac{\mathcal{N}_0|\mathbf{d}_{eg}|^2}{2\hbar} \frac{1}{\omega_\lambda - \omega_{eg} + i\Gamma_{eg}/2} \mathcal{E}_{\omega_\lambda}(\mathbf{r}) \exp(-i\omega_\lambda t) + \text{c.c.} \quad (2.14)$$

where we have used the equivalence  $\Omega_\lambda \mathbf{d}_{ge} \equiv |\mathbf{d}_{eg}|^2 \mathcal{E}_{\omega_\lambda} / \hbar$ . From a phenomenological or macroscopic point of view, the atomic polarization induced by the electromagnetic wave results from a relative displacement of the electrons from the nuclei in the gas. The reaction of the charges is not instantaneous but it builds up after some finite time. Accordingly, the polarization at a certain time is in general a function of the applied field at earlier times. Assuming a spatially local and isotropic atomic medium, as is the case here, the linear relation between the delayed polarization response of the atoms and the applied electric field can be expressed as [101]

$$\mathbf{P}_1(\mathbf{r}, t) = \epsilon_0 \int_{-\infty}^{+\infty} d\tau \chi(\tau) \mathbf{E}(\mathbf{r}, t - \tau), \quad (2.15)$$

where the (dimensionless) response function  $\chi$  is a real quantity satisfying causality,  $\chi(\tau < 0) = 0$ , i.e. the value of the polarization at time  $t$  can not depend on the electric field at future times of  $t$ . For a monochromatic electric field as defined in equation (2.3), the relation (2.15) above reduces to

$$\mathbf{P}_1(\mathbf{r}, t) = \frac{1}{2} \epsilon_0 \underline{\chi}(\omega_\lambda) \mathcal{E}_{\omega_\lambda}(\mathbf{r}) \exp(-i\omega_\lambda t), \quad (2.16)$$

where we introduced the Fourier transform  $\underline{\chi}(\omega) = \int dt \exp(i\omega t) \chi(t)$  of the real valued response function  $\chi(t)$ , and subsequently used  $\underline{\chi}^*(-\omega) = \underline{\chi}(\omega)$ . The frequency dependent function  $\underline{\chi}$  is called the (linear) dielectric susceptibility. Comparing equations (2.14) and (2.16) we find that, under the incidence of a monochromatic electromagnetic wave, the linear dielectric susceptibility for an isotropic gas of atoms evaluated at the frequency of the wave is determined as

$$\underline{\chi}(\omega_\lambda) = -\frac{2\mathcal{N}_0|\mathbf{d}_{eg}|^2}{\epsilon_0\hbar\Gamma_{eg}} \frac{\Gamma_{eg}/2}{\omega_\lambda - \omega_{eg} + i\Gamma_{eg}/2} = 6\pi\mathcal{N}_0|\mathbf{k}_0|^{-3} \frac{i\Gamma_{eg}/2}{\Gamma_{eg}/2 - i\Delta_\lambda}. \quad (2.17)$$

Equations (2.17) and (2.13) yet lead to one more relation:  $\underline{\chi}(\omega_\lambda) = 6\pi|\mathbf{k}_0|^{-3}\Gamma_{eg}\mathcal{R}_{eg}/\Omega_\lambda$ , which shall be formulated after an atomic transient dynamics occurring on a time scale  $\lesssim \Gamma_{eg}^{-1}$ . In the second equality of equation (2.17) we have rewritten the squared of the dipole moment in terms of the natural width of the transition as  $|\mathbf{d}_{eg}|^2 = 3\hbar\pi\epsilon_0|\mathbf{k}_0|^{-3}\Gamma_{eg}$ , with  $|\mathbf{k}_0|^{-1} = c/\omega_{eg}$  the reduced wavelength of the atomic transition. The symbol  $\Delta_\lambda = \omega_\lambda - \omega_{eg}$  denotes the detuning from resonance, that is, the frequency mismatch between the atomic transition frequency and the carrier frequency of the incident wave. The susceptibility  $\underline{\chi}$  is a complex valued and frequency dependent function and, as we will see now, its real  $\underline{\chi}' = \text{Re}[\underline{\chi}]$  and imaginary  $\underline{\chi}'' = \text{Im}[\underline{\chi}]$  parts determine, respectively, the absorptive and dispersive properties of the atomic gas in response to the incident wave. This follows from the wave equation for an electromagnetic mode of frequency  $\omega_\lambda$  inside a linear and isotropic medium (with zero magnetization and devoid of free currents and charges). They lead to a dispersion relation demanding a wavevector fulfilling  $|\mathbf{k}_\lambda| = \omega_\lambda \underline{n}(\omega_\lambda)/c$ , where the index of refraction  $\underline{n}(\omega_\lambda)$  is defined from the linear susceptibility via

$$\underline{n}^2(\omega) = 1 + \underline{\chi}^2(\omega). \quad (2.18)$$

On resonance the real part of the susceptibility vanishes  $\underline{\chi}'(\omega_\lambda = \omega_{eg}) = 0$  whereas the imaginary part reaches its highest value  $\underline{\chi}''(\omega_\lambda = \omega_{eg}) = 6\pi\mathcal{N}_0|\mathbf{k}_\lambda|^{-3}$ . Since we are

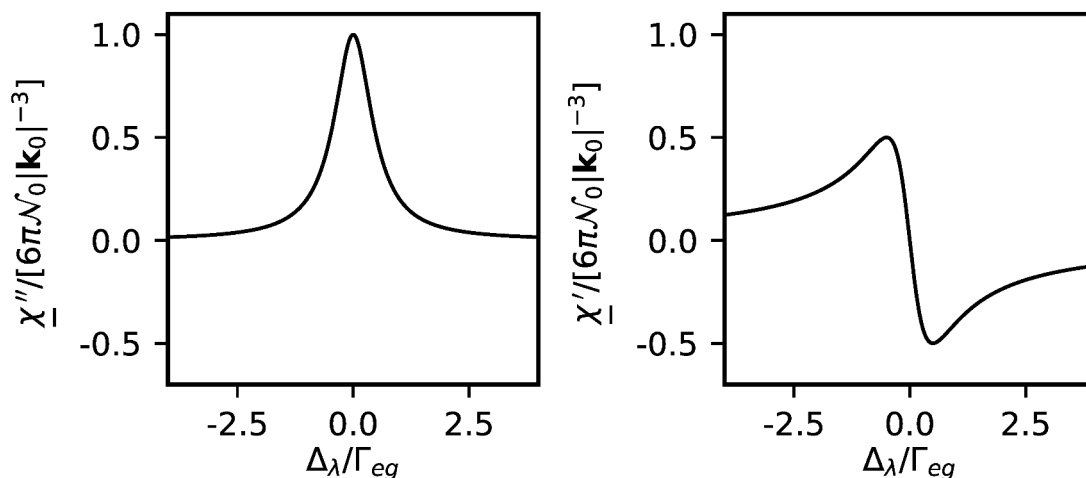


**Figure 2.3** Absorption (left panel) and dispersion (right panel) profiles associated with the electronic transition of a gas of identical two level atoms as a function of the detuning from resonance  $\Delta_\lambda$  in units of  $\Gamma_{eg}/(2\pi) = 6.1$  MHz, the natural width of the transition. The imaginary part  $\underline{\chi}''$  of the susceptibility accounts for absorption (left panel), whereas the real part  $\underline{\chi}'$  accounts for dispersion (right panel).

interested in atomic gases sufficiently diluted with  $\mathcal{N}_0|\mathbf{k}_\lambda|^{-3} < 1$ , we observe that  $\underline{\chi}', \underline{\chi}'' \lesssim 1$ , which enables the approximation  $\underline{n} \simeq 1 + [\underline{\chi}' + i\underline{\chi}'']/2$ . Given a plane wave with electric field (2.3), normally incident from vacuum onto the atomic gas, and propagating along the  $z$ -axis,  $\mathbf{r} = [0, 0, z]^T$  (the superscript T stands for vector transpose), the solution of the electromagnetic wave equation for the electric field  $\mathbf{E}_t$  transmitted through the atomic gas



from 0 (the point at which the medium starts) to  $L$  reads [102]

$$\begin{aligned} \mathbf{E}_t(L, t) &= \frac{1}{2} \frac{2}{\underline{n}(\omega_\lambda) + 1} \mathcal{E}_{\omega_\lambda}(0) \exp(i\omega_\lambda \underline{n}(\omega_\lambda)L/c - \omega_\lambda t) + \text{c. c.} \\ &\simeq \frac{1}{2} \mathcal{E}_{\omega_\lambda}(0) \exp\left(-\frac{\omega_\lambda L}{2c} \underline{\chi}''(\omega_\lambda)\right) \exp\left(i\frac{\omega_\lambda L}{2c} [1 + \underline{\chi}'(\omega_\lambda)] - i\omega_\lambda t\right) + \text{c. c.} \end{aligned} \quad (2.19)$$

The index of refraction determines how the atoms affect the propagation of the electromagnetic wave through the gas. Its real part, and therefore the real part of the susceptibility, characterizes the phase velocity of the wave while propagates through the atomic medium. The frequency dependence of  $\underline{\chi}'$ , shown in figure 2.3, accounts then for dispersion. Figure 2.3 also shows that  $\underline{\chi}''$  is positive. Consequently, upon closer inspection of the expression for the transmitted electric field (2.19), we realize that the amplitude of the wave diminishes exponentially, a phenomenon known as *attenuated wave propagation*. The exponential factor accounts then for the transmission through the medium, which we define as the ratio of transmitted to incident averaged intensity of the wave, averaged over an optical period. The cycle averaged intensity of a plane electromagnetic wave (in vacuum) is given by  $\bar{I} = \varepsilon_0 \overline{\mathbf{E}^2} = \varepsilon_0 \mathcal{E}_{\omega_\lambda}^* \mathcal{E}_{\omega_\lambda} / 2$ . Thus, since  $\mathcal{E}_{\omega_\lambda} = \mathbf{E}_{\omega_\lambda} \exp(i\omega_\lambda \underline{n}(\omega_\lambda)z)$ , the transmission finally reads

$$T_{\omega_\lambda} = \left| \frac{\mathcal{E}_{\omega_\lambda}(L)}{\mathcal{E}_{\omega_\lambda}(0)} \right|^2 \simeq \exp\left(-\omega_\lambda L \underline{\chi}''(\omega_\lambda) / c\right). \quad (2.20)$$

## 2.3 Mechanical resonators

Put simply, a mechanical resonator is a solid undergoing bulk oscillatory motion. To describe the vibrations of a deformable solid one could in principle consider the motion of each atom comprising the underlying crystal lattice of the solid. However, a solution of the ensuing Schrödinger equation is an unfeasible task due to the huge number of degrees of freedom involved in the problem as well as the complexity of the interactions between the ions and electrons in the solid. A more convenient approach consists in obtaining the normal modes of vibration of the mechanical resonator and, subsequently, quantize these modes. The motion of every atom in the crystal lattice can then be expressed through linear superpositions of the normal modes of vibration. Moreover, for a dynamics in the elastic regime, the amplitude of each mode of vibration follows the motion of a harmonic oscillator. Thus, the oscillating motion of the solid formally corresponds to the dynamics of an infinite set of harmonic oscillators. For an elastic solid at a finite temperature the first key question arises. Can quantum mechanical effects have a real impact? The answer depends on how low the temperature  $T$  of its surroundings is or how much we may lower it with respect to the set of frequencies that characterize the mechanical resonator. If the lowest frequency of vibration of the resonator is comparable to the thermal energy  $k_B T$ , where  $k_B$  is the Boltzmann constant, then quantum motion adopts a relevant role. Although mechanical frequencies depend on both the geometry and the material of the solid itself, it is often the

case that smaller structures yield higher mechanical frequencies. As of today, the state of the art fabrication techniques of the material industry can realize a plethora of structures ranging widely in size, geometry and thus frequencies [26]. At usual dilution refrigeration temperatures ( $10 \text{ mK} \lesssim T \lesssim 50 \text{ mK}$ ), mechanical resonators into the nano- or micro-scales possess high enough frequencies so that short wavelength phonon modes become thermally unreachable, prevailing only the long wavelength modes (a type of collective degrees of freedom), [103, 104]. Due to the intrinsic nonlinear nature of wave propagation through a solid medium the short wavelength modes are kept in the description as a source of dissipation for the long wavelength modes. This procedure is analogous to the one adopted in the realm of superconducting quantum circuits. There, instead of using a microscopic theory of superconductivity one relies on an effective quantization of current and voltage (the collective degrees of freedom in this case). This procedure was first introduced by Leggett [25, 105, 106].

At this point we are left yet with another key question, how do we actually test that these mechanical resonators behave in a quantum manner? To do so we interface them with another quantum system over which we can perform measurements and control it coherently. Thus, we may combine a mechanical resonator with an optical or microwave cavity mode to realize a cavity optomechanical system, or with an electric circuit to form an electromechanical setup. The significant range of accessible frequencies that miniature mechanical resonators can embrace also allows them to couple to atoms, molecules and nitrogen vacancy centers in diamond to accomplish yet more complex hybrid systems. Why would we like to couple the resonator to another quantum system apart from wanting to discover its quantum nature? There exists multiple reasons: sensing of very weak forces, so weak that quantum mechanics needs to be taken into consideration; quantum transducers for converting optical signals into microwave signals coherently; fundamental test of quantum mechanics. In this latter respect, we may quote Feynman in his lectures on gravitation [107]: “*It is possible that quantum mechanics fails at large distances and for larger objects*”.

We will shortly review the effective quantization of a mechanical resonator in section 2.3.1. Next we introduce the effects of friction and thermal noise that allow to define a thermodynamic equilibrium of a mechanical resonator mode in 2.3.2, and subsequently discuss cooling and amplification of mechanical motion via viscous forces in 2.3.3.

#### 2.3.1 Quantum motion from the mechanics of miniature solids

We regard a mechanical resonator as a solid that moves and eventually returns to its original form after experiencing a geometrical distortion. Under the action of an external stress (a vectorial force exerted upon a unit of vectorial area), every point (a tiny part) of a deformable solid is moved from its original location  $\mathbf{r}$ . In the framework of continuum mechanics, we quantify this distortion by a displacement field  $\mathbf{v}(\mathbf{r})$ . Relative displacements among different points in the solid, that is in essence the gradient of  $\mathbf{v}(\mathbf{r})$ , are known as strains, which are also assumed to be continuous functions of  $\mathbf{r}$ . If strains in the solid respond linearly to the

action of a small stress we say that the solid is elastic. This proportionality relation between strain and stress is the legendary Hook's law. Therefore, in the elastic regime, the classical dynamics of a mechanical resonator, i.e., the equation of motion for a dynamical displacement  $\mathbf{v}(\mathbf{r}, t)$  is dictated by internal restoring forces reminiscent of the induced deformations. For small amplitude displacements, we may assume that stress waves propagating across the solid are valid solutions for the dynamics of  $\mathbf{v}(\mathbf{r}, t)$ . Note also that the wavelengths of these waves shall also be large in comparison with the separation between the atoms comprising the solid structure, otherwise the continuum mechanics picture does not hold valid. Then we may express any displacement as a superposition of monochromatic modes  $\mathbf{v}(\mathbf{r}, t) = \text{Re} [\sum_{\mathbf{q}} b_{\mathbf{q}}(t) \mathbf{v}_{\mathbf{q}}(\mathbf{r})]$ , wherein each mode  $\mathbf{q}$  is characterized by a shape function  $\mathbf{v}_{\mathbf{q}}(\mathbf{r})$  and a generalized coordinate  $b_{\mathbf{q}}(t) = B_{\mathbf{q}}(t) \exp(-i\omega_{\mathbf{q}}t)$  of complex amplitude  $B_{\mathbf{q}}(t)$  with  $\omega_{\mathbf{q}}$  representing the natural frequency of mode  $\mathbf{q}$ . The frequencies and the shape functions of each mode are determined from their propagation equation across the solid together with the pertinent boundary conditions, which are imposed by the geometry of the mechanical resonator. While every time dependent coordinate  $b_{\mathbf{q}}(t)$  can be regarded as the canonical variable of a harmonic oscillator. This description of stress induced motion can be applied to many cases of interest, such as e.g. an isotropic solid body, or mechanical structures for which their cross sectional area is very small compared to their length (a thin rod) and viceversa (a thin plate or drumhead resonator). In the later examples one may use dimensional reduction to effectively describe the dynamics of the mechanical system in a single spatial dimension [108]. Finally, we will consider that the frequency modes are sufficiently spaced among each other, such that we can constrain ourselves to the study of the dynamics of a single mechanical resonance  $\omega_m$  with displacement field  $\text{Re}[b_m(t)\mathbf{v}_m(\mathbf{r})]$ .

If there was not any loss of mechanical energy, the motion of the canonical coordinate  $z_m = [b_m^*(t) + b_m(t)]/2$  would obey the time evolution of a simple harmonic oscillator. However, elastic waves in a solid do not keep propagating across the medium forever; eventually they vanish due to the intrinsic nonlinear nature of wave propagation through the solid. Nonlinear terms, as well as impurities and defects in the solid material are responsible for the coupling between different modes, giving rise to the so called Akhiezer damping [104]. Likewise, mechanical waves may also be subject to energy dissipation due to clamping losses, i.e. energy radiated to the elements that support the mechanical structure; losses due to thermoelastic damping, that is, thermal relaxation due to gradients of temperature induced by strains in the solid, and more, see e.g. [41, 109] and references therein. In any case, as far as the motion of our mechanical vibration mode is concerned, each of these different intrinsic dissipation mechanisms can be thought of as arising from a weak interaction with a collection of many microscopic degrees of freedom that behave effectively as a heat bath equilibrated at some finite temperature. This introduces friction and noise in the dynamics of our mechanical vibration mode. Thus, we describe the time evolution of  $z_m$  through the

differential equation of a driven damped harmonic oscillator

$$\frac{d^2}{dt^2}z_m(t) + \Gamma_m \frac{d}{dt}z_m(t) + \omega_m^2 z_m(t) = \frac{1}{M}F(t), \quad (2.21)$$

In the equation (2.21) above,  $M$  stands for the effective mass of our mechanical system, the term proportional to the damping rate  $\Gamma_m > 0$  is a friction force characterizing the intrinsic energy losses of the mechanical system and  $F(t)$  represents all the other forces that may act upon it. In the absence of any externally applied drive,  $F(t)$  is a noisy or zero mean stochastic force that is responsible of bringing the resonator mode to a statistical equilibrium; in that case, equation (2.21) is known as a Langevin equation. Note that the value of the effective mass depends on the choice of the normalization of the shape function  $v_m(\mathbf{r})$ . For the case of a translational invariant thin plate or drumhead resonator undergoing linear oscillations we naturally choose  $z_m(t)$  as the center of mass oscillation amplitude, so that  $M$  coincides with the physical mass of the mechanical solid.

For a quantum description of the dynamics of our mechanical vibration mode, we replace the canonical variable  $z_m$  and its associated conjugate momentum  $p_m = iM\omega_m[b_m^* - b_m]/2$  by the corresponding position  $\hat{z}_m$  and momentum  $\hat{p}_m$  operators, satisfying the commutation relation  $[\hat{z}_m, \hat{p}_m] = i\hbar$ . Alternatively, we can also describe the quantum dynamics of our mechanical vibration mode in terms of the dimensionless ladder operator  $\hat{c}$  and its Hermitian adjoint  $\hat{c}^\dagger$ , which relate to  $\hat{z}_m$  and  $\hat{p}_m$  via the following transformation equations

$$\hat{z}_m = \sqrt{\frac{\hbar}{2M\omega_m}} [\hat{c}^\dagger + \hat{c}], \quad (2.22)$$

$$\hat{p}_m = i\sqrt{\frac{\hbar M\omega_m}{2}} [\hat{c}^\dagger - \hat{c}], \quad (2.23)$$

and therefore satisfy the commutation relation  $[\hat{c}, \hat{c}^\dagger] = 1$ . Using the definitions (2.22) and (2.23) the Hamiltonian for our mechanical vibration mode alone reads  $\hat{H}_m = \hat{p}_m^2/(2M) + M\omega_m^2 \hat{z}_m/2 = \hbar\omega_m[\hat{c}\hat{c}^\dagger + \hat{c}^\dagger\hat{c}]/2$ , with eigenenergies  $E_n = \hbar\omega_m[n + 1/2]$  and associated eigenvectors  $|n\rangle$  known as Fock or number states. They represent the number of mechanical quanta  $n$  that are present in our mechanical vibration mode. The classical evolution of our mechanical system is, however, ultimately not free but it is rather driven by noise and friction forces as described by the Langevin equation, see (2.21) above. These noise and friction forces are due to the weak coupling between our mechanical oscillator and its environment or bath. We then treat the environment as another quantum system and embody this coupling in the interaction potential  $\hat{H}_{m-b} = \hat{z}_m \hat{F}$ , where the operator  $\hat{F}$  is the reaction force of the environment assuming now the role of both, the dissipation and noise terms that take part in the classical Langevin equation, see (2.21) above. Since  $\hat{F}$  depends solely on the physical properties of the bath  $[\hat{F}, \hat{z}_m] = 0$ . The Hamiltonian for the combined system of our mechanical vibration mode and its thermal environment reads

$$\hat{H} = \hat{H}_m + \hat{H}_b + \hat{H}_{m-b}, \quad (2.24)$$

where  $\hat{H}_b$  stands for the Hamiltonian governing the dynamics of the bath alone.

A useful quantity to assess how close to the ground state  $|0\rangle$  our mechanical oscillator may be operating is the average energy of the oscillator. If we denote the probability that the oscillator has  $n$  quanta by  $p_n$  we define its average energy as  $\langle E \rangle = \sum_n E_n p_n = \hbar\omega_m(\langle n \rangle + 1/2)$  where  $\langle n \rangle = \sum_n n p_n$  is the so called mean occupation number of the mechanical oscillator. In the quantum ground state  $\langle n \rangle = 0$ . However, in this state the mechanical oscillator still presents a so called zero point motion characterized by its root mean square amplitude fluctuations  $z_{zpm} = \sqrt{\hbar/(2M\omega_m)}$  and its energy  $\hbar\omega_m/2$ . The quantity  $z_{zpm}$  is generally referred to as the standard quantum limit because it corresponds to the minimum length that we can aspire to resolve with a mechanical oscillator, i.e., the root mean square displacement induced by a force acting on a mechanical vibration mode may only be sensed if it exceeds  $z_{zpm}$ . Often, when the oscillator's bath is maintained at some temperature  $T$ , the mechanical oscillator settles into a thermal state at that same temperature, such that all of its properties are determined by the Bose-Einstein statistics. In that case the average energy of the mechanical oscillator reads  $\langle E \rangle = \bar{E} = \hbar\omega_m(\bar{n}_T + 1/2)$ , where

$$\bar{n}_T(\omega_m) = \frac{1}{\exp\left(\frac{\hbar\omega_m}{k_B T}\right) - 1} \quad (2.25)$$

is the so called Bose-Einstein or thermal occupation number. For the mechanical vibration mode to enter the quantum regime it is necessary that  $\bar{n}_T \lesssim 1$ , which reduces to the condition  $\hbar\omega_m > k_B T$ . This condition is very challenging because it demands temperatures that are usually well below the limit achieved so far by state of the art refrigeration techniques (at about 10 mK [27]). As of today, such condition can only be satisfied by mechanical resonances that lie within or above the GHz band. Therefore, for a given environmental temperature, devices with the highest possible mechanical resonances are more appealing if one wants to operate them in the quantum limit. Likewise, since the quantum uncertainty  $z_{zpm}$  scales inversely proportional to the mass of the mechanical oscillator, the lighter the mechanical device the easier it gets to probe the quantum fluctuations of one of its resonances. Fluctuations, either quantum (at  $T \approx 0$ ) or thermal (at  $T \neq 0$ ), set a lower bound for the ability of the oscillator to sense an applied force. Our next task is to learn what determines the strength of these fluctuations and, subsequently, to study how these can be minimized in order to reach the limiting sensitivity provided by the zero point motion of the mechanical oscillator. To that end we start analyzing how does the mechanical oscillator respond to an applied force, i.e., by solving the equation of motion for the displacement coordinate  $z_m$ .

### 2.3.2 Forced mechanical oscillations, friction and noise

The general solution of equation (2.21) for the displacement coordinate  $z_m$  of the vibrational mode consists of two contributions: a transient contribution and a steady-state contribution. The steady state contribution is the part of the solution that accounts for the response of the oscillator to the applied force, and thus it is the part that we are interested in. We consider

first the case of a harmonic forcing  $F(t) = F_0 \cos(\omega_0 t)$ . Then, in the limit  $\Gamma_m t \rightarrow \infty$ , the steady-state solution of  $z_m$  is [110]

$$z_m(t) = \frac{F_0}{M\omega_m^2} G(\omega_0) \cos(\omega_0 t + \delta\phi(\omega_0)), \quad (2.26)$$

where the gain  $G(\omega_0)$  and the phase  $\delta\phi(\omega_0)$  read

$$G(\omega_0) = \frac{\omega_m^2}{\sqrt{(\omega_m^2 - \omega_0^2)^2 + \Gamma_m^2 \omega_0^2}}, \quad \delta\phi(\omega_0) = \arctan \frac{\Gamma_m \omega_0}{\omega_0^2 - \omega_m^2}; \quad (2.27)$$

and they represent the quantities that determine the response of the oscillator relative to the applied force. As long as the oscillator damping is low,  $\Gamma_m < \omega_m$ , resonance occurs for a maximum oscillator amplitude, that is, at the peak of the gain. Hence, the frequency  $\omega_r = \omega_m \sqrt{1 - \Gamma_m^2/(2\omega_m^2)}$  for which the gain reaches its peak is called the *resonance frequency*. Since we are interested in resolving an oscillatory dynamics of the mechanical resonator mode we will focus on an under damped regime for which  $\Gamma_m \ll \omega_m$ , such that we may regard the eigenfrequency  $\omega_m$  as the *resonance frequency* of the mechanical resonator mode, i.e.,  $\omega_r \simeq \omega_m$ . Furthermore, in this well under damped regime we may suitably identify the ratio  $\omega_m/\Gamma_m$  with the so called *quality factor*  $Q$  of the oscillator, which can be defined as the ratio of energy stored in the resonator mode to the energy dissipated by the resonator mode during one cycle  $2\pi/\omega_r$  at resonance, or more explicitly [109]

$$Q = \frac{\omega_m \sqrt{1 - \Gamma_m^2/(2\omega_m^2)}}{\Gamma_m}. \quad (2.28)$$

For small damping equation (2.28) yields  $Q \simeq \omega_m/\Gamma_m$ , which is the definition that we shall adopt throughout this thesis.

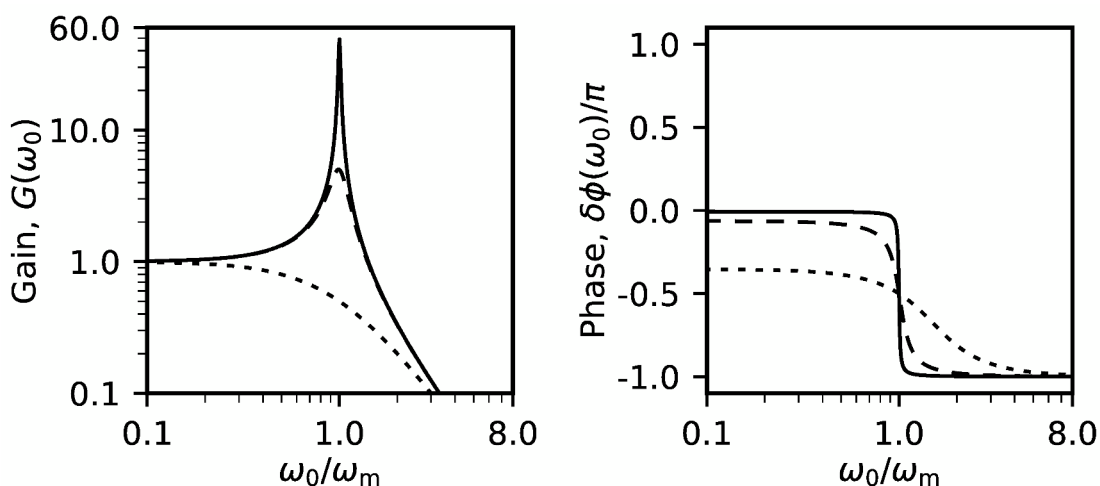


**Figure 2.4** (Left panel) amplitude response and phase response (right panel) of a driven damped harmonic oscillator in its steady state.

The left and right panels of figure 2.4 display, respectively, the gain  $G$  and the phase  $\delta\phi$  as a function of the ratio of the driving frequency to the eigenfrequency of the resonator mode

for different values of  $Q \geq 1$ . We observe that the larger the  $Q$  is, the sharper becomes the resonance. With  $Q$  fixed, for a driving frequency much lower than the resonance frequency, the oscillator follows the drive with almost no gain and no phase lag. As we tune the driving frequency close to the resonance, the gain increases while it emerges a phase lag between the relative motion of the oscillator and the force. On resonance, the gain is maximum and the oscillator is  $-\pi/2$  out of phase with the drive. Whereas for large driving frequencies compared with the eigenfrequency of the oscillator, the gain drops and the phase lag tends to  $-\pi$ . At this point the oscillator motion can no longer follow the drive.

Finally, it is worth mentioning that once the mechanical oscillator attains the steady dynamics described by equation (2.26), an energy balance is established: the transfer of energy from the driving force to the oscillator is compensated by the dissipation of energy due to friction, see [110]. The energy absorbed per driving cycle,  $2\pi/\omega_0$ , is proportional to the square of the gain, which in the limit of a high quality factor,  $Q \gg 1$ , and near resonance can be approximated by a Lorentzian profile, i.e.,  $G^2(\omega_0 \approx \omega_m) \simeq Q\mathcal{L}(\omega_0)/(4\omega_m)$ , where the Lorentzian (normalized to  $2\pi$ ) reads

$$\mathcal{L}(\omega_0) = \frac{\omega_m/Q}{(\omega_m - \omega_0)^2 + (\frac{\omega_m}{2Q})^2}. \quad (2.29)$$

Our next step is to analyze the dynamical consequences that follow when the drive is instead a stochastic force that accounts for the fluctuations of a heat bath or reservoir to which the mechanical resonator mode is coupled to.

### Thermal noise

We first model the heat bath as a fluctuating classical quantity. Later on, we shall regard it as a quantum reservoir that is weakly coupled to the mechanical vibration mode of interest.

If the force  $F$  is a stochastic process a solution of equation (2.21) is meant to be given in statistical terms. Thus, we may conceive an ensemble of identically prepared systems, each consisting of a mechanical oscillator and its surrounding thermal bath, so that the dynamics of every member of the ensemble is influenced by a different realization of the stochastic force  $F$ . We assume that  $F$  is a Gaussian random process (of zero mean), since it derives from a weak coupling of our mechanical vibration mode to an infinitely large collection of microscopic degrees of freedom, in which case the central limit theorem applies accurately. The noisy force  $F$  is then completely characterized by its autocorrelation function  $\mathcal{G}_{FF}(t, t') = \langle F(t)F^*(t') \rangle$ , where the symbol  $\langle \cdot \rangle$  denotes an ensemble average. Finally, since the bath is kept at a constant temperature  $T$ , we also assume that the autocorrelation function is stationary  $\mathcal{G}_{FF}(t, t') = \mathcal{G}_{FF}(\tau) = \langle F(\tau)F^*(0) \rangle$ , i.e., dependent only on the time difference  $\tau = |t - t'|$  between two arbitrary instants of time  $t$  and  $t'$ .

We start writing a formal solution for a given realization of  $F$ . For ease complexity, we operate with the generalized coordinate  $B_m = \exp(i\omega_m t)[z_m + ip_m/(M\omega_m)]$ , where  $p_m = M(dz_m/dt)$  is the conjugate momentum of  $z_m$ , and use the limit  $\Gamma_m \ll \omega_m$  (that is, a

high quality oscillator). In this manner, we may neglect fast rotating terms  $\propto \exp(\pm i2\omega_m t)$  and obtain the following evolution for  $B_m$ :

$$\frac{d}{dt}B_m(t) + \frac{\Gamma_m}{2}B_m(t) \simeq \frac{i}{M\omega_m}F(t) \exp(i\omega_m t). \quad (2.30)$$

After integrating equation (2.30), the solution of the canonical variable  $b_m(t) = B_m(t) \exp(-i\omega_m t)$  reads

$$b_m(t) \simeq b_m(0)e^{-i(\omega_m - i\Gamma_m/2)t} + \frac{i}{M\omega_m} \int_0^t dt' F(t') e^{-i(\omega_m - i\Gamma_m/2)(t-t')}. \quad (2.31)$$

We already saw that for the case of harmonic forcing (cf. equation (2.26)), the steady motion of the mechanical oscillator is directly proportional to the applied force, in other words: the oscillator is a linear system. For times  $\Gamma_m t \rightarrow \infty$ , equation (2.31) reflects that this holds for an arbitrary time dependence of the (linear) drive, and in particular for the stochastic force  $F$ . Likewise, once the mechanical oscillator settles into its steady-state, there exists a balance between the absorption and the dissipation of energy by the mechanical oscillator or, equivalently, a balance between noise and friction: noise allows the mechanical oscillator to absorb energy, whereas friction causes the mechanical oscillator to dissipate energy. The damping rate  $\Gamma_m$  characterizes the magnitude of friction, whereas the strength of noise is quantified by the power spectral density  $S_{FF}$  of the fluctuating force  $F$  which, by virtue of the Wiener-Khintchine theorem [111], may be determined as the Fourier transform of the (stationary) autocorrelation function  $\mathcal{G}_{FF}(\tau)$ ,

$$S_{FF}(\omega) = \int_{-\infty}^{+\infty} d\tau \exp(i\omega\tau) \mathcal{G}_{FF}(\tau) = \int_{-\infty}^{+\infty} d\tau \exp(i\omega\tau) \langle F(\tau)F^*(0) \rangle. \quad (2.32)$$

Clearly, formula (2.32) above shows that the spectral density  $S_{FF}$  is nothing else but the power distribution of the noisy force  $F$  as a function of frequency  $\omega$ , and therefore it is a quantity that one can measure.

Both, friction and noise, originate as a consequence of the weak coupling between our mechanical vibration mode and the heat bath. When this bath is in thermal equilibrium at temperature  $T$ , we may as well expect that the mechanical oscillator equilibrates at the same temperature after a sufficiently long time. Consequently, the balance between noise and friction arising in the steady dynamics of the oscillator shall be in accordance with this presumed thermal equilibrium state at temperature  $T$ . Following references [112, 113, 114], we put this reasoning into quantitative terms by looking at the evolution of the average energy  $\langle E \rangle = M\omega_m^2 [\langle B_m B_m^* \rangle + \langle B_m^* B_m \rangle] / 4$  of the mechanical oscillator. This evolution is obtained from the summation of the differential equation (2.30) multiplied by  $M\omega_m^2 B_m^* / 4$  and added to its complex conjugate counterpart, with the complex conjugate equation, and then averaging on both sides of this final equation. The result reads

$$\frac{d}{dt} \langle E(t) \rangle = -\Gamma_m \langle E(t) \rangle + i \frac{\omega_m}{4} [\langle F(t) b_m^*(t) \rangle - \langle b_m(t) F^*(t) \rangle] + \text{c. c.}, \quad (2.33)$$

where c. c. stands for complex conjugate. In the stationary regime,  $\Gamma_m t \rightarrow \infty$  and  $d \langle E \rangle / dt = 0$ , we can write the term within brackets in the right hand side (rhs) of equation (2.33) in a



more meaningful form. First, we use the definitions of  $\mathcal{S}_{FF}$  and  $b_m$ , equations (2.32) and (2.31) respectively, to find that  $i[\langle Fb_m^* \rangle - \langle b_m F^* \rangle] = \int_{-\infty}^{+\infty} d\omega / (2\pi) \mathcal{L}(\omega) \mathcal{S}_{FF}(\omega)$ . Next, since the region for which  $\mathcal{L}(\omega)$  is sharply peaked happens to be very narrow around  $\omega = \omega_m$ , if  $\mathcal{S}_{FF}(\omega = \omega_m)$  is finite, we may treat  $\mathcal{S}_{FF}$  as constant and equal to  $\mathcal{S}_{FF}(\omega = \omega_m)$  in the integral <sup>5</sup>. Then, using  $\int d\omega / (2\pi) \mathcal{L}(\omega) = 1$  and introducing the symmetrical spectral density  $\tilde{\mathcal{S}}_{FF}(\omega) = [\mathcal{S}_{FF}(\omega) + \mathcal{S}_{FF}^*(\omega)]/2$ , we obtain

$$\frac{d}{dt} \langle E(t) \rangle = -\Gamma_m \langle E(t) \rangle + \frac{1}{2M} \tilde{\mathcal{S}}_{FF}(\omega_m) = 0. \quad (2.34)$$

A thermal equilibrium state for the mechanical oscillator may arise in the stationary regime. Classically, this manifests in the energy equipartition principle,  $\langle E \rangle = k_B T$ , and thus equation (2.34) yields the classical fluctuation-dissipation formula  $\tilde{\mathcal{S}}_{FF}(\omega_m) = 2M\Gamma_m k_B T$  [115, 116], which expresses the balance between noise and friction that we had already anticipated. In accordance with the derivation that we have followed, this classical fluctuation-dissipation formula is valid for bath temperatures such that  $k_B T > \hbar\omega_m$ . Note also the fact that, since we have modeled friction with a frequency independent rate  $\Gamma_m$ , i.e. with ohmic dissipation [117], the above fluctuation-dissipation formula implicitly implies a frequency independent (white-noise) spectrum  $\mathcal{S}_{FF}$ , and hence  $\Gamma_m \tau_c \rightarrow 0$ , where  $\tau_c > 0$  is a so called correlation or relaxation time that characterizes the decay of the noise correlations, i.e.,  $\mathcal{G}_{FF}(\tau > \tau_c) \rightarrow 0$ , see [108]. In general, however, the time scale for which we may speak of a damping rate  $\Gamma_m$  depends on the profile of the power spectral density of the noisy force. Only if the evolution of concern occurs in time steps  $t \gg \tau_c$ , and logically  $\Gamma_m^{-1} \gg \tau_c$ , we may consider valid this so called Markov approximation, in which the memory of the fluctuations are neglected and the power spectral density  $\mathcal{S}_{FF}(\omega)$  of the noise is thus expected to be smooth and nearly constant [118]. As a final remark, we note that  $F$  is a classical, real valued variable, such that  $F^* = F$  and the product  $F(t)F(t') = F(t')F(t)$  is commutative. This implies that  $\mathcal{G}_{FF}(\tau)$  is a real and even function of  $\tau$ , and thus  $\mathcal{S}_{FF}^*(\omega) = \mathcal{S}_{FF}(-\omega) = \mathcal{S}_{FF}(\omega)$ . The power spectral density of a classical dynamical variable is always an even function of the frequency  $\omega$ . Returning to equation (2.34), we can then conclude that the thermal agitation of our mechanical vibration mode is driven by a symmetrical power spectrum  $\tilde{\mathcal{S}}_{FF} = \mathcal{S}_{FF}$ .

### Quantum noise

In the quantum case, we replace every dynamical variable by its corresponding Heisenberg operator. Subsequently, we notice that quantum spectral densities may be asymmetric in frequency since the product of a quantum observable evaluated at different times is generally not commutative. As we shall see momentarily, when evaluated at positive frequencies the

---

<sup>5</sup> If  $\mathcal{S}_{FF}(\omega = \omega_m)$  were not finite we could average its limiting values as  $\omega$  approaches  $\omega_m$  from higher and lower frequencies.

quantum noise spectral density

$$S_{FF}(\omega) = \int_{-\infty}^{+\infty} d\tau \exp(i\omega\tau) \langle \hat{F}(\tau) \hat{F}^\dagger(0) \rangle \quad (2.35)$$

of the noisy observable  $\hat{F}$  (fulfilling  $\hat{F}^\dagger = \hat{F}$ ) symbolizes a transfer of energy to the heat bath, whereas at negative frequencies it symbolizes an extraction of energy from the heat bath. The starting point to unveil these physical effects embodied in the power spectral density  $S_{FF}$  is the Hamiltonian of equation (2.24) that governs the coupled dynamics of the mechanical oscillator and the heat bath. The interaction term  $\hat{H}_{m-b} = \hat{z}_m \hat{F}$ , couples different energy levels of the mechanical oscillator, and hence induces transitions between them. Since the coupling is weak, we may restrict ourselves only to transitions among contiguous levels. Thus, for a given unperturbed energy eigenstate  $|n\rangle$  of the mechanical oscillator, where  $n$  is the number of energy quanta, the transition rates to its neighboring levels can be found using first order perturbation theory. These rates are then determined from Fermi's golden rule. We express them as  $\Gamma_{n \rightarrow n+1} = (n+1)\Gamma_+$  and  $\Gamma_{n \rightarrow n-1} = n\Gamma_-$ , where the upward and downward transition rates relate to the force power spectral density as [114]

$$\Gamma_{\pm} = \frac{z_{zpm}^2}{\hbar^2} S_{FF}(\mp\omega_m). \quad (2.36)$$

From (2.36) we clearly appreciate that  $S_{FF}(-\omega_m)$  quantifies rates of transitions  $|n\rangle \rightarrow |n+1\rangle$  in which the bath transfers an energy quantum  $\hbar\omega_m$  to the oscillator, whereas  $S_{FF}(\omega_m)$  quantifies rates of transitions  $|n\rangle \rightarrow |n-1\rangle$  in which the bath extracts an energy quantum  $\hbar\omega_m$  from the oscillator. With the transition rates  $\Gamma_{n \rightarrow n\pm 1}$  at hand, the probability  $p_n$  that the oscillator has  $n \geq 0$  quanta is found to obey the following rate equation [114]

$$\frac{d}{dt} p_n(t) = \Gamma_{n-1 \rightarrow n} p_{n-1}(t) + \Gamma_{n+1 \rightarrow n} p_{n+1}(t) - [\Gamma_{n \rightarrow n-1} + \Gamma_{n \rightarrow n+1}] p_n(t). \quad (2.37)$$

Thence, we can work out the equation of motion for the average mechanical energy  $\langle E \rangle = \sum_n \hbar\omega_m (n + 1/2) p_n$  of the quantum oscillator,

$$\frac{d}{dt} \langle E(t) \rangle = -\Gamma(\omega_m) \langle E(t) \rangle + \frac{1}{2M} \tilde{S}_{FF}(\omega_m), \quad (2.38)$$

which has exactly the same form as its classical version in equation (2.34), and consequently it is valid only for  $\Gamma \ll \omega_m$  (i.e., a high quality oscillator)<sup>6</sup>. The energy relaxation rate  $\Gamma$  is now wholly specified in terms of the power spectrum of the noise

$$\Gamma(\omega_m) = \Gamma_- - \Gamma_+ = z_{zpm}^2 [S_{FF}(\omega_m) - S_{FF}(-\omega_m)] / \hbar^2. \quad (2.39)$$

Equation (2.39) shows that dissipation of mechanical energy stems from an imbalance in energy absorption and emission processes between the bath and the oscillator, thus

---

<sup>6</sup> The coupling of the oscillator to the bath also induces a Lamb type frequency shift. However, often this shift is unnoticeable, specially if the quality factor of the oscillator is high,  $Q \gg 1$ .

suggesting a quantum foundation for the inclusion of the classical friction force in equation (2.21). At the same time, the frequency symmetric part of the noise spectral density,  $\tilde{S}_{FF}(\omega_m) = [S_{FF}(\omega_m) + S_{FF}(-\omega_m)]/2$ , is, in analogy with the classical case, the source responsible of heating up the mechanical oscillator. Once more, the noise to dissipation ratio  $\tilde{S}_{FF}(\omega_m)/\Gamma$  determines the steady state average energy  $\langle E(t \rightarrow \infty) \rangle$  of the oscillator (the solution of equation (2.38) with  $d\langle E \rangle/dt = 0$ ), such that  $\langle E(t \rightarrow \infty) \rangle = \tilde{S}_{FF}(\omega_m)/\Gamma$ . Remarkably, this ratio shall hold finite even in the limit of a zero temperature heat bath, since at zero temperature  $\langle E(t \rightarrow \infty) \rangle = \hbar\omega_m/2$ . This is a consequence of the quantum version of the fluctuation-dissipation theorem, which is applicable whenever the noise source or bath is in thermal equilibrium. In that case we presume that the mechanical oscillator is in statistical equilibrium with the heat bath, such that  $\langle E(t \rightarrow \infty) \rangle = \bar{E} = \hbar\omega_m(\bar{n}_T + 1/2)$  with  $\bar{n}_T$  the mean thermal occupation number defined in (2.25). This results in the celebrated fluctuation-dissipation formula of Callen and Welton [119]

$$\tilde{S}_{FF}(\omega_m) = 2M\Gamma(\omega_m)\hbar\omega_m(\bar{n}_T(\omega_m) + 1/2). \quad (2.40)$$

So far we have presumed a thermal state for the mechanical oscillator, however, we can corroborate that a thermally equilibrated mechanical oscillator follows directly from the equilibrium condition of the noise source. If the noise source is a quantum reservoir in thermal equilibrium, its state is described by the density operator  $\hat{\rho}_b = \exp(-\hat{H}_b/[k_B T]) / \text{tr}[\exp(-\hat{H}_b/[k_B T])]$ , where  $\hat{H}_b$  is the bath Hamiltonian introduced in equation (2.24) and the symbol  $\text{tr}$  denotes the trace operation<sup>7</sup>. Then, besides fulfilling the stationary property  $\langle \hat{F}(\tau)\hat{F}(0) \rangle = \langle \hat{F}(0)\hat{F}(-\tau) \rangle$ , the correlation function also satisfies<sup>8</sup>  $\langle \hat{F}(\tau)\hat{F}(0) \rangle = \langle \hat{F}(0)\hat{F}(\tau + i\hbar/[k_B T]) \rangle$ , the so called Kubo-Martin-Schwinger (KMS) condition [120, 121]. From the definition (2.35), this KMS condition translates into the following identity for the quantum noise spectral density evaluated at positive and negative frequencies

$$\frac{S_{FF}(-\omega)}{S_{FF}(+\omega)} = \exp\left(-\frac{\hbar\omega}{k_B T}\right). \quad (2.41)$$

We observe that knowing  $S_{FF}$  allows us to find the equilibrium temperature of the bath through equation (2.41) above. More importantly, the relation (2.41) further implies a detailed balance between absorption and emission processes, so that  $\Gamma_+ = \exp(-\hbar\omega_m/[k_B T])\Gamma_-$  or, equivalently,

$$\Gamma_{n \rightarrow n+1} \exp\left(-\frac{\hbar\omega_m n}{k_B T}\right) = \Gamma_{n+1 \rightarrow n} \exp\left(-\frac{\hbar\omega_m(n+1)}{k_B T}\right). \quad (2.42)$$

---

<sup>7</sup> In principle, the coupling of the bath to our mechanical vibration mode could prevent an equilibrium state of the bath, however we keep consistent with our perturbation theory approach and assume that since the bath comprises infinitely many degrees of freedom, this coupling may only have a negligible impact on it, and therefore that its equilibrium condition remains unaltered.

<sup>8</sup> These properties of the force noise autocorrelation function follow from the definition of the freely evolving operator  $\hat{F}(\tau) = \exp(-i\hat{H}_b\tau/\hbar)\hat{F}(0)\exp(i\hat{H}_b\tau/\hbar)$ , and noticing that an ensemble average is now understood as an expectation value  $\langle \cdot \rangle \equiv \text{tr}[\hat{\rho}_b \cdot]$ .

The detailed balance condition (2.42) guarantees that the steady state probabilities  $p_n(t \rightarrow \infty)$  stemming from setting  $dp_n/dt = 0$  in equation (2.37), follow a Boltzmann distribution, i.e.  $p_n(t \rightarrow \infty) \propto \exp(-\hbar\omega_m/[k_B T])$ . Therefore, we can conclude that the mere contact with a thermal equilibrium bath leads to a subsequent thermalization of our mechanical vibration mode too. If the bath were in a stationary state but not in thermal equilibrium (e.g., because it is continually driven by an external force) we could still define a relation identical to the KMS condition, equation (2.41), with  $T$  replaced by an effective (frequency-dependent) temperature  $T_{\text{eff}}(\omega)$  [112, 113].

### 2.3.3 Cooling and amplification of mechanical harmonic motion with a viscous force

Two conclusive points of the previous section 2.3.2 are that a mechanical oscillator reacts linearly against an applied force and that friction and noise go hand in hand. Thus, neither a linear forcing of the oscillator dynamics nor an increase of the damping rate  $\Gamma_m$  can serve to lower the oscillator temperature or, equivalently, to push down to zero the thermal occupation number of the mechanical oscillator. In the absence of any other external agents to the mechanical oscillator and its associated noisy environment with reaction force  $\hat{F}_m$ , it seems that the only way to achieve ground state cooling of the mechanical oscillator motion is to directly lower the equilibrium temperature  $T_m$  of its surrounding heat bath. However, for a great majority of mechanical structures, even the lowest dilution refrigerator temperatures ( $T_m \sim 10$  mK) do not suffice to operate the mechanical vibration mode of interest in the quantum regime, that is, achieving  $\hbar\omega_m > k_B T_m$ , where, as in previous sections,  $\omega_m$  denotes the mechanical resonance frequency. On the other hand, mechanical resonances in the order of GHz or above, for which  $\hbar\omega_m > k_B T_m$  is actually fulfilled, face yet another problem: the higher the frequency of the mode the smaller becomes its root mean square fluctuations  $z_{zpm}$ . Detecting the motion of such a high frequency oscillator at an environmental temperature of a few mK results then very challenging [27]. In order to cool a mechanical vibration mode down to its quantum ground state of motion (and be able to operate with it) we may rather start off in a scenario for which  $\hbar\omega_m > k_B T_m$ , and subsequently use an additional method to reduce the thermal occupation number of the mechanical mode below unity. This cooling method can be performed with the intervention of a nonlinear drive (i.e. a force that may depend on the position and momentum of the vibration mode) in the dynamics of the mechanical vibration mode. A nonlinear coupling to an additional external physical system may introduce into the dynamics of the mechanical oscillator a velocity dependent or viscous like force characterized by some damping rate  $\Gamma_v$ , as well as an associated noisy force  $\hat{F}_v$  that will tend to equilibrate the oscillator towards an effective temperature  $T_v$ . As long as the coupling of the oscillator to the external noise source is weak, we then can use the approach based on perturbation theory of the previous section to determine the damping rate  $\Gamma_v$  in terms of the spectral density  $S_{F_v F_v}$  of the noisy force.

For all practical purposes, the mechanical oscillator is now as if it were in contact with

two different heat baths. If the effective temperature  $T_v$  of the additional bath is much lower than the temperature  $T_m$  of the original environment of the mechanical oscillator and if  $\Gamma_v > \Gamma_m$ , the noise from the additional bath will ultimately set the minimum achievable thermal occupation number for the mechanical oscillator. Since the power spectral density  $S_{\sum_\mu F_\mu F_\mu}$  of uncorrelated observables  $\hat{F}_\mu$  is additive,  $S_{\sum_\mu F_\mu F_\mu} = \sum_\mu S_{F_\mu F_\mu}$ , the equation of motion for the average energy of this mechanical vibration mode coupled to two independent baths reads

$$\frac{d}{dt} \langle E(t) \rangle = - \sum_\mu \Gamma_\mu \langle E(t) \rangle + \frac{1}{2M} \sum_\mu \tilde{S}_{F_\mu F_\mu}(\omega_m), \quad (2.43)$$

where  $\tilde{S}_{F_\mu F_\mu}(\omega_m) = [S_{F_\mu F_\mu}(\omega) + S_{F_\mu F_\mu}(-\omega)]/2$ ,  $\mu \in \{m, v\}$ , and we have assumed that the mechanical mode also starts off with a high quality factor, thus ignoring any frequency shift that may have possibly been induced by its coupling to the additional noise source. In the steady state  $\langle E(t \rightarrow \infty) \rangle = \hbar\omega_m(\bar{n} + 1/2)$ . Then, using the fluctuation-dissipation formula (2.40) for the equilibrium heat bath at temperature  $T_m$  and the KMS condition (2.41) for the external noise source at the effective temperature  $T_v$  we find the following expression for the mean stationary phonon number  $\bar{n}$ ,

$$\bar{n} = \frac{\Gamma_m \bar{n}_{T_m}(\omega_m) + \Gamma_v \bar{n}_v(\omega_m)}{\Gamma_v + \Gamma_m}, \quad (2.44)$$

where we have introduced

$$\bar{n}_v(\omega) \equiv \left[ \frac{S_{F_v F_v}(\omega)}{S_{F_v F_v}(-\omega)} - 1 \right]^{-1}, \quad (2.45)$$

the effective occupation number that results from the coupling of the oscillator to the external effective bath. For a *cold* external bath with minimal quantum fluctuations, i.e. with  $\bar{n}_v \simeq 0$ , the mean occupation number or temperature  $T \equiv \hbar\omega_m \bar{n} / k_B$  of the oscillator is essentially determined by the thermal fluctuations of its environment, such that the equation (2.44) above reduces to

$$T = T_m \frac{\Gamma_m}{\Gamma_m + \Gamma_v}. \quad (2.46)$$

According to this expression the higher the induced damping rate  $\Gamma_v$  is, the lower it gets the oscillator temperature  $T$ . As we approach down to  $T = 0$ , the formula (2.46) starts failing to provide a satisfactory physical description. Eventually, the quantum fluctuations of the external noise source shall manifest in a finite occupation number  $\bar{n}_v > 0$ , thus inhibiting the possibility of reaching  $T = 0$ . In essence,  $\bar{n}_v$  sets the lowest temperature that the oscillator may accomplish. Still, equation (2.46) can be used to gain insight on the capability of the oscillator to attain its ground state of motion. In the limit  $\Gamma_v \gg \Gamma_m$ , and using  $\omega_m > \Gamma_v$ , we obtain  $k_B T / (\hbar\omega_m) \simeq k_B T_m \Gamma_m / (\hbar\omega_m \Gamma_v) \gtrsim k_B T_m / (\hbar\omega_m Q)$ . Ground state cooling of the mechanical vibration mode can be within reach if  $k_B T / (\hbar\omega_m) \sim 1$ . This finally leads to the following relation

$$Q f_m \gtrsim \frac{k_B T_m}{h}, \quad (2.47)$$

where  $f_m = \omega_m/(2\pi)$ . The product (2.47) above is an indicator of how robust the mechanical oscillator may be against thermally induced decoherence [122, 41].

Before we move on to the next section let us remark that we may distinguish different types of cooling techniques depending on the manner in which we realize the nonlinear drive that allows for cooling the motion of the mechanical oscillator, see references [27, 122] for a more detailed discussion. Based on a monitoring of the motion of the displacement coordinate  $z_m$  of the mechanical oscillator we can tailor a friction force that is out of phase with this motion, i.e., proportional to the instantaneous velocity of the oscillator. To damp the amplitude of the mechanical oscillations we feed this force to the dynamics of  $z_m$ . Since the feedback is constructed from a measurement record this cooling technique is commonly known as *active* cooling. Conversely, if we design a mechanical oscillator dynamics in which a viscous force emerges naturally, e.g. from the coupling of the oscillator to a second system, and if we perform no measurement on the oscillator dynamics the cooling mechanism is then called *passive* cooling. This cooling mechanism is the one that we have just presented in this section and the one that we shall focus next in the context of optomechanics, wherein the motion of a mechanical oscillator couples to light waves via the radiation pressure force.

#### 2.3.4 An example: radiation pressure force and optomechanics

First of all, let us note that thermal radiation with frequencies from and above the visible range are considerably higher than frequencies of conventional mechanical resonances. Then according to the discussion of our previous section 2.3.3, the radiation field could in principle act as an excellent *cold* bath for the motion of a mechanical vibration mode.

In the late nineteenth century, Maxwell's theory of classical electromagnetism could definitely confirm the idea that matter objects can undergo a pressure force when they are exposed to radiation<sup>9</sup>. This so called radiation pressure force is the result of a delivery of linear momentum by the radiation field upon reflection from the target object. Remarkably, it was Einstein who showed, in a thought experiment proposed in [124], that also this force may fluctuate, and therefore induce friction in the motion of a radiated object. This frictional phenomenon can be elucidated with the help of the Doppler effect. The radiation pressure  $P_{rp}$  imparted by a light wave normally incident from vacuum onto a stationary matter object, let us say a perfectly reflecting mirror of mass  $M$ , may be written in terms of the light intensity  $\bar{I}$  (averaged in time over a cycle of the wave) as  $P_{rp} = 2\bar{I}/c$ . For a wave with cross sectional area  $\mathcal{A}$ , the corresponding force exerted on the mirror is thus  $F_{rp} = 2\overline{\mathcal{W}}/c$ , with  $\overline{\mathcal{W}} = \bar{I}\mathcal{A}$  the cycle averaged power of the light wave. Now, if the mirror is moving away from and in the propagation direction of the light with uniform speed  $v_m$ ,

---

<sup>9</sup> The contemplation of mechanical effects of light on matter objects may be traced back to J. Kepler who, in his astronomical observations in the seventeenth century, realized that comet tails always opposed the sun. Kepler then argued that this effect could be due to an impulse imparted to the comet by solar rays [123, 114].

the intensity of the, again normally incident light, will be reduced due to the Doppler effect. In the non-relativistic limit  $v_m/c \ll 1$ , and the ensuing Doppler shift for the light intensity is  $\bar{I} \mapsto \bar{I}[1 - v_m/c]$ . As a result, Newton's equation for the mirror,  $dv_m/dt = F_{rp}/M$ , yields a diffusive dynamics with a corresponding diffusion rate<sup>10</sup>  $\gamma = 2\bar{W}/[Mc^2]$ . Unfortunately, for the movable mirrors (mechanical resonators) used in most tabletop experiments, this effect is in practice unnoticeable. Even for the lightest mechanical resonators, the radiative power necessary to observe such a frictional effect is too high in order for the mechanical resonator to be able to support it before it gets destroyed. Using mechanical resonators coated with some unconventional material, such as e. g. a photonic crystal, could be an exception, see [125].

Nowadays, a common procedure to appreciably influence the motion of a mechanical resonator via radiation pressure consists in using a cavity, inside which the radiation field is parametrically coupled to the motion of the mechanical resonator. In a laser driven optical cavity, photons (light particles) may bounce off the cavity walls many times before they abandon it, leading to an enhancement of the radiation field in the interior of the cavity. If the mechanical element is placed either inside the cavity or forming part of one of the cavity walls, the radiation pressure as well as the Doppler scattering process described earlier, will have a much larger impact than in the case of a freely moving mirror. This idea was suggested already back in the 1960s by Braginsky and collaborators in [20, 21], which led to the development of the research field of cavity optomechanics [41]. In order to gain a deeper insight on how the confinement of the radiation field in the cavity may empower the frictional radiative force onto the mechanical element, we shall study the coupled dynamics of both the cavity radiation field and the movable mirror, here assumed to be harmonically bound to one of the end walls of the cavity. To learn the operating method of such frictional force and how we can possibly take advantage of it to cool down the motion of the mechanical resonator we will start with an analysis based on classical physics. After this, we will switch to a quantum framework, in which we will illustrate the utility of the machinery of perturbation theory presented in the previous section 2.3.3.

Let us first consider an optical cavity with fixed walls. In principle a cavity hosts infinitely many modes, the frequencies of which depend on the geometry and the dielectric properties of the device. Additionally, since in a real cavity photons may leak out of it, every mode has a finite life time, or equivalently a finite linewidth. To simplify matters we assume here that the frequency  $\omega_L$  of the driving laser is nearly resonant with the frequency  $\omega_{cav}$  of a single cavity mode, such that  $|\omega_L - \omega_{cav}| \lesssim \kappa$ , where  $\kappa > 0$  is the linewidth of such cavity mode. Thus, as long as there exists an appreciable overlap between the shape function  $\mathbf{u}_{cav}$  of this cavity mode with frequency  $\omega_{cav}$  and that of the laser, the dynamics of the cavity radiation field will be essentially given by that of this single resonantly driven mode with frequency

---

<sup>10</sup> Note that the sign for the rate  $\gamma$  adopted here is a mere convention. A mirror that moves towards the light source would lead to a rate with opposite sign.

$\omega_{\text{cav}}$ , such that no other mode of the cavity will be excited [126]. We then focus here on a single transverse mode, let us say the one with lowest frequency, and restrict ourselves to a one-dimensional analysis, which is a good approximation if the cross sectional area  $\mathcal{A}_{\omega_{\text{cav}}}$  of the cavity mode is considerably larger than its wavelength. We dispose our reference frame such that its  $z$ -axis coincides with the propagation direction of the optical waves. We denote the natural length of the cavity along this axis by  $L_{\text{cav}}$  and write the electric field inside the cavity as  $\mathbf{E}_{\text{cav}}(t) = \sqrt{\hbar\omega_{\text{cav}}/(\epsilon_0 L_{\text{cav}} \mathcal{A}_{\omega_{\text{cav}}})} \text{Re} [a(t) \exp(-i\omega_{\text{L}}t) \mathbf{u}_{\text{cav}}]$ . The complex function  $a(t)$  denotes the normal variable of the cavity mode, and we have normalized it here such that  $|a(t)|^2$  may be viewed as the number of photons that are circulating within the cavity. In the absence of losses and of the laser source, Maxwell's equations show that  $a(t)$  represents the evolution of a free harmonic oscillator  $\sim \exp(-i\omega_{\text{cav}}t)$  [127]. Due to the laser driving and the leakage of photons out of the cavity, the evolution of the slowly varying normal variable  $a(t) \exp(-i\omega_{\text{L}}t)$  may be described by that of a driven damped harmonic oscillator [128, 112]

$$\frac{d}{dt}a(t) = [i(\omega_{\text{L}} - \omega_{\text{cav}}) - \kappa/2]a(t) + \frac{\kappa}{2}a_{\omega_{\text{L}}}. \quad (2.48)$$

Here, the complex constant  $a_{\omega_{\text{L}}}$  accounts for the strength of the normal coordinate of the laser<sup>11</sup>. Following reference [9], we choose  $a_{\omega_{\text{L}}}$  such that on full resonance,  $\omega_{\text{L}} = \omega_{\text{cav}}$ , is  $a = a_{\omega_{\text{L}}}$ . In this manner, we may estimate the power (averaged over one cycle of the wave) of the laser entering the cavity as  $\overline{\mathcal{W}}_{\text{in}} \sim \hbar\omega_{\text{L}}\kappa|a_{\omega_{\text{L}}}|^2 = \kappa\mathcal{W}_{0\omega_{\text{L}}}$ , where  $\mathcal{W}_{0\omega_{\text{L}}}$  is the original laser power.

Let us now go over to the case in which one of the cavity walls, a mirror, is allowed to undergo mechanical motion. The motion of such mirror translates into a time dependent boundary for the radiation field which unavoidably yields a coupling between the different modes of the cavity radiation field. However, as long as the mirror motion is non-relativistic and its characteristic frequencies are much smaller than the free spectral range of the cavity (that is, the frequency separation between adjacent cavity modes) the dynamics of the cavity radiation field may again be accurately described in terms of a single mode [129, 130]. We assume that this is the case here for our harmonically bound mirror, thus requiring  $dz_{\text{m}}/dt \ll c$  and  $\omega_{\text{m}} \ll \tilde{\omega}_{\text{cav}}(z_{\text{m}})$ , where, being true to our usual notation, we have chosen  $z_{\text{m}}$  and  $\omega_{\text{m}}$  to denote the displacement and resonance frequency of the mirror, respectively. The coupling of the radiation field to the motion of the mirror is captured in the frequency  $\tilde{\omega}_{\text{cav}}(z_{\text{m}})$  as well as in the normal variable  $\tilde{a}(z_{\text{m}})$  of the cavity mode, which are parametric functions of the mirror displacement [129]. A change in the mirror position induces a shift in the frequency  $\tilde{\omega}_{\text{cav}}(z_{\text{m}})$  of the cavity. At the same time, a shift in  $\tilde{\omega}_{\text{cav}}(z_{\text{m}})$  modifies the light power inside the optical resonator  $\sim |\tilde{a}(z_{\text{m}})|^2$ , and therefore the radiation pressure

---

<sup>11</sup> As we have pointed out at the beginning of this section 2.3.4, optical radiation can be regarded as a very cold bath for the motion of the resonator. Thus, we have ignored any thermal fluctuations of the cavity field and assumed a vanishing Langevin force in equation (2.48).



delivered to the moving mirror. This phenomenon in which the mirror motion is allowed to influence onto itself is known as dynamical back-action [41]. To address this process more quantitatively we use the fact that  $|z_m| \ll L_{\text{cav}}$ , and expand the canonical amplitude and frequency of the cavity up to first order in  $z_m/L_{\text{cav}}$ . Then, after averaging over an optical period  $2\pi/\omega_L$  to get rid of fast oscillating terms  $\propto \exp(\pm 2i\omega_L t)$ , we obtain the following classical equations of motion describing the coupled dynamics of the radiation field and the moving mirror [9]

$$\frac{d}{dt}a(t) = [i(\omega_L - \omega_{\text{cav}} + g_0 z_m(t)) - \kappa/2]a(t) + \frac{\kappa}{2}a_{\omega_L}, \quad (2.49)$$

$$\frac{d^2}{dt^2}z_m(t) + \Gamma_m \frac{d}{dt}z_m(t) + \omega_m^2 z_m(t) = \frac{\hbar g_0}{M}|a(t)|^2 + \frac{1}{M}F(t). \quad (2.50)$$

In writing equations (2.49) and (2.50) we have used the identities  $\tilde{a}(z_m = 0) = a$  and  $\tilde{\omega}_{\text{cav}}(z_m = 0) = \omega_{\text{cav}}$  and introduced the so called optomechanical frequency shift per mechanical displacement  $g_0 = -\partial\tilde{\omega}_{\text{cav}}(z_m)/\partial z_m|_{z_m=0}$ . The quantity  $\hbar g_0|a(t)|^2$  in the r.h.s. of equation (2.50) corresponds to the radiation pressure force impinging on the movable mirror<sup>12</sup>, whereas  $F$  is as defined in equation (2.21), i. e., it represents any other possible external driving of the mirror motion, including thermal fluctuations. The dynamics described by (2.49) and (2.50) is nonlinear and may give rise to an ample variety of physical phenomena: multistability [131], self-induced oscillations [132], chaos [41].

For a quantitative understanding of the Doppler shift induced on the light intensity of the optical resonator by the moving mirror and the ensuing back action effects onto the mirror motion it is enough an analysis based on a simple harmonic motion of the mirror. Solving equation (2.49) for the steady state with  $z_m = Z_0 \cos(\omega_m t)$  yields [133, 134]

$$a(t) = a_{\omega_L} \kappa/2 \sum_{l=-\infty}^{+\infty} \frac{J_l(x)}{-i(\Delta_L + l\omega_m) + \kappa/2} \exp(-il\omega_m t + ix \sin(\omega_m t)), \quad (2.51)$$

where  $\Delta_L = \omega_L - \omega_{\text{cav}}$  is the laser detuning and  $x = g_0 Z_0/\omega_m$ , while  $J_l$  stands for a Bessel function of the first kind of order  $l$ . For a conventional mechanical resonator, the rate  $g_0 Z_0$  is well below the mechanical resonance frequency, so that  $x \ll 1$ . Therefore, since for a small argument  $x \rightarrow 0$ , the Bessel functions decay increasingly rapidly to zero for increasing  $l$  as  $J_l(x) \approx 2^{-l} x^l/l!$ , we may truncate the series expansion in the equation (2.51) above. Keeping terms up to first order in the small parameter  $x$ , gives  $a = a_0 + a_1$  with

$$a_0 = \frac{\kappa/2}{-i\Delta_L + \kappa/2} a_{\omega_L} \quad (2.52)$$

and

$$a_1(t) = i \frac{g_0 Z_0 a_0(t)}{2} \left[ \frac{\exp(-i\omega_m t)}{-i(\Delta_L + \omega_m) + \kappa/2} + \frac{\exp(i\omega_m t)}{-i(\Delta_L - \omega_m) + \kappa/2} \right]. \quad (2.53)$$

---

<sup>12</sup> The radiation pressure force,  $\hbar g_0|a(t)|^2$ , in equation (2.50) is accurate if the medium filling the cavity is vacuum and the mirror reflectivities are nearly unity.

The radiation pressure force obtained from this solution can be splitted into a contribution oscillating in phase and a contribution oscillating out of phase with respect to  $z_m = Z_0 \cos(\omega_m t)$ . The out of phase contribution accounts for the Doppler shift of the light power inside the resonator and it is thus responsible for an energy loss of the mechanical mirror due to friction. To see this we will compute the power dissipated by the mechanical resonator due to the radiation pressure force. Up to terms of order  $|a_1|$ , the time dependent part of the force is  $\delta F = \hbar g_0 [ |a_0 + a_1|^2 - |a_0|^2 ] \simeq a_0^* a_1 + a_1^* a_0 = \delta F_{\text{IP}} + \delta F_{\text{OP}}$ , with

$$\delta F_{\text{IP}}(t) = -\frac{\hbar g_0^2 Z_0 |a_0|^2}{2} \left[ \frac{2(\Delta_L + \omega_m)}{(\Delta_L + \omega_m)^2 + \kappa^2/4} + \frac{2(\Delta_L - \omega_m)}{(\Delta_L - \omega_m)^2 + \kappa^2/4} \right] \cos(\omega_m t) \quad (2.54)$$

and

$$\delta F_{\text{OP}}(t) = \frac{\hbar g_0^2 Z_0 |a_0|^2}{2} \left[ \frac{\kappa}{(\Delta_L + \omega_m)^2 + \kappa^2/4} - \frac{\kappa}{(\Delta_L - \omega_m)^2 + \kappa^2/4} \right] \sin(\omega_m t) \quad (2.55)$$

the in phase and out of phase contributions, respectively. As we learnt before in section 2.3 a steady state of the mechanical oscillator undergoing driving can be understood as consequence of an equilibrated exchange of energy between the driving source and the mechanical system: the power dissipated by the oscillating mirror is balanced by the energy supplied by the driving. The evolution equation for the ensemble average energy  $\langle E \rangle = M\omega_m^2 \langle z_m^2 \rangle$  of the mechanical mirror can be obtained as we described previously in section 2.3.2, however we depart now from equation (2.50), which takes into account the presence of the radiation pressure force  $\delta F$ . Since the term proportional to  $|a_0|^2$  introduces solely a constant shift we ignore it. The resulting steady state energy  $\langle E(t \rightarrow \infty) \rangle$  is then obtained from

$$\frac{d}{dt} \langle E(t) \rangle = -\Gamma_m \langle E(t) \rangle + \frac{1}{M} [ \langle \delta F(t) p_m(t) \rangle + \langle F(t) p_m(t) \rangle ] = 0, \quad (2.57)$$

where we used the fact that  $F(t)$  and  $\delta F(t)$  are real and our definition  $p_m = iM\omega_m [b_m^* - b_m]/2$ . Assuming that ergodicity is fulfilled, we then interpret ensemble averages as long time averages over many periods  $\tau_m = 2\pi/\omega_m$ . For the harmonic motion  $z_m = Z_0 \cos(\omega_m t)$ , is  $p_m = -M\omega_m Z_0 \sin(\omega_m t)$ , and therefore  $\langle \delta F_{\text{IP}} p_m \rangle = 0$ . While, noticing that  $Z_0^2 = 2 \langle z_m^2 \rangle$ , we find

$$\frac{1}{M} \langle \delta F_{\text{OP}}(t) p_m(t) \rangle = -\omega_m \langle z_m^2 \rangle \frac{\hbar g_0^2 |a_0|^2}{2} \left[ \frac{\kappa}{(\Delta_L + \omega_m)^2 + \kappa^2/4} - \frac{\kappa}{(\Delta_L - \omega_m)^2 + \kappa^2/4} \right]. \quad (2.58)$$

Expression (2.58) accounts for the imbalance of light powers associated with different modes of either frequency upshifted (anti-Stokes) or downshifted (Stokes) photons with respect to the resonance frequency of the cavity. By choosing a laser frequency that falls below the cavity resonance, i.e. a red detuning,  $\omega_L - \omega_{\text{cav}} = \Delta_L < 0$ , we may favor damping of the mirror motion (increase the number of anti-Stokes photons) while suppressing the opposite process of amplification of mirror oscillations, and vice versa, a blue detuning,

$\Delta_L > 0$  may increment the energy supplied to the mirror motion by the optical field (increase the number of Stokes photons), leading to an amplification of its oscillation amplitude. Notably, the cooling method enabled by these light scattering processes is analogous to that of laser cooling of atoms [135]. If we consider that the thermal bath of the mechanical mirror is at temperature  $T_m$ , we have  $\langle Fp_m \rangle = \tilde{\mathcal{S}}_{FF}(\omega_m)/(2M) = \Gamma_m k_B T_m$ , so that, using the formula (2.58) above, we reexpress the steady state energy (2.57) of the mechanical mirror in terms of an effective temperature as

$$\tilde{T} = T_m \frac{\Gamma_m}{\Gamma_{\text{om}} + \Gamma_m}. \quad (2.59)$$

The ratio of power exchange (2.58) between the mechanical mirror and the cavity radiation field to the energy  $\langle E \rangle = M\omega_m^2 \langle z_m^2 \rangle$  stored in the mechanical system accounts for the so called optomechanical energy damping or heating rate  $\Gamma_{\text{om}}$ , i. e.

$$\Gamma_{\text{om}} = -\frac{\langle \delta F_{\text{OP}}(t)p_m(t) \rangle}{M\omega_m^2 \langle z_m^2(t) \rangle} = g_0^2 |a_0|^2 \frac{\hbar}{2\omega_m} \left[ \frac{\kappa}{(\Delta_L + \omega_m)^2 + \kappa^2/4} - \frac{\kappa}{(\Delta_L - \omega_m)^2 + \kappa^2/4} \right]. \quad (2.60)$$

Taking a close look to equation (2.60) we may realize that, as long as  $\omega_m > \kappa$ , a laser detuning  $\Delta_L = \omega_m$  is nearly optimum to maximize processes that yield an excess of Stokes photons relative to anti-Stokes ones (mirror motion amplification) and, oppositely, that if we set  $\Delta_L = -\omega_m$  we allow for an augment of anti-Stokes photons relative to Stokes photons (cooling of mirror motion). This can intuitively be understood if we resort to the energy conservation principle and conceive the full system of mechanical mirror and radiation field from a quantum perspective. Upon excitation, it is clear that the coupled system of cavity plus mechanical mirror always absorbs a laser photon of frequency  $\omega_L$ . However, the frequency of the photon field radiated by the excited system will be given by the resonant frequency of the excited state of the system. Noticing that  $\omega_{\text{cav}} \gg \omega_m$ , we realize that, on average, resonant excitations of the cavity plus mechanical mirror system will radiate at a frequency  $\omega_{\text{cav}}$ . Then, if  $\omega_m > \kappa$ , i.e., if we may distinguish among the laser, anti-Stokes and Stokes photon frequencies,  $\omega_L$ ,  $\omega_L \pm \omega_m$ , respectively, by choosing the frequency of the incident light such that  $\omega_L = \omega_{\text{cav}} - \omega_m$ , excitation and ensuing radiation of the cavity plus mirror system at frequency  $\omega_{\text{cav}}$  implies a reduction of the mechanical mirror's energy by an amount  $\hbar\omega_m$ . This laser cooling strategy in the regime for which  $\omega_m > \kappa$ , i. e., the sideband frequency (here the mechanical frequency  $\omega_m$ ) of the radiated field is larger than the linewidth  $\sim \kappa$  of the excited system (here the weakly coupled cavity plus mechanical modes) is known as resolved sideband cooling, and it was first conceived and realized for atomic systems [136].

What is the minimum mechanical mode temperature that we may aspire to reach by applying this so called resolved sideband cooling process to our optomechanical system? To answer this question, we merely need to know the power spectrum of the radiation pressure force or, equivalently, of the intensity of the quantum radiation field inside the optical resonator in the absence of optomechanical coupling. From the classical equations

of motion (2.49) and (2.50) we can easily write down a Hamiltonian for the corresponding canonical variables  $z_m$  and  $p_m$ , as well as for the normal mode  $a$ . To account for a quantum cavity field we replace  $a$  by the single mode creation  $\hat{a}^\dagger$  and annihilation  $\hat{a}$  operators, satisfying the canonical commutation relation  $[\hat{a}, \hat{a}^\dagger] = 1$ . Using the definitions (2.22)–(2.23) for the position and momentum operators of the mechanical mirror, the optomechanical Hamiltonian can be written as [137]

$$\hat{H}_{\text{om}} = \hbar\omega_{\text{cav}}[\hat{a}^\dagger\hat{a} - \langle\hat{a}^\dagger\hat{a}\rangle] + \hbar\omega_m\hat{c}^\dagger\hat{c} - \hbar g_0 z_{\text{zpm}}[\hat{a}^\dagger\hat{a} - \langle\hat{a}^\dagger\hat{a}\rangle][\hat{c}^\dagger + \hat{c}] + \hat{H}_{\text{ld}} + \hat{H}_\kappa + \hat{H}_{\Gamma_m}. \quad (2.61)$$

Here,  $\hat{H}_{\text{ld}}$  stands for the Hamiltonian of the laser drive, whereas the Hamiltonians  $\hat{H}_\kappa$  and  $\hat{H}_{\Gamma_m}$  describe, respectively, the interactions of the optical resonator and the mechanical resonator with all the other infinitely many modes of their corresponding environments, and account for the friction and stochastic forces of the quantum mechanical version of the classical Langevin equations of the operators  $\hat{a}$  and  $\hat{c}$ . Knowledge of the Hamiltonian (2.61), finally allows us to evaluate the dynamics of every observable of concern, in particular that of the correlator  $\langle\hat{F}_{\text{rp}}(t)\hat{F}_{\text{rp}}(0)\rangle$  where  $\hat{F}_{\text{rp}} = \hbar g_0[\hat{a}^\dagger\hat{a} - \langle\hat{a}^\dagger\hat{a}\rangle]$  is the radiation pressure force operator. Determining  $\langle\hat{F}_{\text{rp}}(t)\hat{F}_{\text{rp}}(0)\rangle$  (with vanishing optomechanical coupling,  $g_0 = 0$ , in the Hamiltonian (2.61) above) and, subsequently, its Fourier transform, provides us with the wanted power spectrum of  $\hat{F}_{\text{rp}}$ . The outcome reads

$$S_{F_{\text{rp}}F_{\text{rp}}}(\omega) = \int_{-\infty}^{+\infty} d\tau \exp(i\omega\tau) \langle\hat{F}_{\text{rp}}(\tau)\hat{F}_{\text{rp}}^\dagger(0)\rangle = \bar{n} \frac{\kappa}{(\Delta_L + \omega)^2 + \kappa^2/4}, \quad (2.62)$$

where  $\bar{n} = |a_0|^2$  is the mean photon number of the cavity radiation field. For details on the calculation the reader is referred to [9, 114]. The minimum temperature or, equivalently, mean occupation number of the mechanical resonator will be limited by the quantum noise of the cold bath to which the mechanical mirror is coupled to, i. e., by the quantum fluctuations of the radiation pressure force. Formula (2.45), presented in the previous section 2.3.3, provides the effective occupation number of a mechanical resonator resulting from the quantum fluctuations of an external noisy drive. Applied here to the radiation pressure force yields

$$\bar{n}_{\text{om}}(\omega_m) = \left[ \frac{S_{F_{\text{rp}}F_{\text{rp}}}(\omega_m)}{S_{F_{\text{rp}}F_{\text{rp}}}(-\omega_m)} - 1 \right]^{-1} = -\frac{(\Delta_L + \omega_m)^2 + \kappa^2/4}{4\omega_m\Delta_L}, \quad (2.63)$$

where we used the power spectral density (2.62) above. For  $\Delta_L = -\omega_m$ , and in the resolved sideband regime,  $\omega_m \gg \kappa$ , we obtain  $\bar{n}_{\text{om}} \simeq \kappa^2/(4\omega_m)^2 < 1$ , the minimum achievable occupation number of the mechanical mode under laser sideband cooling. Finally, we note that to approach this limit it is necessary to overcome the original thermal fluctuations of the mechanical mode. We can estimate the necessary conditions for this from the equation (2.44) for the steady state occupation number of the mechanical mode under an external noisy drive. Particularized for our optomechanical system with  $\Delta_L = -\omega_m$  and  $\omega_m \gg \kappa$ , this reads

$$\bar{n} = \frac{\Gamma_m \bar{n}_{T_m}(\omega_m)}{\Gamma_{\text{om}} + \Gamma_m} + \frac{\Gamma_{\text{om}} \bar{n}_{\text{om}}(\omega_m)}{\Gamma_{\text{om}} + \Gamma_m} \simeq \frac{\Gamma_m \bar{n}_{T_m}(\omega_m)/\Gamma_{\text{om}}}{1 + \Gamma_m/\Gamma_{\text{om}}} + \frac{\Gamma_{\text{om}}}{\Gamma_{\text{om}} + \Gamma_m} \frac{\kappa^2}{16\omega_m^2}. \quad (2.64)$$

From equation (2.63) we see that to get close to the minimum occupation number  $\bar{n}_{\text{om}} \simeq \kappa^2 / (4\omega_m)^2 \ll 1$ , we need a small thermal decoherence rate  $\Gamma_m \bar{n}_{T_m} \ll \Gamma_{\text{om}}$ . Noting as well that, since we determine the optomechanical rate from a perturbation approach either as  $\Gamma_{\text{om}} = z_{\text{zpm}}^2 [S_{F_{\text{rp}}F_{\text{rp}}}(\omega_m) - S_{F_{\text{rp}}F_{\text{rp}}}(-\omega_m)] / \hbar^2$  or as given in equation (2.60) (both expressions coincide), we should take into account that both times  $\Gamma_{\text{om}}^{-1}$  and  $\Gamma_m^{-1}$  must be much longer than the autocorrelation time of the radiation pressure force correlator. The latter is given by the cavity linewidth as  $\kappa^{-1}$ . Therefore, we may conclude that for a good performance of resolved sideband cooling of the mechanical oscillator mode we shall look for a laser power, and mechanical resonator parameters (mass, frequency, quality factor) that satisfy  $\Gamma_m \bar{n}_{T_m} \ll \Gamma_{\text{om}} \ll \kappa \ll \omega_m$ .



### 3 A nanomechanical resonator remotely coupled to an ultracold atomic gas

In the previous chapter 2 we learnt that cavity optomechanics enables an active control over the motion of a mechanical oscillator with an electromagnetic mode of radiation inside of an optical or microwave resonator. Here, we present instead a scheme to affect the motion of a linearly vibrating nanomirror (our mechanical oscillator) by means of the dielectric response of an ultracold atomic gas. Two electric dipole transitions of the atoms in the ultracold ensemble are relevant for our scheme. Each transition is characterized by a different Bohr frequency, and therefore we use two laser beams to mediate a mutual coupling between the ultracold atoms and the mechanically oscillating nanomirror. One laser beam serves us to probe the absorption of the atoms at the Bohr frequency of one of the atomic transitions as well as to drive the nanomirror oscillations, and is thus called the probe beam. The probe beam interacts first with the atoms before hitting the mirror surface. The other laser beam is aimed to control the dielectric response of the atoms and so is referred to as the control beam. Unlike the probe beam, the control beam reflects off the mirror surface before interacting with the atoms. For a fixed mirror, the control beam remains essentially unperturbed after reflecting off the mirror surface, so that by carefully adjusting its frequency to the Bohr frequency of the other atomic transition, one can render the resonantly absorbing atomic gas transparent at the frequency of the probe beam, an effect known as electromagnetically induced transparency. The mirror, however, is allowed to mechanically oscillate. An oscillating mirror imprints a phase modulation onto the control beam, producing sidebands of the control field detuned by the mirror frequency. Feeding the atoms with this control light reflected off the oscillating mirror allows to alter the transparency of the atoms with respect to the probe light. The optical response of the atoms may now generate counterpart sidebands into the probe light transmitted through the atoms. In this way, the intensity of the resulting probe light is ultimately modulated by the mechanical vibrations of the mirror. This effect is maximal when the mirror frequency matches the energy gap between two eigenstates of the coupled system of atoms plus light fields. Upon incidence onto the mirror surface the probe light couples to the mirror motion through radiation pressure force, thus enabling that these vibrations act back on themselves. This feedback translates then into a viscous like force. Whether this driving amplifies or damps the mirror motion depends on the relative phase shift between probe beam amplitude modulations and mirror oscillation. We show that this relative phase shift can be adjusted by choice of the frequency mismatch between the probe and control light waves. At the semi-classical level discussed here, the scheme allows phase-locking the amplitude modulations of a laser to motion of a mechanical element. Equivalently, the atomic cloud allows the conversion of phase-modulations of one light-field (the control beam), into amplitude modulations of another (the probe beam). This chapter is organized

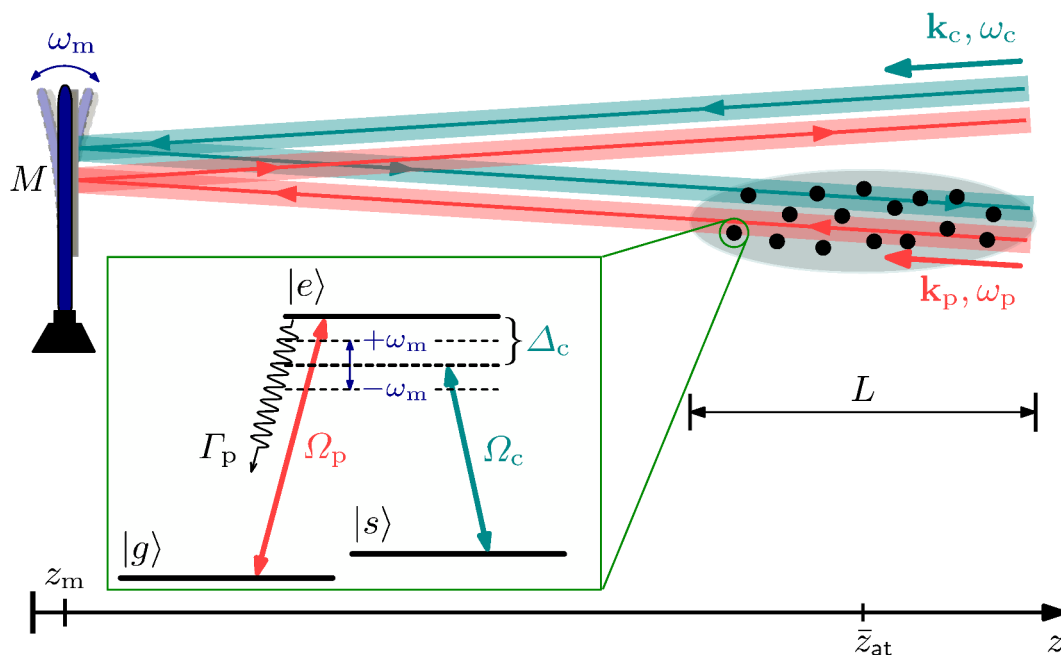


**Figure 3.1** Schematic diagram of an electromagnetically rendered transparent medium (dots) coupled to mechanically oscillating mirror via probe and control lasers with different optical paths. (inset) Energy level diagram of the electromagnetically rendered transparent medium, realizing a  $\Lambda$  scheme. We also indicate the control laser sidebands due to mirror vibrations and spontaneous decay<sup>1</sup>.

as follows: in section 3.1 we discuss our setup of mirror, atomic cloud and light fields with a brief parenthetical remark on the phenomenon of electromagnetically induced transparency, followed by the physical model describing this arrangement in section 3.2. Subsequently we analyse the dynamical response of the system, first of the atomic medium to a constantly oscillating mirror, section 3.3, and then of the mirror being driven by the response of that medium, section 3.4. In section 3.4.2 we investigate in which parameter regime the ensuing coupling between mirror and medium shows prospects for manipulations of the mirror, before concluding in section 3.5.

### 3.1 Atom-optomechanical setup

This section introduces those properties of the physical system under concern that will set the grounds of our dynamical description presented in the following sections. It is convenient to address in turn the different elements that constitute the system, a mechanical oscillator, a gas of atoms and a pair of electromagnetic fields that mediate the mutual coupling between the atomic gas and the mechanical oscillator, see figure 3.1. We adopt a semiclassical model, like the one discussed in section 2.2.1, in which the atoms are described quantum mechanically whereas the electromagnetic fields are assumed to be sufficiently intense and coherent so as

<sup>1</sup> For simplicity we consider only decay from  $|e\rangle$  to  $|g\rangle$ . In our parameter regimes, the physics is unchanged if decay from  $|e\rangle$  to  $|s\rangle$  is also possible.



to describe them classically.

**Mechanical oscillator:** The mechanical element consists of a thin plate (a perfectly conducting mirror) of mass  $M$  that may oscillate linearly with frequency  $\omega_m$ . We assume that the amplitude of such oscillations is large compared with the quantum fluctuations of the mirror's motion. Then we also describe the oscillatory dynamics of the mirror classically, and by means of a single displacement coordinate  $z_m(t) = [b_m^*(t) + b_m(t)]/2$ , the center of mass oscillation amplitude of the mirror around its equilibrium position  $z_0 = 0$ . The dynamical variable  $b_m(t) = B_m(t) \exp(-i\omega_m t)$  with complex amplitude  $B_m(t)$  denotes the generalized coordinate of the mechanical oscillator (see section 2.3.1). To facilitate the task of judging whether or not mechanical losses are externally induced by other coupling scheme, we focus on the case in which  $z_m$  obeys the time evolution of an ideal harmonic oscillator with no intrinsic dissipation. Nonetheless, we could easily extend the model to include intrinsic damping and driving of the mirror induced by its coupling to a thermal environment at a finite temperature due to the mirror clamping, as described in section 2.3.2 of the previous chapter.

**Atomic gas:** We envisage an isotropic atomic medium that confines  $N$  identical non interacting  $^{87}\text{Rb}$  atoms and extends over a length  $L$  along the  $z$ -axis as depicted in figure 3.1. Then, if  $\mathcal{N}_0$  is the (uniform) density of the atomic medium, our non interacting description of the atoms demands a dilute regime for which  $\mathcal{N}_0 |\mathbf{k}_\lambda|^{-3} \lesssim 1$ , where  $|\mathbf{k}_\lambda|^{-1}$  stands for any of the reduced wavelengths of the electromagnetic waves that drive optical transitions of the atoms. The atoms are also kept at an ultracold temperature, and hence we will neglect Doppler motion as well as collisional dephasing.

Concerning the electronic structure of the atoms, we consider three relevant states,  $|g\rangle$ ,  $|e\rangle$  and  $|s\rangle$ , i.e., we effectively describe every multilevel atom as a three level atom, see section 2.2 for the details and validity of such effective reduction of the states space of the atom. Then, the Hamiltonian for the internal states of atom  $n$  at position  $\mathbf{r}_n$  is

$$\hat{H}_0^{(n)} = \sum_{\mu} \hbar\omega_{\mu} \hat{\sigma}_{\mu\mu}^{(n)}, \quad (3.1)$$

with the states space restricted to  $\mu \in \{g, e, s\}$  and  $n = 1, 2, \dots, N$ . We keep the notation of section 2.2.1, such that  $\{\hbar\omega_{\mu}\}$  denotes the set of eigenenergies of  $\hat{H}_0^{(n)}$  (identical for every atom in the gas) and  $\hat{\sigma}_{\mu\mu'}^{(n)} = [|\mu\rangle\langle\mu'|]_n$  denotes the atomic transition operator between eigenstates  $|\mu\rangle_n$  and  $|\mu'\rangle_n$  acting on atom  $n$  only. The states  $|g\rangle$ ,  $|s\rangle$  are long-lived meta-stable ground states, while  $|e\rangle$  decays to  $|g\rangle$  with a rate  $\Gamma_p$ , as sketched in the inset of figure 3.1. They form a so called three level  $\Lambda$ -type atom with only two dipole allowed transitions, one (similar to the one introduced in section 2.2.1) involving states  $|e\rangle$  and  $|g\rangle$  with dipole matrix element  $\mathbf{d}_{eg}$ , and another one involving states  $|e\rangle$  and  $|s\rangle$  with dipole matrix element  $\mathbf{d}_{es}$ .

Finally, following also section 2.2.1, we characterize the dynamical state of the non interacting atoms with the density operator  $\hat{\rho} = \hat{\rho}^{(1)} \otimes \hat{\rho}^{(2)} \otimes \dots \otimes \hat{\rho}^{(N)}$ , where  $\hat{\rho}^{(n)} = \hat{\rho}^{(n)}(\mathbf{r}_n)$  is the single-particle density operator for the  $n$ th atom at  $\mathbf{r}_n$ .

**Electromagnetic waves:** To attain a mutual coupling between the vibrating mirror and the atoms we use two running electromagnetic waves (laser beams) that impinge normally from vacuum on the atomic gas. The two light waves reach atoms and nanomirror only once along their paths, as shown in figure 3.1. We express the total electric field as a superposition of two quasi-monochromatic waves,

$$\mathbf{E}(\mathbf{r}, t) = \frac{1}{2} \sum_{\omega_\lambda} \mathcal{E}_{\omega_\lambda}(\mathbf{r}, t) \exp(-i\omega_\lambda t) + \text{c.c.} \quad (3.2)$$

In equation (3.2) the summation runs over the carrier frequencies  $\omega_\lambda \in \{\omega_p, \omega_c\}$ , and  $\mathcal{E}_{\omega_\lambda} = \mathbf{E}_{\omega_\lambda} \exp(i\mathbf{k}_\lambda \cdot \mathbf{r})$  denotes a complex valued envelope where  $\mathbf{k}_\lambda$  is the wavevector of the carrier wave (such that, in vacuum,  $|\mathbf{k}_\lambda| = \omega_\lambda/c$ ) and  $\mathbf{E}_{\omega_\lambda}$  is a slowly varying field amplitude in space over an optical wavelength and in time over an optical period. We assume each beam follows an unidirectional propagation along the  $z$ -axis, which it is a good approximation if both light beams have finite transverse cross sectional areas fulfilling  $\mathcal{A}_{\omega_\lambda} \gg |\mathbf{k}_\lambda|^{-2}$ . For Gaussian laser beams and atoms focused at the beam waists  $w_\lambda$ , the cross sectional areas are approximately given by  $\mathcal{A}_{\omega_\lambda} = \pi w_\lambda^2/2$ .

The probe light wave (carrier frequency  $\omega_p$  and wavevector  $\mathbf{k}_p$ ) couples the states  $|g\rangle$  and  $|e\rangle$  resonantly with Rabi frequency  $\Omega_p = \mathbf{d}_{eg} \cdot \mathcal{E}_{\omega_p}/\hbar$ . It traverses first through the atoms before reflecting off the nanomirror surface and propagating freely away from the setup. The control light wave (carrier frequency  $\omega_c$  and wavevector  $\mathbf{k}_c$ ) couples the states  $|s\rangle$  and  $|e\rangle$  with Rabi frequency  $\Omega_c = \mathbf{d}_{es} \cdot \mathcal{E}_{\omega_c}/\hbar$ . In contrast to the probe light wave, it impinges and reflects off the nanomirror surface first, then passes through the atomic cloud and finally leaves the system. Therefore, we may conceive each light wave as the combination of a beam incident on the nanomirror surface and a beam reflected from the nanomirror surface. The atomic gas then couples to the incident probe light beam (on the way to the mirror surface) and to the reflected control light beam. In the following, unless otherwise expressly stated, whenever we mention the probe light wave we shall be referring to its incident beam, while an allusion to the control light wave shall refer to its reflected beam.

Given a motionless mirror, the electric field in equation (3.2) would be a continuous wave (c. w.) form and the amplitudes  $\mathbf{E}_{\omega_\lambda}$  would be constant in time. However, a light wave reflected off a perfectly conducting mirror in oscillatory motion undergoes modulations. In the non-relativistic limit (speed of mirror oscillations much smaller than speed of light in vacuum  $\sim \omega_m z_m/c \ll 1$ ) the next adiabatic picture holds: the light beam at successive instants of time can be computed as if the mirror were at rest. Assuming nearly normal incidence on the mirror surface along the  $z$ -axis, this quasistationary picture yields the following modulated control electric field amplitude [138, 139, 140]

$$\mathbf{E}_{\omega_c}(\mathbf{r}, t) = -\tilde{\mathbf{E}}_{\omega_c}(\mathbf{r}, t) \exp(-i2|\mathbf{k}_c|z_m(t)) \simeq -\tilde{\mathbf{E}}_{\omega_c}(\mathbf{r}, t)[1 - 2i|\mathbf{k}_c|z_m(t)], \quad (3.3)$$

where  $\tilde{\mathbf{E}}_{\omega_c}$  is the slowly varying part of the control electric field amplitude. Upon reflecting off the mirror surface the wave experiences a sign flip, hence the minus sign in the first equality of equation (3.3), whereas in the last equality we have assumed that the oscillation

amplitude of the mirror is way smaller than the wavelength of the control light beam, which is well satisfied in the atom-optomechanical setup under consideration.

We will show that the phase modulation of the control field causes a time-dependent modulation of the transmission of the probe beam through the medium, or in short, the phase modulation of the control beam is turned into an amplitude modulation of the probe beam. Thus, due to the radiation pressure exerted by the probe beam on the mirror, we obtain a closed feedback loop, where the running wave fields are used to separately mediate the two directions of mutual coupling between the nano-mechanical mirror and the atomic medium.

### 3.1.1 Electromagnetically induced transparency

Electromagnetically induced transparency (EIT) is a phenomenon in which a resonant absorbing atomic gas becomes transparent via the proper application of electromagnetic radiation [141, 142, 143]. The phenomenon of EIT constitutes a central feature in our setup, which we could clearly observe it if the control field would be devoid of optomechanical sidebands. Let us assume for now that this is the case, and hence that the Rabi frequencies  $\Omega_p$  and  $\Omega_c$  are time independent. Transparency of the atomic medium to electromagnetic radiation on resonance at a given transition frequency may then be achieved by establishing an atomic coherence between two meta stable (non-decaying) states that remains uncoupled from the decaying excited state  $|e\rangle$  while the atom is irradiated with electromagnetic waves. For a concrete illustration we consider that the electronic state of every atom in our ultracold atomic gas is settled in a quantum superposition of the meta stable levels  $|g\rangle$  and  $|s\rangle$ . In particular, for atom  $n$ , we define this state as

$$|d\rangle_n = \frac{1}{\sqrt{|\Omega_p(\mathbf{r}_n)|^2 + |\Omega_c(\mathbf{r}_n)|^2}} [\Omega_c(\mathbf{r}_n)|g\rangle_n - \Omega_p(\mathbf{r}_n)|s\rangle_n]. \quad (3.4)$$

Remarkably, under a proper calibration of the probe and control beams the superposition state (3.4) can be made *invisible* to light, and hence  $|d\rangle$  is usually known as a *dark* state. To show this potential feature of *invisibility* of  $|d\rangle$  we shall compute the overlap of the excited state  $|e\rangle_n$  and the superposition state  $|d\rangle_n$  with the Hamiltonian describing the electric dipole interaction of atom  $n$  with the probe and control light fields. In the dipole approximation and following the recipe of section 2.2.1, the total Hamiltonian  $\hat{H}_\Lambda^{(n)}$  for the  $n$ th three level  $\Lambda$ -type atom of the gas coupled to the probe and control light fields is found to be

$$\hat{H}_\Lambda^{(n)} = \sum_{\mu \neq g} \omega_{\mu g} \hat{\sigma}_{\mu\mu}^{(n)} + \hat{V}^{(n)}(\mathbf{r}_n, t), \quad (3.5)$$

$$\hat{V}^{(n)}(\mathbf{r}_n, t) = -[\Omega_p(\mathbf{r}_n)\hat{\sigma}_{eg}^{(n)} + \text{h. c.}] \cos(\omega_p t) - [\Omega_c(\mathbf{r}_n)\hat{\sigma}_{es}^{(n)} + \text{h. c.}] \cos(\omega_c t). \quad (3.6)$$

The overlap of  $|e\rangle_n$  and  $|d\rangle_n$  with the interaction Hamiltonian (3.6) (at all times) is given by the interaction picture matrix element  ${}_n\langle e|\hat{U}_0 \hat{V}^{(n)} \hat{U}_0^\dagger |d\rangle_n$  with  $\hat{U}_0 = \exp(i \sum_n \sum_{\mu \neq g} \omega_{\mu g} \hat{\sigma}_{\mu\mu}^{(n)} t)$ .

### 3.1 Atom-optomechanical setup

The result is

$${}_n\langle e|\hat{\mathcal{U}}_0\hat{V}^{(n)}\hat{\mathcal{U}}_0^\dagger|d\rangle_n \simeq \frac{\Omega_p(\mathbf{r}_n)\Omega_c(\mathbf{r}_n)}{\sqrt{|\Omega_p(\mathbf{r}_n)|^2 + |\Omega_c(\mathbf{r}_n)|^2}} \left[ e^{-i(\omega_p - \omega_{eg})t} - e^{-i(\omega_c - \omega_{es})t} \right], \quad (3.7)$$

after neglecting non resonant terms proportional to  $\exp(i\omega_{eg}t + i\omega_p t)$  and  $\exp(i\omega_{es}t + i\omega_c t)$ . The matrix element (3.7) vanishes for all times whenever the two photon resonance condition  $\Delta_p = \omega_p - \omega_{eg} = \omega_c - \omega_{es} = \Delta_c$  is fulfilled. In that case, and provided that the relative phase between the states  $|g\rangle_n$  and  $|s\rangle_n$  remains constant in the course of time, an atom  $n$  initially settled in  $|g\rangle_n$  and subsequently evolved under the action of the Hamiltonian (3.5), will eventually reach the dark state (3.4) (up to a global phase factor). Certainly, due to the finite lifetime of its excited level  $|e\rangle_n$  the atom will absorb and emit light waves for some time, however, if the two photon resonance condition is satisfied, equation (3.7) shows that the transition amplitude from  $|g\rangle_n$  to  $|e\rangle_n$  and the transition amplitude from  $|s\rangle_n$  to  $|e\rangle_n$  will cancel each other (destructively interfere), precluding the excitation of atom  $n$  to level  $|e\rangle_n$ . At that point, the atom no longer fluoresces, i.e., it becomes transparent (*invisible*) to light, exhibiting a so called dark resonance. We can further corroborate this physical picture by examining the absorption profile of the atom, i.e. the imaginary part of the atomic susceptibility near the two photon resonance. To determine the susceptibility close to the

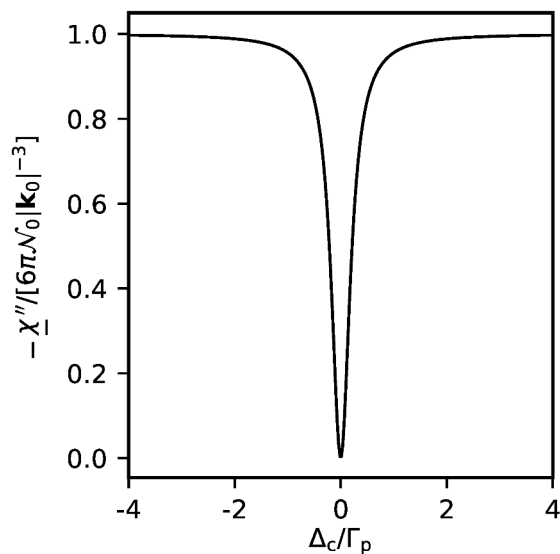


**Figure 3.2** Absorption profile for the probe transition of a gas of noninteracting  $\Lambda$ -type three level atoms vs the detuning  $\Delta_\lambda$  in units of  $\Gamma_p/(2\pi) = 6.1$  MHz. We set  $\Delta_p = 0$  and  $\Omega_c/(2\pi) = 4$  MHz.

resonance we solve the internal dynamics of atom  $n$  initially prepared in the ground state  $|g\rangle_n$  and subject to the dipole interaction (3.5). In the dynamics we also take into account decoherence due to spontaneous decay of level  $|e\rangle$  with rate  $\Gamma_p$ . Switching to a rotating frame to drop fast oscillating terms in (3.5) and assuming a weak coupling to the probe beam, we use first order perturbation theory in  $\Omega_p$  to find the following expression for the linear susceptibility (the one that is proportional to an electric field oscillating with the carrier

frequency  $\omega_p$ )

$$\underline{\chi}(\omega_p) = 6\pi\mathcal{N}_0|\mathbf{k}_0|^{-3} \frac{i\Gamma_p/2}{\Gamma_p/2 - i\Delta_p + \frac{i|\Omega_c|^2/4}{\Delta_p - \Delta_c}}. \quad (3.8)$$

The details on the derivation of equation (3.8) can be found in Appendix A.2.1. As expected, at the two photon resonance,  $\Delta_p = \Delta_c$ , equation (3.8) completely vanishes. The physical scenario that we want to study operates the probe beam on resonance with the  $|e\rangle$ - $|g\rangle$  transition, therefore from now on we set  $\Delta_p = 0$  and  $|\mathbf{k}_0| = |\mathbf{k}_p|$ . Figure 3.2 shows a plot of the imaginary part  $\text{Im}[\underline{\chi}] = \underline{\chi}''$  of the susceptibility as a function of the detuning  $\Delta_c$ . The curve is a particular example of a Fano resonance profile (an antiresonance profile) [144], which is symmetric on both sides of the two photon resonance,  $\Delta_p = \Delta_c = 0$ , where it drops to zero. The width of the resonance is  $|\Omega_c|^2/(4\Gamma_p)$  and it is intimately related with the so called EIT window or bandwidth: the frequency range around the resonance on which the transparency and the linear dispersive properties of the medium are supported [145]. Changing the Rabi frequency  $\Omega_c$ , that is to say, the power of the control field, enables to widen or narrow this width, and thus the EIT bandwidth of the medium. It is noteworthy to mention that for large control light intensities,  $|\Omega_c| \gg \{|\Omega_p|, \Gamma_p\}$ , we could be tempted to attribute the EIT phenomenon to the emergence of an Autler-Townes doublet [146]. However, EIT persists even in the case for which the doublet can not be resolved, i.e. for  $|\Omega_c| < \Gamma_p$ , since vanishing absorption on resonance is still observed (see figure 3.2). For a thorough discussion on the distinction between EIT and the Autler-Townes splitting the reader is referred to [147, 148].

Therefore, as we have already mentioned above, in the three level  $\Lambda$ -type atomic gas considered here, the EIT effect is ultimately a direct consequence of a destructive interference between the transition amplitude from  $|g\rangle$  to  $|e\rangle$  and the transition amplitude from  $|s\rangle$  to  $|e\rangle$  that takes place at the two photon resonance. A complete transparency of the atomic medium ceases to be observable if there exists dephasing between the levels  $|g\rangle$  and  $|s\rangle$ . The more rapidly these states lose their coherence the less transparent becomes the medium. This is due to the fact that the dark state (the emerging steady state of the optically driven atoms) of equation (3.4) loses its feature of *invisibility* to light as soon as it undergoes decoherence, i.e., as soon as the relative phase between the states  $|g\rangle$  and  $|s\rangle$  varies in the course of time. Taking a closer look at equation (3.4) we notice that this relative phase between  $|g\rangle$  and  $|s\rangle$  is strongly dependent on the relative phase between the probe and control fields.

Let us return to our original physical setup, thus recovering the time dependence of the probe and control Rabi frequencies. Since the phase of the control beam is modulated by the mechanical oscillations of the mirror (cf. equation (3.3)), the internal dynamics of the atoms can effectively couple to the mechanically oscillating mirror. Then we may exploit the sensitivity of the dark resonance to the phase mismatch between the probe and control Rabi frequencies to study the effect of the mechanical motion in the dielectric response of the atoms and vice versa. That will be the task of concern in the remaining of the chapter, after

presenting our dynamical model of the full physical system in the following section 3.2. We will then start with a physical scenario involving a constant harmonic motion of the mirror,  $z_m(t) \propto \cos(\omega_m t)$ , whereby the power spectrum of the control Rabi frequency acquires sidebands  $\omega_c \pm \omega_m$  as in multi-chromatic EIT [149, 150, 151, 152, 153].

## 3.2 Coupled dynamics of atomic gas, light waves and nanomechanical mirror

The aim of this section is to present a reduced set of equations describing an effective coupled dynamics between the internal states of the atoms in the gas and the linearly vibrating mirror. In Appendix A.1 we provide a more extended discussion of the approach followed here. We assume that the atoms are initially in equilibrium, all settled in the ground state  $|g\rangle$ , and at a large distance away and completely isolated from the presence of the nanomechanical mirror. The applied electromagnetic fields disturb the atoms and bring them out of equilibrium. We will neglect any magnetic effects induced in the atomic medium and study only the electrical response of the atomic gas to these applied fields. This response is then characterized by the medium's polarization  $\mathbf{P}$ , which acts as a source term in the electromagnetic wave equation. Considering the atomic gas as a medium with zero magnetization and lacking of free sources of charge and current, the electromagnetic wave equation reads

$$\nabla \times \nabla \times \mathbf{E}(\mathbf{r}, t) + \frac{1}{c^2} \frac{\partial^2}{\partial t^2} \mathbf{E}(\mathbf{r}, t) = -\frac{1}{\epsilon_0 c^2} \frac{\partial^2}{\partial t^2} \mathbf{P}(\mathbf{r}, t). \quad (3.9)$$

To evaluate the polarization we shall compute the expectation value of every atomic dipole in the gas, which requires knowledge of the dynamics of the electronic state of the atoms represented here by the density operator  $\hat{\rho}$ . The dynamics of any atom in the ensemble are ruled by the Hamiltonian (3.5) describing the dipole coupling of the atom to the probe and control light waves. Rather than working directly with (3.5), we switch to a rotating frame that enables us to drop all of the non resonant terms in (3.5). The switch to this rotating frame is performed with the help of the unitary operator  $\hat{U}_\Lambda = \exp(i\hat{\mathcal{H}}_\Lambda t/\hbar)$  where

$$\hat{\mathcal{H}}_\Lambda/\hbar = \omega_p \sum_{n=1}^N \hat{\sigma}_{ee}^{(n)} + (\omega_p - \omega_c) \sum_{n=1}^N \hat{\sigma}_{ss}^{(n)}. \quad (3.10)$$

Using  $\hat{U}_\Lambda$ , we transform the Hamiltonian for the  $n$ th atom into  $\hat{H}_\Lambda^{(n)} = \hat{U}_\Lambda \hat{H}_\Lambda^{(n)} \hat{U}_\Lambda^\dagger + i\hbar \dot{\hat{U}}_\Lambda \hat{U}_\Lambda^\dagger$  which, after neglecting non resonant terms and recalling that we have set  $\Delta_p = 0$ , reads

$$\hat{H}_\Lambda^{(n)}/\hbar = \Delta_c \hat{\sigma}_{ss}^{(n)} - \frac{1}{2} [\Omega_c(\mathbf{r}_n, t) \hat{\sigma}_{es}^{(n)} + \Omega_p(\mathbf{r}_n, t) \hat{\sigma}_{eg}^{(n)} + \text{h. c.}]. \quad (3.11)$$

Likewise, the density operator changes according to  $\hat{\rho} \mapsto \hat{U} \hat{\rho} \hat{U}^\dagger = \hat{\rho} = \hat{\rho}^{(1)} \otimes \dots \otimes \hat{\rho}^{(N)}$ . Then, if we take into account the relaxation process  $\mathcal{L}[\hat{\rho}^{(n)}] = \hat{L}_n \hat{\rho}^{(n)} \hat{L}_n^\dagger - (\hat{L}_n^\dagger \hat{L}_n \hat{\rho}^{(n)} + \hat{\rho}^{(n)} \hat{L}_n^\dagger \hat{L}_n)/2$  with  $\hat{L}_n = \sqrt{\Gamma_p} \hat{\sigma}_{ge}^{(n)}$ , due to the spontaneous decay of level  $|e\rangle$  to  $|g\rangle$ , the density operator  $\hat{\rho}^{(n)}$  for the  $n$ th atom evolves according to the Lindblad master equation

$$\frac{\partial}{\partial t} \hat{\rho}^{(n)}(t) = -\frac{i}{\hbar} [\hat{H}_\Lambda^{(n)}, \hat{\rho}^{(n)}(t)] + \mathcal{L}[\hat{\rho}^{(n)}(t)]. \quad (3.12)$$

In combination, and in the absence of the optomechanical sidebands (3.3) imprinted onto the control light field, equations (3.9) and (3.12) (the Maxwell Bloch equations) allow for a self-consistent solution of the coupled dynamics of the electric fields (3.2) and the polarization, since the latter is given by

$$\mathbf{P}(\mathbf{r}, t) = \left\langle \sum_n \delta(\mathbf{r} - \mathbf{r}_n) \sum_{\mu, \mu'} \mathbf{d}_{\mu\mu'} \hat{U}_\Lambda(t) \hat{\sigma}_{\mu\mu'}^{(n)} \hat{U}_\Lambda^\dagger(t) \right\rangle = \sum_{n=1}^N \sum_{\mu, \mu'} \rho_{\mu'\mu}^{(n)}(t) \delta(\mathbf{r} - \mathbf{r}_n) \mathbf{d}_{\mu\mu'} e^{-i\nu_{\mu'\mu} t}, \quad (3.13)$$

with the summation indices  $\mu, \mu' \in \{g, e, s\}$  and  $\mathbf{d}_{sg} = \mathbf{d}_{gs} = 0$ . The frequencies  $\nu_{\mu'\mu} = \nu_{\mu'} - \nu_\mu$  in equation (3.13) stem from the definition of (3.10), and hence  $\nu_{eg} = \omega_p$  and  $\nu_{es} = \omega_c$ . We can express the polarization more compactly in terms of collective slowly varying atomic density matrix elements,  $\mathcal{R}_{\mu\mu'}(\mathbf{r}) = \sum_{n=1}^N \rho_{\mu\mu'}^{(n)} \delta(\mathbf{r} - \mathbf{r}_n)$ , defined already in equation (2.9) of the previous chapter 2. Moreover, in section 2.2.1 of chapter 2 we saw that for a non interacting gas of atoms, as is the case here, these collective density matrix elements are, for all practical purposes, equivalent to the density of the gas  $\mathcal{N}_0$  times the matrix elements of a single atom density operator  $\hat{\rho}(\mathbf{r})$  standing representative for the entire medium, i.e.,  $\mathcal{R}_{\mu\mu'}(\mathbf{r}) \equiv \mathcal{N}_0 \rho_{\mu\mu'}(\mathbf{r})$ , and hence

$$\mathbf{P}(\mathbf{r}, t) = \mathcal{N}_0 [\rho_{eg}(\mathbf{r}, t) \mathbf{d}_{ge} \exp(-i\omega_p t) + \rho_{es}(\mathbf{r}, t) \mathbf{d}_{se} \exp(-i\omega_c t) + \text{c. c.}]. \quad (3.14)$$

In order to make the notation clearer, we omit from now on the superscript of one-particle operators used to label a given atom  $n$  within the whole atomic ensemble. Thus, e.g.,  $\hat{\rho}^{(n)} \equiv \hat{\rho}$  and  $\hat{H}_\Lambda^{(n)} \equiv \hat{H}_\Lambda$ .

As we mentioned earlier in section 3.1, a scenario without optomechanical sidebands affecting the atomic medium is also a scenario of unperturbed c.w. fields. In that case the atoms in the medium settle into a steady state beyond some initial transient time  $\sim \Gamma_p^{-1}$ , providing, in a linear regime with the probe field, the complex susceptibility  $\underline{\chi} = \underline{\chi}' + i\underline{\chi}''$  of equation (3.8); in what follows we split complex numbers  $s \in \mathbb{C}$  as  $s = s' + is''$  into real part  $s' = \text{Re}[s]$  and imaginary part  $s'' = \text{Im}[s]$ . For our dilute homogeneous gas and within an infinite plane wave approximation (no spatial dependence on coordinates perpendicular to the propagation direction,  $\mathbf{E}_{\omega_\lambda}(\mathbf{r}, t) \simeq \mathbf{E}_{\omega_\lambda}(z, t)$ ) a solution of the Maxwell Bloch equations yields a probe field amplitude transmitted across the entire medium  $\mathbf{E}_{\omega_p} \simeq \mathbf{E}_{0\omega_p} \exp(-|\mathbf{k}_p|L\underline{\chi}''(\omega_p)/2)$ , and thus an average power per optical period  $\overline{\mathcal{W}}_{\omega_p} = \varepsilon_0 c \mathcal{A}_{\omega_\lambda} \mathbf{E}_{\omega_\lambda} \cdot \mathbf{E}_{\omega_\lambda}^* / 2 \simeq \mathcal{W}_{0\omega_p} \exp(-|\mathbf{k}_p|L\underline{\chi}''(\omega_p))$ , where the input field strength<sup>2</sup>  $|\mathbf{E}_{0\omega_p}| = \sqrt{2\mathcal{W}_{0\omega_p} / [\varepsilon_0 c \mathcal{A}_{\omega_p}]}$  is determined from the input power  $\mathcal{W}_{0\omega_p}$ . Evaluated at  $z = z_m$ , the average powers  $\overline{\mathcal{W}}_{\omega_\lambda}$  per optical period of each beam impinging on the mirror, determine the radiation pressure force

$$F_{\text{rp}}(t) = 2[\mathcal{W}_{\omega_p}(t) + \mathcal{W}_{\omega_c}(t)]/c, \quad (3.15)$$

---

2 We assume that the phase of the input amplitude can be taken as a phase reference and thus we set it to zero without loss of generality.

with  $\mathcal{W}_{\omega_\lambda}(t) = \overline{\mathcal{W}_{\omega_\lambda}(z, t)}|_{z=z_m}$ , that both beams exert on the perfectly reflecting surface of the mirror. The classical motion of the mechanically oscillating mirror is then described by Newton's equation for a driven harmonic oscillator

$$M \frac{d^2}{dt^2} z_m(t) + M\omega_m^2 z_m(t) = F_{rp}(t). \quad (3.16)$$

The force due to the incident control beam is always constant and determined from its input power  $\mathcal{W}_{\omega_c} = \mathcal{W}_{0\omega_c}$ , since the control light wave only passes the medium that could absorb it *after* reflection off the mirror<sup>3</sup>. For the scenario exempt of optomechanical sidebands the power  $\mathcal{W}_{\omega_p} \simeq \mathcal{W}_{0\omega_p} \exp(-|\mathbf{k}_p|L\chi''(\omega_p))$  of the probe beam impinging on the mirror is also constant, and therefore in this case the ensuing radiation pressure force gives only rise to a shift of the equilibrium position of the mirror. However, for our setup shown in figure 3.1 the modulation (3.3) of the control field precludes a genuine steady state for the atoms. If the modulation period is slow enough compared to the time it takes probe beam phase-fronts to pass through the atomic gas, we can nevertheless obtain a simple response of the atoms, as argued in Appendix A.2.2. The atomic medium is then described by a modulated susceptibility  $\chi(\omega_p; t) = 6\mathcal{N}_0\pi|\mathbf{k}_p|^{-3}\Gamma_p\rho_{eg}(t)/\Omega_p$ . From a solution of (3.12), linear in the probe field, and that includes the influence of the optomechanical sidebands, we assume the following probe power to impinge on the mirror:

$$\mathcal{W}_{\omega_p}(t) \simeq \mathcal{W}_{0\omega_p} \exp(-|\mathbf{k}_p|L\chi''(\omega_p; t)) \approx \mathcal{W}_{0\omega_p} \left( 1 - 6\mathcal{N}_0\pi|\mathbf{k}_p|^{-2}L \operatorname{Im} \left[ \frac{\Gamma_p}{\Omega_p} \rho_{eg}(t) \right] \right). \quad (3.17)$$

When writing equation (3.17) we assume that any effects that may arise in the course of an atomic transient dynamics (times  $\lesssim \Gamma_p^{-1}$ ) are minimal. Equation (3.17), just like our whole dynamical model, also neglects the travel time of light waves between mirror and all atomic positions in the atom cloud, which hence has to be much shorter than the dynamical time scale of the problem that we study. The latter time scale is given by the mirror period  $\tau_m = 2\pi/\omega_m$ , so that the above assumptions are well satisfied for mirrors with frequencies in the MHz-GHz range and typical optical path lengths.

Using the power (3.17) for the probe radiation pressure force (3.15), together with the definition (3.3) for the phase modulation of the control field, the master equation (3.12) and Newton's equation (3.16) become a coupled system of differential equations.

---

<sup>3</sup> Possible backscattering of the control light beam by the atoms can be fully avoided by shielding and optical diodes.



### 3.3 Interaction between multiple monochromatic light waves and atomic gas

In the following we analyse the consequences of coupling a vibrating mirror to an atomic  $\Lambda$ -type EIT medium with the model developed in section 3.2. In a first step, we take into account the phase-modulation of the control beam by the vibrating mirror, but neglect all radiation pressure on the mirror. This yields an analytically solvable time-periodic model, presented in section 3.3.2. In a second step, we close the feedback loop by incorporating radiation pressure on the mirror. As shown in section 3.4 this gives rise to interesting dynamics, which can be understood using the results of section 3.3.2.

#### 3.3.1 Linearly oscillating nanomirror coupled to atomic gas

If the driving force is switched off in equation (3.16),  $F_{\text{rp}}(t) = 0$ , the mirror will undergo harmonic oscillations  $z_m(t) = [B_{0m} \exp(-i\omega_m t) + \text{c. c.}]/2$  with amplitude  $Z_0 = |B_{0m}|$ . These oscillations give rise to constant strength sidebands in the control light field, such that  $\Omega_c = -\tilde{\Omega}_c[1 - i(\eta \exp(-i\omega_m t) + \text{c. c.})]$ , where  $\tilde{\Omega}_c = \mathbf{d}_{es} \cdot \tilde{\mathbf{E}}_{\omega_c} \exp(i\mathbf{k}_c \cdot \mathbf{r})/\hbar$  and  $|\eta| = |\mathbf{k}_c|Z_0$  is the relative amplitude of the sidebands.

#### 3.3.2 Time periodic model

We are interested in a description of the long term dynamics ( $\Gamma_p t > 1$ ) of the optically driven atoms linear in the probe field and that is also suitable for a limit of weak modulations of the control field, such that  $|\eta||\tilde{\Omega}_c| \ll \Gamma_p |\tilde{\Omega}_c|$ . We then rely on a solution based on perturbation theory with respect to those terms in the Hamiltonian (3.11) that are proportional to  $\Omega_p$ . Within this perturbative approach we also presume that the c.w. form of the input beams prevails as such during the entire dynamics, i.e., that both Rabi frequencies  $\Omega_p$  and  $\tilde{\Omega}_c$  remain as time independent quantities during the evolution of the coupled system of atoms and light waves (see Appendix A.2.2 for an extended discussion). Having clarified this, we start recognizing that the presence of the sidebands in the control field prevents the atomic system (3.12) from settling into a genuine steady state, which suggests the construction of an asymptotic solution in terms of Fourier components of the density operator:  $\hat{\rho} = \sum_{l=-\infty}^{\infty} \hat{\rho}_{l\omega_m} \exp(-il\omega_m t)$ , see for example references [154] and [149, 155]. Using this expression for the density operator in the master equation (3.12) leads to an infinite hierarchy of coupled equations for the  $\hat{\rho}_{l\omega_m}$ . We truncate the hierarchy by neglecting all  $\hat{\rho}_{l\omega_m}$  with  $|l| > 1$ , which allows us to retain terms up to first order in  $|\eta||\tilde{\Omega}_c|/\omega_m$ . For long times ( $\Gamma_p t \gtrsim 1$ ) we demand the Fourier amplitudes  $\hat{\rho}_{l\omega_m}$  to become steady,

$$\frac{\partial}{\partial t} \hat{\rho}_{l\omega_m} = 0. \quad (3.18)$$

Next, by demanding  $|\Omega_p| \lesssim \Gamma_p \ll |\tilde{\Omega}_c|$ , which amounts to typical EIT conditions, we expand the amplitudes  $\hat{\rho}_{l\omega_m}$  to first order in  $\Omega_p/\tilde{\Omega}_c$ . The zeroth order density operator results in the

usual steady state solution for  $\eta = 0$ , which yields the linear susceptibility of equation (3.8). Knowledge of  $\hat{\rho}_0$  allows us to solve equation (3.18) for  $l = 1$  to find (see Appendix A.2.2 for more details)

$$\rho_{+\omega_m, eg}(\Delta_c) = \frac{2i\omega_m\eta\Omega_p|\tilde{\Omega}_c|^2}{(2i\Gamma_p\Delta_c + |\tilde{\Omega}_c|^2)(2i[\Gamma_p - 2i\omega_m][\Delta_c - \omega_m] + |\tilde{\Omega}_c|^2)}. \quad (3.19)$$

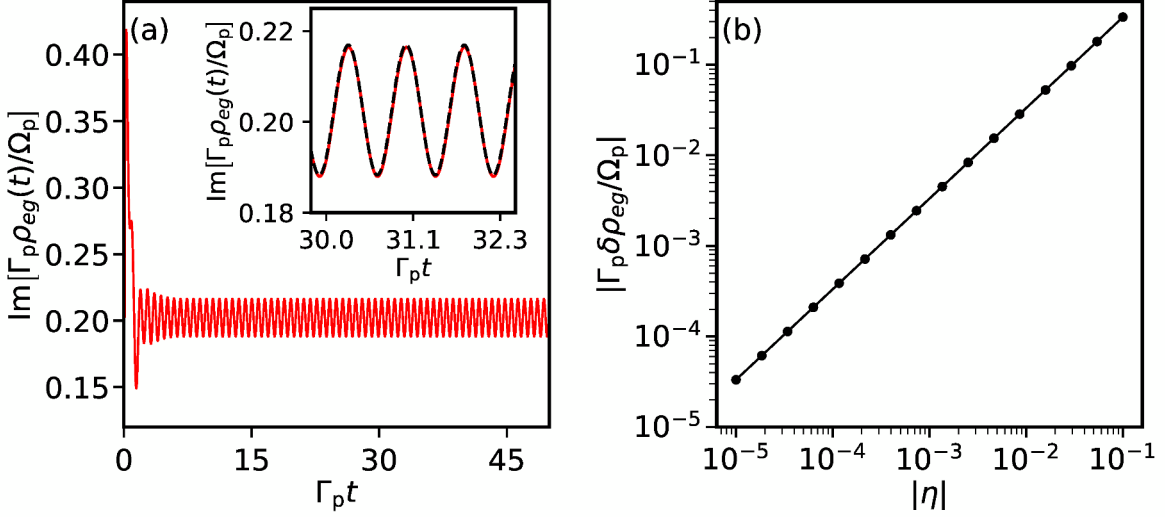


**Figure 3.3** Asymptotic response of atomic system to constant control beam sidebands, from numerical solutions of equation (3.12). We show the imaginary part of the probe transition coherence  $\text{Im} [\Gamma_p \rho_{eg}(t)/\Omega_p]$  that causes absorption, using  $\Delta_c/(2\pi) = -4.13$  MHz,  $\omega_m/(2\pi) = 8.00$  MHz,  $\Omega_p/(2\pi) = 0.32$  MHz and  $\tilde{\Omega}_c/(2\pi) = 10.00$  MHz,  $\Gamma_p/(2\pi) = 6.10$  MHz. (a) Evolution of  $\text{Im} [\Gamma_p \rho_{eg}(t)/\Omega_p]$  as a function of time (in units of  $\Gamma_p^{-1}$ ) for  $\eta = 0.009$ . The inset shows a zoom on the asymptotic behaviour, where the black dashed stems from our analytic solution equation (3.19). (b) The amplitude  $|\Gamma_p \delta\rho_{eg}/\Omega_p|$  of these oscillations scales linearly with the sideband strength  $|\eta|$ ; (●) are data points, and the line guides the eye.

### 3.3.3 Linear response in the presence of optomechanical sidebands

Our approximate solution,  $\hat{\rho} = \hat{\rho}_0 + \hat{\rho}_{+\omega_m} \exp(-i\omega_m t) + \hat{\rho}_{-\omega_m} \exp(i\omega_m t)$ , determines the medium's susceptibility (linear in the probe field), and hence its optical absorptive properties. Of particular interest for us are the modulations of the imaginary part of the probe coherence  $\text{Im} [\Gamma_p \rho_{eg}/\Omega_p]$ . These modulations will affect absorption by the medium according to equation (3.17). We define

$$\text{Im} \left[ \frac{\Gamma_p}{\Omega_p} \rho_{eg}(t) \right] = \text{Im} \left[ \frac{\Gamma_p}{\Omega_p} \rho_{0, eg} \right] + \left| \frac{\Gamma_p}{\Omega_p} \delta\rho_{eg} \right| \cos(\omega_m t + \alpha), \quad (3.20)$$

where  $\alpha$  is the relative phase between absorption modulations and mirror motion and the factor  $|\Gamma_p \delta\rho_{eg}/\Omega_p|$  is the amplitude of such modulations. From equation (3.19) we can determine  $\delta\rho_{eg}$  and  $\alpha$  in equation (3.20) as  $\delta\rho_{eg} = \rho_{+\omega_m, eg}(\Delta_c) - \rho_{+\omega_m, eg}(-\Delta_c)$  and

$\alpha = \arg [\Gamma_p \delta \rho_{eg} / \Omega_p] - \pi/2$ , where  $\arg[s]$  is the argument of the complex number  $s$ . Here, we have used the fact that the density operator is Hermitian, which demands  $\hat{\rho}_{-l\omega_m} = \hat{\rho}_{+l\omega_m}^\dagger$ , and exploited the symmetry  $\rho_{+\omega_m, eg}(\Delta_c) / \Omega_p^* = \rho_{+\omega_m, eg}(-\Delta_c) / \Omega_p$ .

Figure 3.3(a) demonstrates that equation (3.19) correctly describes the long-term evolution of the atomic system. We show  $\text{Im} [\Gamma_p \rho_{eg} / \Omega_p]$  from a numerical solution to the master equation (3.12) with Newton's equation (3.16), ignoring the driving force in equation (3.16),  $F_{rp}(t) = 0$ , but initializing mirror oscillations in the form  $z_m(t) = Z_0 \cos(\omega_m t)$  with  $Z_0 > 0$ . This numerical solution is compared with the predictions of equations (3.19) and (3.20). After an initial transient phase of the full model until  $\Gamma_p t \lesssim 1$ , the probe coherence is modulated at the mirror frequency with amplitude and phase described by equation (3.20). The modulation scales linearly with  $\eta$ , justifying our early truncation of the hierarchy of coupled equations for the  $\hat{\rho}_{l\omega_m}$ . Note that any mean coherence is nearly suppressed ( $\text{Im} [\Gamma_p \rho_{0, eg} / \Omega_p] \approx 0$ ).

Through changes in radiation pressure, the periodic modulation of the transparency of the atomic medium just discussed will give rise to a periodic driving of the mirror through equation (3.17). This driving is automatically resonant. By determining the phase-relation between driving and mirror motion as well as the amplitude of this driving, we can predict the response of the mirror from classical mechanics. To this end we plot in figure 3.4 the amplitude  $|\Gamma_p \delta \rho_{eg} / \Omega_p|$  and phase  $\alpha$  of equation (3.20) according to equation (3.19) for various mirror frequencies  $\omega_m$  and detunings  $\Delta_c$ . The amplitude  $|\Gamma_p \delta \rho_{eg} / \Omega_p|$  is maximal approximately at  $\Delta_c = \pm \Delta_{\max}$ , with

$$\Delta_{\max} = \frac{\omega_m}{2} \left[ 1 + \frac{|\tilde{\Omega}_c|^2}{\Gamma_p^2} - \sqrt{\left(1 - \frac{|\tilde{\Omega}_c|^2}{\Gamma_p^2}\right)^2 + \frac{|\tilde{\Omega}_c|^4 / \Gamma_p^2}{\omega_m^2}} \right] \quad (3.21)$$

as shown in figure 3.4(a) as red dashed line. Equation (3.21) is valid when  $\Omega_p$  is small compared to other energies. We can further expand equation (3.21) in the quantities  $\Gamma_p^2 / |\tilde{\Omega}_c|^2$  and  $\Gamma_p / \omega_m$ , which are small for cases considered here and get the even simpler expression

$$\Delta_{\max} \simeq \left| \frac{|\tilde{\Omega}_c|^2 - 4\omega_m^2}{4\omega_m} \right|, \quad (3.22)$$

which we will exploit in section 3.4.2.

We can also see in figure 3.4 that a wide range of relative phases between the amplitude modulation of the probe beam, and the phase modulation of the control beam (or mirror motion) can be accessed through variations of the detuning  $\Delta_c$ .

The physical origin of the sharp features in figure 3.4 is a resonance between the mirror frequency and energy gaps in the atomic system. To see this, let us decompose equation (3.11) for one atom as  $\hat{H}_\Lambda(t) = \hat{H}_{0\Lambda} + \sum_{l=\pm 1} \hat{V}_{l\omega_m} \exp(-il\omega_m t)$ , where  $\hat{H}_{0\Lambda} / \hbar = \Delta_c \hat{\sigma}_{ss} - [\Omega_p \hat{\sigma}_{eg} - \tilde{\Omega}_c \hat{\sigma}_{es} + \text{h. c.}] / 2$  is the unperturbed part whereas the terms  $\hat{V}_{+\omega_m} / \hbar = -i\eta [\tilde{\Omega}_c \hat{\sigma}_{es} - \text{h. c.}] / 2$  and  $\hat{V}_{-\omega_m} = \hat{V}_{+\omega_m}^\dagger$ , weighted by complex exponentials, are the perturbation. Let us define eigenstates  $|\Lambda_j\rangle$  of  $\hat{H}_{0\Lambda}$  via  $\hat{H}_{0\Lambda} |\Lambda_j\rangle = E_j |\Lambda_j\rangle$ . We now assume the system has relaxed into

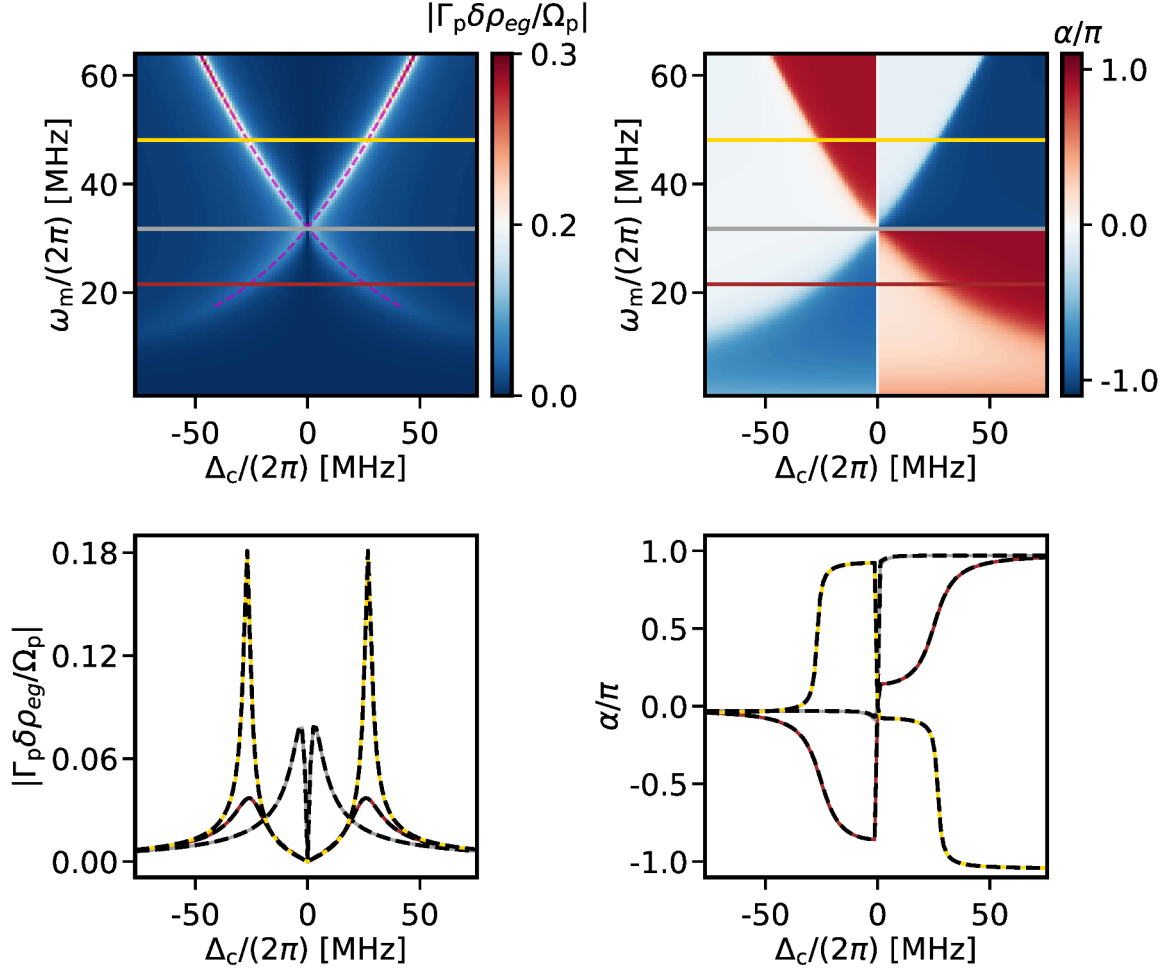


**Figure 3.4** (a) Amplitude  $|\Gamma_p \delta \rho_{eg} / \Omega_p|$  of the oscillations in the imaginary part of the scaled probe transition coherence,  $\text{Im} [\Gamma_p \rho_{eg} / \Omega_p]$ , as a function of mirror frequency  $\omega_m$  and optical detuning  $\Delta_c$ , using equation (3.19). Here,  $\tilde{\Omega}_c / (2\pi) = 64.00$  MHz, and  $\eta = 0.08$ ; other parameters as in figure 3.3. The red dashed line shows the peak position according to equation (3.21). (b) The phase  $\alpha$  of the first harmonic of  $\text{Im} [\Gamma_p \rho_{eg} / \Omega_p]_{eg}$  relative to the mirror oscillation, see equation (3.20). Note that the apparent discontinuity for  $\Delta_c > 0$  is a meaningless  $2\pi$  jump arising from plotting the phase continuously along the  $\Delta_c$  axis. Plots in (c) and (d) are cuts through (a) and (b) respectively at the indicated values of mirror frequency  $\omega_m / (2\pi) = 21.30$  MHz (brown),  $\omega_m / (2\pi) = 32.00$  MHz (gray) and  $\omega_m / (2\pi) = 48.00$  MHz (gold). Black dashed lines are a comparison of equation (3.19) with direct numerical solutions of equation (3.12).

the EIT ground-state,  $|\Lambda_d\rangle$ , but otherwise we ignore spontaneous decay here. It is clear that whenever  $\omega_m = |E_d - E_j| / \hbar$  for some  $j \neq d$ , the perturbation will cause resonant transitions to  $|\Lambda_j\rangle$ . This is the case for  $\omega_m$  fulfilling equation (3.22). Since in this scenario the superposition of  $|\Lambda_d\rangle$  and  $|\Lambda_j\rangle$  will beat at the mirror frequency, also  $\rho_{eg}$  is modulated with  $\omega_m$ . We have confirmed this picture using time-dependent perturbation theory.

### 3.4 Optomechanical interface between atomic gas and oscillating nanomirror

Based on the previous section, we now determine the consequences of enabling feedback from the atomic medium onto the mirror through varying radiation pressure forces in equations (3.16) and (3.15). We only consider radiation pressure from the modulated part of the probe beam,

$$F_{\text{rp}}(t) = -F_{0\text{p}}6\mathcal{N}_0\pi|\mathbf{k}_{\text{p}}|^{-2}L \operatorname{Im} \left[ \frac{\Gamma_{\text{p}}}{\Omega_{\text{p}}}\rho_{+\omega_{\text{m}},eg} \exp(-i\omega_{\text{m}}t) + \frac{\Gamma_{\text{p}}}{\Omega_{\text{p}}}\rho_{-\omega_{\text{m}},eg} \exp(i\omega_{\text{m}}t) \right], \quad (3.23)$$

thereby assuming that the mirror is already oscillating around a new equilibrium position

$$\bar{z} = \frac{F_{0\text{c}}}{M\omega_{\text{m}}^2} + \frac{F_{0\text{p}}}{M\omega_{\text{m}}^2} \left( 1 - 6\mathcal{N}_0\pi|\mathbf{k}_{\text{p}}|^{-2}L \operatorname{Im} \left[ \Gamma_{\text{p}}\rho_{0,eg}/\Omega_{\text{p}} \right] \right), \quad (3.24)$$

due to the radiation pressure by the control beam and the constant part of the probe beam, with  $F_{0\lambda} = 2\mathcal{W}_{0\omega_{\lambda}}/c$  and  $\omega_{\lambda} \in \{\omega_{\text{p}}, \omega_{\text{c}}\}$ . For simplicity we set  $\bar{z} = 0$  from now on.

#### 3.4.1 Dynamics of oscillating nanomirror driven by a viscous like radiation pressure force

Using the driving force (3.23), we numerically solve the coupled Newton (3.16) and master equations (3.12). As can be seen in figure 3.5, the mirror can be driven such that its oscillation amplitude increases or decreases depending on  $\Delta_{\text{c}}$ . For a more quantitative description, we make the Ansatz  $z_{\text{m}}(t) = [B_{\text{m}}(t) \exp(-i\omega_{\text{m}}t) + \text{c. c.}]/2$ , the amplitude of which,  $Z(t) = |B_{\text{m}}(t)|$ , is expected to vary very little during one mirror period  $\tau_{\text{m}}$ . The energy of the oscillator  $E(t) = 1/2M\omega_{\text{m}}^2 Z^2(t)$ . Inserting the Ansatz into equation (3.16), exploiting the slow variation of  $Z(t)$  and using equation (3.23), we find the solution

$$\bar{Z}(t) = \bar{Z}(0) \exp(-\Gamma_{\text{eff}}t/2), \quad (3.25)$$

$$\begin{aligned} \Gamma_{\text{eff}} &= \frac{F_{0\text{p}}}{M\omega_{\text{m}}} 6\mathcal{N}_0\pi|\mathbf{k}_{\text{p}}|^{-2}L \operatorname{Re} \left[ \frac{\Gamma_{\text{p}}}{\Omega_{\text{p}}} \delta\rho_{eg} \right] \\ &= \frac{|\mathbf{k}_{\text{c}}|F_{0\text{p}}}{M\omega_{\text{m}}} 6\mathcal{N}_0\pi|\mathbf{k}_{\text{p}}|^{-2}L \left| \frac{\Gamma_{\text{p}}}{\Omega_{\text{p}}} \frac{\delta\rho_{eg}}{\eta} \right| \sin(\alpha), \end{aligned} \quad (3.26)$$

where the bar denotes a time average over one mirror period. Details are shown in Appendix A.3. In equation (3.26), the phase  $\alpha$  can be determined from equation (3.19). Note that depending on the relative phase shift  $\alpha$  between mirror motion and transparency modulations, the quantity  $\Gamma_{\text{eff}}$  can actually describe damping or amplification. In figure 3.4 we see that the effect on the mirror will be largest at the resonant feature near  $\Delta_{\text{max}}$ , with damping for negative detuning and amplification for positive detuning as long as  $\omega_{\text{m}} < |\tilde{\Omega}_{\text{c}}|/2$ . For  $\omega_{\text{m}} > |\tilde{\Omega}_{\text{c}}|/2$  the two phenomena are swapped.

We validate the model solution (3.25) by comparing the predicted energy of a driven oscillator, using the analytical result for the atomic coherence (3.19), with the energy from

a full numerical solution of Newton (3.16) and master equations (3.12). We find good agreement as shown in figure 3.5. Our conclusions on damping and amplification are not altered by the inclusion of mirror coupling to an additional external heat bath, e.g. through mirror clamping. To this end we have included friction and a stochastic driving force as usual [156], which for small but realistic environmental coupling rates up to 1 kHz did not alter the mechanism.

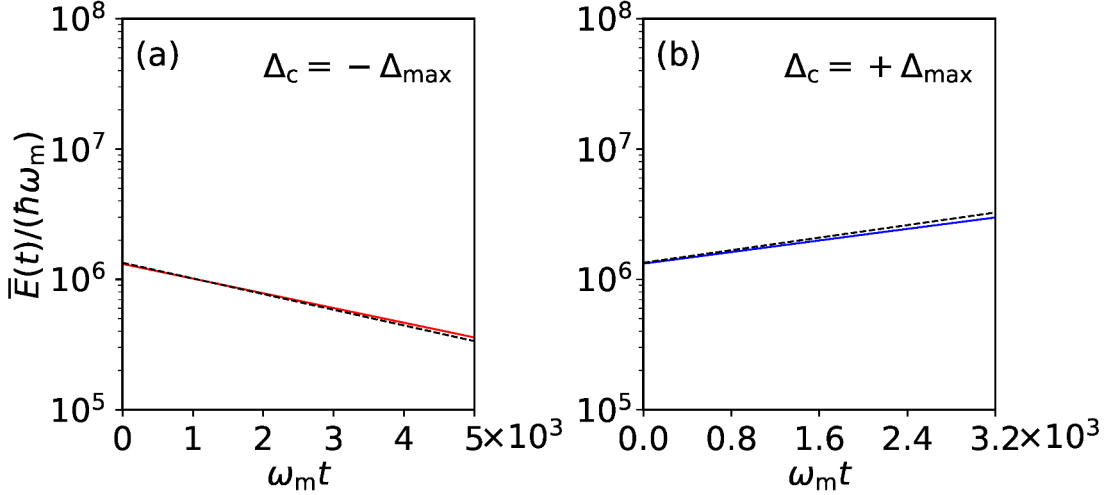


**Figure 3.5** Average energy  $\bar{E}(t)$  of the vibrating mirror per mechanical period  $\tau_m = 2\pi/\omega_m$  in units of  $\hbar\omega_m$  from a numerical integration of equations (3.16) and (3.12), with the values of the time axis being scaled in units of  $\tau_m$  and using  $M = 2.00 \times 10^{-20}$  kg,  $\eta = 0.08$ ,  $\tilde{\Omega}_c/(2\pi) = 64$  MHz,  $\Omega_p/(2\pi) = 1.6$  MHz,  $\omega_m/(2\pi) = 22$  MHz, and  $\Gamma_p/(2\pi) = 6.1$  MHz. In this parameter regime, for red detuning  $\Delta_c = -\Delta_{\max}$ , the mirror motion gets damped (a), whereas for a blue detuning  $\Delta_c = +\Delta_{\max}$  it gets amplified (b). Black dashed curves represent the model developed in section 3.4.1 and we find good agreement.

The results of the present section suggest an optical technique that makes use of atomic absorption to obtain a tailored optical driving force in order to control the mechanical state of a vibrating mirror.

### 3.4.2 Range of applicability

For given oscillator parameters  $\omega_m$  and  $M$ , the results of the preceding sections enable us to determine optical EIT parameters  $\Omega_p$ ,  $\tilde{\Omega}_c$ ,  $\Delta_c$ , for which the damping or amplification of the mirror is maximal [equation (3.21)]. For these we show the effective damping rate  $\Gamma_{\text{eff}}$  of equation (3.26) in figure 3.6 for a variety of mirror parameters. Additionally, we also show the performance as a function of  $\Omega_p$  and  $\tilde{\Omega}_c$  for fixed mirror parameters.

Crucially underlying figure 3.6 are our assumptions for light-field and medium properties. We have assumed a  $^{87}\text{Rb}$  medium of density  $\mathcal{N}_0 = 8.00 \times 10^{12} \text{ cm}^{-3}$  and length  $L = 512.00 \mu\text{m}$ . Assigning the states  $|g\rangle = |5S_{1/2}, F = 1\rangle$ ,  $|s\rangle = |5S_{1/2}, F = 2\rangle$  and  $|e\rangle = |5P_{1/2}, F' = 2\rangle$ , the Rabi frequencies used in figure 3.6 then roughly correspond to powers  $\mathcal{W}_{0\omega_p} \simeq 0.43 \text{ nW}$  and  $\mathcal{W}_{0\omega_c} \simeq 1.76 \text{ mW}$  at beam waists of  $w_p = 560.00 \mu\text{m}$  for the

probe- and  $w_c = 720.00 \mu\text{m}$  for the control beam. The transition frequencies used are  $\omega_p/(2\pi) \approx \omega_c/(2\pi) \simeq 3.77 \times 10^8 \text{ MHz}$ . The decay rate  $\Gamma_p/(2\pi) \simeq 6.10 \text{ MHz}$ .

For this set of parameters, cooling rates in excess of typical environmental coupling strengths are accessible for rather light mirrors  $M \lesssim 10^{-18} \text{ kg}$  with frequencies  $\omega_m/(2\pi) \approx 10 - 100 \text{ MHz}$ . Note that the feature at  $\omega_m = |\tilde{\Omega}_c|/2$  is due to the absence of atomic response at this frequency, as evident in figure 3.4(a). Larger damping rates for heavier mirrors could be obtained with a larger probe power  $\mathcal{W}_{0\omega_p}$ . In the present scheme, they are restricted by the requirement  $|\Omega_p| < |\tilde{\Omega}_c|$ . Variations of the scheme can be achieved by choosing a higher lying decaying state  $|e\rangle$ , which would decrease the transition matrix element  $|\mathbf{d}_{eg}|$  and thus allow larger  $\mathcal{W}_{0\omega_p}$  for identical Rabi frequency  $\Omega_p$ . However, simultaneously this would typically reduce the decay rate  $\Gamma_p$ .

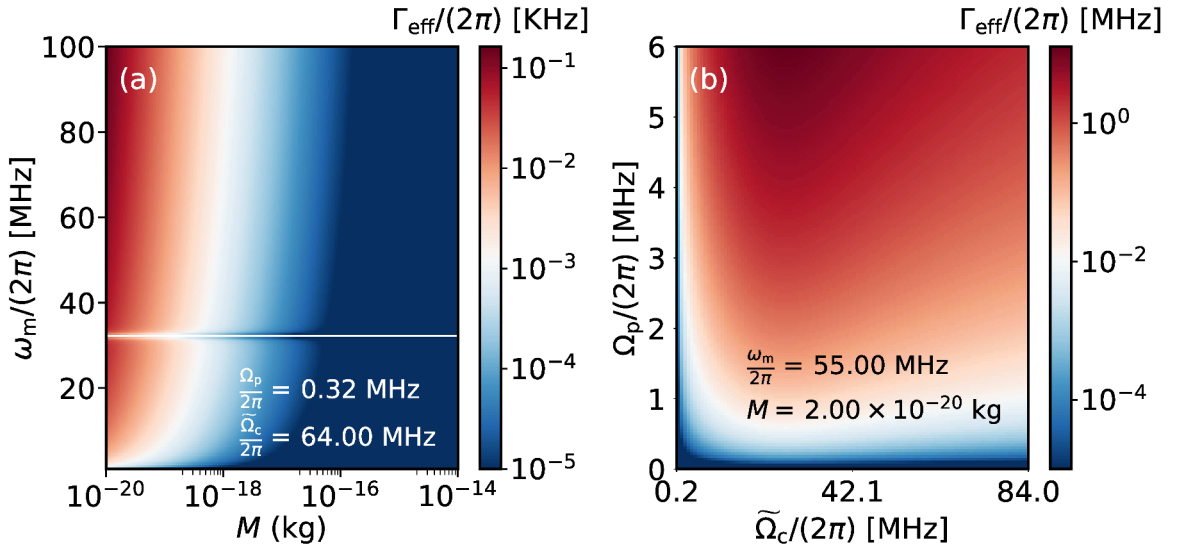


**Figure 3.6** Effective optical damping rate  $\Gamma_{\text{eff}}$  for  $\Delta_c = \Delta_{\text{max}}$ . In (a) we show the dependence on the mirror mass  $M$  and the mirror frequency  $\omega_m$  for fixed Rabi frequencies  $\Omega_p$  and  $\tilde{\Omega}_c$ ; in (b) we fixed  $M$  and  $\omega_m$  and vary the Rabi frequencies. The dependence of the rate  $\Gamma_{\text{eff}}$  on the probe Rabi frequency occurs only via the input power,  $\mathcal{W}_{0\omega_p} \simeq \hbar c \omega_p^2 |\Omega_p|^2 |\mathbf{k}_p|^3 / (12\Gamma_p)$ .

### 3.5 Conclusions

We have described an interface of the classical motion of a harmonically oscillating nano-mechanical mirror with the internal state dynamics and hence optical properties of a three-level,  $\Lambda$ -type atomic medium. Our atom-optomechanical setup exists in free-space, without any cavity. Coupling between mirror and atomic system is provided by the probe and control light fields that render the ultracold atomic gas transparent, due to electromagnetically induced transparency (EIT).

Depending on the choice of the EIT two-photon detuning, amplitude modulations of the probe light beam caused by the atomic medium are phase locked to the mirror oscillation. We have provided analytical expressions for the dependence of phase and strength of the

### 3.5 Conclusions

modulations on the detuning. The setup can also be seen as transferring phase modulations on one optical beam onto amplitude modulations of another.

When the modulated probe beam is made to interact with the mirror, oscillatory motion of the latter can be damped or amplified. We derive the effective damping (amplification) rate of the mirror, using a single atom type description of the EIT medium and a Fourier expansion of the density matrix in the presence of constant sidebands. The achievable damping rates exceed typical coupling strength of mirror to their thermal environment for light and fast mirrors ( $M \lesssim 10^{-18}$  kg,  $\omega_m/(2\pi) \gtrsim 20$  MHz).

Our results provide the basis for a thorough understanding of the corresponding quantum-mechanical setup, which appears as a good candidate for a cavity-free cooling scheme [50, 59], that may complement established cavity cooling techniques [41, 156, 137, 157]. This will be the subject of future work.



## 4 *In situ* monitoring of the quantum state of a nano-scale torsion pendulum with Rydberg atoms

Our goal in the following study is to acquire information about the quantum state of motion of a torsion mechanical resonator mode. Directly measuring a quantum system usually entails a subsequent destruction of it or the loss of its original state. To circumvent this issue we couple the mechanical mode to an ancillary system and let them both evolve together for some finite time. Then we measure the ancillary system. Recording this measurement will in general enable us to gain knowledge about the dynamical state of the mechanical resonator mode without losing it. The mechanical element of interest is a torsion mode of a carbon nanotube and we probe the dynamics of this torsion mechanical mode with a guided beam of two level Rydberg atoms. Every single atom interacts in turn with the torsion mechanical mode and serves as the ancillary system. We use the guided Rydberg atoms with a twofold purpose. On the one hand, we may perform Ramsey interferometry on a series of Rydberg atoms to readout sequentially the dynamical state of the torsion mechanical mode. On the other hand, if we externally drive a Rydberg atom while it interacts with the torsion mechanical mode we may achieve a coherent displacement of the torsion mechanical mode in its dynamical phase space. With a few Rydberg atoms and varying the parameters of the external driving we can sample the dynamical phase space of the torsion pendulum. Then we can combine an exhaustive sampling of the dynamical phase space of the torsion pendulum with several records of Ramsey measurements to realize quantum state tomography of the torsion mechanical mode.

### 4.1 Hybrid platform of nano-torsional oscillator and Rydberg atom

For torsional oscillators [158, 159], we develop in the following a scheme without direct cavity interfacing, allowing for integration of mechanical and measurement elements into the same nano-fabricated substrate using Rydberg atoms. As we mentioned previously in 2.1, Rydberg atoms furnish accessible atomic transition frequencies spanning orders of magnitude when varying the principal quantum number  $\nu$ . This enables them to interface to a wide range of nanomechanical elements with different oscillation frequencies [27, 41, 156]. Furthermore, with their long life times and strong long range interactions [160], Rydberg atoms have proven to be an excellent tool to probe electric fields [161, 94]. Therefore, to use a Rydberg atom as an information carrier of the quantum state of motion of a mechanical resonator we will rely on a coupling between atom and oscillator based on electromagnetic radiation. To this end let us consider the prototype setup shown in figure 4.1. Here a single isolated Rydberg atom is used to sense the motion of a torsion pendulum that oscillates

with angular frequency  $\omega_{\text{osc}}$  and is equipped with a permanent electric dipole  $\mathbf{d}_{\text{osc}}$  due to a spherical ferroelectric load [162] or nanoparticle that we attach at one of its ends, as in [163, 164]. This provides a simple and adjustable interaction between the mechanical oscillator and the Rydberg atom, independent of surface and material properties. Small

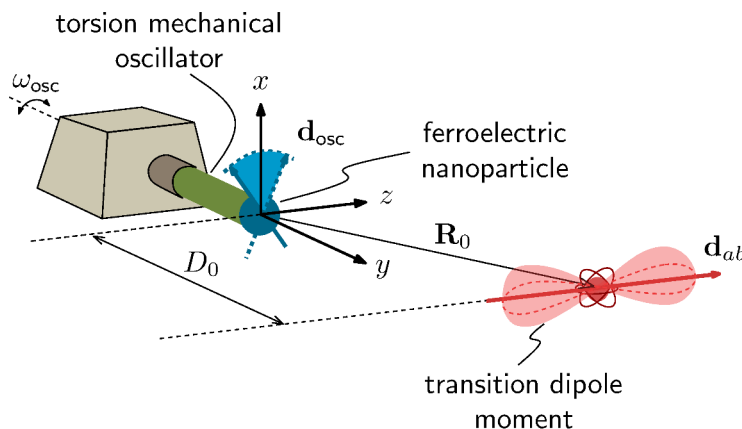


**Figure 4.1** A Rydberg atom is positioned at  $\mathbf{R}_0$  with respect to a ferroelectric nanoparticle attached at one of the ends of a torsional mechanical oscillator with resonant frequency  $\omega_{\text{osc}}$ . The permanent electric dipole moment  $\mathbf{d}_{\text{osc}}$  of the ferroelectric load provides then a strong coupling between a transition dipole moment of the Rydberg atom and the motion of the torsional oscillator. The coupling is highest for a minimum separation  $D_0$  between the atom and the nanoparticle.

oscillation amplitudes of the torsion pendulum produce a time dependent dipolar field that causes Stark shifts in the Rydberg atom depending on the occupation number of the torsion pendulum. A detailed discussion on the radiated electromagnetic field by the swinging electric dipole can be found in Appendix B.2.1.

The peak value of the frequency shift associated with a single mechanical excitation quantum is  $\mathcal{K}_0 = \varphi_{\text{zpm}} V_0 / \hbar$ , where  $V_0 = |\mathbf{d}_{ba}| |\mathbf{d}_{\text{osc}}| / (4\pi\epsilon_0 D_0^3)$  denotes the energy strength of a dipole-dipole coupling with the transition dipole  $\mathbf{d}_{ba} = \langle b | \hat{\mathbf{d}}_{\text{at}} | a \rangle$  between atomic Rydberg states  $|a\rangle$  and  $|b\rangle$  ( $\hat{\mathbf{d}}_{\text{at}}$  is the atomic dipole operator),  $D_0$  the minimum separation (impact parameter) between the atom and the center of the spherical ferroelectric load and  $\epsilon_0$  the vacuum permittivity. The quantity  $\varphi_{\text{zpm}} = \sqrt{\hbar / (2\omega_{\text{osc}} I)}$  represents the amplitude of the zero point motion for a torsional oscillator with total moment of inertia  $I$ . As we discuss later in section 4.4.4, if, e.g., we specifically consider a carbon nanotube (CNT) as the torsional oscillator, we can easily adjust parameters to achieve a coupling strength  $\mathcal{K}_0$  at resonance exceeding both the decoherence rate of Rydberg states  $|a\rangle$  and  $|b\rangle$ , and the rate of mechanical dissipation. This is essential to resolve any correlated dynamics between the atom and the oscillator.

Our general idea is to subject the Stark shifted Rydberg atoms in a waveguide to a Ramsey interference measurement, and hence to read out the mechanical occupation number before the system dynamics settles into a stationary regime. If the oscillator is in a Fock

state, such a Ramsey measurement leaves the oscillator state unchanged, thus furnishing a quantum non-demolition measurement [165]. For more general oscillator states, a series of these measurements will gradually collapse the state towards a phonon number (Fock) state [166]. Repeating such series multiple times eventually reveals the entire phonon-number distribution.

Full quantum state tomography requires knowledge of the phases between different number states, which can be obtained after quantum coherently displacing the oscillator prior to the phonon number distribution measurement. To obtain a well defined displacement, we propose to externally drive Rydberg atoms while they interact together with the mechanical oscillator as discussed below. For a well defined coupling the driving should target only the Rydberg atoms and not directly the oscillator by using well localized evanescent fields from a coplanar microwave guide [167, 161] or a three-photon off-resonant Raman transition [168].

## 4.2 Dynamics of a Rydberg atom and a torsion pendulum interacting electrostatically

The dynamics of our coupled system of a single guided Rydberg atom and the torsion pendulum is described with the following Hamiltonian

$$\hat{H}' = \hat{H}_{\text{osc}} + \hat{H}_{\text{at}} + \hat{H}_{\text{int}} + \hat{H}'_{\text{coup}}. \quad (4.1)$$

The term  $\hat{H}_{\text{osc}} = \hbar\omega_{\text{osc}}(\hat{c}^\dagger\hat{c} + \hat{\mathbb{1}}/2)$ , rules the motion of the torsional oscillator with corresponding number states  $|n\rangle$  and ladder operators  $\hat{c}$ ,  $\hat{c}^\dagger$  and where  $\hat{\mathbb{1}}$  denotes the identity operator on the Hilbert space of the total system of atom plus torsional oscillator. The Hamiltonian for the internal state of a single atom is  $\hat{H}_{\text{at}} = \hbar\sum\omega_\mu\hat{\sigma}_{\mu\mu}$ , where  $\hat{\sigma}_{\mu'\mu} = |\mu'\rangle\langle\mu|$  denotes the atomic transition operator between levels  $|\mu'\rangle$  and  $|\mu\rangle$ , and  $\hbar\omega_\mu$  the energy of level  $|\mu\rangle$ , with  $\mu, \mu' \in \{a, b\}$ . We consider  $\omega_b > \omega_a$ . Motion of the atoms in the waveguide is treated classically as we discuss in section 4.2.3. The atom-oscillator coupling  $\hat{H}_{\text{int}}$  is due to electric dipole-dipole interactions between the transition dipole of the atom and the permanent dipole of the nano-particle attached to the oscillator. Finally, the Hamiltonian  $\hat{H}'_{\text{coup}}$  is due to a microwave field in regions  $R_1$ ,  $R_2$  and possibly  $C$ , with the carrier frequency of the field chosen to be equal to  $\omega_{\text{osc}}$ . To simplify matters, we set the energy origin to the ground state energy of the total system of atom plus mechanical oscillator and get rid of the oscillator's free evolution. This is achieved in an interaction picture with respect to the Hamiltonian

$$\hat{\mathcal{H}}_{\text{mw}}/\hbar = (\omega_a + \omega_{\text{osc}}/2)\hat{\mathbb{1}} + \omega_{\text{osc}}(\hat{c}^\dagger\hat{c} + \hat{\sigma}_{bb}). \quad (4.2)$$

Then, by choosing the atomic transition dipole  $\mathbf{d}_{ba}$  along the z-axis<sup>1</sup> and neglecting counter rotating terms we find  $\hat{H}' \mapsto \hat{H}$ , where (Appendix B.3)

$$\hat{H} = -\hbar\delta\hat{\sigma}_{bb} - \hbar\mathcal{K}[\hat{c}\hat{\sigma}_{ba} + \hat{c}^\dagger\hat{\sigma}_{ab}] + \hat{H}_{\text{coup}}. \quad (4.3)$$

Here,  $\delta = \omega_{\text{osc}} - \omega_{ba}$  is the frequency mismatch between the oscillator frequency and the Bohr frequency  $\omega_{ba} = \omega_b - \omega_a$ . The interaction strength is  $\mathcal{K}(\mathbf{R}_0) = \mathcal{K}_0 f(\mathbf{R}_0)$ . The coordinate vector  $\mathbf{R}_0 = [X_0, Y_0, Z_0]^T$ , points from the center of the nanoparticle in equilibrium (origin of our Cartesian coordinate system) to the atom in the waveguide, as shown in figure 4.4. Then the interaction amplitude becomes  $f(\mathbf{R}_0) = [D_0/R_0]^3 [1 - 3Z_0^2/R_0^2]$ , with  $R_0 = |\mathbf{R}_0|$ . We have assumed small excursions of the oscillator from an equilibrium torsional angle  $\varphi_0 = \pi/2$ . The last term  $\hat{H}_{\text{coup}} = -\hbar[\Omega(t)\hat{\sigma}_{ba} + \text{h. c.}]/2$  represents the controllable inter-state coupling in regions  $R_1, R_2$  and possibly C, with Rabi frequency  $\Omega(t)$  in the dipole and rotating wave approximations.

Before we enter into a description of our probing scheme for the oscillator dynamics using Ramsey measurements we shall consider first the correlated dynamics of the torsional oscillator and the Rydberg atom that results solely from their dipole coupling in equation (4.3). Subsequently, we will build up step by step a model that can describe the whole probing scheme.

### 4.2.1 The Jaynes-Cummings Hamiltonian

Our scheme exploits the phonon dependent phase shifts incurred by the Rydberg atoms to probe the oscillator dynamics. Therefore, we analyze first how and under which conditions these phase shifts may emerge. For that, it is enough to start with the Hamiltonian (4.3) with  $\hat{H}_{\text{coup}}$  set to zero. We also consider a fixed atom, so that the coupling strength is time independent. Thus, the Hamiltonian reads

$$\hat{H}/\hbar = -\delta\hat{\sigma}_{bb} - \mathcal{K}[\hat{c}\hat{\sigma}_{ba} + \hat{c}^\dagger\hat{\sigma}_{ab}]. \quad (4.4)$$

This so called Jaynes Cummings Hamiltonian couples only states within a given doublet  $\mathcal{E}_n$ ; for every  $n \in \mathbb{Z}^+$  a doublet comprises two states:  $|n, a\rangle$  and  $|n-1, b\rangle$ . To determine the spectrum of Hamiltonian (4.4) we decompose it into an infinite direct product of two-dimensional Hamiltonians, each of them associated with a subspace  $\mathcal{E}_n$  of fixed  $n$ . The matrix form of the two-dimensional Hamiltonian  $\hat{H}_n$  constrained to the subspace  $\mathcal{E}_n$  reads

$$H_n/\hbar = - \begin{bmatrix} 0 & \mathcal{K}\sqrt{n} \\ \mathcal{K}\sqrt{n} & \delta \end{bmatrix}. \quad (4.5)$$

---

<sup>1</sup> We can for example define a quantisation axis  $\parallel z$  through Rydberg excitation laser polarisation and work with  $m_J = 1/2$  states only.

Its eigenstates and eigenenergies are given by

$$|n, +\rangle = \cos \Theta_n |n, a\rangle - \sin \Theta_n |n-1, b\rangle, \quad (4.6)$$

$$|n, -\rangle = \sin \Theta_n |n, a\rangle + \cos \Theta_n |n-1, b\rangle, \quad (4.7)$$

and

$$E_{n,\pm}/\hbar = \frac{\delta}{2} \left[ -1 \pm \sqrt{1 + \frac{4n\mathcal{K}^2}{\delta^2}} \right], \quad (4.8)$$

respectively, where the mixing angle is  $\Theta_n = 1/2 \arctan(2|\mathcal{K}|\sqrt{n}/\delta)$ . We observe that the ground state  $|0, a\rangle$  separates from the rest and remains unaltered by the interaction part of the Hamiltonian. The eigenstates  $|n, \pm\rangle$  and eigenenergies  $E_{n,\pm}$  are commonly known as dressed states and dressed energies, respectively [127]. Figure 4.2 displays the dressed

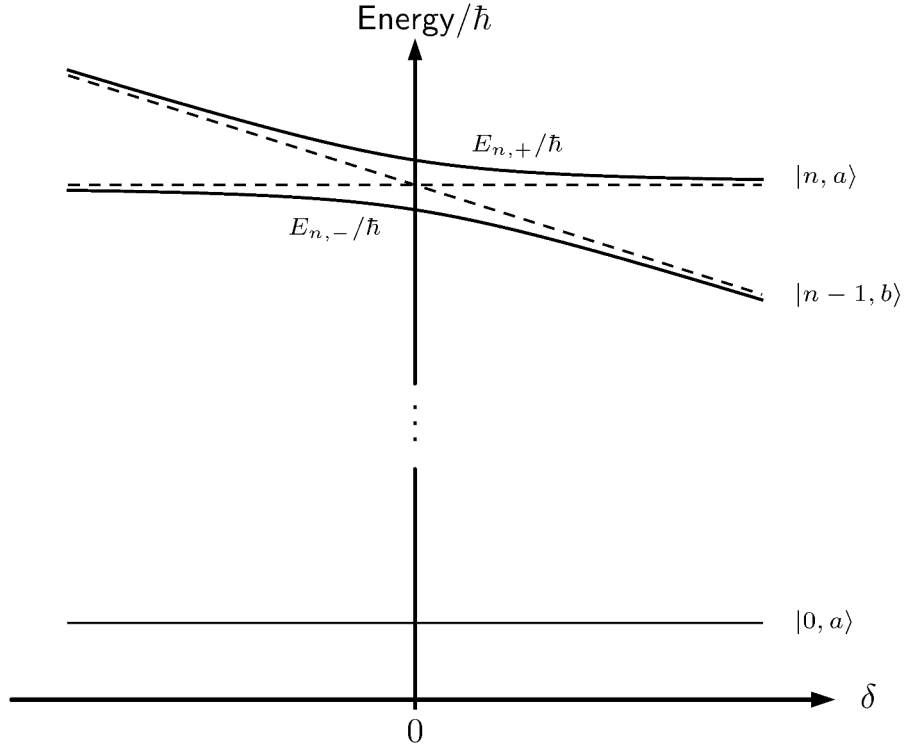


**Figure 4.2** Frequency spectrum of the Jaynes-Cummings Hamiltonian (4.4) as a function of the detuning  $\delta$ . In the limit of large detunings the eigenfrequencies  $E_{\pm}/\hbar$  converge to the ones corresponding to the uncoupled system of atom plus torsion pendulum, associated to states  $|n, \mu\rangle$ , with  $\mu \in \{a, b\}$ .

frequencies  $E_{n,\pm}/\hbar$ , as well as the frequencies corresponding to the decoupled or bare states  $|n, a\rangle$  and  $|n-1, b\rangle$  as a function of the detuning  $\delta$ . There, we may distinguish two phenomenologically distinct scenarios associated with two limiting values of the detuning. On resonance  $\delta = 0$ , the bare energies cross, and therefore the bare states constituting each

doublet  $\mathcal{E}_n$  are degenerate. However, due to the interaction, an avoided crossing appears for the dressed energies and the degeneracy breaks up for the corresponding eigenstates. The time evolution of the joint system comprising the Rydberg atom and the torsion pendulum may lead in this case to Rabi oscillations, that is, a coherent exchange of mechanical and electronic excitation energies among the bare states  $|n, a\rangle$  and  $|n - 1, b\rangle$ , provided that the oscillator is initially prepared in a Fock state, see e.g. [169]. Other interesting dynamics involving an energy exchange between the atom and the mechanical oscillator can also emerge for different initial states.

The other limiting case arises from increasingly high values of the detuning, for which the dressed energies tend to their asymptotes, i.e., to the uncoupled energies. Therefore, in this limit we expect a scenario with very little chances of an energy exchange between the atom and the mechanical oscillator. Next, we examine in more detail the dynamical consequences of this limit.

### 4.2.2 Time evolution in the dispersive regime

We first start evaluating the time evolution operator of the full system of atom plus torsion pendulum. The dressed states (4.6) and (4.7) of each doublet  $\mathcal{E}_n$ , together with the ground state  $|0, a\rangle$ , form a complete basis of the state space of the joint system of atom plus torsion pendulum. Hence, we can represent the time evolution operator as

$$\hat{U}(\tau_0) = |0, a\rangle\langle 0, a| + \sum_{n=1}^{\infty} \sum_{\bar{\mu} \in \{\pm\}} e^{-iE_{n,\bar{\mu}}\tau_0/\hbar} |n, \bar{\mu}\rangle\langle n, \bar{\mu}|, \quad (4.9)$$

where  $\tau_0 = t_2 - t_1$  is the time interval between two distinct instants of time  $t_1$  and  $t_2$ . In the far detuned limit,  $|\delta| \gg |\mathcal{K}|\sqrt{n}$ , we may use perturbation theory to approximate the separation between the dressed energies and their asymptotes. This amounts to a series expansion of (4.8) in the small parameter  $\mathcal{K}\sqrt{n}/\delta$ ,

$$E_{n,+}/\hbar = \frac{\mathcal{K}^2}{\delta}n + \mathcal{O}(\mathcal{K}\sqrt{n}/\delta)^3, \quad (4.10)$$

$$E_{n,-}/\hbar = -\delta - \frac{\mathcal{K}^2}{\delta}n + \mathcal{O}(\mathcal{K}\sqrt{n}/\delta)^3. \quad (4.11)$$

The resulting dressed energies, (4.10) and (4.11), are thus very close to the bare energies of the uncoupled system except for a small correction that, in the lowest non zero order of perturbation theory, is proportional to the number  $n$  of mechanical excitation quanta (phonons). A similar expansion for the corresponding eigenstates, (4.6) and (4.7), shows that they are nearly identical to the bare states, i.e., we may write  $|n, +\rangle \approx |n, a\rangle$ , and  $|n, -\rangle \approx |n - 1, b\rangle$ . With the above approximations the time evolution operator (4.9) simplifies considerably and we may express it in the following compact form

$$\hat{U}(\tau_0) \simeq \exp\left(-i\frac{\mathcal{K}^2}{\delta}\hat{n}\tau_0\right) \otimes \hat{\sigma}_{aa} + \exp\left(i\delta\tau_0 + i\frac{\mathcal{K}^2}{\delta}(\hat{n} + 1)\tau_0\right) \otimes \hat{\sigma}_{bb}. \quad (4.12)$$

We observe that under this unitary dynamics, transitions between atomic states  $|b\rangle$  and  $|a\rangle$  via the absorption or emission of a phonon are suppressed, and thus the phonon number operator  $\hat{n} = \hat{c}^\dagger \hat{c}$  remains unchanged.

### 4.2.3 Adiabatic evolution

So far we have assumed a static scenario, in which the atom is in a fixed location with respect to the torsion pendulum. However, in the scenario that we actually envisage, the atom flies by the torsional oscillator, such that the internal and translational dynamics of the atom are unavoidably coupled. An exact description of the system dynamics should therefore include the quantization of the atomic motion to take into account the excitation of transverse modes of motion, recoil effects (due to the presence of microwave photons) and Doppler shifts [170, 171].

Fortunately, we will assume atoms moving in a waveguide, wherein the transverse spatial spread of their wavepackets remains always considerably smaller than the reduced wavelength of the microwave radiation. We will also work in a regime for which the initial kinetic energy of the atom is large compared with both, the detuning and the coupling between the atom and the torsional oscillator during the entire motion of the atom. All these considerations allow for a classical treatment of the atomic motion with a trajectory, along which the velocity  $\mathbf{v}_0$  and position  $\mathbf{R}_0(t) = \mathbf{R}_0(0) + \mathbf{v}_0 t$  of the atom are well defined for every instant of time [172]. Since the interaction between the atom and the torsional oscillator is a function of the distance that separates them, a moving atom generates a time dependent coupling  $\mathcal{K}(\mathbf{R}_0(0) + \mathbf{v}_0 t)$ . In this way, a diagonalization of the previous Hamiltonian matrix (4.5) gives rise to sets of instantaneously dressed states and dressed energies, that are known as adiabatic states and adiabatic energies [173]. By contrast, in this time dependent framework, bare states are usually termed as diabatic states. In figure 4.3 we show the adiabatic energies for a given atom trajectory. The shaded areas enclosed under the energy curves indicate the accumulated phase shifts.

We may say that the state of our system follows an adiabatic evolution if it can be written as a stationary superposition of adiabatic states, such that the non-adiabatic transitions are approximately zero. This turns out to be particularly the case if the condition for a dispersive interaction between the atom and the torsion pendulum is fulfilled during the whole course of an atom trajectory. Then the evolution of the interacting eigenstates of the compound system of atom plus torsion pendulum may be accounted for diabatic states that accumulate a phase shift conditioned to the state of the atom. The resulting time evolution operator is thus equivalent to equation (4.12). However, as we expect from a collisional process, the accumulated phase shifts shall be written now in terms of the time duration of the collision  $\sim D_0/|\mathbf{v}_0|$ , which is proportional to the integrated squared of the interaction amplitude during the time  $\tau_0$ ,

$$\tau_{\text{col}} = \int^{\tau_0} dt f^2(\mathbf{R}(t)) = \frac{D_0}{|\mathbf{v}_0|} \int^{\zeta_{\tau_0}} d\zeta f^2(\zeta), \quad \zeta = (Z_0(0) + |\mathbf{v}_0|t)/D_0, \quad (4.13)$$

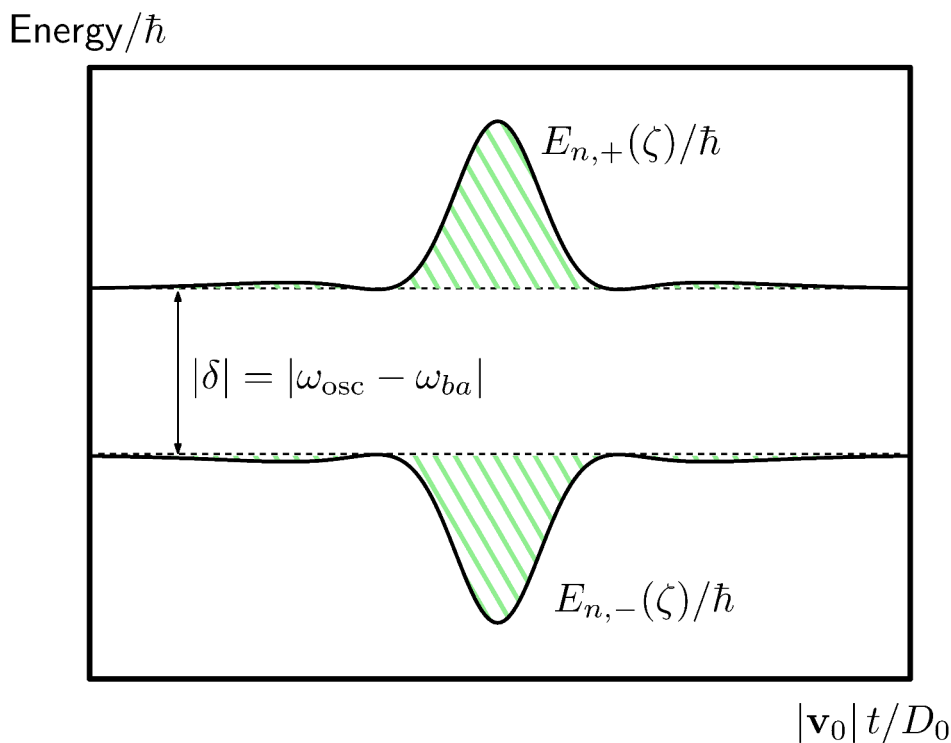


**Figure 4.3** Dressed energy curves  $E_{n,\pm}$  as a function of the relative distance  $|\mathbf{R}_0|$  as this evolves in the course of an atom trajectory  $\mathbf{R}_0 = D_0[X_0/D_0, Y_0/D_0, \zeta]^T$ , where  $\zeta = (Z_0(0) + |\mathbf{v}_0|t)/D_0$ . The dashed lines represent the energies of the atom oscillator compound in the absence of interaction. The shaded areas enclosed between solid and dashed lines then quantify the accumulated energy phase shifts that the bare atom-oscillator states undergo.

where the interaction amplitude recast as a function of the rescaled variable  $\zeta$  reads  $f(\zeta) = [1 + \zeta^2]^{-3/2}[1 - 3\zeta^2/(1 + \zeta^2)]$ , and  $\zeta_{\tau_0} = |\mathbf{v}_0|\tau_0/D_0$ . For a sufficiently long trajectory,  $\zeta_{\tau_0} > 1$ , the integral approaches to  $\tau_{\text{col}} = 27\pi/128$ . Thus, the unitary evolution of the system reads now

$$\hat{U}(\tau_0) \simeq \exp(-i\hat{n}\Phi_0) \otimes \hat{\sigma}_{aa} + \exp(i\delta\tau_0 + i(\hat{n} + 1)\Phi_0) \otimes \hat{\sigma}_{bb}, \quad (4.14)$$

where we have introduced the phase  $\Phi_0 = \mathcal{K}_0^2\tau_{\text{col}}/\delta$ . Since the validity of the dispersive regime relies on perturbation theory, transition probabilities between different nearly time independent adiabatic states shall automatically be negligibly small. To be more specific, if the system is initially prepared in the uncoupled state  $|n, -\rangle \simeq |n-1, b\rangle$ , the transition probability to a neighboring state  $|n, +\rangle \simeq |n, a\rangle$  shall be proportional to the absolute square of the Fourier transform of the interaction amplitude, evaluated at the frequency mismatch  $\delta$ . Then from the uncertainty relation for Fourier transforms, we estimate that these non-adiabatic transitions are smothered out for values of the detuning larger than the inverse of the time duration of the collision, that is, for  $|\delta| \gtrsim |\mathbf{v}_0|/D_0$ . Thus, for a sufficiently slow atom,



non adiabatic transitions will be suppressed, guaranteeing the constancy of the phonon number during the entire motion of the atom. Next, we will analyze a scheme that enables a quantum nondemolition measurement of the phonon number observable via the observation of the atomic coherence between the two Rydberg levels  $|b\rangle$  and  $|a\rangle$ . The method in question was originally developed in the context of quantum cavity electrodynamics [94] and led Haroche, together with his group, to win the Nobel prize award in 2012 [174]. The prize was shared with Wineland, who achieved similar results with his collaborators from experiments with trapped ions [175].

### 4.3 Quantum non demolition measurement of torsional mechanical excitation quanta

The time dynamics governed by (4.14) leads to energy phase shifts proportional to the phonon number, which are conditioned by the electronic state of the atom. That is, it generates a correlation between the eigenstates of the phonon number observable and the energies of the Rydberg states  $|a\rangle$  and  $|b\rangle$  of the atom. Then, in the dispersive regime, by observing the energy state of the atom we may reduce any (low energy) state<sup>2</sup> of the torsional oscillator to an eigenstate of the phonon number observable, and thus realize an accurate measurement of the phonon number. A projective measurement onto an eigenstate of an observable is said quantum non-demolition (QND) if such observable commutes with the system Hamiltonian. Therefore, since the phonon number observable is, under the unitary evolution (4.14), a constant of the motion, this measurement would also be quantum non-demolition. [176, 177, 178]. To determine the energy state of the atom we will use Ramsey interferometry [179].

#### 4.3.1 Ramsey interferometry

Ramsey interferometry enables us to measure the phase difference between two Rydberg levels  $|a\rangle$  and  $|b\rangle$  of an atom, and is therefore sensitive to a phase modulation of the atomic levels  $|a\rangle$  and  $|b\rangle$ . Since the phase modulations that these levels undergo during the unitary time evolution (4.14) are proportional to the phonon number of our torsional oscillator, a Ramsey measurement may serve us for the monitoring of the phonon number observable.

To implement a single interferometric measurement we subject an atom in uniform motion with position vector  $\mathbf{R}_0(t)$  and constant velocity  $\mathbf{v}_0$  to a sequence of two identical microwave pulses (mw), as we depict in figure 4.4. We confine and apply the two mw pulses in the zones  $R_1$  and  $R_2$ . And we assume that the atom interacts with the torsion pendulum only during the time period  $\tau_0 = L/|\mathbf{v}_0|$ , which is the time of flight of the atom

---

<sup>2</sup> The linearity of the phaseshift with the phonon number works only for low energy oscillator states, that is, for average phonon numbers  $\langle \hat{n} \rangle \lesssim \delta^2 / \mathcal{K}_0^2$ .

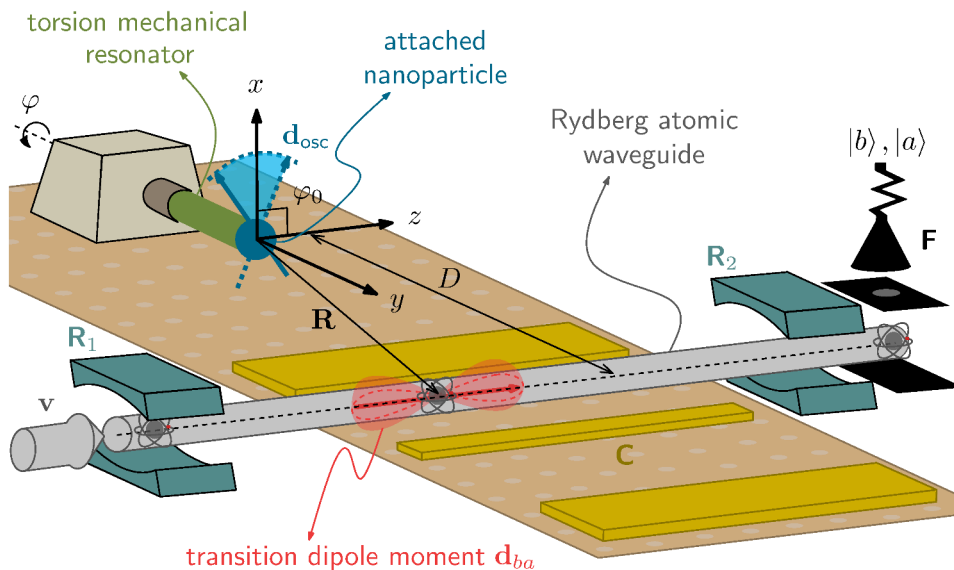


**Figure 4.4** Schematic of the coupled Rydberg atomic wave-guide (grey) and torsion mechanical oscillator (green). The beam passes the oscillator with impact parameter  $D$  and velocity  $v$ . Oscillations of the torsion angle  $\varphi$  modulate the interaction between the permanent electric moment  $\mathbf{d}_{\text{osc}}$  of a ferroelectric load (blue) and the transition dipole moment  $\mathbf{d}_{ba}$  involving atomic Rydberg states  $|b\rangle$  and  $|a\rangle$ . While a train of atoms interacts one-by-one with the oscillator, the states incur a phase-shift dependent on the state of the oscillator. This shift is interferometrically read out using microwave  $\pi/2$ -pulses in regions  $R_{1/2}$  and state detection in F. Quantum coherent manipulation of the oscillator for quantum tomography uses additional external driving of the atoms through a coplanar microwave waveguide in region C.

along the distance of length  $L$  that separates the centers of the two zones  $R_1$  and  $R_2$ . For this assumption to be valid we shall use pulses with temporal length  $\tau_{\text{mw}} \ll D_0/|\mathbf{v}_0|$ , i.e., much shorter than the duration of the effective collision between the atom and the torsion pendulum. This allows us to ignore interactions between the atom and the mechanical oscillator across the locations  $R_1$  and  $R_2$ . In this way, we use each pulse just to drive the atom into an equally weight superposition of the states  $|a\rangle$  and  $|b\rangle$ . We model this operation by using a unitary transformation  $\hat{A}_{\pi/2}(\phi)$ , the matrix form of which, in the basis  $\{|a\rangle, |b\rangle\}$ , reads (see Appendix B.4)

$$A_{\pi/2}(\phi) = \frac{1}{\sqrt{2}} \begin{bmatrix} 1 & e^{i\phi} \\ -e^{-i\phi} & 1 \end{bmatrix}. \quad (4.15)$$

This matrix represents a so called  $\pi/2$ -rotation with a phase  $\phi$  that in practice can be controlled by tuning the microwave pulse<sup>3</sup>. To simplify matters, we work in an interaction picture with respect to the Hamiltonian (4.2) with the frequency of the mw pulses chosen to be equal to  $\omega_{\text{osc}}$ . Then, the unitary evolution of the total system of atom plus torsion

<sup>3</sup> Note that this  $\pi/2$ -pulse could be achieved without additional microwave cavities, but microwave fields should not directly affect the oscillator.

pendulum across the interferometer may be written as

$$\hat{U}_{\text{RM}}(\tau_0, \phi) = \hat{A}_{\pi/2}(\phi_2 = \phi) \hat{U}(\tau_0) \hat{A}_{\pi/2}(\phi_1 = \pi), \quad (4.16)$$

where the operator  $\hat{U}$  is the unitary evolution (4.14) of the system dynamics in the course of the collisional process between the Rydberg atom and the torsional oscillator given in section 4.2.2.

In every single Ramsey measurement, we assume that atom and mechanical resonator states are initially uncorrelated. Before the atom enters the interferometer we prepare it in the Rydberg state  $|a\rangle$ , so that if  $\hat{\rho}_0$  denotes the initial density operator of the mechanical resonator, the initial density operator of the Rydberg atom plus resonator compound reads  $\hat{\rho}_0 \otimes \hat{\sigma}_{aa}$ . After the atom leaves the interferometer the dynamics of the mechanical oscillator and that of the Rydberg atom becomes correlated, evolving into the joint state

$$\begin{aligned} \hat{U}_{\text{RM}}(\tau_0, \phi) [\hat{\rho}_0 \otimes \hat{\sigma}_{aa}] \hat{U}_{\text{RM}}^\dagger(\tau_0, \phi) &= \hat{\mathcal{M}}_a(\tau_0, \phi) \hat{\rho}_0 \hat{\mathcal{M}}_a^\dagger(\tau_0, \phi) \otimes \hat{\sigma}_{aa} + \hat{\mathcal{M}}_b(\tau_0, \phi) \hat{\rho}_0 \hat{\mathcal{M}}_b^\dagger(\tau_0, \phi) \otimes \hat{\sigma}_{bb} \\ &+ \hat{\mathcal{M}}_a(\tau_0, \phi) \hat{\rho}_0 \hat{\mathcal{M}}_b^\dagger(\tau_0, \phi) \otimes \hat{\sigma}_{ab} + \hat{\mathcal{M}}_b(\tau_0, \phi) \hat{\rho}_0 \hat{\mathcal{M}}_a^\dagger(\tau_0, \phi) \otimes \hat{\sigma}_{ba}, \end{aligned} \quad (4.17)$$

where the  $\hat{\mathcal{M}}_\mu$ , with  $\mu \in \{a, b\}$ , are measurement or Kraus operators [180] that apply only to the oscillator state and are determined from the unitary evolution  $\hat{U}$  and the initial state  $|a\rangle$  of the Rydberg atom (see below). After the pulse sequence the atom reaches a state recorder at F, where its electronic state is projected into one of the states  $|\mu\rangle$  with probabilities  $P_\mu = \text{tr}[\hat{\mathcal{M}}_\mu \hat{\rho}_0 \hat{\mathcal{M}}_\mu^\dagger]$ . We use  $\hat{A}_{\pi/2}(\phi_1 = \pi)$  in region R<sub>1</sub> and choose the phase of  $\hat{A}_{\pi/2}(\phi)$  in region R<sub>2</sub> to ensure that  $P_b$  equals zero when the mechanical oscillator mode is in its ground state. Then, except for an irrelevant phase factor, the Kraus operators above read explicitly

$$\hat{\mathcal{M}}_a(\tau_0, \phi) \equiv \hat{\mathcal{M}}_+(\tau_0, \phi) = \frac{1}{2} \left[ \exp \left( i\delta\tau_0/2 + i[\hat{n} + 1/2]\Phi_0 + i\phi/2 \right) + \text{h. c.} \right], \quad (4.18)$$

$$\hat{\mathcal{M}}_b(\tau_0, \phi) \equiv \hat{\mathcal{M}}_-(\tau_0, \phi) = \frac{1}{2} \left[ \exp \left( i\delta\tau_0/2 + i[\hat{n} + 1/2]\Phi_0 + i\phi/2 \right) - \text{h. c.} \right]. \quad (4.19)$$

Once the Rydberg atom hits the detector at F the atom is lost. If we assume an instantaneous detection event, then the (normalized) quantum state of the torsional oscillator reduces into one of the next two possibilities

$$\hat{\rho}_{\bar{\mu}} = \hat{\mathcal{M}}_{\bar{\mu}}(\tau_0, \phi) \hat{\rho}_0 \hat{\mathcal{M}}_{\bar{\mu}}^\dagger(\tau_0, \phi) / P_{\bar{\mu}}, \quad (4.20)$$

with  $\bar{\mu} \in \{\pm\}$ . Equation (4.20) constitutes the outcome of what is commonly known as positive operator-valued measure (POVM) [181].

The resulting signals of the probabilities  $P_a \equiv P_+$  and  $P_b \equiv P_-$  yield fringes oscillating with the phase difference between  $|b\rangle$  and  $|a\rangle$ :

$$P_\pm = \frac{1}{2} \pm \frac{1}{2} \text{tr} \left[ \cos(\delta\tau_0 + [2\hat{n} + 1]\Phi_0 + \phi) \hat{\rho}_0 \right], \quad (4.21)$$

from which we recognize that the adjustable phase shall be tuned to  $\phi = -\delta\tau_0 - \Phi_0$ , so that the probability  $P_-$  will vanish when the torsion pendulum is in its ground state.

To resolve a maximum of  $n_0$  phonons we can adjust the phaseshift  $2\Phi_0 = 2\mathcal{K}_0^2\tau_{\text{col}}/\delta$  according to  $2\Phi_0 = \pi/n_0$ . This enables the construction of a one-to-one correspondence between the values of the phonon number within the range  $n = 0, 1, \dots, n_0$ , and the experimentally observable values of the associated atomic probabilities  $P_{\pm}$ . The result is an effective monitoring of the phonon number operator, and thus a direct proof of the discrete nature of the energy spectrum of our torsional oscillator. In the next section we explain the details and limitations of this QND measurement.

### 4.3.2 Projecting the quantum state of motion of a torsion pendulum onto a phonon number eigenstate

We are interested in illustrating measurements of phonon numbers corresponding to quantum states the energy of which is very close to that of the quantum ground state of motion of the torsional oscillator. Thus, we choose  $n_0 = 5$  and set  $2\Phi_0 = \pi/n_0$ , just as we have explained at the end of the section 4.3.1 above. This allows us to associate every different outcome of the population difference  $\mathcal{P}$  between levels  $|a\rangle$  and  $|b\rangle$  with a single value of the phonon number observable in the interval  $0, 1, \dots, n_0 = 5$ . The population difference  $\mathcal{P}$  is an experimentally measurable quantity defined as

$$\mathcal{P} = P_+ - P_- = \text{tr} [\cos(2\hat{n}\Phi_0)\hat{q}_0]. \quad (4.22)$$

Here, we have explicitly replaced the auxiliary phase by  $\phi = -\delta\tau_0 - \Phi_0$ . An experiment that performs a series of Ramsey interference measurements, starting with the torsional oscillator in a Fock state  $|n\rangle$ , can serve to determine the outcome of  $\mathcal{P}$ , and hence the eigenvalue  $n$  of the phonon number operator in the corresponding Fock state  $|n\rangle$ . This is possible because a Fock state is an eigenstate of the phonon number operator, in which case is  $\langle\hat{n}\rangle \equiv n$ . In such a case, the initial quantum state of motion of the torsion pendulum is such that  $\langle n|\hat{q}_0|n'\rangle = \delta_{nn'}$ , and it will remain exactly the same either after the detection of the first atom or of an arbitrarily large number of them in the given series, since  $[\hat{\mathcal{M}}_{\pm}, |n\rangle\langle n|] = [\hat{\mathcal{M}}_{\pm}^{\dagger}, |n\rangle\langle n|] = 0$ , which implies that  $\hat{q}_{\pm} = \hat{\mathcal{M}}_{\pm}\hat{\mathcal{M}}_{\pm}^{\dagger}|n\rangle\langle n|/\|\hat{\mathcal{M}}_{\pm}^{\dagger}|n\rangle\|^2$ , and thus  $\langle n|\hat{q}_{\pm}|n'\rangle = \delta_{nn'}$ . If we cannot design an experiment that initializes the torsional oscillator into a Fock state, we actually may drive an arbitrary oscillator state into a Fock state through the detection of a few atoms in a series of Ramsey measurements. The original phonon distribution eventually peaks into a single phonon number state as long as its domain falls within a range of phonon numbers that allows to allocate a different value of the atomic probabilities  $P_{\pm}$  to each phonon number in such domain. That is to say, in order for the oscillator state to collapse into a Fock state, there cannot exist a value of the atomic probabilities  $P_{\pm}$  that repeats for any two distinct phonon numbers in the domain of the initial phonon distribution.

This is argued in very detailed mathematical terms in references [182, 183], and it has also been corroborated in the experiments of reference [166]. The interested reader may also consult the Appendix B.5, wherein we provide a numerical test of this fact using two different phonon distributions. Another interesting feature worth mentioning, is that this

### 4.3.2 Projecting the quantum state of motion of a torsion pendulum onto a phonon number eigenstate

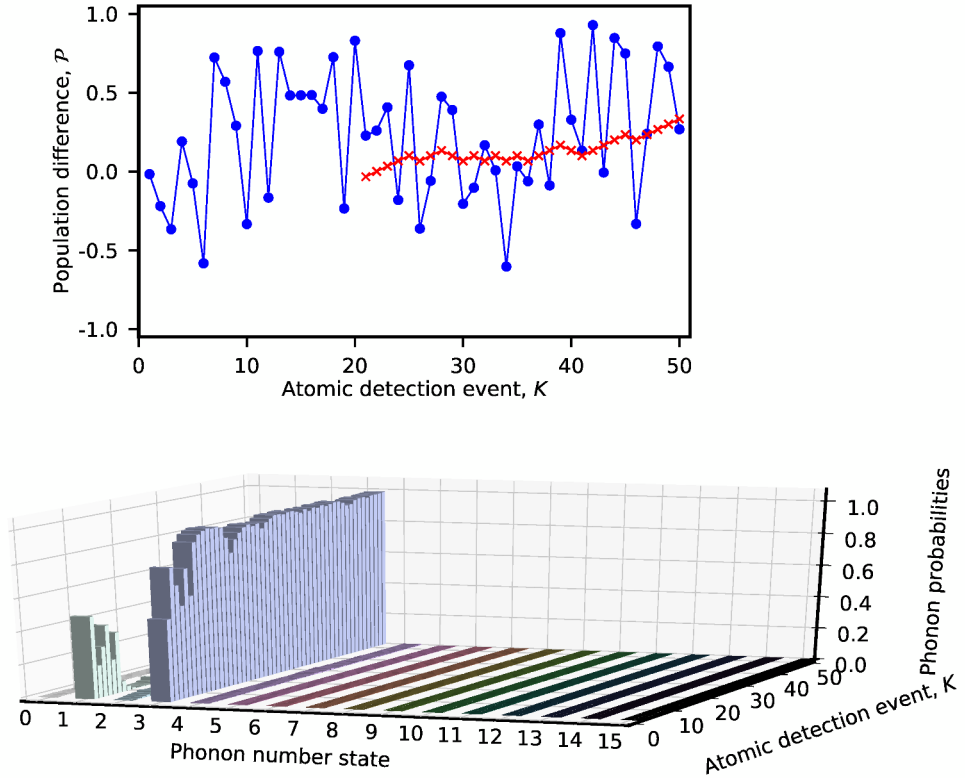


**Figure 4.5** Gradual collapse of the mechanical oscillator state  $|\Psi_0\rangle = [|1\rangle + |3\rangle]/\sqrt{2}$  into an eigenstate of the phonon number observable after a series of  $K = 50$  Ramsey measurements. (Top) The population difference  $\mathcal{P}$  (blue) converges close to its exact value associated to the phonon number  $n = 3$  at the end of the series. (Red x) values of the population difference obtained by tracking the number of times an atom is measured in the states  $|a\rangle$  and  $|b\rangle$  relative to the total number  $K$  of atomic samples. (Bottom) phonon probabilities evolving towards the Fock state with  $n = 3$ .

collapse of the mechanical oscillator into a Fock state will generally take place at a faster pace if we engineer the phase shift  $\Phi_0$  to be a random quantity (see [183] for a detailed discussion). Later on in section 4.4.2 we will explain how we may achieve a fluctuating phase shift by considering initial position and velocity uncertainties of the guided atoms traversing the interferometer. Let us focus now on figure 4.5. There, we show the outcome of a numerical simulation of a sequential projection of the mechanical oscillator state into a Fock state using a series of detection atoms with such a randomized set of initial atomic conditions and taking into account the decoherence processes that we list in section 4.4.1 (details regarding the numerical simulations are found in section 4.4). In the lower panel of the figure we observe the evolution of the phonon probability distribution of the initial mechanical oscillator state  $\hat{\rho}_0 = |\Psi_0\rangle\langle\Psi_0|$ , with  $|\Psi_0\rangle = [|1\rangle + |3\rangle]/\sqrt{2}$ , in the course of a succession of  $K = 50$  consecutive Ramsey measurement events. Every time we measure an atom in the basis  $\{|+\rangle \equiv |a\rangle, |-\rangle \equiv |b\rangle\}$ , we reallocate the mechanical oscillator state into a reduced subspace of Fock states. This constitutes a weak measurement [112] of the phonon number. Several of these weak measurements then leads to a projective measurement of the phonon number observable resulting in  $n = 3$  for a Fock state  $|3\rangle$  of the mechanical oscillator.

At this point, the remaining detection events in the series reproduce a similar result, which allows us to estimate the probabilities  $P_{\pm}$  to check that they tend to the value associated with a mechanical oscillator in  $|3\rangle$  as we approach the end of the series of the  $K = 50$  measurements. This can be seen in the top panel of the figure, where we plot the population difference  $\mathcal{P}$  as a function of  $K$ . The data in blue refer to the values of  $\mathcal{P} = P_+ - P_-$  when we compute the probabilities from the numerical solution of  $\hat{\rho}$  as  $P_{\pm} = \text{tr}[\hat{\mathbb{1}}_{\text{osc}} \otimes |\pm\rangle\langle\pm| \hat{\rho}]$ , with  $\hat{\mathbb{1}}_{\text{osc}}$  being the identity operator on the mechanical oscillator's Hilbert space. The data in red are counterpart values of  $\mathcal{P}$  that we obtain in this case by keeping track of the quantity  $\mathcal{C}_{\pm}$ , which designates the number of times that an atom is measured in the states  $|\pm\rangle$  after the initial phonon distribution has peaked into a single phonon number during a series of  $K$  measurements. This typically occurs after a few  $i_c \sim 10$  measurements,  $i_c < K$ . Then the probabilities can be alternatively computed as  $P_{\pm} = \mathcal{C}_{\pm}/(K - i_c)$ .

## 4.4 Simulation of Ramsey measurement series subject to decoherence and statistical noise

To attain a sequential collapse of the mechanical oscillator state into a Fock state we numerically solve the dynamics of the density operator  $\hat{\rho}$  of the full system of a single atom plus mechanical oscillator. We take into account decoherence sources to explore the practical limitations arising through the vicinity of a micro-chip surface and the Rydberg atom waveguide. In addition, we will address statistical errors that may manifest as a consequence of the finite spread of the atoms in the waveguide.

### 4.4.1 Decoherence

As stated in section 4.3.1, every Ramsey sequence starts with the uncorrelated state  $\hat{\rho}_0 \otimes \hat{\sigma}_{aa}$ , and we work in a frame rotating with the oscillator frequency. The microwave pulses in the regions  $R_1$  and  $R_2$  are thought to act onto the atom fast enough so that we may neglect any decoherence effects therein, and therefore they are emulated via an instantaneous application of the operator  $\hat{A}_{\pi/2}(\phi)$  defined in equation (4.15). During the fly-by of the atom between  $R_1$  and  $R_2$ , we evolve the system state by means of a Lindblad master equation

$$\frac{\partial}{\partial t} \hat{\rho}(t) = -\frac{i}{\hbar} [\hat{H}(t), \hat{\rho}(t)] + \mathcal{L}_{\text{th}}[\hat{\rho}(t)] + \mathcal{L}_{\text{bbr}}[\hat{\rho}(t)] + \mathcal{L}_{\text{deph}}[\hat{\rho}(t)]. \quad (4.23)$$

The Hamiltonian is time dependent due to the classical motion of the atom in the waveguide, given by the uniform trajectory  $\mathbf{R}_0(t) = \mathbf{R}_0(0) + \mathbf{v}_0 t$ . The three linear maps  $\mathcal{L}_{\text{th}}$ ,  $\mathcal{L}_{\text{bbr}}$  and  $\mathcal{L}_{\text{deph}}$  acting on  $\hat{\rho}$  in equation (4.23) describe all the relevant decoherence sources that we consider in our setup. Thus, the term

$$\begin{aligned} \mathcal{L}_{\text{th}}[\hat{\rho}(t)] = & \frac{\Gamma_{\text{osc}}}{2} [\bar{n}_T(\omega_{\text{osc}}) + 1] [2\hat{c}\hat{\rho}(t)\hat{c}^\dagger - \hat{c}^\dagger\hat{c}\hat{\rho}(t) - \hat{\rho}(t)\hat{c}^\dagger\hat{c}] \\ & + \frac{\Gamma_{\text{osc}}}{2} \bar{n}_T(\omega_{\text{osc}}) [2\hat{c}^\dagger\hat{\rho}(t)\hat{c} - \hat{c}\hat{c}^\dagger\hat{\rho}(t) - \hat{\rho}(t)\hat{c}\hat{c}^\dagger] \end{aligned} \quad (4.24)$$

models the decay of mechanical oscillator states due to their weak coupling to a heat bath equilibrated at temperature  $T = 25$  mK, where  $\bar{n}_T(\omega) = (\exp[\hbar\omega/(k_B T)] - 1)^{-1}$  is the thermal occupation number with  $k_B$  being the Boltzmann constant, and  $\Gamma_{\text{osc}}/(2\pi) = 50$  Hz is the mechanical energy damping rate for a given quality factor  $Q = \omega_{\text{osc}}/\Gamma_{\text{osc}}$  of the mechanical oscillator<sup>4</sup>.

As far as the atom is concerned, we assume that the Rydberg states  $|a\rangle$  and  $|b\rangle$  undergo pure relaxation due to black body radiation induced transitions between them, which we capture with another Lindblad term

$$\mathcal{L}_{\text{bbbr}}[\hat{\rho}(t)] = \frac{\Gamma_{\text{bbbr}}}{2} \sum_{\mu \neq \mu'} [2\hat{\sigma}_{\mu\mu'}\hat{\rho}(t)\hat{\sigma}_{\mu'\mu} - \hat{\sigma}_{\mu'\mu'}\hat{\rho}(t) - \hat{\rho}(t)\hat{\sigma}_{\mu'\mu'}], \quad (4.25)$$

where  $\Gamma_{\text{bbbr}}$  is the black-body radiation transition rate and the summation indices  $\mu, \mu' \in \{a, b\}$ . we employ  $\Gamma_{\text{bbbr}}/(2\pi) = 988.63$ Hz, determined following [184].

Likewise, we consider that Rydberg states are subject to pure dephasing due to stray electric fields from the bearing surface of the mechanical oscillator. We take this effect into account through the last linear map appearing in equation (4.23), which yields

$$\mathcal{L}_{\text{deph}}[\hat{\rho}(t)] = \frac{\Gamma_{\text{deph}}}{2} \sum_{\mu \in \{a, b\}} [2\hat{\sigma}_{\mu\mu}\hat{\rho}(t)\hat{\sigma}_{\mu\mu} - \hat{\sigma}_{\mu\mu}\hat{\rho}(t) - \hat{\rho}(t)\hat{\sigma}_{\mu\mu}], \quad (4.26)$$

where  $\Gamma_{\text{deph}}$  is the dephasing rate. The latter effect, a major challenge for Rydberg atom quantum technologies near solid state surfaces, has been steadily reduced [185, 68]. We employ  $\Gamma_{\text{deph}}/(2\pi) = 1.50$  kHz, the same order of magnitude as reported in [68].

Of crucial importance for modelling the experimental sequence is the final atom state detection at F. We assume that detection events are uncorrelated and that every atom is successfully detected in either of the two states  $|a\rangle$  or  $|b\rangle$ , i.e., there is no atom loss. Likewise, we neglect any decoherence processes while an atom is detected and during the time a new atom is launched into the interferometer. To carry out this measurement numerically, we compare a pseudorandom number  $\eta$ , drawn from a standard uniform distribution, with the probability  $P_b = \text{tr}[\hat{\sigma}_{bb}\hat{\rho}]$  that the atom is found in  $|b\rangle$ . The output of the measurement is  $\hat{\sigma}_{aa}\hat{\rho}\hat{\sigma}_{aa}/[1 - P_b]$  if  $P_b < \eta$  and  $\hat{\sigma}_{bb}\hat{\rho}\hat{\sigma}_{bb}/P_b$  otherwise, thus collapsing the state onto  $|a\rangle$  or  $|b\rangle$  in the subspace of the atom [186].

Finally, in view of both, its help for accelerating the mechanical oscillator state collapse and of being an inherent feature while coping with an experimental realization of the setup, we will also take into consideration a finite spread of the interrogating atomic beam across the waveguide.

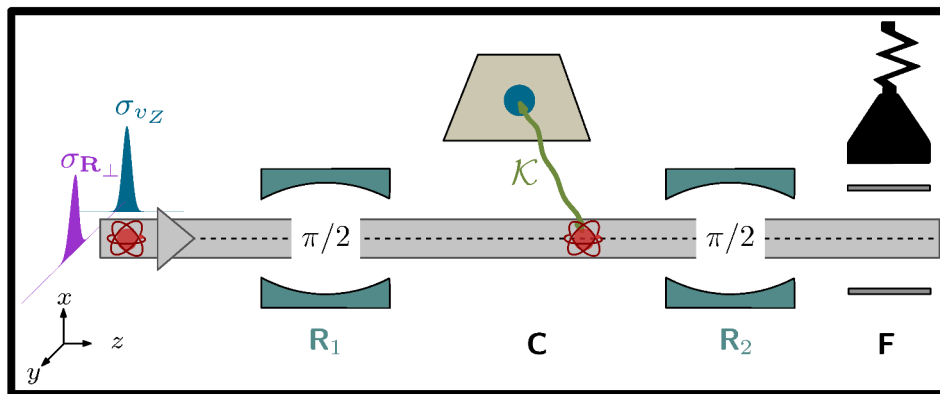


**Figure 4.6** Sketch map of a simulated Ramsey measurement sequence. The finite widths of the atomic beam in the waveguide (grey beam) are modeled by using uniform probability distributions that describe the initial longitudinal velocity spread  $\sigma_{v_z}$  (blue) of an atom along the beam axis and the initial spatial spread  $\sigma_{R_\perp} = \sigma_X = \sigma_Y$  (violet) of the atom in a plane perpendicular to the beam axis. The Rydberg atom experiences  $\pi/2$  pulses in zones  $R_1$  and  $R_2$  and a coupling  $\mathcal{K}$  with the torsional mechanical oscillator in region  $C$  before its electronic state is measured at  $F$ .

#### 4.4.2 Guided atomic motion with initial position and momentum spreads. Statistical averages

We describe the width of the interrogating atomic beam across the waveguide through a random distribution of initial atomic positions in a plane transverse to the beam axis and a random distribution of initial coaxial atomic velocities, see figure 4.6. We set transverse atomic velocities to zero in accordance with the confinement of the atoms in the waveguide [187, 188]. The fact that each detection event involves an atom  $k$ ,  $k \in \mathbb{N}^+$ , with randomized initial coordinate vector  $\mathbf{R}_k(0) = [X_k(0), Y_k(0), Z_0(0)]^T$  and velocity  $\mathbf{v}_k = [0, 0, v_{Z_k}]^T$  affects the probabilities of the measurement outcomes of every physical observable. This is because each atomic detection leads to a slightly different Hamiltonian (recall that the later depends on  $\mathbf{R}_k(t) = \mathbf{R}_k(0) + \mathbf{v}_k t$ ). Note, however, that every atomic trajectory evolves independently from the others. Therefore, the probabilities to be contrasted with an experiment shall be the result of a statistical average of its counterpart values obtained from considering separate time evolutions. To numerically address the problem, we start by identifying a sample of our statistical ensemble of atomic detection events with a series of  $K$  Ramsey measurements, whereas a single atomic detection event is recognized as a sample unit. Then, we obtain the average probabilities for the measurement outcomes of a given observable operator  $\hat{O}$  by solving the master equation (4.23) for many sample units, each sample unit evaluated for a set of discrete values accounting for the initial location  $\mathbf{R}_k(0)$  and initial velocity  $\mathbf{v}_k$  of the atom. If  $\mathbb{P}_{o,j}$  denotes the probability of the measurement outcome  $o$  of  $\hat{O}$  in

4 This rather low oscillator decoherence rate are required by the slow measurement chosen here. Higher values could be dealt with by a higher launching rate of atoms into the interferometer.



the sample  $j$ , its corresponding statistical average in an experiment involving  $N_s$  samples is

$$\bar{\mathbb{P}}_o = \frac{1}{N_s} \sum_{j=1}^{N_s} \mathbb{P}_{o,j}. \quad (4.27)$$

To evaluate statistical averages the initial transverse location  $\mathbf{R}_{\perp,k}(0) = [X_k(0), Y_k(0)]^T$  and the coaxial velocity  $v_{Z_k}$  of the atom are both drawn from gaussian distributions with mean values  $\mathbf{R}_{\perp,0}$  and  $v_{Z_0}$ , respectively. The covariances of both distributions are diagonal with diagonal entries given by  $\sigma_X$  and  $\sigma_Y$  for the case of the spatial distribution, and by  $\sigma_{v_z}$  for the case of the velocity distribution. The widths  $\sigma_X = \sigma_Y = \sigma_{\mathbf{R}_{\perp}}$  in the position plane transverse to the beam and  $\sigma_{v_z}$  in the velocity along the beam, are chosen to mimic the relevant uncertainties for a beam of atoms travelling within a very tight waveguide. Finally, in order to run the simulations with a fixed interferometer length while taking into account the effects of dealing with different atomic speeds, we translate the distribution of initial velocities  $\mathbf{v}_k$  into a distribution of time of flights  $\tau_k$  via the relation  $\tau_k = \tau_0 |\mathbf{v}_0| / |\mathbf{v}_k|$ .

#### 4.4.3 Averaged atomic probabilities $P_{\pm}$ and phonon statistics

For a mechanical oscillator initially prepared in a Fock state a sequence of QND measurements using atoms can yield the probabilities  $P_{\pm}$ . Numerically, we can model an experimental sequence of this type by following the steps of the previous sections 4.4.1 and 4.4.2. The observables that we may measure are  $|\pm\rangle\langle\pm|$  and the statistical average is over sample probabilities  $P_{\pm,j} = \mathcal{C}_{\pm,j} / (K - i_c)$ , where  $j$  is the index that labels the sample. As before,  $\mathcal{C}_{\pm,j}$  is a frequency count for detection events in states  $|\pm\rangle$  of sample  $j$ , while  $K$  is the total number of atoms used in a sequence or series of measurements and  $i_c$  is the number of atoms detected in the series until the mechanical oscillator state to collapse into a Fock state.

Measurement sequences are meaningful for a given range of phonon numbers as long as the outcomes of  $\mathcal{P}$  for adjacent Fock states can be distinguished from each other. This is the case of the example that we show in figure 4.7, wherein we evaluate  $\mathcal{P}$  for initial oscillator states  $\hat{q}_0 = |n \leq n_0\rangle\langle n \leq n_0|$ , such that the horizontal axis spans a range of phonon numbers  $0, 1, \dots, n_0 = 5$ . The set of blue data results from considering an ideal scenario in which every single atom travels along the waveguide centre. In this case a single sample is enough to reproduce the outcomes of  $\mathcal{P}$  for every initial Fock state of the oscillator. The red data are the result of averaging  $\mathcal{P}_j = P_{+,j} - P_{-,j}$  over the distributions of initial transverse positions and initial coaxial velocity of the atomic beam in the waveguide, using a total of  $N_s = 512$  samples. That average is  $\bar{\mathcal{P}} = 1/N_s \sum_{j=1}^{N_s} \mathcal{P}_j$ . The error bars are the statistical standard deviation.

Note that the broader we choose the range of phonon numbers, the harder does it get to resolve each eigenvalue  $n$ , because different values of the probabilities  $P_{\pm}$  for adjacent eigenvalues of  $\hat{n}$  turn closer and closer for increasing  $n$ , and eventually saturate for  $n \sim \delta^2 / \mathcal{K}_0^2$ .

If the initial target state  $\hat{q}_0$  of the oscillator is not a Fock state, a sequence of measurements initially quickly collapses it into one, say  $|n\rangle$ , with probability  $q_{0nn} = \text{tr}[|n\rangle\langle n| \hat{q}_0]$ . Indeed,

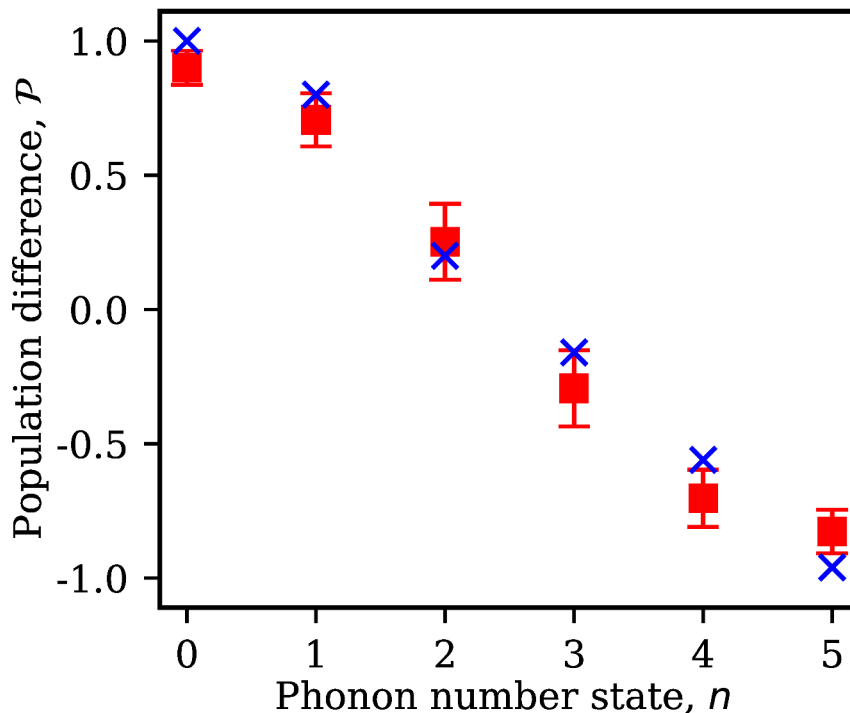


**Figure 4.7** Population difference  $\mathcal{P}$ , between Rydberg levels  $|b\rangle$  and  $|a\rangle$ , as a function of phonon number eigenvalues  $n$ . (Blue x) ideal values for an atom traveling across the waveguide center, (red square areas and error bars) average and root mean square deviation accounting for the finite spatial and velocity widths of an atomic beam in the waveguide. Red data include as well decoherence.

just as we showed in figure 4.5, after the detection of  $K \sim 43$  atoms typically all but one of the phonon probabilities are depopulated, such that the final phonon distribution  $p_n$  is nearly equal to that of a Fock state,  $p_n \simeq \delta_{nn'}$ , with  $\delta_{nn'}$  being the Kronecker delta and  $n'$  a positive integer, the final phonon number. The mechanical oscillator is then assumed to have collapsed into the *a priori* unknown Fock state  $|n'\rangle$ . In the theory, we can directly extract the phonon distribution  $p_{n,j}$  of sample  $j$  from the simulation, repeat the process multiple times and thus extract the entire phonon distribution after averaging over all the  $N_s$  samples,  $\bar{p}_n = 1/N_s \sum_{j=1}^{N_s} p_{n,j}$ . We call this approach “Method A”. However, an experiment would not have access to  $p_{n,j}$  directly, instead it would extract the probabilities  $P_{\pm,j}$  from the measurement results of the  $K$  probing atoms. Using figure 4.7, these can then be translated into Fock state distributions  $p_{n,j}$ , but this translation may be subject to different error sources. We also extract a second value of  $\bar{p}_n$  from the simulation in this manner, called “Method B”.

In figure 4.8 we compare the exact phonon distribution (green histogram) of an initial coherent state  $\hat{\rho}_0 = |\alpha\rangle\langle\alpha|$  of the mechanical oscillator with amplitude  $\alpha = \sqrt{2}$  against a reconstructed version of it (red horizontal segments) as obtained from the statistics of “Method A” using  $N_s = 512$  samples. We will offer a test of “Method B” in section 4.5, where we exploit further the capabilities of the Rydberg atom probes in a next step towards a measurement of the full state of the mechanical oscillator.

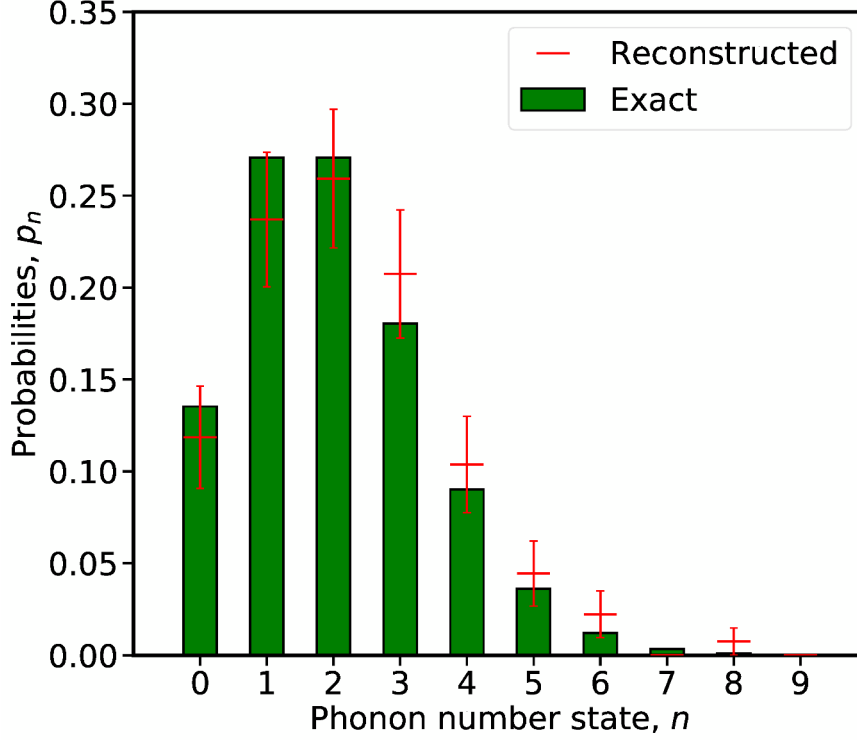


**Figure 4.8** Phonon probabilities corresponding to a mechanical oscillator in a coherent state  $|\alpha\rangle$  with amplitude  $\alpha = \sqrt{2}$ . Green bars display the exact probability distribution, whereas red horizontal lines account for the inferred phonon probabilities. The error bars (red vertical lines) are the standard statistical deviation.

Before embarking into the task of reconstructing the full quantum state of motion of the mechanical oscillator we provide and discuss next the values of the system parameters that enable the good agreement between the exact and the reconstructed phonon distributions shown in figure 4.8.

#### 4.4.4 System design and parameter choices

The choice of the values of the system parameters is dictated by a few requirements that are important for the realization of a QND readout of the phonon observable through a series of Ramsey measurements:

- A fulfillment of a rotating wave approximation so that the original interaction Hamiltonian  $\hat{H}_{\text{int}}$  can be reduced into a Jaynes Cummings Hamiltonian. This demands that  $\mathcal{K}_0 \ll \omega_{ba}, \omega_{\text{osc}}$ .
- A large interferometer length to impact parameter ratio  $L/D_0 = |\mathbf{v}_0|\tau_0/D_0 > 1$  to ensure a constant collision time  $\tau_{\text{col}}$ .
- An atom (mass  $m$ ) with an initial kinetic energy  $m|\mathbf{v}_0|^2/2$ , considerably higher than  $\hbar\mathcal{K}_0, \hbar\delta, \hbar\Omega$ , i.e., than the interaction energy of the atom with both the permanent

#### 4.4 Simulation of Ramsey measurement series subject to decoherence and statistical noise

**Table 4.1** Parameters used for our simulations underlying figures 4.7, 4.8, 4.9, 4.10 and 4.12 of the main text.

Atomic system (Rubidium, $^{87}\text{Rb}$ )	Symbol	Value	Unit
Mass	$M$	$1.44 \times 10^{-25}$	kg
Initial atom position	$\mathbf{R}_0(0) = [X_0(0), Y_0(0) = D_0, Z_0(0)]^T$	$[0.0, 21.675, -15.436]^T$	$\mu\text{m}$
Atomic spatial spread	$\sigma_X = \sigma_Y = \sigma_{\mathbf{R}_\perp}$	0.51	$\mu\text{m}$
Initial atom velocity:			
displacement sequence	$\mathbf{v}_0 = [v_{X_0}, v_{Y_0}, v_{Z_0}]^T$	$[0.0, 0.0, 14.0]^T$	$\text{m s}^{-1}$
measurement sequence	$\mathbf{v}_0 = [v_{X_0}, v_{Y_0}, v_{Z_0}]^T$	$[0.0, 0.0, 8.0]^T$	$\text{m s}^{-1}$
Atomic velocity spread	$\sigma_{v_Z}$	0.01	$\text{m s}^{-1}$
Principal quantum number	$\nu$	80	
Rydberg state basis	$\{ vL_J, m_J\rangle\}$	$\{ a\rangle =  80S_{1/2}, 1/2\rangle,  b\rangle =  80P_{1/2}, 1/2\rangle\}$	
Transition frequency ( $ b\rangle \leftrightarrow  a\rangle$ )	$\omega_{ba}/(2\pi)$	6835.81	MHz
Electric dipole moment strength	$d_{ba}$	$5.69 \times 10^{-26}$	C m
<b>Torsional mechanical oscillating mode</b>			
Torsional spring constant of the nanotube	$\kappa$	$2.085 \times 10^{-11}$	N m
Total moment of inertia with respect to the tube axis	$I$	$1.126 \times 10^{-32}$	$\text{kg}^2 \text{m}$
Permanent dipole moment strength of ferroelectric load	$d_{\text{osc}}$	$2.58 \times 10^{-20}$	C m
Frequency	$\omega_{\text{osc}}/(2\pi) = (2\pi)^{-1} \sqrt{\kappa/I}$	6848.69	MHz
Number state basis	$\{ n\rangle\}$	$\{ 0\rangle,  1\rangle, \dots,  15\rangle\}$	
Quality factor	$Q = \omega_{\text{osc}}/\Gamma_{\text{osc}}$	$1.37 \cdot 10^8$	
Heat bath temperature	$T_{\text{osc}}$	0.025	K
<b>Coupling and decoherence rates</b>			
Atom-oscillator coupling rate	$\mathcal{K}_0/(2\pi) = \frac{d_{ba}d_{\text{osc}}}{8\pi^2\epsilon_0 D^3} \frac{1}{\sqrt{2\hbar\omega_{\text{osc}}I}}$	0.64	MHz
Effective Rabi frequency	$\Omega_0/(2\pi)$	0.0 to 1.8	MHz
Mechanical damping rate	$\Gamma_{\text{osc}}/(2\pi)$	50.0	Hz
Pure relaxation rate due to black body radiation induced transitions ( $ b\rangle \leftrightarrow  a\rangle$ )	$\Gamma_{\text{bb}}/(2\pi)$	988.63	Hz
Pure dephasing rate of $ a\rangle$ and $ b\rangle$ levels due to noisy stray electric fields	$\Gamma_{\text{deph}}/(2\pi)$	1.50	kHz
<b>Protocol of state tomography</b>			
Dimensions (number of pixels) of the reconstructed Wigner function	$S \times S$	$11 \times 11$	
Number of atoms per displacement sequence to reach a given phase space pixel	$N$	8	
Number of atoms per measurement sequence to collapse oscillator into Fock state	$K$	43	
Number of repetitions (samples) of a displacement plus measurement sequence to obtain a set of phonon probabilities at a given pixel	$N_s$	512	
Atom-oscillator detuning	$ \delta /(2\pi) =  \omega_{\text{osc}} - \omega_{ba} /(2\pi)$	12.88	MHz
Passage time per atom in a displacement sequence	$\tau_{\text{disp}}$	2.205	$\mu\text{s}$
Passage time per atom in a measurement sequence	$\tau_{\text{meas}}$	3.859	$\mu\text{s}$

electric dipole of the torsion pendulum, and the microwave drive. In this regime the center of mass motion of the atom can be described classically and separately from the dynamics of its internal states [172].

- A strong coupling within the dispersive regime. For a measurable phase shift,  $n\Phi_0 = n\mathcal{K}_0^2\tau_{\text{col}}/\delta \sim \pi$ , we need an effective coupling constant,  $\mathcal{K}_0\sqrt{n}$ , the inverse of which is smaller than the time during which takes place the collision between the atom and the oscillator,  $\tau_{\text{col}} \sim |\mathbf{v}_0|/D_0$ . That is  $\tau_{\text{col}} > 1/(\mathcal{K}_0\sqrt{n})$ . This follows from the large detuning condition  $\delta > \mathcal{K}_0\sqrt{n}$ , which guarantees that the mechanical oscillator contains  $n$  phonons before and after an atom traverses the interferometer in a Ramsey measurement. This is an essential requirement for our QND detection scheme.
- An average fly-by time  $\tau_0$  of an atom across the interferometer that is short compared to the lifetimes of Rydberg states  $|a\rangle$  and  $|b\rangle$ , and short as well compared to the ring down time  $\sim 1/\Gamma_{\text{osc}}$  of the torsion pendulum.

Based on the above conditions we adjust all parameter values but the beam widths. For an estimate of the beam widths we demanded a relative uncertainty on the probabilities  $P_{\pm}$  of about 0.05 and then find corresponding values for the beam uncertainties through a propagation of error for equation (4.21) with the full phaseshift being replaced by its randomized counterpart. The estimate for the beam uncertainties is plausible<sup>5</sup> in experiments using atomic waveguides [187].

In our simulations, we then consider states  $|a\rangle = |\nu S_{1/2}, m_J = 1/2\rangle$  and  $|b\rangle = |\nu P_{1/2}, m_J = 1/2\rangle$  of  $^{87}\text{Rb}$  with principal quantum number  $\nu = 80$ . Their resonance frequency is  $\omega_{ba}/(2\pi) \simeq 6835.81$  MHz with transition dipole moment  $|\mathbf{d}_{ba}| \simeq 6711 ea_0$  (where  $e$  is the electron charge and  $a_0$  the Bohr radius). A 148.54 nm long and 75.79 nm wide CNT with a spherical ferroelectric load can yield a moment of inertia  $I \simeq 1.12 \times 10^{-32} \text{ kg}^2 \text{ m}$  with torsional oscillation frequency  $\omega_{\text{osc}}/(2\pi) \simeq 6848.69$  MHz (see Appendix B.1), and thus a small atom-oscillator detuning  $\delta/(2\pi) \simeq 12.88$  MHz. A dipole of strength  $|\mathbf{d}_{\text{osc}}| \simeq 3.04 \times 10^9 ea_0$  can be attached. We choose an impact parameter  $D_0 = 21.68 \mu\text{m}$ , and hence a coupling constant  $\mathcal{K}_0/(2\pi) = 0.64$  MHz. The transverse atomic waveguide widths are  $\sigma_X = \sigma_Y = 0.51 \mu\text{m}$ . The standard deviation of the longitudinal (on-axis) atomic velocity is  $\sigma_{v_z} = 0.01 \text{ m s}^{-1}$ .

## 4.5 Direct sampling of the Wigner function of a torsion pendulum

Phonon-state QND measurements yield the probabilities  $p_n = \varrho_{nn} = \text{tr}[|n\rangle\langle n| \hat{\varrho}]$ , where  $\hat{\varrho}$  is the reduced density operator of the mechanical oscillator after a series of measurements, but

---

<sup>5</sup> For a sufficiently large impact parameter  $D_0$ , as is the case here, the force exerted on the atoms by the electric field of the ferroelectric nanoparticle becomes negligible. If an experiment was able to reduce the transverse atomic beam velocity and position spreads also without confinement, a waveguide would be dispensable and the scheme could also utilize free atomic motion.

no coherences between  $|n\rangle, |n'\rangle$ . The full quantum state of the mechanical oscillator may be inferred from a tomographic reconstruction of the Wigner function

$$W(\alpha) = \frac{2}{\pi} \text{tr}[\hat{\mathcal{D}}^\dagger(\alpha) \hat{\rho} \hat{\mathcal{D}}(\alpha) \hat{\Pi}], \quad (4.28)$$

where  $\hat{\mathcal{D}}(\alpha) = \exp[\alpha \hat{c}^\dagger - \alpha^* \hat{c}]$  is the displacement operator [87, 189] for a complex variable  $\alpha$  and  $\hat{\Pi} = e^{i\pi \hat{n}}$  is the phonon number parity operator. There exists a plethora of articles that deals with the Wigner function. The interested reader may, e.g., consult references [190, 191], or the textbook [192] and references therein for more thorough discussion of the topic. Here we only want to point out a few remarks that may help us to elucidate better the physical meaning of the Wigner function, before we actually discuss how to compute it.

#### 4.5.1 Phase space representation of the quantum state of motion of a torsion pendulum

Equation 4.28 is the expectation value of  $2\hat{\Pi}/\pi$  in the state  $\hat{\rho}(-\alpha) = \hat{\mathcal{D}}(-\alpha) \hat{\rho} \hat{\mathcal{D}}^\dagger(-\alpha)$ . Therefore, the Wigner function represents a measurable quantity. In fact, it is a one to one representation of the quantum state of our mechanical oscillator. However, this representation is based on an alternative framework to the Hilbert space of the density operator  $\hat{\rho}$ . To manifestly show this, we start by clarifying that every complex variable  $\alpha$  together with its conjugate counterpart  $\alpha^*$ , may be regarded as a pair of canonical coordinates, and thus the complex two-dimensional space of these variables may be thought of as the phase space of our torsion pendulum, see e.g. [193]. Consequently, the unitary operator  $\hat{\mathcal{D}}(\alpha)$  is called the *displacement* operator because it enables us to carry out translations in phase space. Indeed, using the Baker-Campbell-Hausdorff formula and the Hadamard's lemma [194], one easily finds that under a unitary operation induced by  $\hat{\mathcal{D}}(\alpha)$ , the annihilation operator undergoes the shift

$$\hat{c} \mapsto \hat{\mathcal{D}}(\alpha) \hat{c} \hat{\mathcal{D}}^\dagger(\alpha) = \hat{c} - \alpha. \quad (4.29)$$

Alternatively, we can recast equation (4.29) in terms of the quadratures  $\hat{x} = (\hat{c}^\dagger + \hat{c})/\sqrt{2}$  and  $\hat{p} = i(\hat{c}^\dagger - \hat{c})/\sqrt{2}$ , which account respectively for a rescaled version of the torsion angle and its associated canonical momentum. With this notation the displacement operator reads  $\hat{\mathcal{D}}(\alpha) = \exp(-ix_\alpha \hat{p}) \exp(ip_\alpha \hat{x}) \exp(ix_\alpha p_\alpha/2)$  and we have

$$\hat{x} \mapsto \hat{\mathcal{D}}(\alpha) \hat{x} \hat{\mathcal{D}}^\dagger(\alpha) = \hat{x} - x_\alpha, \quad \hat{p} \mapsto \hat{\mathcal{D}}(\alpha) \hat{p} \hat{\mathcal{D}}^\dagger(\alpha) = \hat{p} - p_\alpha, \quad (4.30)$$

with  $x_\alpha = (\alpha^* + \alpha)/\sqrt{2}$  and  $p_\alpha = i(\alpha^* - \alpha)/\sqrt{2}$ . At this point, equation (4.28) suggests us now that the Wigner function provides a picture of the quantum state of our torsion pendulum using solely the phase space formalism. We actually may conceive it as a sort of classical phase space distribution, yet with some subtle differences. Classically, the phase space variables may fluctuate, but they are uncorrelated quantities. Every complex amplitude  $\alpha$  or, equivalently, every pair of values of the canonical variables,  $x_\alpha$  and  $p_\alpha$ ,

unequivocally defines a point in phase space. Thus, we may use a collection of phase space points to account for the overall state of the torsion pendulum. Every single realization of a particular state of the torsion pendulum is then given by a point in phase space. In this way, we can completely describe the state of the torsion pendulum by introducing a distribution that quantifies the probability of realizing every single phase space point. In the quantum case, however, we cannot use just a single phase space point to define the state of our torsion pendulum. A natural extension of the phase space formalism into the

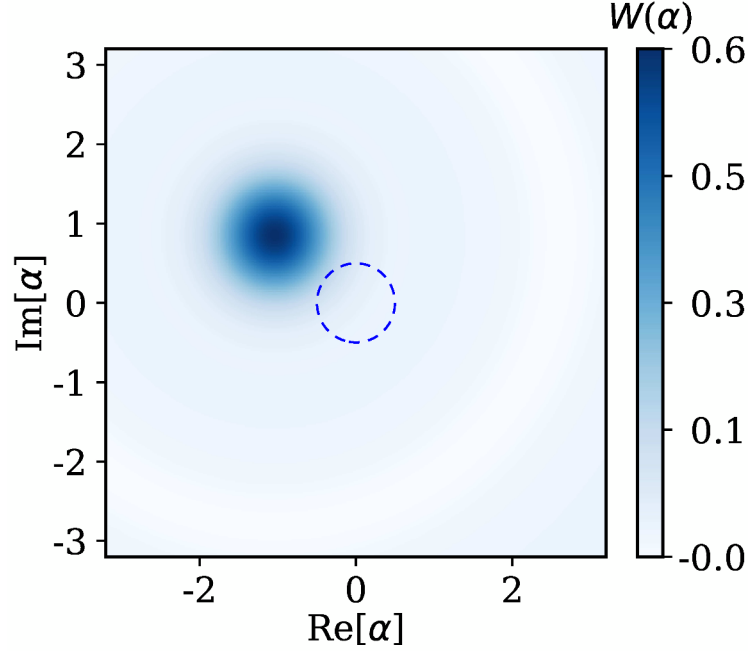


**Figure 4.9** Wigner function of mechanical oscillator state. Before displacement we take the ground state (contour), after displacement operation  $\hat{D}(\alpha_N(\tau))$  we obtain a coherent state (color). We use  $\alpha_N(\tau)/|\alpha_N(\tau)| = -[1 - i]/\sqrt{2}$ , with  $|\alpha_N(\tau)| \simeq 1.35$ ,  $\Omega/(2\pi) = \sqrt{2}/2$  MHz, see text.

quantum realm replaces the canonical coordinates  $x_\alpha$  and  $p_\alpha$ , by the quadrature operators  $\hat{x}$  and  $\hat{p}$ , respectively. As opposed to the paradigm of classical physics, the quadratures  $\hat{x}$  and  $\hat{p}$  are now correlated quantities. A simultaneous and arbitrarily precise measurement of the quadratures is then unfeasible, because a disturbance in one of them necessarily generates (quantum) noise in the other one. Hence, rather than a point we use a region in phase space to picture the dynamical state of the torsion pendulum. The minimal size of this region is given by the Heisenberg uncertainty principle concerning the two quadratures. This blur of phase space points caused by such quantum fluctuations is captured by the Wigner function. The result is that, unlike a regular probability distribution, the Wigner function may account for negative values. For this reason, the Wigner function is referred to as a *quasi-probability* distribution. Although rigorously it is not a joint probability measure for the two quadratures, the Wigner function is then used to compute quantum-mechanical expectation values of observables, similarly to statistical averages of dynamical functions in the framework of classical physics. Moreover, the probability densities for each of the

quadratures alone are naturally obtained as the marginal distributions of the Wigner function, resembling again very closely a classical phase space distribution. We can see this last fact more clearly if we evaluate the trace form in equation (4.28) in terms of the quadratures  $\hat{x}$  and  $\hat{p}$ . The result is Wigner's original formula [195]

$$W(\alpha_R, \alpha_I) = \frac{2}{\pi} \int_{-\infty}^{+\infty} dx \langle \sqrt{2}\alpha_R + x | \hat{\rho}_0 | \sqrt{2}\alpha_R - x \rangle e^{-2i\sqrt{2}\alpha_I x}, \quad (4.31)$$

where real and imaginary parts of  $\alpha$ ,  $\alpha_R$  and  $\alpha_I$  respectively, relate to the canonical coordinates via the relations  $\sqrt{2}\alpha_R = x_\alpha$  and  $\sqrt{2}\alpha_I = p_\alpha$ . The marginal distribution  $\int d\alpha_I W(\alpha_R, \alpha_I) / \sqrt{2} = \langle x_\alpha | \hat{\rho}_0 | x_\alpha \rangle = \text{Pr}(x_\alpha)$ , that is, a partial integration over the quadrature  $\alpha_I$  yields the probability distribution of the conjugate quadrature  $\sqrt{2}\alpha_R = x_\alpha$ , (the same holds for the other quadrature).

Having clarified that the Wigner function is just another means to represent the full quantum state of motion of our torsion pendulum we will discuss now a way to evaluate it in our setup.

#### 4.5.2 Sampling the phase space of a torsion pendulum. Wigner function reconstruction

Returning to equation (4.28) we thus recognize that we can picture the quantum state of the mechanical oscillator in phase space from the evaluation of the Wigner function at a given  $\alpha$  as  $W(\alpha) = [2/\pi] \sum_n (-1)^n \tilde{p}_n$ , i.e, from a phonon-distribution after a coherent displacement by  $-\alpha$ . We illustrate  $W(\alpha)$  in Figure 4.9, for a mechanical oscillator initially prepared in its ground state of motion.

An established method for the quantum coherent displacement of nano-mechanical oscillators does not yet exist. A major advantage of the on-chip architecture proposed here, is that this coherent displacement can be conveniently achieved with the same Rydberg atomic wave guide used for phonon-state measurement. To this end the atomic dipole transition has to be strongly driven in region C. Therefore, we switch on the driving  $\hat{H}_{\text{coup}}$  in the Hamiltonian defined in (4.3). Under appropriate conditions, see Appendix B.6, this leads to an effective coherent drive for the oscillator. The evolution operator describing the reduced dynamics of the oscillator for a succession of  $N$  atoms reads  $\hat{U}_N(\tau) = \hat{\mathcal{D}}(\alpha_N(\tau)) \exp[-iN\theta(\tau)\hat{n}]$ , a product of a displacement with complex amplitude  $\alpha_N(\tau)$  depending on  $\Omega$  and  $\delta$ , as well as a phase-shift with  $\theta(\tau) = \int^\tau dt \mathcal{K}^2(\mathbf{R}(t)) / \delta$  that can be compensated (see Appendix B.6 for details). Figure 4.9 shows an exemplary oscillator Wigner function before- and after a sequence of  $N = 8$  displacement atoms, modelled explicitly as in the previous section. To sample the entire Wigner function with displacements of this kind, one can vary the amplitude and complex phase of the effective Rabi-frequency through parameters of the external drive in region C, see Appendix B.6.

To assess the impact of the decoherence sources and imperfections mentioned earlier, we now simulate the complete Wigner tomography sequence:



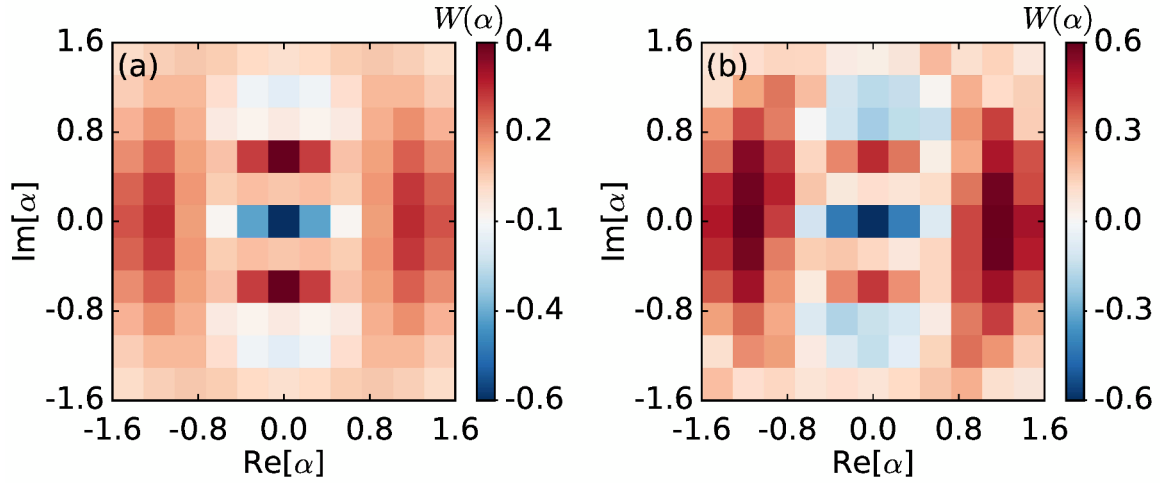


**Figure 4.10** Quantum state tomography of oscillator state using QND-detection sequences and coherent displacements all with the same atomic beam. (a) Ideal Wigner-function of the oscillator in state  $|\Psi_0\rangle = [|1\rangle + |3\rangle]/\sqrt{2}$ . (b) Reconstruction including practical imperfections as discussed in the text.

- (i) Initialise the oscillator in the state  $\hat{q}_0$  to be measured. This initialisation must be reproducible.
- (ii) Effectuate a coherent displacement,  $\hat{q}_0 \mapsto \hat{q}(-\alpha)$ , using a flyby sequence of  $N$  explicitly modelled displacement atoms.
- (iii) Measure the phonon number with a flyby sequence of  $K = 43$  atomic Ramsey interference measurements. The first few atoms collapse the oscillator into a Fock state  $|n'\rangle$ , which is read out by the remaining majority of the  $K = 43$  atoms, that is,  $K - i_c$  with  $i_c = 10$ .
- (iv) Repeat steps (i)-(iii)  $N_s = 512$  times, to obtain the phonon probability distribution  $\tilde{p}_n$  for the displacement  $-\alpha$ .
- (v) Repeat step (iv) for an  $(S \times S)$  array of different values for  $\alpha \in \mathbb{C}$  to obtain the Wigner function  $W(\alpha)$ .

See also figure 4.11 for a pictorial flow of these steps.

Figure 4.12 illustrates the Wigner densities reconstructed with this sequence through “Method A” and the ideal expectation for the mechanical oscillator superposition state  $|\Psi_0\rangle = [|1\rangle + |3\rangle]/\sqrt{2}$ . It can be seen that all major qualitative features of the Wigner function, particularly the non-classical negativity, are correctly inferred. Quantitative deviations indicate that the decoherence rates employed here should not be exceeded.

Remember that both, “Method A” and “Method B”, refer to two different ways of reconstructing the phonon distribution from a numerical simulation of steps (i)-(iv). “Method A” applies a statistical average directly to phonon probabilities as extracted from the numerical solution of  $\hat{\rho}$ , whereas “Method B” performs a statistical average over phonon probabilities

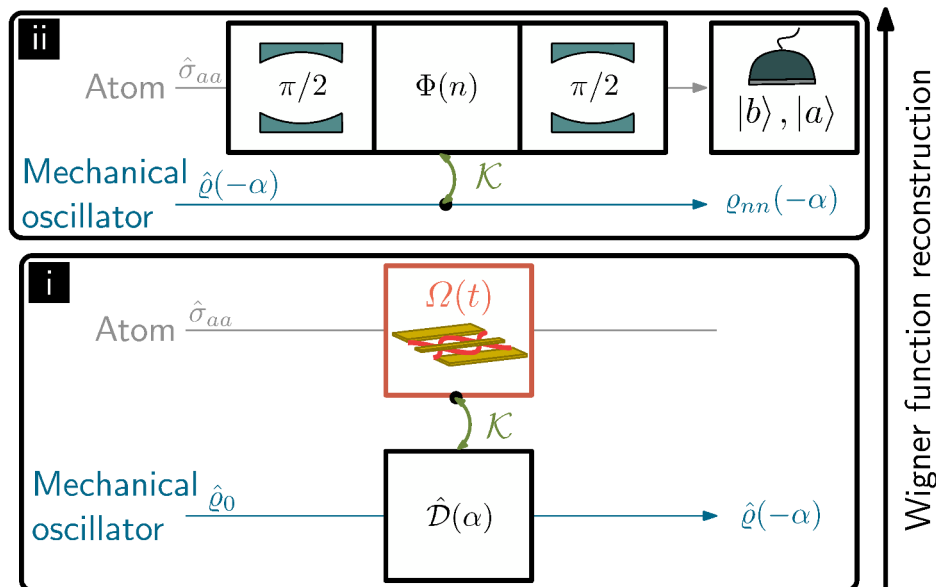


**Figure 4.11** Diagrammatic protocol to reconstruct the Wigner function of a mechanical oscillator state. The bottom to top arrow indicates the timeline of the protocol; timelines of the atom (grey) and the mechanical oscillator (blue) in steps (i) and (ii) of the protocol are shown from left to right. The curved green arrows account for the coupling  $\mathcal{K}$  between atom and torsion pendulum in each step of the protocol. Step (i) initializes the mechanical oscillator in a reproducible target state  $\hat{q}_0$  and uses a series of atoms, each atom initialized in  $\hat{\sigma}_{aa}$ , to carry out the phase space translation  $\hat{q}_0 \mapsto \hat{q}(-\alpha) \simeq \hat{D}^\dagger(\alpha)\hat{q}_0\hat{D}(\alpha)$ . A displacement operation  $\hat{D}$  is achieved by driving every atom in the series while it interacts with the mechanical oscillator in the coupling region through a coplanar microwave cavity (see red box). In step (ii) a series of Ramsey measurements (RMs) collapses  $\hat{q}$  into a Fock state  $|n\rangle$ ,  $n \in \{0, \dots, n_0 = 5\}$ . A RM is enclosed by two  $\pi/2$  pulses, so that atomic populations in  $|a\rangle, |b\rangle$  are recorded as a function of the phaseshift  $\Phi(n)$ , and thus as a function of  $n$ , the eigenvalue of the phonon number operator in the state  $|n\rangle$ . Many runs of (i) and (ii), with  $\hat{D}(\alpha)$  mapped out for the same phase space point  $\alpha$ , reveals the phonon distribution  $\{q_{nn}(-\alpha)\} \simeq \{q_{0nn}(-\alpha)\}$  and enables the reconstruction of a single pixel of the Wigner function of  $\hat{q}_0$ . Varying the amplitude and phase of the Rabi frequency  $\Omega$  in step (ii) allows to sample many points  $\alpha$  and thus to reconstruct the full Wigner function of  $\hat{q}_0$ .

that we deduce from the atomic population difference  $\mathcal{P}$  using the one to one correspondence that exists between  $\mathcal{P}$  and the range of phonon numbers  $n$  that we are interested in,  $n \in \{0, 1, \dots, n_0 = 5\}$ . See section 4.4.3 for further information.

In figure 4.12, we contrast the values of  $W(\alpha)$  representing the state  $|\Psi_0\rangle = [|1\rangle + |3\rangle]/\sqrt{2}$  as obtained through “Method A” with the ones derived in this case from “Method B”. The Wigner density computed via “Method A” resembles the exact outcome more than the counterpart result determined through “Method B”. Considering that occasionally a series of  $K = 43$  Ramsey measurements may not be sufficient to project the mechanical oscillator state into a Fock state, we expect a higher inaccuracy of “Method B” compared to “Method A”. Indeed, if a complete Fock state collapse is not realized, applying “Method B” may lead to a wrong Fock state record or to the loss of a statistical sample. Contrarily, if we apply “Method A” in a similar situation, a statistical loss never occurs and the error for a Fock state

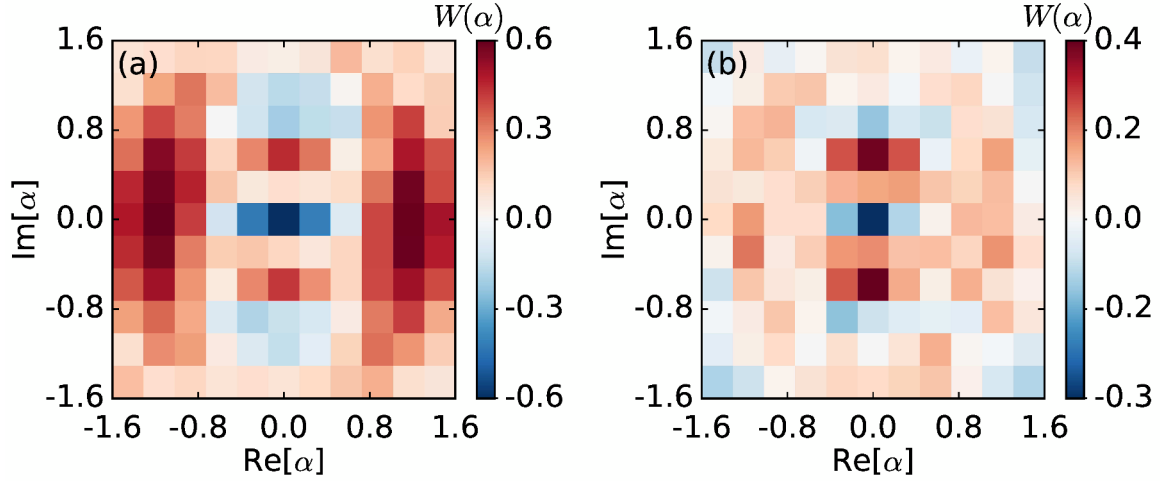


**Figure 4.12** Tomographic reconstruction of the Wigner density  $W(\alpha)$  of the mechanical oscillator superposition state  $|\Psi_0\rangle = [|1\rangle + |3\rangle]/\sqrt{2}$ . (a) Evaluation of  $W(\alpha)$  using the reconstruction protocol of “Method A”. (b) The outcome of the same  $W(\alpha)$  applying instead the protocol of “Method B”. Both, “Method A” and “Method B”, are defined in 4.4.3.

miscount is lower.

## 4.6 Conclusions

By porting technologies from cavity quantum electrodynamics to nano-mechanics, our scheme addresses two outstanding challenges for quantum nano-mechanics, namely phonon QND-detection and quantum state tomography. Thereby, we have also described a technique for the quantum coherent state displacement of nano-mechanical elements. The ingredients of the hybrid setup proposed, nano fabricated oscillators and Rydberg atomic waveguides, can naturally co-exist on the same chip surface [196], and our numerical simulations demonstrate that in combination they can be used to monitor the quantum state of nano-scale oscillators despite realistic noise and decoherence sources.



## 5 Summary and outlook

Atoms in excited electronic states can assist in the preparation, measurement and control of the dynamics of a miniature mechanical resonator that is free of any coupling to an electromagnetic field confined in the interior of a cavity. Fortunately, the responsiveness to external forces of miniature mechanical systems is often high enough to enable them to interface with a multitude of different physical systems. This feature may be especially valuable in the realm of hybrid quantum systems (HQS)s [46]. HQSs integrate different physical components that may communicate at the level of single energy quanta, thereby offering promising vistas for the development of quantum technologies [48]. Among these kind of composite setups we find systems in which a miniature mechanical resonator is interfaced with atoms [197]. Our work aims to contribute in this undertaking from a theoretical perspective. To this end we have developed two prospective schemes in which a mechanical resonator is interfaced with atoms. Given that the existing trend to miniaturize mechanical structures for a potential quantum enhancement of a great number of technological devices might hinder an efficient design of cavity opto- and electro-mechanical systems [42], we have focused instead on arrangements in which the mechanical element is not enclosed or forming part of a cavity. Our strategy harnesses excited electronic states of atoms to assist in monitoring and controlling the dynamics of miniature mechanical resonators as an alternative and possibly complementary route to other recent proposals [59, 198]. Today's level of control over atoms through the use of electromagnetic radiation enables the generation and combination of oscillating atomic dipoles associated with a specific and desired coherent superposition of electronic atomic levels (atomic coherence). The extreme sensitivity of an atomic coherence to changes in the relative phase or frequency of the levels that comprise such a coherent superposition state is a pivotal resource in the two schemes that we have envisaged. In order to probe a coupling between a mechanical resonator and an atomic system we rely on the response of a given atomic coherence subject to a radiation field that is precisely modulated by the oscillating motion of the mechanical resonator.

The first scheme is described in chapter 3. There we have conceived a distant coupling between a mechanical resonator and an ultracold gas of non-interacting alkali metal (rubidium) atoms mediated by laser light. The setup makes possible a remote control of the motion of the mechanical resonator in the classical regime. This remote control is enabled through the dielectric response of the atoms in the gas. A linearly vibrating and perfectly reflecting mirror of nano-scale dimensions plays the role of the mechanical resonator. We use two laser beams, and hence consider only two dipole allowed atomic transitions involving two meta-stable states and an excited state. Furthermore, we initialize all the atoms in the lowest energy state. One of the laser beams firstly interacts resonantly with the atoms, such that its carrier frequency exactly matches a single Bohr atomic frequency, and nextly hits the mirror. This beam allows probing the absorption of the atoms and is usually referred

to as the probe beam. Contrarily, the other laser beam, the carrier frequency of which is close to the remaining Bohr atomic frequency, reflects off the moving mirror before it couples to the atoms with a finite detuning. Since it enables certain control over atomic absorption this beam is known as the control beam. The oscillating motion of the mirror modulates the reflected part of the control beam. Both beams reach atoms and mirror only once along their paths. For vanishing detuning the optically driven atoms display a dark resonance: they become effectively transparent with respect to the resonant probe beam, featuring a phenomenon known as electromagnetically induced transparency (EIT). The dark resonance, and thus EIT, arise because every atom in the gas settles into a stationary coherence between the two meta-stable states, in which atomic fluorescence is inhibited. For a non-zero detuning the coherence breaks, atoms populate the excited state and absorption takes place. At the same time, the optical response of the atoms may transfer the mechanical modulations onto the probe beam. By directing the transmitted probe beam towards the mirror surface we allow these mechanical modulations to influence back in the dynamics of the oscillating mirror. Ultimately, this gives rise to a friction force that enables us either to damp or amplify the oscillation amplitude of the mechanical resonator. Each of these effects, damping and amplification of the mirror motion, can be controlled by means of the detuning and is maximum when the oscillation frequency of the mechanical resonator matches a transition frequency between two eigenstates of the dressed system of atoms plus laser light.

The second scheme, presented in chapter 4, considers instead a short distance coupling in which atoms and a mechanical resonator are expected to be integrated into an on-chip platform. The coupling is enabled by attaching a ferroelectric material to the mechanical resonator. Atoms are guided next to the mechanical resonator and interact with it one by one through an electromagnetic coupling. In this way the energy levels of an atom experience Stark shifts that depend on the state of motion of the mechanical system. Importantly, when the frequency of the mechanical element is nearly resonant with the transition frequency between two Rydberg levels of the atom, a strong coupling is realized due to the large electric dipole moment of such atomic transition, and the ensuing Stark shifts affecting these Rydberg levels become high enough to be detected. The arrangement is then well suited for the study of the quantum dynamics of the mechanical resonator. We use two level Rydberg atoms as probes, such that performing measurements on their electronic states we may readout quantum features of the mechanical system. For concreteness, the mechanical resonator takes on the form here of a carbon nanotube (CNT) undergoing torsion oscillations. From a fundamental point of view, torsion vibration modes for these mechanical systems are expected to have negligibly small clamping losses, and therefore rather high quality factors [199]. This facilitates the task of reading out the quantum dynamical state of the mechanical system before it decoheres. We monitor the atomic coherence between the Stark shifted levels of the Rydberg atoms through Ramsey interference measurements. This in turn allows us to access the quantum state of the torsion pendulum, the torsion vibration mode of concern. For a mechanical frequency sufficiently detuned from the transition frequency of

the two level Rydberg atoms, the aforementioned Stark shifts showcase an approximately linear dependence with the phonon number of the torsion pendulum. We demonstrate that a record of several Ramsey measurements drives the state of motion of the torsion pendulum towards a Fock state, thus making a quantum non-demolition measurement of the phonon number possible. Many repetitions of this Ramsey sequence, all of them using the same initial quantum state of the mechanical system, reproduces the initial phonon distribution. In addition, we show how the guided Rydberg atoms may serve to sample the dynamical phase space of the torsion pendulum. To explore the phase space we propose to drive the atoms with the evanescent field of a coplanar microwave cavity while they interact with the CNT. By exhaustively sampling the phase space of the torsion pendulum while reproducing the phonon number distribution of its initial quantum state, we suggest a recipe for the reconstruction of the quantum dynamical state of the torsion pendulum. It is noteworthy to mention that although we consider rubidium atoms to assess the performance of this on-chip platform for the monitoring of the state of motion of quantum limited nanoscale torsion mechanical resonators due to their prominence in experiments, the use of lithium atoms could offer some advantages. Lithium Rydberg states with a principal quantum number between 80 and 100 can still provide long lived coherences, while featuring a higher coupling and transition frequencies of a few MHz. In contrast with our  $\sim$  GHz torsion mechanical resonance, a few MHz is a figure already found in a wide range of torsion mechanical resonators [163, 200, 159, 158].

## Prospective work

Our work raises new questions which may lead to further research.

Chapter 3 provides a semiclassical description of the remote interface between a mechanical resonator and a gas of  $\Lambda$ -type three level atoms in which only the internal dynamics of the atoms is treated on a quantum mechanical basis. A natural next step would then consist in formulating a full quantum-mechanical model of the entire system of atoms, light and mechanical resonator and assess the possibility of achieving ground state cooling of the mechanical resonator motion. Further interesting perspectives arise when our setup is extended towards Rydberg physics: EIT media where one of the hyperfine states is replaced by a highly excited (and therefore also long-lived) Rydberg state [201, 202, 203, 204, 205, 206, 207], have recently been used for the creation of single-photon sources [208, 209] and proposed to enable nonlocal nonlinear optics [210]. Replacing a hyperfine state by a Rydberg state could serve to enhance the optically induced damping rate of the mechanical resonator dynamics. Furthermore, since such Rydberg state would be highly sensitive to interactions with other Rydberg atoms, the control of the mechanical resonator motion by further quantum mechanical atomic elements could be feasible also without the use of an optical cavity.

Within the context of the on-chip interface between a mechanical resonator and a system of atoms as described in chapter 4, an interesting problem to address is the design of a method that allows for the reconstruction of arbitrary quantum states of the mechanical

torsion mode. The state reconstruction protocol exposed in chapter 4 is based on a quantum non-demolition measurement of the phonon number observable and is in turn enabled by a dispersive coupling between the torsion pendulum and guided two level Rydberg atoms. Given a finite coupling strength, a successful application of the protocol is thus restricted to a torsion pendulum prepared in low energy quantum states of motion, with a small phonon occupation number. We could circumvent this limitation if we calibrated the Ramsey interferometer to allow for the measurement of the expectation value of appropriate Heisenberg-Weyl (phase space displacement) operators. By appropriate we mean that they form a complete basis of phase space observables. For every point in the dynamical phase space of the torsion pendulum, reading out the population difference between the two Rydberg levels would now yield knowledge of the expectation value of the wanted Heisenberg-Weyl operator. With this at hand a reconstruction of the Wigner function of the torsion pendulum may be possible [211].

Going a step further in the realization of hybrid systems with atoms and solids we envisage a promising avenue in interfaces between Rydberg atoms and nano- or micro-particles. Bonding and nonbonding interactions between a Rydberg state atom and a metallic nano-particle may lead to novel synthetic phenomena of chemical physics, which could be exploited in the realm of photovoltaics. Likewise, a long-range coupling between the Rydberg electron of an atom and a nanoparticle offers a plausible scenario to explore electronic friction [212]. The combination of nanoparticles and Rydberg atoms may also enable us to push forward the interplay between the motion of solid structures and atoms. An arrangement in which we allocate one or several Rydberg atoms within a lattice of nano- or micro-particles could serve as a platform to investigate charge induced motion and possibly charge migration at unconventional length scales [213].



# A Supplement: optical absorption of an ultracold gas of three-level atoms

This complement provides a more detailed account of our semiclassical treatment of light-matter interactions of chapter 3. In particular, we address the problem of electromagnetic wave propagation across the atoms. Likewise, we present the steps that we use to obtain an expression for the dielectric response of the optically driven atomic vapor both in the absence and in the presence of mechanically modulated radiation fields.

## A.1 Linear polarization and electromagnetic wave propagation inside the atomic gas

For the system shown in figure 3.1, the probe and control beams are coupled to the atomic medium with Rabi frequencies  $\Omega_p$  and  $\Omega_c$ . Our goal is to calculate the transmission, and thus the atomic absorption, of the probe light field normally incident from vacuum onto the ensemble of  $N$  atoms. Thus we start looking at the evolution of the light beams inside the medium, which is governed by the electromagnetic wave equation (3.9). For light beams with transverse widths  $\mathcal{A}_{\omega_\lambda} \gg |\mathbf{k}_\lambda|^{-2}$ , as it is the case here, we use an infinite plane wave approximation in which the fields take on an unidirectional propagation along the  $z$ -direction, and so  $\nabla \times \nabla \times \mapsto -\partial^2/\partial z^2$ . The wave equation (3.9), then reduces to

$$\frac{\partial^2}{\partial z^2} \mathbf{E}(z, t) - \frac{1}{c^2} \frac{\partial^2}{\partial t^2} \mathbf{E}(z, t) = \frac{1}{\epsilon_0 c^2} \frac{\partial^2}{\partial t^2} \mathbf{P}(z, t). \quad (\text{A.1})$$

For a one dimensional description of the medium along  $z$ , the polarization is given by the collective slowly varying atomic coherences,

$$\mathcal{R}_{\mu\mu'}(z, t) = (1/\mathcal{A}_0) \sum_{n=1}^N \rho_{\mu\mu'}^{(n)} \delta(z - z_n), \quad (\text{A.2})$$

with  $\mathcal{A}_0 = \max\{\mathcal{A}_{\omega_p}, \mathcal{A}_{\omega_c}\}$ , via

$$\mathbf{P}(z, t) = \mathcal{R}_{eg}(z, t) \mathbf{d}_{ge} \exp(-i\omega_p t) + \mathcal{R}_{es}(z, t) \mathbf{d}_{se} \exp(-i\omega_c t) + \text{c. c.} \quad (\text{A.3})$$

$$= \frac{1}{2} \sum_{\omega_\lambda} \mathbf{P}_{\omega_\lambda}(z, t) \exp(i\mathbf{k}_\lambda \cdot \mathbf{r} - i\omega_\lambda t) + \text{c.c.} \quad (\text{A.4})$$

In writing equation (A.4) with  $\omega_\lambda \in \{\omega_p, \omega_c\}$ , we have introduced the slowly varying polarization amplitudes  $\mathbf{P}_{\omega_p} = 2\mathcal{R}_{eg} \mathbf{d}_{ge} \exp(i|\mathbf{k}_p|z)$  and  $\mathbf{P}_{\omega_c} = 2\mathcal{R}_{es} \mathbf{d}_{se} \exp(-i|\mathbf{k}_c|z)$ . Note that the probe beam propagates along the negative direction of the  $z$ -axis, and thus  $\mathbf{k}_p \cdot \mathbf{r} = -|\mathbf{k}_p|z$ , whereas the control beam propagates in the positive direction, such that  $\mathbf{k}_c \cdot \mathbf{r} = |\mathbf{k}_c|z$ . Just like the electric field amplitudes  $\mathbf{E}_{\omega_\lambda}$ , defined in section 3.1, the vector fields  $\mathbf{P}_{\omega_\lambda}$  undergo appreciable changes in time and space at a pace much slower than

an optical period and wavelength, respectively. Mathematically, this may be written as  $|\partial(\mathbf{E}_{\omega_\lambda}, \mathbf{P}_{\omega_\lambda})/\partial t| \ll \omega_\lambda |(\mathbf{E}_{\omega_\lambda}, \mathbf{P}_{\omega_\lambda})|$  and  $|\partial(\mathbf{E}_{\omega_\lambda}, \mathbf{P}_{\omega_\lambda})/\partial z| \ll |\mathbf{k}_\lambda| |(\mathbf{E}_{\omega_\lambda}, \mathbf{P}_{\omega_\lambda})|$ . Making use of these relations upon insertion of the definitions (3.2) and (A.4) in the wave equation (A.1), we obtain an approximate evolution for the slowly varying amplitudes  $\mathbf{E}_{\omega_\lambda}$ . After separating out the different frequency component amplitudes at  $\omega = \omega_\lambda$ , this so called slowly varying envelope approximation (SVEA) [99, 214] leads to the following wave equation for each electric field amplitude

$$\left[ \frac{\partial}{\partial t} \pm c \frac{\partial}{\partial z} \right] \mathbf{E}_{\omega_\lambda}(z, t) = i \frac{\omega_\lambda}{2\varepsilon_0} \mathbf{P}_{\omega_\lambda}(z, t), \quad (\text{A.5})$$

where the plus (minus) sign indicates a wave traveling along the positive (negative) direction of the  $z$ -axis.

Solving equation (A.5) requires also evaluating the internal dynamics of the atoms. Given that we have assumed that the atoms do not interact with one another, these dynamics are characterized by the single particle density operator  $\hat{\rho}^{(n)}$ , with  $n \in \{1, \dots, N\}$ . Its matrix elements,  $\rho_{\mu\mu'}^{(n)}$ , settle into a steady state after a characteristic time scale, set by the rate  $\Gamma_p$  of spontaneous emission from  $|e\rangle$  to  $|g\rangle$ . Since the duration of the optical laser fields that drive the atoms is considerably longer than this time scale ( $\sim \Gamma_p^{-1}$ ), we will reduce here the complexity of the problem and focus only in a regime in which the  $\rho_{\mu\mu'}^{(n)}$  are settled into their steady state, which can be computed from the master equation (3.12). If we restrict the calculation to a scenario in which the probe light field is rather weaker than the control one, a solution of equation (3.12) can yield a polarization that is linearly related to the electric field of the incident wave via (a real and stationary) dielectric response function  $\chi$ , as expressed in equation (2.15). Let us assume for now that this is the case. This allows us to solve the wave equation (A.5) by means of the Fourier transform. We adopt the following convention for the Fourier transform of a time dependent vector field  $\mathbf{C}(t)$  (that admits it)

$$\mathcal{F}[\mathbf{C}(t)](\omega) = \underline{\mathbf{C}}(\omega) = \int_{-\infty}^{+\infty} dt \mathbf{C}(t) \exp(i\omega t), \quad (\text{A.6})$$

$$\mathcal{F}^{-1}[\underline{\mathbf{C}}(\omega)](t) = \mathbf{C}(t) = \int_{-\infty}^{+\infty} \frac{d\omega}{2\pi} \underline{\mathbf{C}}(\omega) \exp(-i\omega t). \quad (\text{A.7})$$

Consequently, in Fourier space, the relation (2.15) between the linear polarization and the electric field in the medium simply reads

$$\underline{\mathbf{P}}_1(z, \omega) = \varepsilon_0 \underline{\chi}(z, \omega) \underline{\mathbf{E}}(z, \omega). \quad (\text{A.8})$$

Likewise, in terms of its slowly varying components, the Fourier transforms of the electric field (3.2) and the polarization (A.4) are

$$\underline{\mathbf{E}}(z, \omega) = \frac{1}{2} \sum_{\omega_\lambda} [\underline{\mathbf{E}}_{\omega_\lambda}(z, \omega - \omega_\lambda) \exp(i\mathbf{k}_\lambda \cdot \mathbf{r}) + \underline{\mathbf{E}}_{\omega_\lambda}^*(z, -\omega - \omega_\lambda) \exp(-i\mathbf{k}_\lambda \cdot \mathbf{r})], \quad (\text{A.9})$$

$$\underline{\mathbf{P}}(z, \omega) = \frac{1}{2} \sum_{\omega_\lambda} [\underline{\mathbf{P}}_{\omega_\lambda}(z, \omega - \omega_\lambda) \exp(i\mathbf{k}_\lambda \cdot \mathbf{r}) + \underline{\mathbf{P}}_{\omega_\lambda}^*(z, -\omega - \omega_\lambda) \exp(-i\mathbf{k}_\lambda \cdot \mathbf{r})]. \quad (\text{A.10})$$

By substituting equation (A.9) into equation (A.8) we identify

$$\underline{\mathbf{P}}_{1,\omega_\lambda}(z, \omega) = \varepsilon_0 \underline{\chi}(z, \omega_\lambda + \omega) \underline{\mathbf{E}}_{\omega_\lambda}(z, \omega), \quad (\text{A.11})$$

with the Fourier transform of the linear, slowly varying polarization amplitude  $\mathbf{P}_{1,\omega_\lambda}$ . Then, applying the Fourier transform to both sides of the wave equation (A.5) and neglecting all the nonlinear polarization terms  $\underline{\mathbf{P}}_{k>1,\omega_\lambda}$ , leads to

$$\frac{\partial}{\partial z} \underline{\mathbf{E}}_{\omega_\lambda}(z, \omega) = \pm i \left[ \frac{\omega}{c} + \frac{\omega_\lambda}{2c} \underline{\chi}(z, \omega_\lambda + \omega) \right] \underline{\mathbf{E}}_{\omega_\lambda}(z, \omega). \quad (\text{A.12})$$

Solving the ordinary differential equation (A.12) above in the interval  $[z_1, z_2]$ , and subsequently inverting the resulting Fourier transform, yields

$$\underline{\mathbf{E}}_{\omega_\lambda}(z_2, t) = \int_{-\infty}^{+\infty} \frac{d\omega}{2\pi} \underline{\mathbf{E}}_{\omega_\lambda}(z_1, \omega) \exp \left[ -i\omega \left( t \mp \frac{z_2 - z_1}{c} \right) \pm \frac{i\omega_\lambda}{2c} \int_{z_1}^{z_2} dz \underline{\chi}(z, \omega + \omega_\lambda) \right]. \quad (\text{A.13})$$

Since each amplitude  $\underline{\mathbf{E}}_{\omega_\lambda}$  is presumed to be highly confined around the carrier frequency  $\omega_\lambda$  of its associated wave, we could simplify further the expression (A.13) above if we expanded  $\underline{\chi}(\omega + \omega_\lambda)$  in a Taylor series (up to first order) around  $\omega_\lambda$ . In this way, the integral over frequencies in equation (A.13) would approximately represent a wave packet traveling with a smaller (group) velocity than  $c$ , multiplied by both a phase and an attenuating factor. Such a wave packet would then be delayed by the gas of atoms relative to an identical wave packet that traveled the same distance in vacuum, see, e. g., references [215, 216, 217] for a more detailed discussion. For the setup described in chapter 3 we are ultimately concerned with ideal monochromatic radiation fields as well as with a spatially uniform atomic medium. In that case  $\underline{\mathbf{E}}_{\omega_\lambda}(\omega - \omega_\lambda) = \underline{\mathbf{E}}_{\omega_\lambda} 2\pi\delta(\omega - \omega_\lambda)$ , while  $\underline{\chi}$  becomes independent of the spatial coordinates, such that at the exit of the atomic medium the electric field envelopes  $\underline{\mathcal{E}}_{\omega_\lambda}(z) = \underline{\mathbf{E}}_{\omega_\lambda}(z) \exp(i\mathbf{k}_\lambda \cdot \mathbf{r})$  take on the simple form<sup>1</sup>

$$\underline{\mathcal{E}}_{\omega_p}(-L/2 + \bar{z}_{\text{at}}) = \underline{\mathcal{E}}_{\omega_p}(L/2 + \bar{z}_{\text{at}}) \exp(-i\omega_p \underline{n}(\omega_p)L/c), \quad (\text{A.14})$$

$$\underline{\mathcal{E}}_{\omega_c}(L/2 + \bar{z}_{\text{at}}) = \underline{\mathcal{E}}_{\omega_c}(-L/2 + \bar{z}_{\text{at}}) \exp(i\omega_c \underline{n}(\omega_c)L/c). \quad (\text{A.15})$$

Here,  $\bar{z}_{\text{at}}$  denotes the average distance from the origin of our reference frame to the center of the atomic cloud, of length  $L$ , along the  $z$ -axis (see figure 3.1). We have also used  $\underline{n} \simeq 1 + \underline{\chi}/2$ , a valid approximation whenever  $\underline{\chi}', \underline{\chi}'' \ll 1$ . Using equation (A.14) we compute the transmission of the probe field through the medium as

$$T_{\omega_p} = \left| \frac{\underline{\mathcal{E}}_{\omega_p}(-L/2 + \bar{z}_{\text{at}})}{\underline{\mathcal{E}}_{\omega_p}(L/2 + \bar{z}_{\text{at}})} \right|^2 \simeq \exp(-\omega_p L \underline{\chi}''(\omega_p)/c) \approx 1 - \omega_p L \underline{\chi}'' \omega_p / c. \quad (\text{A.16})$$

---

1 The equations (A.14) and (A.15), representing the electric field envelopes transmitted through the medium, provide an accurate description of the electric field when the index of refraction is close to unity, as is the case for our dilute atomic gas. Otherwise, the right hand side of equations (A.14) and (A.15) should actually be weighted by the factor  $2/[\underline{n} + 1]$ , as required by the Fresnel relations at the atom-vacuum boundaries, see [102].

## A.2 Dynamics of the optically driven atoms

The semiclassical theory that we adopt to describe the light-matter interaction of a three-level  $\Lambda$ -type atom  $n$ , in the dipole and rotating wave approximations, relies on the Hamiltonian  $\hat{H}_\Lambda^{(n)} = \hbar[\Delta_c - \Delta_p]\hat{\sigma}_{ss}^{(n)} - \hbar\Delta_p\hat{\sigma}_{ee}^{(n)} - \hbar[\Omega_c(\mathbf{r}_n, t)\hat{\sigma}_{es}^{(n)} + \Omega_p(\mathbf{r}_n, t)\hat{\sigma}_{eg}^{(n)} + \text{h. c.}]/2$ , which results in that of equation (3.11) for  $\Delta_p = 0$ . Since the atoms are continually driven by the optical fields, we only focus in a regime in which  $\hat{\rho}^{(n)}$  reaches a steady state. To be consistent with chapter 3 and the theory presented in the Appendix A.1 above, we also restrict the analysis to the case in which the atoms respond linearly to the applied probe electric field. Note finally, that we shall be interested in ideal monochromatic radiation fields. Thus, for a scenario in which the waves are not mechanically modulated, the Rabi frequencies may be treated as time independent quantities. We first provide a solution for this scenario and then consider the case for which the radiation fields are modulated by the oscillating motion of the nano-scale mechanical mirror as described in chapter 3.

### A.2.1 Linear susceptibility. Free radiation

We start expanding the one-particle density operator up to first order in the probe field,  $\hat{\rho}^{(n)} \simeq \hat{\rho}_0^{(n)} + \hat{\rho}_1^{(n)}$ , and substitute it into the master equation (3.12) to obtain the time evolution of the density operator of order  $k = 0, 1$  in a recursive manner, just like we do in section 2.2.2. Since we assume all the atoms start off (far in the past) in  $|g\rangle$ , we have  $\hat{\rho}_0^{(n)} = \hat{\sigma}_{gg}^{(n)}$ . The ensuing dynamics of  $\hat{\rho}_1^{(n)}$ , resulting from the master equation (3.12), is governed by the following set of differential equations

$$\frac{\partial}{\partial t}\rho_{1,gg}^{(n)}(t) = \Gamma_p\rho_{1,ee}^{(n)}(t), \quad (\text{A.17})$$

$$\frac{\partial}{\partial t}\rho_{1,ge}^{(n)}(t) = -\frac{i}{2}\Omega_p^*(z_n, t) - [\Gamma_p/2 + i\Delta_p]\rho_{1,ge}^{(n)}(t) - \frac{i}{2}\Omega_c^*(z_n, t)\rho_{1,gs}^{(n)}(t), \quad (\text{A.18})$$

$$\frac{\partial}{\partial t}\rho_{1,gs}^{(n)}(t) = -\frac{i}{2}\Omega_c(z_n, t)\rho_{1,ge}^{(n)}(t) + i[\Delta_c - \Delta_p]\rho_{1,gs}^{(n)}(t), \quad (\text{A.19})$$

$$\frac{\partial}{\partial t}\rho_{1,eg}^{(n)}(t) = \frac{i}{2}\Omega_p(z_n, t) - [\Gamma_p/2 - i\Delta_p]\rho_{1,eg}^{(n)}(t) + \frac{i}{2}\Omega_c(z_n, t)\rho_{1,sg}^{(n)}(t), \quad (\text{A.20})$$

$$\frac{\partial}{\partial t}\rho_{1,ee}^{(n)}(t) = \frac{i}{2}\Omega_c(z_n, t)\rho_{1,se}^{(n)}(t) - \frac{i}{2}\Omega_c^*(z_n, t)\rho_{1,es}^{(n)}(t) - \Gamma_p\rho_{1,ee}^{(n)}(t), \quad (\text{A.21})$$

$$\frac{\partial}{\partial t}\rho_{1,es}^{(n)}(t) = -[\Gamma_p/2 - i\Delta_c]\rho_{1,es}^{(n)}(t) - \frac{i}{2}\Omega_c(z_n, t)[\rho_{1,ee}^{(n)}(t) - \rho_{1,ss}^{(n)}(t)], \quad (\text{A.22})$$

$$\frac{\partial}{\partial t}\rho_{1,sg}^{(n)}(t) = \frac{i}{2}\Omega_c^*(z_n, t)\rho_{1,eg}^{(n)}(t) - i[\Delta_c - \Delta_p]\rho_{1,sg}^{(n)}(t), \quad (\text{A.23})$$

$$\frac{\partial}{\partial t}\rho_{1,se}^{(n)}(t) = -[\Gamma_p/2 + i\Delta_c]\rho_{1,se}^{(n)}(t) + \frac{i}{2}\Omega_c^*(z_n, t)[\rho_{1,ee}^{(n)}(t) - \rho_{1,ss}^{(n)}(t)], \quad (\text{A.24})$$

$$\frac{\partial}{\partial t}\rho_{1,ss}^{(n)}(t) = \frac{i}{2}\Omega_c^*(z_n, t)\rho_{1,es}^{(n)}(t) - \frac{i}{2}\Omega_c(z_n, t)\rho_{1,se}^{(n)}(t). \quad (\text{A.25})$$

For time independent Rabi frequencies, we may set all time derivatives to zero in the coupled system of differential equations (A.17) – (A.25) above in order to find the steady state of the  $\rho_{1,\mu\mu'}^{(n)}$ . More generally, even if only the control Rabi frequency were time independent,

we still could easily find a steady state solution by means of the Fourier transform. Let us consider, just for illustrative purposes, this latter case, i.e., we consider that only  $\Omega_c$  is time independent. In such scenario equations (A.17) – (A.25) are equivalent to a linear vector differential equation with a constant coefficient matrix, and a driving term the entries of which are either zero or proportional to  $\Omega_p(z_n, t)$  (or to its complex conjugate). We find, either with the help of the Fourier transform or equating to zero time derivatives in equations (A.17), (A.21), (A.22), (A.24) and (A.25), that the steady state populations  $\rho_{1,\mu\mu}^{(n)}(t \rightarrow \infty)$  as well as the steady state coherence  $\rho_{1,es}^{(n)}(t \rightarrow \infty)$  (and its complex conjugate) are identically zero. This means that, up to first order in the probe field, the control field is undisturbed by the response of the atoms, and thus propagates inside the vapor with group velocity  $c$ . The probe field, however, generates a non vanishing polarization characterized by a linear susceptibility. We can determine this susceptibility from the solution of the coupled system of differential equations (A.20) and (A.23) in the Fourier domain. Fourier transforming equations (A.20) and (A.23), yields

$$-i\omega \underline{\rho}_{1,eg}^{(n)}(\omega) = \frac{i}{2} \underline{\Omega}_p(z_n, \omega) - [\Gamma_p/2 - i\Delta_p] \underline{\rho}_{1,eg}^{(n)}(\omega) + \frac{i}{2} \Omega_c(z_n) \underline{\rho}_{1,sg}^{(n)}(\omega), \quad (\text{A.26})$$

$$-i\omega \underline{\rho}_{1,sg}^{(n)}(\omega) = \frac{i}{2} \Omega_c^*(z_n) \underline{\rho}_{1,eg}^{(n)}(\omega) - i[\Delta_c - \Delta_p] \underline{\rho}_{1,sg}^{(n)}(\omega). \quad (\text{A.27})$$

The solution for the matrix element  $\underline{\rho}_{1,eg}^{(n)}$  is

$$\underline{\rho}_{1,eg}^{(n)}(\omega) = \frac{i \underline{\Omega}_p(z_n, \omega) / 2}{\Gamma_p/2 - i[\Delta_p + \omega] + \frac{i|\Omega_c|^2/4}{[\Delta_p + \omega - \Delta_c]}}. \quad (\text{A.28})$$

The linear susceptibility relates the Fourier transforms  $\underline{\mathbf{P}}_{1,\omega_p}$  and  $\underline{\mathbf{E}}_{\omega_\lambda}$  of the polarization and electric field amplitudes, respectively, via equation (A.11). Therefore, we combine our perturbative expansion  $\hat{\rho}^{(n)} \simeq \hat{\rho}_0^{(n)} + \hat{\rho}_1^{(n)}$  together with the definitions (A.2), (A.3) and (A.4), to recognize that  $\underline{\mathbf{P}}_{1,\omega_p} = 2\mathcal{R}_{1,eg} \mathbf{d}_{ge} \exp(i|\mathbf{k}_p|z)$ . Taking into account that for our isotropic gas of atoms is  $\underline{\Omega}_p \mathbf{d}_{ge} \equiv |\mathbf{d}_{eg}|^2 \underline{\mathbf{E}}_{\omega_p} \exp(-i|\mathbf{k}_p|z) / \hbar$ , we then obtain the Fourier transform  $\underline{\mathbf{P}}_{1,\omega_p} = 2\mathcal{R}_{1,eg} \mathbf{d}_{ge} \exp(i|\mathbf{k}_p|z)$ , via equation (A.28), as

$$\underline{\mathbf{P}}_{1,\omega_p}(z, \omega) = \frac{2\mathcal{N}(z) |\mathbf{d}_{eg}|^2}{\hbar} \frac{1}{\Gamma_p/2 - i[\Delta_p + \omega] + \frac{i|\Omega_c|^2/4}{[\Delta_p + \omega - \Delta_c]}} \frac{i}{2} \underline{\mathbf{E}}_{\omega_p}(z, \omega), \quad (\text{A.29})$$

from which, after comparing it with equation (A.11) and using  $|\mathbf{d}_{eg}|^2 \simeq 3\hbar\pi\epsilon_0 |\mathbf{k}_0|^{-3} \Gamma_p$ , we finally find that the susceptibility is given by

$$\underline{\chi}(z, \omega_p + \omega) = 6\pi\mathcal{N}(z) |\mathbf{k}_0|^{-3} \frac{i\Gamma_p/2}{\Gamma_p/2 - i[\Delta_p + \omega] + \frac{i|\Omega_c|^2/4}{[\Delta_p + \omega - \Delta_c]}}. \quad (\text{A.30})$$

In the equations (A.29) and (A.30) we have introduced the one-dimensional atomic density  $\mathcal{N}(z) = (1/\mathcal{A}_0) \sum_{n=1}^N \delta(z - z_n)$ . For a homogeneous gas of atoms, as we consider throughout

this thesis,  $\mathcal{N}(z) = \mathcal{N}_0$  is constant, and therefore equation (A.30) evaluated at  $\omega = 0$  yields the susceptibility (3.8) introduced in section 3.1.1, corresponding to an ideal monochromatic amplitude  $\underline{\mathbf{E}}_{\omega_p}(\omega - \omega_p) = \mathbf{E}_{\omega_p} 2\pi\delta(\omega - \omega_p)$ .

### A.2.2 Linear susceptibility. Mechanically modulated radiation

First of all, since we are interested in a solution of  $\hat{\rho}^{(n)}$  that is linear in the probe field we use the same perturbation expansion of the previous section, which leads us to the set of equations (A.17) – (A.25). Once again, since the atoms are all initialized in  $|g\rangle$ , a linear dynamics in the probe field results in an unperturbed propagation of the control field through the atomic medium, with group velocity  $c$ . Thus, for a c. w. form we may write

$$\Omega_c(t - z_n/c) = -\tilde{\Omega}_c(z_n) \exp(-i2|\mathbf{k}_c|z_m(t - z_n/c)) \simeq -\tilde{\Omega}_c(z_n)[1 - 2i|\mathbf{k}_c|z_m(t - z_n/c)], \quad (\text{A.31})$$

where  $\tilde{\Omega}_c$  is time independent, and the mirror displacement coordinate is given by  $z_m(t) = [B_m(t) \exp(-i\omega_m t) + \text{c.c.}]$ . Due to the finite propagation speed,  $c$ , of the control radiation field, we have evaluated equation (A.31) at the retarded time  $t_- = t - z_n/c$ . However, for sufficiently small distances between the oscillating mirror and the atoms we may neglect retardation effects. Writing  $z_n = \bar{z}_{at} + \delta z_n$  with  $|\delta z_n| \ll \bar{z}_{at}$ , a sufficiently small distance means that  $z_m(t - z_n/c) \simeq z_m(t)$ , which is fulfilled if  $(\bar{z}_{at}/c) dz_m/dt \sim \omega_m \bar{z}_{at} z_m/c \ll z_m$ , i. e., if  $\omega_m \bar{z}_{at}/c \ll 1$ , a condition that applies to our setup. Consequently, we will replace  $t_-$  by the instantaneous time  $t$  in subsequent calculations.

The mirror motion introduces a residual time dependence with a characteristic time given by the mirror oscillation frequency  $\omega_m$ . The presence of this time dependent modulation precludes a steady state of the dynamics ruled by the set of equations (A.17) – (A.25). To remove the explicit oscillations with the mirror frequency we decompose the density operator in the series

$$\hat{\rho}^{(n)}(t) = \sum_{l=-\infty}^{\infty} \hat{\rho}_{l\omega_m}^{(n)}(t) \exp(-il\omega_m t), \quad (\text{A.32})$$

omitting the subscript  $k = 1$  of our first order perturbation expansion to maintain a clearer notation. Using the series (A.32) of every matrix element  $\rho_{\mu\mu'}^{(n)}$  in the equations (A.17) – (A.25) and assuming the amplitudes  $\rho_{l\omega_m, \mu\mu'}^{(n)}$ , as well as the Rabi frequency  $\Omega_p$ , to be constant during a mirror period  $\tau_m = 2\pi/\omega_m$ , we then can average over  $\tau_m$  on both sides of each of the resulting equations and use the identity  $\tau_m^{-1} \int^{\tau_m} dt \exp(-i[l - l']\omega_m t) = \delta_{ll'}$  to identify the following coupled dynamics for the slowly varying  $\hat{\rho}_{l\omega_m}^{(n)}$

$$\frac{\partial}{\partial t} \hat{\rho}_{l\omega_m}^{(n)} = i l \omega_m \hat{\rho}_{l\omega_m}^{(n)} - \frac{i}{\hbar} [\hat{H}_{0\Lambda}^{(n)}, \hat{\rho}_{l\omega_m}^{(n)}] - \frac{i}{\hbar} \sum_{l'=\pm 1} [\hat{V}_{l'\omega_m}^{(n)}, \hat{\rho}_{(l-l')\omega_m}^{(n)}] + \mathcal{L}[\hat{\rho}_{l\omega_m}^{(n)}] - \frac{i}{\hbar} [\hat{H}_{1\Lambda}^{(n)}, \hat{\sigma}_{gg}] \delta_{l0}. \quad (\text{A.33})$$

In (A.33) the terms in the sum are  $\hat{V}_{+\omega_m}^{(n)} = -i|\mathbf{k}_c|B_m[\tilde{\Omega}_c \hat{\sigma}_{es}^{(n)} - \text{h. c.}]/2$  and  $\hat{V}_{-\omega_m}^{(n)} = [\hat{V}_{+\omega_m}^{(n)}]^\dagger$ , whereas  $\hat{H}_{0\Lambda}^{(n)} = \hbar\Delta_c \hat{\sigma}_{ss}^{(n)} + \hbar[\tilde{\Omega}_c \hat{\sigma}_{es}^{(n)} + \text{h. c.}]/2$  and  $\hat{H}_{1\Lambda}^{(n)} = -\hbar[\Omega_p \hat{\sigma}_{eg}^{(n)} + \text{h. c.}]/2$  conform

the usual (mechanically unmodulated) Hamiltonian of a  $\Lambda$ -atomic medium (except for the sign flip of the control Rabi frequency). Since for increasingly large values of  $l$  the factor  $il\omega_m$  in (A.33) becomes an increasingly high effective detuning, in order to find an approximate solution of the dynamics of the full density operator  $\hat{\rho}^{(n)}$  we may use the following strategy. We start adiabatically eliminating the motion of an amplitude  $\hat{\rho}_{l\omega_m}^{(n)}$  with a high enough  $\bar{l}$  and substitute the result into the dynamical equation for the immediately lower order amplitude,  $\hat{\rho}_{(\bar{l}-1)\omega_m}^{(n)}$ . We then apply this combo of adiabatic elimination and backward substitution successively, until we reach the equation of motion for  $\hat{\rho}_0^{(n)}$ . Finally, solving the dynamics of  $\hat{\rho}_0^{(n)}$  allows us to recursively find all the other amplitudes  $\hat{\rho}_{l \leq \bar{l}}^{(n)}$ . Fortunately, for the values of interest of the optical detunings, Rabi frequencies and mirror displacements taking part in (A.33), this task becomes simpler. We pursue a solution of (A.33) for small mirror oscillation amplitudes and high mirror oscillation frequency, i. e., up to first order in the small parameter  $|\hat{V}_{+\omega_m}^{(n)} / [\hbar\omega_m]| \sim |\mathbf{k}_c|Z_{\max}|\tilde{\Omega}_c|/\omega_m$ , where  $Z_{\max} = \max\{|B_m|\}$ . This approximately amounts to solve (A.33) up to  $|l| \leq 1$ , neglecting the contributions proportional to  $\hat{\rho}_{\pm\omega_m}^{(n)}$  in the equation for  $l = 0$ , as well as those proportional to  $\hat{\rho}_{\pm 2\omega_m}^{(n)}$  in the equations for  $l = \pm 1$ . As in the previous section A.2.1, the pair of coherences  $\rho_{l\omega_m, eg}^{(n)}$  and  $\rho_{l\omega_m, sg}^{(n)}$  decouple from the rest (for each value of  $|l| \leq 1$ ). Next, we shall outline the solution for the positive frequency amplitude  $\rho_{\omega_m, eg}^{(n)}$ , the solution for its negative frequency counterpart being obtained in a similar way. After taking the considerations above, namely retaining terms up to first order in  $|\mathbf{k}_c|B_m|\tilde{\Omega}_c|/\omega_m$ , the coupled equations that we need to solve are

$$\frac{\partial}{\partial t}\rho_{0, eg}^{(n)}(t) = \frac{i}{2}\Omega_p(z_n, t) - [\Gamma_p/2 - i\Delta_p]\rho_{0, eg}^{(n)}(t) - \frac{i}{2}\tilde{\Omega}_c(z_n)\rho_{0, sg}^{(n)}(t), \quad (\text{A.34})$$

$$\frac{\partial}{\partial t}\rho_{0, gs}^{(n)}(t) = -\frac{i}{2}\tilde{\Omega}_c^*(z_n)\rho_{0, eg}^{(n)}(t) - i[\Delta_c - \Delta_p]\rho_{0, sg}^{(n)}(t), \quad (\text{A.35})$$

$$\frac{\partial}{\partial t}\rho_{\omega_m, eg}^{(n)}(t) = -[\Gamma_p/2 + i\omega_m]\rho_{\omega_m, eg}^{(n)}(t) - \frac{i}{2}\tilde{\Omega}_c(z_n)\rho_{\omega_m, sg}^{(n)}(t) - \frac{1}{2}|\mathbf{k}_c||B_m(t)|\tilde{\Omega}_c(z_n)\rho_{0, sg}^{(n)}(t), \quad (\text{A.36})$$

$$\frac{\partial}{\partial t}\rho_{\omega_m, gs}^{(n)}(t) = -i[\Delta_c - \omega_m]\rho_{\omega_m, sg}^{(n)}(t) - \frac{i}{2}\tilde{\Omega}_c^*(z_n)\rho_{\omega_m, eg}^{(n)}(t) + \frac{1}{2}|\mathbf{k}_c||B_m(t)|\tilde{\Omega}_c^*(z_n)\rho_{0, eg}^{(n)}(t). \quad (\text{A.37})$$

Equations (A.34) – (A.37) are easily solvable in the Fourier domain for a time independent sideband strength, i. e.  $|\mathbf{k}_c|B_m = |\mathbf{k}_c|B_{0m} = \eta$ . We will assume so from now on<sup>2</sup>. Thus, the solution for the amplitude  $\rho_{\omega_m, eg}^{(n)}$  in Fourier space reads

$$\underline{\rho}_{\omega_m, eg}^{(n)}(\omega) \left[ \Gamma_p/2 - i[\Delta_p + \omega_m + \omega] + \frac{i|\tilde{\Omega}_c|^2/4}{\Delta_p + \omega_m + \omega - \Delta_c} \right] = -\frac{\omega_m\eta|\tilde{\Omega}_c|^2\rho_{0, eg}^{(n)}(\omega)}{(\Delta_p - \Delta_c + \omega)^2 + \omega_m(\Delta_p - \Delta_c + \omega)}, \quad (\text{A.38})$$

---

2 Should the amplitude  $B_m$  be time dependent we could first adiabatically eliminate the first harmonics  $\rho_{\omega_m, \mu\mu'}^{(n)}$ , while solving via Fourier transformation the zeroth order harmonics  $\rho_{0, \mu\mu'}^{(n)}$ .

## A.2 Dynamics of the optically driven atoms

with  $\rho_{0,eg}^{(n)}(\omega)$  given by the r.h.s. of equation (A.28) (note that  $|\tilde{\Omega}_c|^2 = |\Omega_c|^2$ ). Hence, the close form for  $\rho_{\omega_m,eg}^{(n)}$  reads

$$\rho_{\omega_m,eg}^{(n)}(\omega) = \frac{2i\omega_m\eta\Omega_p(z_n,\omega)|\tilde{\Omega}_c|^2}{\mathcal{B}(\omega_p + \omega)\mathcal{B}(\omega_p + \omega_m + \omega)}, \quad (\text{A.39})$$

with

$$\mathcal{B}(\omega_p + \omega) = 2i[\Gamma_p - 2i(\Delta_p + \omega)][\Delta_c - \Delta_p - \omega] + |\tilde{\Omega}_c|^2. \quad (\text{A.40})$$

Here, we shall note that for  $\Delta_p = 0$  and a monochromatic probe field,  $\Omega_p(z_n) = 2\pi\Omega_p(z_0)\delta(\omega)$ , the inverse Fourier transform of equation (A.39) yields (3.19), the coherence  $\rho_{\omega_m}(\Delta_c)$  that we introduced in chapter 3. We obtain the negative frequency counterpart of (A.39) through a similar procedure. The outcome is

$$\rho_{-\omega_m,eg}^{(n)}(\omega) = \frac{-2i\omega_m\eta^*\Omega_p(z_n,\omega)|\tilde{\Omega}_c|^2}{\mathcal{B}(\omega_p + \omega)\mathcal{B}(\omega_p - \omega_m + \omega)}. \quad (\text{A.41})$$

Together with the r. h. s. of equation (A.28), which determines  $\rho_{0,eg}$ , the expressions (A.39), (A.40) and (A.41) fully determine the linear polarization of the medium. By integrating the electromagnetic wave equation we can finally obtain the radiation pressure force impinging on the nano-mechanical mirror. For ease of readability, it is convenient to express the equations above more compactly. We can do this in terms of the so called polarizability, that is, the average atomic dipole per unit electric field. In Fourier space, and with the help of the definitions (A.32) and (A.38) – (A.41), the average atomic dipole,  $\sum_{\mu,\mu'} \rho_{\mu'\mu}^{(n)}(\omega) \mathbf{d}_{\mu\mu'} \exp(-i\nu_{\mu'\mu}t)$ , is found to be

$$4\pi\epsilon_0\alpha_p(\omega_p + \omega) \left\{ 1 - \frac{2|\mathbf{k}_0|^3}{3} \left[ \alpha_p(\omega_p + \omega_m + \omega) \frac{\omega_m|\mathbf{k}_c|b_m(t)|\tilde{\Omega}_c|^2/4}{(\Delta_p - \Delta_c + \omega)^2 + \omega_m(\Delta_p - \Delta_c + \omega)} \right. \right. \\ \left. \left. - \alpha_p(\omega_p - \omega_m + \omega) \frac{\omega_m|\mathbf{k}_c|b_m^*(t)|\tilde{\Omega}_c|^2/4}{(\Delta_p - \Delta_c + \omega)^2 - \omega_m(\Delta_p - \Delta_c + \omega)} \right] \right\} \mathcal{E}_{\omega_p}(z_n,\omega) e^{-i\omega_p t} \\ + \text{c.c.}, \quad (\text{A.42})$$

where we have used the fact that  $\eta \exp(-i\omega_m t) = |\mathbf{k}_c|b_m(t)$  and introduced the aforementioned polarizability,

$$\alpha_p(\omega_p + \omega) = \frac{3}{2}|\mathbf{k}_0|^{-3} \frac{i\Gamma_p/2}{\Gamma_p/2 - i[\Delta_p + \omega] + \frac{i|\Omega_c|^2/4}{[\Delta_p + \omega - \Delta_c]}}. \quad (\text{A.43})$$

Multiplying equation (A.42) by  $\mathcal{N}(z) \exp(i|\mathbf{k}_p|z)$ , where  $\mathcal{N}(z) = (1/\mathcal{A}_0) \sum_{n=1}^N \delta(z - z_n)$  denotes the distribution function, and integrating over the Fourier frequency  $\omega$ , we obtain the polarization in a form which allows us to identify its slowly varying amplitude very easily. With the latter one we may integrate the corresponding electromagnetic wave equation (A.5).



For that, we introduce new variables  $\tau = \pm[t - z/c]$  and  $\xi = z$ , so that the wave propagator transforms into  $\partial/\partial t \pm c\partial/\partial z \mapsto \pm c\partial/\partial \xi$ ; here, as in equation (A.5), the plus and minus signs indicate, respectively, a wave propagation in the positive or negative direction along the  $z$ -axis. In the new variables the wave equation reads

$$-c \frac{\partial}{\partial \xi} \mathbf{E}_{\omega_p}(\xi, \tau) = i \frac{\omega_p}{2} \int_{-\infty}^{+\infty} dt' \tilde{\chi}(\xi, t'; \tau + t') \mathbf{E}_{\omega_p}(\xi, \tau - t'), \quad (\text{A.44})$$

where the response function  $\tilde{\chi}(\xi, t'; \tau + t') = \int d\omega / (2\pi) \underline{\chi}(\xi, \omega_p + \omega; \tau + t') \exp(-i\omega t')$  is given in terms of the susceptibility as

$$\begin{aligned} \frac{\underline{\chi}(\xi, \omega_p + \omega; \tau + t')}{4\pi\alpha_p(\omega_p + \omega)} = \mathcal{N}(z) \left\{ 1 - \frac{2|\mathbf{k}_0|^3}{3} \left[ \alpha_p(\omega_p + \omega_m + \omega) \frac{\omega_m |\mathbf{k}_c| b_m(\tau + t') |\tilde{\Omega}_c|^2 / 4}{(\Delta_p - \Delta_c + \omega)^2 + \omega_m(\Delta_p - \Delta_c + \omega)} \right. \right. \\ \left. \left. - \alpha_p(\omega_p - \omega_m + \omega) \frac{\omega_m |\mathbf{k}_c| b_m^*(\tau + t') |\tilde{\Omega}_c|^2 / 4}{(\Delta_p - \Delta_c + \omega)^2 - \omega_m(\Delta_p - \Delta_c + \omega)} \right] \right\}. \end{aligned} \quad (\text{A.45})$$

A solution of the wave equation (A.5) above provides us the probe electric field transmitted through the medium. Particularizing for our homogeneous medium  $\mathcal{N}(z) = \mathcal{N}_0$ , driven by monochromatic fields, so that  $\underline{\mathbf{E}}_{\omega_p} = 2\pi \mathbf{E}_{\omega_p} \delta(\omega)$ , the positive frequency part of the transmitted field reads

$$\frac{1}{2} \mathcal{E}_{\omega_p}(L/2 + \bar{z}_{\text{at}}) \exp\left(-\frac{\omega_p L}{2c} \underline{\chi}''(\omega_p; t - L/c)\right) \exp\left(i \frac{\omega_p L}{2c} [1 + \underline{\chi}'(\omega_p; t - L/c)] - i\omega_p t\right). \quad (\text{A.46})$$

As we mentioned earlier, retarded effects can be neglected. Therefore, the transmission of the probe field is

$$T_{\omega_p}(t) = \left| \frac{\mathcal{E}_{\omega_p}(-L/2 + \bar{z}_{\text{at}}, t)}{\mathcal{E}_{\omega_p}(L/2 + \bar{z}_{\text{at}})} \right|^2 \simeq \exp(-\omega_p L \underline{\chi}''(\omega_p; t)/c) \approx 1 - |\mathbf{k}_p| L \underline{\chi}''(\omega_p; t), \quad (\text{A.47})$$

where we used the dispersion relation in free space  $|\mathbf{k}_p| = \omega_p/c$ . The transmission (A.47) times the input power of the beam gives us equation (3.17) of chapter 3.

### A.3 Radiation damping of mirror's oscillation amplitude

Here we sketch out a derivation of the effective damping rate induced by the radiation pressure force of the probe field. Since this carries the mechanical modulations back to the mirror dynamics it gives rise to friction, having an impact on the oscillation amplitude of the mirror displacement coordinate. As we learnt in chapter 2, this effect can be analyzed appropriately via the equation of motion for the averaged energy of the oscillator.

Written in units of length and neglecting fast rotating terms ( $\propto e^{\pm 2i\omega_m t}$ ), the time evolution of the amplitude of motion of the mirror,  $Z = \sqrt{b_m^* b_m}$ , reads

$$\dot{Z}(t) \simeq \frac{F_{0p} 6\mathcal{N}_0 \pi |\mathbf{k}_p|^{-2} L}{2M\omega_m} \text{Re}[\Gamma_p \delta\rho_{eg} / \Omega_p |e^{i(\alpha + \pi/2)}]. \quad (\text{A.48})$$

### A.3 Radiation damping of mirror's oscillation amplitude

Here,  $|\Gamma_p \delta \rho_{eg} / \Omega_p|$  and  $\alpha$  are derived in section 3.3.3 for constant mirror oscillations. Since the amplitude of mirror oscillations is now allowed to change in time, we make the replacement  $|\delta \rho_{eg}(t)| \mapsto [|\delta \rho_{eg} / \eta|] |\mathbf{k}_c| Z(t)$  in equation (A.48), where we used the linear dependence of  $\delta \rho_{eg}$  on the mirror oscillation amplitude  $\sim \eta$  found in section 3.3.2. The relative phase  $\alpha$  does not depend on  $Z(t)$  and hence remains constant. We can finally solve equation (A.48) coarse grained in time ( $t > \tau_m$ ) by averaging over one mirror period to remove small variations of  $Z(t)$ , and obtain

$$\dot{\bar{Z}}(t) = -\frac{|\mathbf{k}_c| F_{0p}}{2M\omega_m} 6\mathcal{N}_0\pi |\mathbf{k}_p|^{-2} L \left[ \frac{|\Gamma_p \delta \rho_{eg} / \Omega_p|}{|\eta|} \right] \bar{Z}(t) \sin \alpha, \quad (\text{A.49})$$

with the solution (3.25) – (3.26) in section 3.4.1.

# B Supplement: parameters, electromagnetic coupling and joint evolution of a torsion pendulum and a Rydberg atom

## B.1 Mechanical frequency of torsion pendulum

We consider that the resonance frequency of the oscillating motion of the torsion mechanical resonator (a singly clamped nanotube) introduced in chapter 4, section 4.1, is given by the eigenfrequency of the lowest torsion mechanical mode the resonator. This is assumed to be [163]

$$\omega_{\text{osc}} = \sqrt{\frac{\kappa}{I}}. \quad (\text{B.1})$$

Here,  $I$  is the total moment of inertia with respect to the symmetry axis of the nanotube. It takes into account the entire assembly of ferroelectric particle, and nanotube that comprises the oscillator. The quantity  $\kappa$  denotes the torsional spring constant of the nanotube. We consider a value of  $\kappa = 2.085 \times 10^{-11}$  N m. For a carbon nanotube of mass  $m_{\text{cnt}} = 8.71 \times 10^{-19}$  kg (length  $\ell = 148.54$  nm) and diameter  $w = 75.79$  nm with a spherical ferroelectric load of mass  $m_{\text{sfl}} = 6.31 \times 10^{-18}$  kg and radius  $r = 63.3$  nm we obtain a total moment of inertia  $I \approx m_{\text{cnt}}w^2/4 + 2m_{\text{sfl}}r^2/5 \simeq 1.126 \times 10^{-32}$  kg<sup>2</sup> m. This finally corresponds to a frequency  $\omega_{\text{osc}}/(2\pi) \simeq 6848.69$  MHz as specified in the main text.

## B.2 Coupling a two-level atom and a torsion pendulum

In this complement we derive the interaction energy between a ferroelectric load mounted on the torsion pendulum of chapter 4 and a two-level atom.

To enable an interaction between the motion of our torsion pendulum and an atom we rely on electromagnetic radiation. We equip the torsion pendulum with a ferroelectric material. We consider an approximately spherical ferroelectric load with net charge equal to zero. However, the charges in the material are distributed so as to confer the ferroelectric load a permanent electric dipole moment  $\mathbf{d}_{\text{osc}}$ . Due to the oscillatory motion of the torsion pendulum this electric dipole swings back and forth around an equilibrium configuration, and hence accounts for an electromagnetic source current. While we can formally write down an exact solution for the electromagnetic field radiated by an arbitrary time dependent source current, the outcome is normally too intricate for further practical uses. It is often more convenient to employ assumptions relative to the average size of the source charge, in our case the diameter  $2r$  of the spherical load, the characteristic wavelength of the emitted radiation  $\lambda$ , and the distance from the source to the observation point  $\mathbf{R}$ ; then one may use instead approximate expressions to describe the radiated electric and magnetic fields

that arise from those assumptions, as well as their potential influence on a test particle. Of particular interest for us will be the so called near zone limit, which can be thought to emerge for a hierarchy of length scales fulfilling  $2r \ll |\mathbf{R}| \ll \lambda$ . In the following, we will show how does apply this near zone limit in the case of our particular source current, and what consequences does it entail for the ensuing radiated fields. Note that, since the signal of our source current is of a rather arbitrary time dependence, the emitted radiation will in principle be constituted by an infinite number of modes. Hence, the main goal of the following analysis will be to identify those physical circumstances that may enable us to consider only a few modes of the signal, the modes that will be relevant for the coupling of the field to a test atom.

### B.2.1 Electromagnetic radiation of a point electric dipole attached to a torsion pendulum

We will consider that  $r \ll \lambda$ , i.e., the size of the ferroelectric load containing the current is many times smaller than a typical wavelength of the emitted radiation,  $\lambda \sim ct_0$  with  $t_0$  being a characteristic period of time during which the charges undergo an appreciable change. This amounts to a non relativistic limit in which all the charges in the ferroelectric load will move with velocities  $\sim r/t_0$  considerably smaller than the speed of light  $c$ . Additionally, we will be interested in distances  $|\mathbf{R}| \gg r$ . In such case we will be able to think of a point electric dipole current [140, 218, 219], well localized at the center of the ferroelectric load, where we will place the origin of our Cartesian coordinate system, see sketch figure 4.1. We will further assume that vacuum is the space surrounding our mechanical device. The magnetic and electric fields,  $\mathbf{B}$  and  $\mathbf{E}$  respectively, of the point dipole are then found to be [102]

$$\mathbf{B}(\mathbf{R}, t) = -\frac{1}{4\pi\epsilon_0 c} \left[ \frac{1}{c R^2} \frac{\partial}{\partial t} + \frac{1}{c^2 R} \frac{\partial^2}{\partial t^2} \right] [\mathbf{u} \times \mathbf{d}_{\text{osc}}(t - R/c)], \quad (\text{B.2})$$

$$\mathbf{E}(\mathbf{R}, t) = \mathbf{E}_{\parallel}(\mathbf{R}, t) + \mathbf{E}_{\perp}(\mathbf{R}, t). \quad (\text{B.3})$$

The magnetic field is purely transverse, i.e, perpendicular to the direction of the unit norm vector  $\mathbf{u} = \mathbf{R}/R$ , with  $R = |\mathbf{R}|$ , that accounts for the propagation direction of the emitted electromagnetic signal. While the electric field comprises both a longitudinal and a transverse part,  $\mathbf{E}_{\parallel}$  and  $\mathbf{E}_{\perp}$  respectively, which read

$$\mathbf{E}_{\parallel}(\mathbf{R}, t) = \frac{1}{4\pi\epsilon_0} \left( \frac{2}{R^3} + \frac{2}{c R^2} \frac{\partial}{\partial t} \right) \mathbf{u} \cdot \mathbf{d}_{\text{osc}}(t - R/c) \mathbf{u}, \quad (\text{B.4})$$

$$\mathbf{E}_{\perp}(\mathbf{R}, t) = \frac{1}{4\pi\epsilon_0} \left( \frac{1}{R^3} + \frac{1}{c R^2} \frac{\partial}{\partial t} + \frac{1}{c^2 R} \frac{\partial^2}{\partial t^2} \right) [\mathbf{u} \cdot \mathbf{d}_{\text{osc}}(t - R/c) \mathbf{u} - \mathbf{d}_{\text{osc}}(t - R/c)]. \quad (\text{B.5})$$

Equations (B.2), (B.4) and (B.5) tell us that the magnetic and electric fields observed at the spatial location  $\mathbf{R}$  and time  $t$  derive from the point electric dipole  $\mathbf{d}_{\text{osc}}$  located in the origin of our reference frame and evaluated at an earlier or retarded time  $t_r = t - R/c$ . The retarded time as well as the terms proportional to the velocity (first time derivative) and acceleration (second time derivative) of the charges representing the point dipole arise both from the

finite nature of the speed of light. The remaining terms, proportional to  $R^{-3}$ , are due to the Coulomb's law, characteristic of a static scenario of charges. In order to assess and contrast the relevance of the contributions due to static and retarded effects in formulas (B.2), (B.4) and (B.5) we shall specify further an explicit form for the spectrum of the source (the point electric dipole).

### B.2.2 Frequency spectrum of the radiated signal. The *near zone* limit

The torsion angle  $\varphi = \varphi_0 + \delta\varphi$  describes the oscillating dynamics of the torsion pendulum, and hence the swinging of the point electric dipole representing the source current (see sketch figure 4.1). The angle  $\varphi_0$  defines the equilibrium configuration of the torsional oscillator. Angular displacements  $\delta\varphi$  take place around the symmetry axis of the torsional oscillator, which extends along the  $y$ -axis. The point dipole moves then in the  $x$ - $z$  plane and we may write it in vector components as

$$\mathbf{d}_{\text{osc}}(t_r) = |\mathbf{d}_{\text{osc}}| [\cos(\varphi_0 + \delta\varphi(t_r))\mathbf{u}_z + \sin(\varphi_0 + \delta\varphi(t_r))\mathbf{u}_x], \quad (\text{B.6})$$

where  $\mathbf{u}_x$  and  $\mathbf{u}_z$  are unit norm vectors in the  $x$  and  $z$  directions, respectively. To proceed with our analysis it will be sufficiently for us to consider the case of a force-free motion of the torsion pendulum. Harmonic oscillations  $\delta\varphi(t_r) = \delta\varphi_0 \cos(\omega_{\text{osc}}t_r + \theta_0)$  of the torsion angle will then determine the dynamics of the torsion pendulum, where  $\delta\varphi_0 > 0$  and  $\theta_0$  stand for the initial angle and phase of the angular displacements. This allows us to expand  $\varphi$ , and thus the equation (B.6), in a Fourier series, so that we can explicitly write the fields as  $\underline{\mathbf{E}}_{\parallel(\perp)}(\mathbf{R}, \omega) = 2\pi \sum_{n=0}^{\infty} 1/2 [\mathbf{E}_{\parallel(\perp), \omega_n}(\mathbf{R})\delta(\omega - \omega_n) + \mathbf{E}_{\parallel(\perp), \omega_n}^*(\mathbf{R})\delta(\omega + \omega_n)]$  and  $\underline{\mathbf{B}}(\mathbf{R}, \omega) = 2\pi \sum_{n=0}^{\infty} 1/2 [\mathbf{B}_{\omega_n}(\mathbf{R})\delta(\omega - \omega_n) + \mathbf{B}_{\omega_n}^*(\mathbf{R})\delta(\omega + \omega_n)]$ , where  $\delta(\omega)$  and the asterisk denote the Dirac delta function and complex conjugation respectively, and  $\underline{\mathbf{C}}(\omega) = \int_{-\infty}^{+\infty} dt / (2\pi) e^{-i\omega t} \mathbf{C}$  is the Fourier transform of the vector field  $\mathbf{C}$ . For  $n \geq 1$ , the complex coefficients  $\mathbf{B}_{\omega_n}(\mathbf{R})$  and  $\mathbf{E}_{\parallel(\perp), \omega_n}(\mathbf{R})$  read

$$\mathbf{B}_{\omega_n}(\mathbf{R}) = \frac{2|\mathbf{d}_{\text{osc}}| J_n(\delta\varphi_0) e^{-in\theta_0}}{4\pi\epsilon_0 c} \frac{e^{ik_n R}}{R} k_n^2 \left( \frac{i}{k_n R} + 1 \right) [\mathbf{u} \times \boldsymbol{\epsilon}_n], \quad (\text{B.7})$$

$$\mathbf{E}_{\parallel, \omega_n}(\mathbf{R}) = \frac{2|\mathbf{d}_{\text{osc}}| J_n(\delta\varphi_0) e^{-in\theta_0}}{4\pi\epsilon_0} \frac{e^{ik_n R}}{R} k_n^2 \left( \frac{2}{k_n^2 R^2} - \frac{2i}{k_n R} \right) (\mathbf{u} \cdot \boldsymbol{\epsilon}_n) \mathbf{u}, \quad (\text{B.8})$$

$$\mathbf{E}_{\perp, \omega_n}(\mathbf{R}) = \frac{2|\mathbf{d}_{\text{osc}}| J_n(\delta\varphi_0) e^{-in\theta_0}}{4\pi\epsilon_0} \frac{e^{ik_n R}}{R} k_n^2 \left( \frac{1}{k_n^2 R^2} - \frac{i}{k_n R} - 1 \right) [(\mathbf{u} \cdot \boldsymbol{\epsilon}_n) \mathbf{u} - \boldsymbol{\epsilon}_n], \quad (\text{B.9})$$

where we introduce the wavenumber  $k_n = \omega_n/c$ , with  $\omega_n = n\omega_{\text{osc}}$ , and the unit norm vector

$$\boldsymbol{\epsilon}_n = \cos(\varphi_0 + n\pi/2)\mathbf{u}_z + \sin(\varphi_0 + n\pi/2)\mathbf{u}_x, \quad (\text{B.10})$$

while  $J_n(\delta\varphi_0)$  is the Bessel function of the first kind of order  $n$ . The coefficients for  $n = 0$  describe the fields of a stationary point electric dipole, and thus (using  $\underline{\mathcal{C}}(\omega)\delta\omega \equiv \underline{\mathcal{C}}(0)\delta(\omega)$  with  $\underline{\mathcal{C}}$  an arbitrary function)  $\mathbf{B}_{\omega_0}(\mathbf{R}) = \mathbf{0}$ , whereas  $\mathbf{E}_{\parallel, \omega_0}(\mathbf{R}) = 2|\mathbf{d}_{\text{osc}}| J_0(\delta\varphi_0) (\mathbf{u} \cdot$

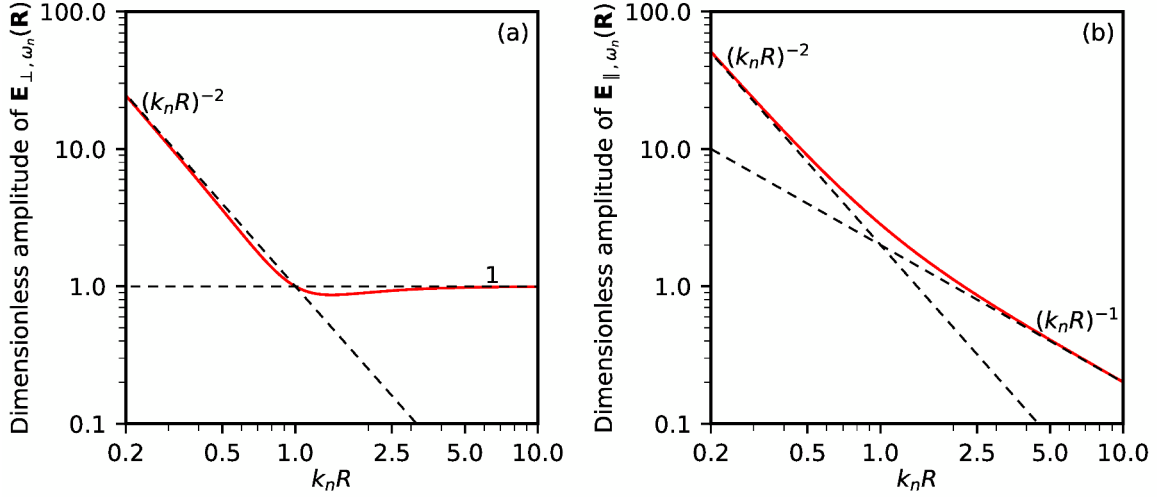


**Figure B.1** Radial behavior of the transverse (a) and longitudinal (b) amplitudes of the frequency spectrum of the electric field. The plots correspond to the norm of the polynomials in  $k_n R$  within parenthesis in formulas (B.8) and (B.9).

$\epsilon_0 \mathbf{u} / (4\pi\epsilon_0 R^3)$  and  $\mathbf{E}_{\perp,\omega_n}(\mathbf{R}) = |\mathbf{d}_{\text{osc}}| J_0(\delta\varphi_0) [(\mathbf{u} \cdot \epsilon_0) \mathbf{u} - \epsilon_0] / (4\pi\epsilon_0 R^3)$ . Equations (B.7), (B.8) and (B.9) are proportional to polynomials in  $k_n R$  which dictate the radial behavior of the spectrum of the fields. At this point, we learn that the *near zone* limit, corresponding to  $k_n R \ll 1$  for each mode  $n \neq 0$ , is predominantly electric, with amplitudes  $|\mathbf{E}_{\parallel(\perp),\omega_n}(\mathbf{R})|$  that scale with the distance to the observation point as  $R^{-3}$ . In the *near zone* the fields are then quasi-static and retarded effects do not play any relevant role. We can clearly appreciate the scaling of the electric field with  $R$  if we look at figure B.1. There, we plot the longitudinal and transverse amplitudes of a given mode  $n \neq 0$  of the electric field spectrum, equations (B.8) and (B.9) respectively, in units of the amplitude  $|\mathbf{E}_{\text{FF},\omega_n}(\mathbf{R})| = 2|\mathbf{d}_{\text{osc}}| J_n(\delta\varphi_0) k_n^2 / (4\pi\epsilon_0 R)$  that describes the electric field spectrum in the so called *far zone* limit  $k_n R \gg 1$ .

### B.2.3 Interaction between a two level atom and a mechanically modulated point electric dipole

The interaction Hamiltonian for an atom (with dipole operator  $\hat{\mathbf{d}}_{\text{at}}$ ) placed at  $\mathbf{R} = \mathbf{R}_0$  under the action of the field radiated by the ferroelectric nanoparticle is given, in the dipole approximation, by  $\hat{H}_{\text{int}} = -\hat{\mathbf{d}}_{\text{at}} \cdot \mathbf{E}(\mathbf{R}_0, t)$ , the magnetic contribution being small enough to be neglected (see section B.2.2 above). From the expressions (B.8) and (B.9) above we observe that if the amplitude of the angular displacements is small,  $\delta\varphi_0 \ll 1$ , we may envisage a *near zone* regime for distances such that  $R \ll c/\omega_{\text{osc}}$ . This follows from the fact that Bessel functions for small argument are all increasingly vanishing for increasing  $n$ . In general, we may conclude that a *near zone* description, devoid of retarded effects, is accurate if the motion of the source is tightly bounded, with a characteristic frequency  $\omega_s$  such that  $R \ll c/\omega_s$  is fulfilled. For the frequency of our torsion mechanical mode is  $c/\omega_{\text{osc}} \sim 4$  cm, a figure nearly four orders of magnitude larger than the distances  $R$  that we consider here (of the order of a

few microns). Thus, in what follows, we let  $\delta\varphi$  to be subjected to a Langevin dynamics while assuming valid a *near zone* description. For that, we require small angular displacements, in the sense that  $|\delta\varphi| \ll \varphi_0$ . This allows us to expand in a Taylor series the sinusoidal functions in the expression for the dipole (B.6), around the equilibrium value  $\varphi_0$ . We substitute the series in the expressions (B.4) and (B.5) of the longitudinal and transverse electric fields, neglect time derivatives and replace  $t_r$  by  $t$ . Then, retaining terms up to second order in  $\delta\varphi$ , the total electric field  $\mathbf{E} = \mathbf{E}_{\parallel} + \mathbf{E}_{\perp}$  is found to be

$$\mathbf{E}(\mathbf{R}, t) \simeq \frac{|\mathbf{d}_{\text{osc}}|}{4\pi\epsilon_0 R^3} \left\{ \frac{3}{R^2} \mathbf{R} \cdot \left[ \epsilon_0 \left( 1 - \frac{\delta\varphi^2(t)}{2} \right) + \delta\varphi(t) \epsilon_1 \right] \mathbf{R} - \epsilon_0 \left[ 1 - \frac{\delta\varphi^2(t)}{2} \right] + \delta\varphi(t) \epsilon_1 \right\}. \quad (\text{B.11})$$

For a two-level atom with levels  $|a\rangle$  and  $|b\rangle$  we can write the dipole operator as  $\hat{\mathbf{d}}_{\text{at}} =$

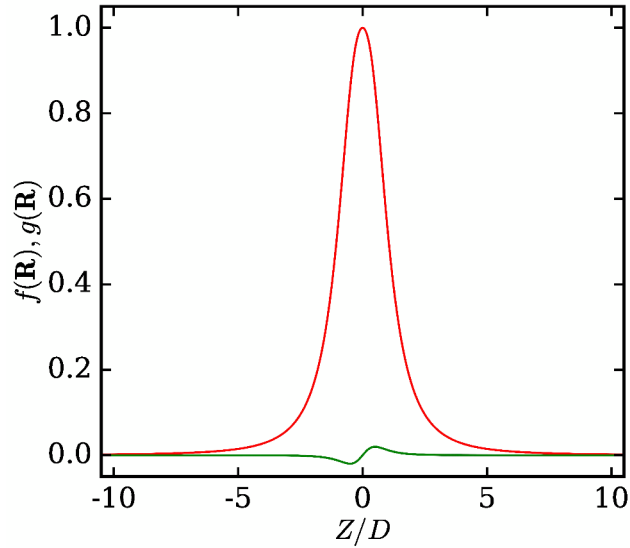


**Figure B.2** Coupling functions  $f(X, Y, Z)$  (red) and  $g(X, Y, Z)$  (green) along the axis of the waveguide. Parameters are  $D \simeq 21.68 \mu\text{m}$ ,  $X/D \simeq 0.0231$ , and  $Y/D = 0.9997$ .

$\mathbf{d}_{ba}[\hat{\sigma}_{ba} + \hat{\sigma}_{ab}]$  (see section 2.2.1), where we assume here a real transition dipole moment  $\mathbf{d}_{ba} = \langle b | \hat{\mathbf{d}}_{\text{at}} | a \rangle = \langle a | \hat{\mathbf{d}}_{\text{at}} | b \rangle$ . In principle, the direction of  $\mathbf{d}_{ba}$  depends on the states in question. To simplify matters we choose the two levels such that  $\mathbf{d}_{ba} = |\mathbf{d}_{ba}| \mathbf{u}_z$ . Using rectangular coordinates, so that  $\mathbf{R} = [X, Y, Z]^T$ , and the definition (B.10) for the unit vectors  $\epsilon_n$ , the interaction Hamiltonian can be written as

$$\hat{H}_{\text{int}} \simeq -V_0 [\hat{\sigma}_{ba} + \hat{\sigma}_{ab}] \left[ g(\mathbf{R}_0) \delta\varphi(t) - f(\mathbf{R}_0) \left( 1 - \frac{\delta\varphi^2(t)}{2} \right) \right] \cos \varphi_0 \quad (\text{B.12})$$

$$-V_0 [\hat{\sigma}_{ba} + \hat{\sigma}_{ab}] \left[ f(\mathbf{R}_0) \delta\varphi(t) + g(\mathbf{R}_0) \left( 1 - \frac{\delta\varphi^2(t)}{2} \right) \right] \sin \varphi_0, \quad (\text{B.13})$$

where  $f(\mathbf{R}_0) = [D_0/R_0]^3[1 - 3Z_0^2/R_0^2]$  and  $g(\mathbf{R}_0) = 3X_0Z_0D_0^3/R_0^5$  are the coupling functions depicted in figure B.2 and  $V_0 = |\mathbf{d}_{ba}||\mathbf{d}_{\text{osc}}|/(4\pi\epsilon_0D_0^3)$  is the interaction energy strength with  $D_0 = \sqrt{X_0^2 + Y_0^2}$  the minimum separation (for the geometry we chose) between atom and center of the nanoparticle. For an equilibrium configuration of the torsion mechanical mode such that  $\varphi_0 = \pi/2$ , the terms proportional to  $\cos \varphi_0$  in the r. h. s. of equation (B.13) can be ignored. We choose such a configuration from now on. Next, since the radiation field is completely specified in terms of the canonical variable  $\delta\varphi$ , we use Born's quantization rule and replace  $\delta\varphi$  and its conjugate momentum (the angular momentum  $L_{\delta\varphi}$  along the axis of rotation) by its associated operators, and subsequently express them in terms of the mechanical phonon creation  $\hat{c}^\dagger$  and annihilation  $\hat{c}$  operators. The latter ones are then subject to the usual commutation relation  $[\hat{c}, \hat{c}^\dagger] = 1$  (here written in the global Hilbert space of atom plus torsion pendulum), so that

$$\hat{\delta\varphi} = \varphi_{\text{zpm}}[\hat{c} + \hat{c}^\dagger], \quad (\text{B.14})$$

$$\hat{\delta\varphi}^2 = \varphi_{\text{zpm}}^2[\hat{c} + \hat{c}^\dagger]^2 = \varphi_{\text{zpm}}^2[\hat{c}^2 + (\hat{c}^\dagger)^2 + 2\hat{c}^\dagger\hat{c} + 1], \quad (\text{B.15})$$

where  $\varphi_{\text{zpm}} = \sqrt{\hbar/(2\omega_{\text{osc}}I)}$  represents the amplitude of the zero point motion of the torsion pendulum. In terms of creation and annihilation operators, the interaction Hamiltonian (B.13) with  $\varphi_0 = \pi/2$ , reads

$$\begin{aligned} \hat{H}_{\text{int}}/\hbar \simeq & \varphi_{\text{zpm}}^2 \frac{V_0}{\hbar} g(\mathbf{R}_0) [\hat{\sigma}_{ba} + \hat{\sigma}_{ab}] \hat{c}^\dagger \hat{c} - \frac{V_0}{\hbar} g(\mathbf{R}_0) [1 - \varphi_{\text{zpm}}^2/2] [\hat{\sigma}_{ba} + \hat{\sigma}_{ab}] \\ & - \varphi_{\text{zpm}} \frac{V_0}{\hbar} f(\mathbf{R}_0) [\hat{\sigma}_{ba} + \hat{\sigma}_{ab}] [\hat{c} + \hat{c}^\dagger] - \varphi_{\text{zpm}}^2 \frac{V_0}{2\hbar} g(\mathbf{R}_0) [\hat{\sigma}_{ba} + \hat{\sigma}_{ab}] [\hat{c}^2 + (\hat{c}^\dagger)^2]. \end{aligned} \quad (\text{B.16})$$

### B.3 Hamiltonian of torsion pendulum and driven atom

In this section we want to derive the simple Hamiltonian written in equation (4.3) of section 4.2 that we use along the entire chapter 4 to describe the joint unitary evolution of the torsion mechanical oscillator and the Rydberg states  $|a\rangle$  and  $|b\rangle$  of an atom driven by microwave fields.

We shall first complete the explicit form of the total Hamiltonian  $\hat{H}'$  of equation (4.1). To this end we need to describe the microwave driving of the Rydberg excited atom, which may take place at the locations  $R_1$  and  $R_2$ , as well as in region C of the interferometer setup (see figure 4.4). We account for this driving via an electric dipole interaction, the Hamiltonian of which we write as

$$\hat{H}'_{\text{coup}} = -\mathbf{d}_{ba} \cdot \mathbf{E}_{\text{mw}}(t) [\hat{\sigma}_{ba} + \hat{\sigma}_{ab}] \sin(\omega_{\text{mw}}t + \phi), \quad (\text{B.17})$$

where  $\omega_{\text{mw}}$  is the carrier frequency of the microwave,  $\mathbf{E}_{\text{mw}}$  its slowly varying electric field envelope, and  $\phi$  its phase. Since we now know explicitly all Hamiltonian terms appearing in the total Hamiltonian  $\hat{H}'$  of equation (4.1), we can derive the Hamiltonian (4.2) by switching to the frame rotating with  $\omega_{\text{mw}}$ . We achieve this by performing a unitary transformation of



the form  $\hat{U}_{\text{mw}} = \exp(i\hat{\mathcal{H}}_{\text{mw}}t/\hbar)$ , where

$$\hat{\mathcal{H}}_{\text{mw}}/\hbar = (\omega_a + \omega_{\text{osc}}/2)\hat{1} + \omega_{\text{mw}}(\hat{c}^\dagger \hat{c} + \hat{\sigma}_{bb}). \quad (\text{B.18})$$

In this way, the total Hamiltonian transforms into  $\hat{H}' \mapsto \hat{U}_{\text{mw}}\hat{H}'\hat{U}_{\text{mw}}^\dagger + i\hbar\dot{\hat{U}}_{\text{mw}}\hat{U}_{\text{mw}}^\dagger = \hat{H}$ . The outcome reads

$$\begin{aligned} \hat{H}/\hbar \simeq & -\delta\hat{\sigma}_{bb} - \delta_{\text{osc}}\hat{c}^\dagger\hat{c} + \varphi_{\text{zpm}}^2 \frac{V_0}{\hbar} g(\mathbf{R}_0) \left[ \hat{\sigma}_{ba}e^{i\omega_{\text{mw}}t} + \hat{\sigma}_{ab}e^{-i\omega_{\text{mw}}t} \right] \hat{c}^\dagger\hat{c} \\ & - \frac{V_0}{\hbar} g(\mathbf{R}_0) \left[ 1 - \varphi_{\text{zpm}}^2/2 \right] \left[ \hat{\sigma}_{ba}e^{i\omega_{\text{mw}}t} + \hat{\sigma}_{ab}e^{-i\omega_{\text{mw}}t} \right] \\ & - \varphi_{\text{zpm}} \frac{V_0}{\hbar} f(\mathbf{R}_0) \left[ \hat{\sigma}_{ba}e^{i\omega_{\text{mw}}t} + \hat{\sigma}_{ab}e^{-i\omega_{\text{mw}}t} \right] \left[ \hat{c}e^{-i\omega_{\text{mw}}t} + \hat{c}^\dagger e^{i\omega_{\text{mw}}t} \right] \\ & - \varphi_{\text{zpm}}^2 \frac{V_0}{2\hbar} g(\mathbf{R}_0) \left[ \hat{\sigma}_{ba}e^{i\omega_{\text{mw}}t} + \hat{\sigma}_{ab}e^{-i\omega_{\text{mw}}t} \right] \left[ \hat{c}^2 e^{-2i\omega_{\text{mw}}t} + (\hat{c}^\dagger)^2 e^{2i\omega_{\text{mw}}t} \right] \\ & - \frac{\mathbf{d}_{ba} \cdot \mathbf{E}_{\text{mw}}(t)}{i2\hbar} \left[ \hat{\sigma}_{ba}e^{i\omega_{\text{mw}}t} + \hat{\sigma}_{ab}e^{-i\omega_{\text{mw}}t} \right] \left[ e^{i(\omega_{\text{mw}}t+\phi)} - e^{-i(\omega_{\text{mw}}t+\phi)} \right]. \end{aligned} \quad (\text{B.19})$$

Here, the microwave detunings read  $\delta = \omega_{\text{mw}} - \omega_{ba}$  and  $\delta_{\text{osc}} = \omega_{\text{mw}} - \omega_{\text{osc}}$ . Then, provided the conditions  $|\mathbf{d}_{ba} \cdot \mathbf{E}_{\text{mw}}/\hbar|, |\varphi_{\text{zpm}}^q V_0 g(\mathbf{R}_0)/\hbar|, |\delta|, |\delta_{\text{osc}}| \ll |\omega_{\text{mw}}|, |\omega_{\text{osc}}|$ , with  $q \in \{0, 1, 2\}$  and  $\mathbf{R}_0 = [X_0, D_0 + \Delta Y_0, Z_0]^\top$ , with  $X_0/D_0, \Delta Y_0/D_0 \ll 1$ , are fulfilled, off resonant terms can be neglected. For the parameters that we use these conditions hold, and hence, the Hamiltonian (B.19) reduces to

$$\hat{H}/\hbar \simeq -\delta\hat{\sigma}_{bb} - \delta_{\text{osc}}\hat{c}^\dagger\hat{c} - \mathcal{K}(\mathbf{R}_0)[\hat{c}\hat{\sigma}_{ba} + \hat{c}^\dagger\hat{\sigma}_{ab}] - \frac{1}{2}[\Omega(t)\hat{\sigma}_{ba} + \Omega^*(t)\hat{\sigma}_{ab}], \quad (\text{B.20})$$

where we have defined the Rabi frequency  $\Omega = \mathbf{d}_{ba} \cdot \mathbf{E}_{\text{mw}} \exp(-i\phi + i\pi/2)/\hbar$ , and introduced the interaction strength  $\mathcal{K}(\mathbf{R}_0) = \mathcal{K}_0 f(\mathbf{R}_0)$ , with  $\mathcal{K}_0 = \varphi_{\text{zpm}} V_0/\hbar$ . Choosing  $\omega_{\text{mw}} = \omega_{\text{osc}}$ , as we indicate in section 4.2, is  $\delta = \omega_{\text{osc}} - \omega_{ba}$  and  $\delta_{\text{osc}} = 0$ , thus recovering the Hamiltonian of equation (4.3).

## B.4 Unitary evolution of joint atom-oscillator system during a Ramsey sequence

Here we shall derive the time evolution operator describing the unitary dynamics of the atom-oscillator system across each of the microwave pulses exerted in the zones  $R_1$  and  $R_2$  of a Ramsey sequence. With this at hand we construct next an expression for the state at the exit of the pulse sequence. After that we show under which conditions the results obtained here reduce to those presented in section 4.3.1. We assume that the atom traverses the interferometer in a time interval comprised between the instants  $t_i$  and  $t_f$ . Between  $t_i$  and  $t_1$  the atom crosses the region  $R_1$ , during  $\tau_0 = t_2 - t_1$  it interacts with the torsion pendulum, and finally, between  $t_2$  and  $t_f$  goes through the region  $R_2$ . We then write the time evolution operator as  $\hat{U}_{\text{RM}}(t_f, t_i) = \hat{U}(t_f, t_2)\hat{U}(t_2, t_1)\hat{U}(t_1, t_0)$ . The operator  $\hat{U}(t_2, t_1) \equiv \hat{U}(\tau_0)$  is that of equation (4.14) describing the joint atom-oscillator evolution while they interact with each

#### B.4 Unitary evolution of joint atom-oscillator system during a Ramsey sequence

other in the dispersive and adiabatic limits. During any of the remaining time windows  $t_i \leq t \leq t_1$  and  $t_2 \leq t \leq t_f$  we use rectangular pulses (time independent Rabi frequency) and assume that the evolution of the system is governed by the following Hamiltonian

$$\hat{H}/\hbar = -\delta\hat{\sigma}_{bb} - \delta_{\text{osc}}\hat{c}^\dagger\hat{c} - \frac{1}{2}[\Omega\hat{\sigma}_{ba} + \Omega^*\hat{\sigma}_{ab}]. \quad (\text{B.21})$$

Equation (B.21) is a good approximation provided the time lapse  $\tau_{\text{mw}} = t_1 - t_i = t_f - t_2$  of the pulse is sufficiently short and the atom-oscillator distance  $|\mathbf{R}_0|$  sufficiently large so that  $\tau_{\text{mw}}\mathcal{K}_0 < 1$ . The unitary evolution can be readily found after diagonalizing the Hamiltonian (B.21) and expanding the corresponding eigenstates in the original basis  $\{|a\rangle, |b\rangle\}$ . The outcome yields  $\hat{U}(t_1, t_i) = \hat{U}(t_f, t_2) \equiv \hat{U}(\tau_{\text{mw}}, \phi)$ , where

$$\hat{U}(\tau_{\text{mw}}, \phi) = \sum_{\mu\mu'} \exp(i\delta_{\text{osc}}\tau_{\text{mw}}\hat{c}^\dagger\hat{c} + i\delta\tau_{\text{mw}}\hat{\sigma}_{bb}) A_{\mu\mu'}(\tau_{\text{mw}}, \phi) \otimes \hat{\sigma}_{\mu\mu'}, \quad (\text{B.22})$$

the matrix elements of which are given by

$$A_{aa}(\tau_{\text{mw}}) = \left[ \cos\left(\frac{\Delta}{2}\tau_{\text{mw}}\right) - i\frac{\delta}{\Delta}\sin\left(\frac{\Delta}{2}\tau_{\text{mw}}\right) \right] e^{i\delta\tau_{\text{mw}}/2} = c_a(\tau_{\text{mw}})e^{i\delta\tau_{\text{mw}}/2}, \quad (\text{B.23})$$

$$A_{ab}(\tau_{\text{mw}}, \phi) = \frac{|\Omega|e^{i(\delta\tau_{\text{mw}}/2+\phi)}}{\Delta} \sin\left(\frac{\Delta}{2}\tau_{\text{mw}}\right) = c_b(\tau_{\text{mw}})e^{i(\delta\tau_{\text{mw}}/2+\phi)}, \quad (\text{B.24})$$

$$A_{ba}(\tau_{\text{mw}}, \phi) = -[A_{ab}(\tau_{\text{mw}}, \phi)]^*, \quad A_{bb}(\tau_{\text{mw}}) = [A_{aa}(\tau_{\text{mw}})]^*. \quad (\text{B.25})$$

with  $\Delta = \sqrt{\delta^2 + |\Omega|^2}$ . Knowledge of (B.22) allows us to propagate the initial joint state  $|\Psi_0\rangle \otimes |a\rangle \equiv |\Psi_0, a\rangle$  of atom plus oscillator system in the course of a Ramsey sequence. We fix the phase of the first pulse in  $R_1$  to  $\phi = \pi$  and let the phase of the second pulse in  $R_2$  to be adjustable, so that  $\hat{U}_{\text{RM}}(\tau_{\text{fi}}, \phi) = \hat{U}(\tau_{\text{mw}}, \phi)\hat{U}(\tau_0)\hat{U}(\tau_{\text{mw}}, \phi = \pi)$ , with  $\tau_{\text{fi}} = t_f - t_i$ . Using expression (4.14) for  $\hat{U}(\tau_0)$  and the definitions (B.22) – (B.25) above for the evolution in  $R_1$  and  $R_2$  we find that the initial state evolves into

$$\begin{aligned} \hat{U}_{\text{RM}}(\tau_{\text{fi}}, \phi) |\Psi_0, a\rangle &= e^{i(\delta\tau_{\text{mw}} - [\hat{n} + 1/2]\Phi_0)} \left[ c_a^2(\tau_{\text{mw}}) + |c_b(\tau_{\text{mw}})|^2 e^{i(\delta\tau_0 + [2\hat{n} + 1]\Phi_0 + \phi)} \right] \hat{U}_{\text{osc}}(\tau_{\text{fi}}) |\Psi_0, a\rangle \\ &+ ie^{i(\delta\tau_{\text{mw}} - [\hat{n} + 1/2]\Phi_0 - \phi)} c_b(\tau_{\text{mw}}) \left[ c_a(\tau_{\text{mw}}) - c_a^*(\tau_{\text{mw}}) e^{i(\delta\tau_0 + [2\hat{n} + 1]\Phi_0 + \phi)} \right] \hat{U}_{\text{osc}}(\tau_{\text{fi}}) |\Psi_0, b\rangle, \end{aligned} \quad (\text{B.26})$$

where  $|\Psi_0, b\rangle \equiv |\Psi_0\rangle \otimes |b\rangle$  and  $\hat{U}_{\text{osc}}(\tau_{\text{fi}}) = \exp(i\delta_{\text{osc}}\hat{c}^\dagger\hat{c}\tau_{\text{fi}})$  is the free unitary evolution of the oscillator. We may reduce the state (B.26) further by resorting to the definition of a  $\pi/2$  half pulse: one that provides a transition probability  $|A_{ab}|^2 = |c_b|^2 = 1/2$  between states  $|a\rangle$  and  $|b\rangle$ , which implies a pulse length  $\tilde{\tau}_{\text{mw}} = 2 \arcsin(\Delta/|\Omega|\sqrt{2})/\Delta$ . Then, writing  $c_b(\tilde{\tau}_{\text{mw}}) = 1/\sqrt{2}$  and  $c_a(\tilde{\tau}_{\text{mw}}) = \exp(-i\vartheta)/\sqrt{2}$  with  $\vartheta = \arcsin(\delta/|\Omega|)$ , the final state after a Ramsey sequence simplifies to

$$\begin{aligned} \hat{U}_{\text{RM}}(\tau_{\text{fi}}, \phi) |\Psi_0, a\rangle &= e^{i(\delta\tau_{\text{fi}} + \phi - 2\vartheta)/2} \cos(\delta\tau_{\text{fi}}/2 + \Phi_0[\hat{n} + 1/2] + \vartheta) \hat{U}_{\text{osc}}(\tau_{\text{fi}}) |\Psi_0, a\rangle \\ &+ e^{i(\delta\tau_{\text{fi}} - \phi)/2} \sin(\delta\tau_{\text{fi}}/2 + \Phi_0[\hat{n} + 1/2] + \vartheta) \hat{U}_{\text{osc}}(\tau_{\text{fi}}) |\Psi_0, b\rangle. \end{aligned} \quad (\text{B.27})$$

From equation (B.27) we may extract the full version of the measurement operators (4.18) and (4.19) introduced in section 4.3.1. It is important to emphasize that this outcome has been obtained for an atom following an ideal uniform trajectory across the pulse sequence of the Ramsey interferometer. For an atom traveling with a different velocity, it would be necessary to readjust the pulse sequence so that we could again obtain a  $\pi/2$  pulse and generate a similar state (B.27). Fortunately, we can overcome this difficulty by requiring either a sufficiently small detuning  $\delta$  or a large enough microwave power, i. e. Rabi frequency  $\Omega$ , or both. From the definition of the transition probability between states  $|a\rangle$  and  $|b\rangle$ ,  $|c_b|^2 = |\Omega|^2 \sin^2(\delta\tau_{\text{mw}} \sqrt{\delta^2 + |\Omega|^2}/2) / [\delta^2 + |\Omega|^2]$ , it follows that  $|c_b|^2 = 1/2$  is only possible for  $|\delta| < |\Omega|$ . Therefore, in our platform we presume Rabi pulses in  $R_1$  and  $R_2$  with a sufficiently high intensity and strong confinement, ensuring both a small ratio  $|\delta/\Omega| \ll 1$  and  $\delta\tau_{\text{mw}} \ll 1$ , such that  $A_{aa} \rightarrow \cos(|\Omega|\tau_{\text{mw}}/2)$ ,  $A_{ab} \rightarrow \exp(i\phi) \sin(|\Omega|\tau_{\text{mw}}/2)$  and  $\vartheta \rightarrow 0$ . In this limit, we can achieve  $|\Omega|\tau_{\text{mw}} \approx \pi/2$  for every trajectory, and hence  $A_{aa} \approx 1/\sqrt{2}$ ,  $A_{ab} \approx \exp(i\phi)/\sqrt{2}$ . The latter values reproduce then the matrix  $A_{\pi/2}(\phi)$  defined in equation (4.15), and the final state (B.27) supplies the measurement operators defined in section 4.3.1, wherein, for simplicity, we also used  $\omega_{\text{mw}} = \omega_{\text{osc}}$ , and thus  $\hat{U}_{\text{osc}} = \hat{\mathbb{1}}$ .

Finally, let us note that  $\hat{U}_{\text{RM}}$  provides the time evolution in an interaction picture with respect to the Hamiltonian (B.18) written in the previous section B.3. The evolution between  $t_i$  and  $t_f$  in the original frame would be given by  $\exp(-i\hat{\mathcal{H}}_{\text{mw}}t_f/\hbar)\hat{U}_{\text{RM}}(t_f, t_i)\exp(i\hat{\mathcal{H}}_{\text{mw}}t_i/\hbar)$ . However, since after all we are interested in measuring probabilities, our results remain unaltered disregarding the choice of the frame in which the evolution is computed.

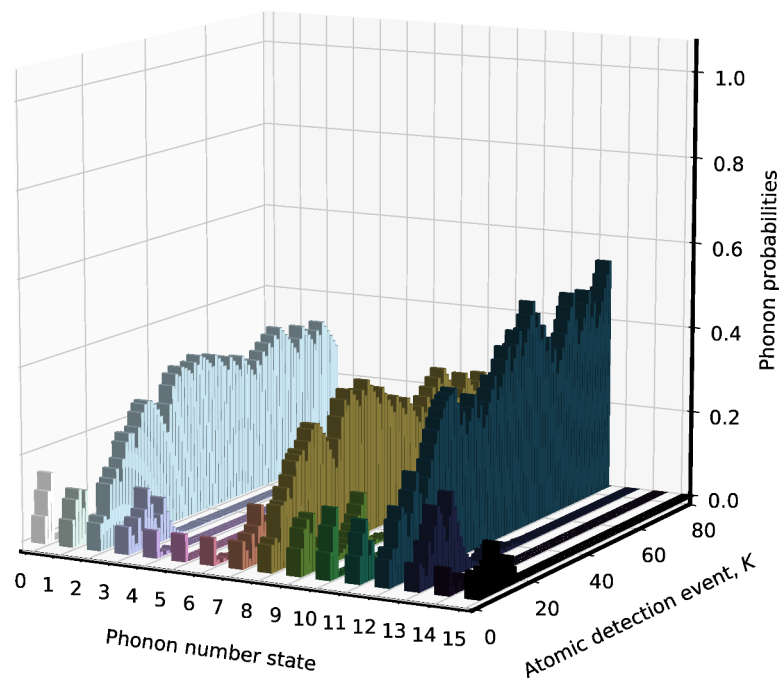


**Figure B.3** Probability distribution  $q_{nm}$  of (discrete) phonon numbers  $n$  as it evolves during a series of  $K = 80$  Ramsey measurements. The initial distribution is flat and its domain,  $n = 0, \dots, n_c = 15$  exceeds the range of phonon numbers  $n = 0, \dots, n_0 = 5$  onto which different outcomes of the atomic probabilities are mapped. This prevents that the phonon probability distribution allocates into a single Fock state at the end of the series.

## B.5 Numerical test of the mechanical oscillator state collapse

The goal of this section is to test that a mechanical oscillator state collapse will hardly occur if the outcomes of the atomic probabilities  $P_{\pm}$  are such that they coincide for any pair of different phonon numbers that fall within the range of phonon numbers accounting for the initial phonon distribution. We test this non degeneracy condition numerically. Figure B.3 displays the evolution of a flat probability distribution of phonon numbers in the course of a sequence of  $K = 80$  measurements. Initially, the set of Fock states  $\{|n\rangle\}_{n=0}^{n_c}$  are all occupied with the same probability,  $1/(n_c + 1)$ . We set  $n_c = 15$ . Now, the probabilities  $P_{\pm}$ , as well as  $\mathcal{P}$ , are periodic functions of period  $\pi$  and we have mapped the phase shifts from the range of phonon numbers  $n = 0, 1, \dots, n_0 = 5$  onto the interval  $[0, \pi]$ . Since  $n_0 < n_c$ , the non degeneracy of the atomic probabilities breaks down over the range of phonon numbers  $n = 0, 1, \dots, n_c$  spanned by the original phonon distribution, i.e., there exists different phonon numbers  $n$  that yield an equivalent value for  $P_{\pm}$ . Then, as we observe in figure B.3, the mechanical oscillator does not collapse into a Fock state after the entire sequence of Ramsey measurements. However, the phonon distribution corresponding to a mechanical oscillator initially prepared in the superposition of Fock states  $|\Psi\rangle = [ |1\rangle + |3\rangle ] / \sqrt{2}$ , does indeed collapse into a phonon number state after a sequence of

$K = 80$  Ramsey measurements. We show this in figure B.4.

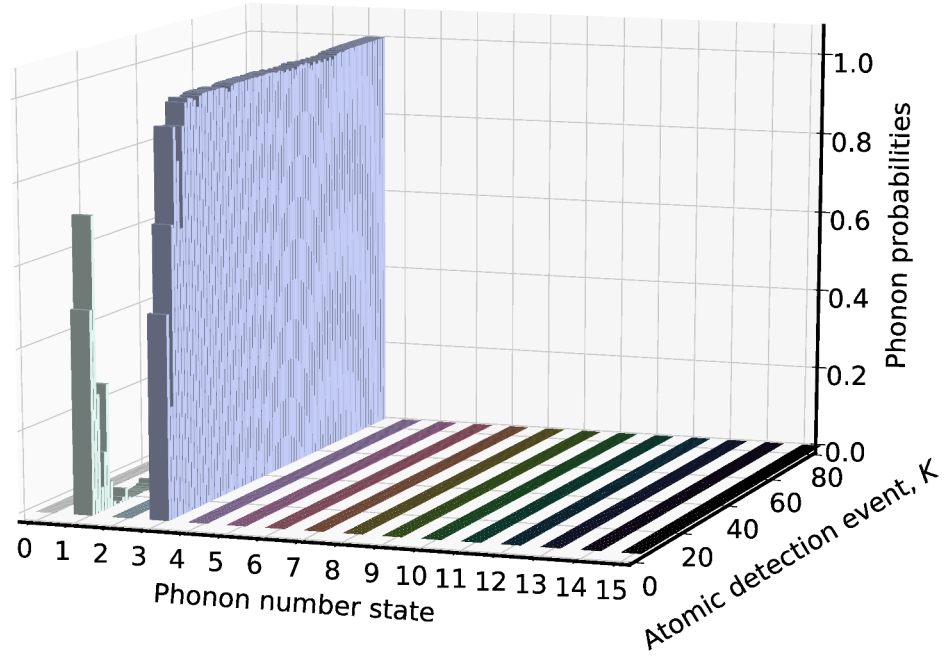


**Figure B.4** Probability distribution  $q_{nm}$  of (discrete) phonon numbers  $n$  as it evolves during a series of  $K = 80$  Ramsey measurements. The mechanical oscillator starts in the state  $[|1\rangle + |3\rangle]/\sqrt{2}$ . Thus, the domain of the initial distribution falls within the range of phonon numbers onto which different outcomes of the atomic probabilities can be resolved, and the final distribution converges to that of a single Fock state with  $n = 3$ .

## B.6 Effective coherent driving of mechanical oscillator

In this supplementary section we provide a derivation of the effective coherent driving of the quantum torsion pendulum that may result from the Hamiltonian (4.3) of chapter 4 when we use that Hamiltonian to describe the simultaneous interaction of an atom with both, the torsion pendulum and the microwave drive in region C (see figure 4.4).

If we operate the Hamiltonian (4.3) with  $|\delta| > |\Omega(t)|, |\mathcal{K}(\mathbf{R})|$ , and initialize all the atomic population in  $|a\rangle$ , we then can adiabatically eliminate the second Rydberg state  $|b\rangle$  to obtain the effective Hamiltonian  $\hat{H}_{\text{dho}}(t) \otimes \hat{\sigma}_{aa}$ , where

$$\hat{H}_{\text{dho}}(t) = \frac{\mathcal{K}^2(\mathbf{R})}{\delta} \hat{c}^\dagger \hat{c} - \frac{\mathcal{K}(\mathbf{R})\Omega(t)}{2\delta} \hat{c} - \frac{\mathcal{K}(\mathbf{R})\Omega^*(t)}{2\delta} \hat{c}^\dagger + \frac{|\Omega(t)|^2}{4\delta}. \quad (\text{B.28})$$

Like in previous occasions we can work in a shifted picture to remove the c-number  $\frac{|\Omega(t)|^2}{4\delta}$  from the Hamiltonian. Then, while the atom essentially remains in the Rydberg state  $|a\rangle$ , the evolution for the mechanical oscillator can be written as

$$\hat{\rho}(\tau) = \hat{U}(\tau) \hat{\rho}(0) \hat{U}^\dagger(\tau), \quad (\text{B.29})$$

where  $\hat{\rho}$  denotes the density matrix describing the oscillator. The quantity  $\hat{U}(\tau)$  equals the time development operator for a driven quantum harmonic oscillator, which one can see by exploiting the commutation relations of  $\hat{c}, \hat{c}^\dagger$  [220]

$$\begin{aligned} \hat{U}(\tau) &= e^{i\lambda(\tau)} \hat{\mathcal{D}}\left(\tilde{\zeta}(\tau) e^{-i\theta(\tau)}\right) e^{-i\theta(\tau) \hat{c}^\dagger \hat{c}}, \\ \lambda(\tau) &= -\frac{1}{2\hbar^2} \int_0^\tau dt \int_0^t dt' [\hat{H}_{\text{dho}}(t), \hat{H}_{\text{dho}}(t')], \\ \tilde{\zeta}(\tau) &= i \int^\tau dt \frac{\Omega^*(t) \mathcal{K}(t)}{2\delta} e^{i\theta(t)}, \\ \theta(\tau) &= \int^\tau dt \frac{\mathcal{K}^2(t)}{\delta}. \end{aligned} \quad (\text{B.30})$$

Here we adopted the shortened notation  $\mathcal{K}(t) = \mathcal{K}(\mathbf{R}(t))$  and  $\hat{\mathcal{D}}$  is the displacement operator introduced in the main text. Since  $\lambda(\tau)$  is a c-number,  $\exp[i\lambda(\tau)]$  is a global phasor that we will ignore from now on. The  $N$ -th power of  $\hat{U}(\tau)$  then accounts for the state evolution of the mechanical oscillator after a successive fly-by of  $N$  atoms, each atom passing through the oscillator in a time interval  $\tau$ . To compute  $\hat{U}_N(\tau) \equiv [\hat{U}(\tau)]^N$  we use the following properties of the displacement operator:

$$\begin{aligned} \hat{\mathcal{D}}(\alpha) \hat{\mathcal{D}}(\beta) &= \exp[(\alpha\beta^* - \alpha^*\beta)/2] \hat{\mathcal{D}}(\alpha + \beta), \\ \exp[i\theta \hat{c}^\dagger \hat{c}] \hat{\mathcal{D}}(\alpha) &= \hat{\mathcal{D}}(\alpha \exp[i\theta]) \exp[i\theta \hat{c}^\dagger \hat{c}], \end{aligned} \quad (\text{B.31})$$

such that, ignoring again global phasors, one has

$$\begin{aligned} \hat{U}_N(\tau) &= \hat{\mathcal{D}}\left(\tilde{\zeta}(\tau) \sum_{l=1}^N e^{-il\theta(\tau)}\right) e^{-iN\theta(\tau) \hat{c}^\dagger \hat{c}} = \hat{\mathcal{D}}(\alpha_N(\tau)) e^{-iN\theta(\tau) \hat{c}^\dagger \hat{c}}, \\ \alpha_N(\tau) &= \frac{\sin(N\theta(\tau)/2)}{\sin(\theta(\tau)/2)} \tilde{\zeta}(\tau) e^{-i[N+1]\theta(\tau)/2}. \end{aligned} \quad (\text{B.32})$$

In chapter 4, all the numerical calculations involving the Hamiltonian  $\hat{H}_{\text{coup}}$  describing the microwave driving of an atom in the coupling region  $C$  were assuming continuous waves with  $\Omega(t) = \Omega_0$ . Sampling the dynamical phase space of the mechanical oscillator is then achieved by adjusting the amplitude and phase of the complex Rabi frequency  $\Omega_0$ , while taking into account the additional phase offset generated by  $\exp[-iN\theta(\tau)\hat{c}^\dagger\hat{c}]$ .





# References

- [1] Barry C. Barish and Rainer Weiss. LIGO and the detection of gravitational waves. *Physics Today*, 52(10):44–50, 1999.
- [2] B P Abbott et al. Ligo: the laser interferometer gravitational-wave observatory. *Reports on Progress in Physics*, 72(7):076901, 2009.
- [3] Sung Chang. LIGO detects gravitational waves. *Physics Today*, 69(4):14–16, 2016.
- [4] B. P. Abbott et al. Observation of gravitational waves from a binary black hole merger. *Phys. Rev. Lett.*, 116:061102, 2016.
- [5] Nobelprize.org. The 2017 Nobel Prize in Physics - Press Release. [http://www.nobelprize.org/nobel\\_prizes/physics/laureates/2017/press.html](http://www.nobelprize.org/nobel_prizes/physics/laureates/2017/press.html), 2017.
- [6] W. Heisenberg. Über den anschaulichen inhalt der quantentheoretischen kinematik und mechanik. *Zeitschrift für Physik*, 43(3):172–198, 1927.
- [7] Jürgen Fritz. Cantilever biosensors. *The Analyst*, 133(7):855, 2008.
- [8] J.L. Arlett, E.B. Myers, and M.L. Roukes. Comparative advantages of mechanical biosensors. *Nature Nanotechnology*, 6(4):203–215, 2011.
- [9] Markus Aspelmeyer, Tobias J. Kippenberg, and Florian Marquardt. *Cavity optomechanics : nano- and micromechanical resonators interacting with light*. Springer, Heidelberg, 2014.
- [10] Oriol Romero-Isart, Mathieu L Juan, Romain Quidant, and J Ignacio Cirac. Toward quantum superposition of living organisms. *New Journal of Physics*, 12(3):033015, 2010.
- [11] O. Romero-Isart, A. C. Pflanzer, F. Blaser, R. Kaltenbaek, N. Kiesel, M. Aspelmeyer, and J. I. Cirac. Large quantum superpositions and interference of massive nanometer-sized objects. *Phys. Rev. Lett.*, 107:020405, 2011.
- [12] Igor Pikovski, Michael R. Vanner, Markus Aspelmeyer, M. S. Kim, and Časlav Brukner. Probing planck-scale physics with quantum optics. *Nature Physics*, 8:393, 2012.
- [13] A. Asadian, C. Brukner, and P. Rabl. Probing macroscopic realism via ramsey correlation measurements. *Phys. Rev. Lett.*, 112:190402, 2014.
- [14] H Pino, J Prat-Camps, K Sinha, B Prasanna Venkatesh, and O Romero-Isart. On-chip quantum interference of a superconducting microsphere. *Quantum Science and Technology*, 3(2):025001, 2018.

- [15] Oriol Romero-Isart. Coherent inflation for large quantum superpositions of levitated microspheres. *New Journal of Physics*, 19(12):123029, 2017.
- [16] Wojciech H. Zurek. Decoherence and the transition from quantum to classical. *Phys. Today*, 44(10):36, 1991.
- [17] T. H. Maiman. Stimulated optical radiation in ruby. *Nature*, 187(4736):493–494, 1960.
- [18] Michael Riordan, Lillian Hoddeson, and Conyers Herring. The invention of the transistor. *Rev. Mod. Phys.*, 71:S336–S345, 1999.
- [19] Bruce Rosenblum and Fred Kuttner. *Quantum enigma: physics encounters consciousness*. Oxford University Press, New York, 2011.
- [20] V. B. Braginsky and A. B. Manukin. Ponderomotive effects of electromagnetic radiation. *Sov. Phys. JETP*, 25(4):653–655, 1967.
- [21] V. B. Braginsky, Anatoli B. Manukin, and M. Yu. Tikhonov. Investigation of dissipative ponderomotive effects of electromagnetic radiation. *Soviet Journal of Experimental and Theoretical Physics*, 31:829, 1970.
- [22] Carlton M. Caves, Kip S. Thorne, Ronald W. P. Drever, Vernon D. Sandberg, and Mark Zimmermann. On the measurement of a weak classical force coupled to a quantum-mechanical oscillator. i. issues of principle. *Reviews of Modern Physics*, 52(2):341–392, 1980.
- [23] Florian Marquardt and Steven Girvin. Optomechanics. *Physics*, 2, 2009.
- [24] Pierre Meystre. A short walk through quantum optomechanics. *ANNALEN DER PHYSIK*, 525(3):215–233, 2012.
- [25] G. J. Milburn and M. J. Woolley. Quantum nanoscience. *Contemporary Physics*, 49(6):413–433, 2008.
- [26] Markus Aspelmeyer, Pierre Meystre, and Keith Schwab. Quantum optomechanics. *Phys. Today*, 65(7):29, 2012.
- [27] Menno Poot and Herre S.J. van der Zant. Mechanical systems in the quantum regime. *Phys. Rep.*, 511:273, 2012.
- [28] Miles Blencowe. Quantum electromechanical systems. *Physics Reports*, 395(3):159 – 222, 2004.
- [29] Jasper Chan, P. Mayer Alegre, Amir H. Safavi-Naeini, Jeff T. Hill, Alex Krause, Simon Gröblacher, Markus Aspelmeyer, and Oskar Painter. Laser cooling of a nanomechanical oscillator into its quantum ground state. *Nature*, 478:89, 2011.

- [30] Aashish Clerk. Seeing the “quantum” in quantum zero-point fluctuations. *Physics*, 5, 2012.
- [31] Amir H. Safavi-Naeini, Jasper Chan, Jeff T. Hill, Thiago P. Mayer Alegre, Alex Krause, and Oskar Painter. Observation of quantum motion of a nanomechanical resonator. *Phys. Rev. Lett.*, 108:033602, 2012.
- [32] Sh. Barzanjeh, D. Vitali, P. Tombesi, and G. J. Milburn. Entangling optical and microwave cavity modes by means of a nanomechanical resonator. *Phys. Rev. A*, 84:042342, 2011.
- [33] Sh. Barzanjeh, M. Abdi, G. J. Milburn, P. Tombesi, and D. Vitali. Reversible optical-to-microwave quantum interface. *Phys. Rev. Lett.*, 109:130503, 2012.
- [34] Joerg Bochmann, Amit Vainsencher, David D. Awschalom, and Andrew N. Cleland. Nanomechanical coupling between microwave and optical photons. *Nature Physics*, 9:712, 2013.
- [35] R. W. Andrews, R. W. Peterson, T. P. Purdy, K. Cicak, R. W. Simmonds, C. A. Regal, and K. W. Lehnert. Bidirectional and efficient conversion between microwave and optical light. *Nat Phys*, 10(4):321–326, 2014.
- [36] T. Bagci, A. Simonsen, S. Schmid, L. G. Villanueva, E. Zeuthen, J. Appel, J. M. Taylor, A. Sørensen, K. Usami, A. Schliesser, and E. S. Polzik. Optical detection of radio waves through a nanomechanical transducer. *Nature*, 507(7490):81–85, 2014.
- [37] E. E. Wollman, C. U. Lei, A. J. Weinstein, J. Suh, A. Kronwald, F. Marquardt, A. A. Clerk, and K. C. Schwab. Quantum squeezing of motion in a mechanical resonator. *Science*, 349(6251):952–955, 2015.
- [38] J.-M. Pirkkalainen, E. Damskägg, M. Brandt, F. Massel, and M. A. Sillanpää. Squeezing of quantum noise of motion in a micromechanical resonator. *Phys. Rev. Lett.*, 115:243601, 2015.
- [39] C. U. Lei, A. J. Weinstein, J. Suh, E. E. Wollman, A. Kronwald, F. Marquardt, A. A. Clerk, and K. C. Schwab. Quantum nondemolition measurement of a quantum squeezed state beyond the 3 db limit. *Phys. Rev. Lett.*, 117:100801, 2016.
- [40] F. Lecocq, J. B. Clark, R. W. Simmonds, J. Aumentado, and J. D. Teufel. Quantum nondemolition measurement of a nonclassical state of a massive object. *Phys. Rev. X*, 5:041037, 2015.
- [41] Markus Aspelmeyer, Tobias J. Kippenberg, and Florian Marquardt. Cavity optomechanics. *Reviews of Modern Physics*, 86(4):1391–1452, 2014.

- [42] Ignacio Wilson-Rae, Jack C Sankey, and Herman L Offerhaus. Editorial for special issue on nano-optomechanics. *Journal of Optics*, 19(8):080401, 2017.
- [43] Taejoon Kouh, M. Hanay, and Kamil Ekinici. Nanomechanical motion transducers for miniaturized mechanical systems. *Micromachines*, 8(4):108, 2017.
- [44] J.-M. Pirkkalainen, S.U. Cho, F. Massel, J. Tuorila, T.T. Heikkilä, P.J. Hakonen, and M.A. Sillanpää. Cavity optomechanics mediated by a quantum two-level system. *Nature Communications*, 6:6981, 2015.
- [45] Michele Montinaro, Gunter Wüst, Mathieu Munsch, Yannik Fontana, Eleonora Russo-Averchi, Martin Heiss, Anna Fontcuberta i Morral, Richard J. Warburton, and Martino Poggio. Quantum dot opto-mechanics in a fully self-assembled nanowire. *Nano Letters*, 14(8):4454–4460, 2014.
- [46] M Wallquist, K Hammerer, P Rabl, M Lukin, and P Zoller. Hybrid quantum devices and quantum engineering. *Phys. Scr.*, T137:014001, 2009.
- [47] Nikos Daniilidis and Hartmut Häffner. Quantum interfaces between atomic and solid-state systems. *Annual Review of Condensed Matter Physics*, 4(1):83–112, 2013.
- [48] Gershon Kurizki, Patrice Bertet, Yuimaru Kubo, Klaus Mølmer, David Petrosyan, Peter Rabl, and Jörg Schmiedmayer. Quantum technologies with hybrid systems. *Proceedings of the National Academy of Sciences*, 112(13):3866–3873, 2015.
- [49] C. Genes, D. Vitali, and P. Tombesi. Emergence of atom-light-mirror entanglement inside an optical cavity. *Phys. Rev. A*, 77:050307, 2008.
- [50] Stephan Camerer, Maria Korppi, Andreas Jöckel, David Hunger, Theodor W. Hänsch, and Philipp Treutlein. Realization of an optomechanical interface between ultracold atoms and a membrane. *Phys. Rev. Lett.*, 107:223001, 2011.
- [51] K. Hammerer, K. Stannigel, C. Genes, P. Zoller, P. Treutlein, S. Camerer, D. Hunger, and T. W. Hänsch. Optical lattices with micromechanical mirrors. *Phys. Rev. A*, 82:021803(R), 2010.
- [52] Claudiu Genes, Helmut Ritsch, Michael Drewsen, and Aurélien Dantan. Atom-membrane cooling and entanglement using cavity electromagnetically induced transparency. *Phys. Rev. A*, 84(5):051801, 2011.
- [53] K. Hammerer, M. Aspelmeyer, E. S. Polzik, and P. Zoller. Establishing einstein-poldosky-rosen channels between nanomechanics and atomic ensembles. *Phys. Rev. Lett.*, 102:020501, 2009.
- [54] Swati Singh and Pierre Meystre. Atomic probe wigner tomography of a nanomechanical system. *Phys. Rev. A*, 81(4), 2010.

- [55] S. Singh, M. Bhattacharya, O. Dutta, and P. Meystre. Coupling nanomechanical cantilevers to dipolar molecules. *Phys. Rev. Lett.*, 101(26), 2008.
- [56] F Bariani, S Singh, L F Buchmann, M Vengalattore, and P Meystre. Hybrid optomechanical cooling by atomic  $\Lambda$  systems. *Phys. Rev. A*, 90:033838, 2014.
- [57] C Genes, H Ritsch, and D Vitali. Micromechanical oscillator ground-state cooling via resonant intracavity optical gain or absorption. *Phys. Rev. A*, 80:061803(R), 2009.
- [58] Aurélien Dantan, Bhagya Nair, Guido Pupillo, and Claudiu Genes. Hybrid cavity mechanics with doped systems. *Phys. Rev. A*, 90:033820, 2014.
- [59] B Vogell, T Kampschulte, M T Rakher, A Faber, P Treutlein, K Hammerer, and P Zoller. Long distance coupling of a quantum mechanical oscillator to the internal states of an atomic ensemble. *New Journal of Physics*, 17(4):043044, 2015.
- [60] Shuo Zhang, Jian-Qi Zhang, Jie Zhang, Chun-Wang Wu, Wei Wu, and Ping-Xing Chen. Ground state cooling of an optomechanical resonator assisted by a  $\Lambda$ -type atom. *Opt. Express*, 22(23):28118, 2014.
- [61] Klaus D. Sattler. *Handbook of Nanophysics: Functional Nanomaterials*. CRC Press, 2011.
- [62] Steven Chu. Cold atoms and quantum control. *Nature*, 416(6877):206–210, 2002.
- [63] József Fortágh and Claus Zimmermann. Magnetic microtraps for ultracold atoms. *Rev. Mod. Phys.*, 79:235–289, 2007.
- [64] Matthias Weidemüller and Claus Zimmermann. *Cold atoms and molecules : a testground for fundamental many particle physics*. Wiley-VCH, Weinheim, 2009.
- [65] Maciej Lewenstein, Anna Sanpera, and Verònica Ahufinger. *Ultracold Atoms in Optical Lattices: Simulating quantum many-body systems*. Oxford University Press, 2012.
- [66] Nikolay V. Vitanov, Andon A. Rangelov, Bruce W. Shore, and Klaas Bergmann. Stimulated raman adiabatic passage in physics, chemistry, and beyond. *Rev. Mod. Phys.*, 89:015006, 2017.
- [67] Philipp Treutlein, Peter Hommelhoff, Tilo Steinmetz, Theodor W. Hänsch, and Jakob Reichel. Coherence in microchip traps. *Phys. Rev. Lett.*, 92:203005, 2004.
- [68] C. Hermann-Avigliano, R. Celistrino Teixeira, T. L. Nguyen, T. Cantat-Moltrecht, G. Nogues, I. Dotsenko, S. Gleyzes, J. M. Raimond, S. Haroche, and M. Brune. Long coherence times for Rydberg qubits on a superconducting atom chip. *Phys. Rev. A*, 90:040502, 2014.

- [69] Gerardo Adesso, Thomas R Bromley, and Marco Cianciaruso. Measures and applications of quantum correlations. *Journal of Physics A: Mathematical and Theoretical*, 49(47):473001, 2016.
- [70] Max F. Riedel, Pascal Böhi, Yun Li, Theodor W. Hänsch, Alice Sinatra, and Philipp Treutlein. Atom-chip-based generation of entanglement for quantum metrology. *Nature*, 464(7292):1170–1173, 2010.
- [71] Robert McConnell, Hao Zhang, Jiazhong Hu, Senka Ćuk, and Vladan Vuletić. Entanglement with negative wigner function of almost 3,000 atoms heralded by one photon. *Nature*, 519(7544):439–442, 2015.
- [72] Daniel Kleppner, Michael G. Littman, and Myron L. Zimmerman. Highly excited atoms. *Scientific American*, 244(5):130–149, may 1981.
- [73] Henning Labuhn, Sylvain Ravets, Daniel Barredo, Lucas Béguin, Florence Nogrette, Thierry Lahaye, and Antoine Browaeys. Single-atom addressing in microtraps for quantum-state engineering using Rydberg atoms. *Phys. Rev. A*, 90:023415, 2014.
- [74] Y.-Y. Jau, A. M. Hankin, T. Keating, I. H. Deutsch, and G. W. Biedermann. Entangling atomic spins with a Rydberg-dressed spin-flip blockade. *Nature Physics*, 12(1):71–74, 2015.
- [75] Tyler Keating, Robert L. Cook, Aaron M. Hankin, Yuan-Yu Jau, Grant W. Biedermann, and Ivan H. Deutsch. Robust quantum logic in neutral atoms via adiabatic Rydberg dressing. *Phys. Rev. A*, 91:012337, 2015.
- [76] M. Saffman, T. G. Walker, and K. Mølmer. Quantum information with Rydberg atoms. *Reviews of Modern Physics*, 82(3):2313–2363, 2010.
- [77] T Pohl, C S Adams, and H R Sadephpour. Cold Rydberg gases and ultra-cold plasmas. *Journal of Physics B: Atomic, Molecular and Optical Physics*, 44(18):180201, 2011.
- [78] O Firstenberg, C S Adams, and S Hofferberth. Nonlinear quantum optics mediated by Rydberg interactions. *Journal of Physics B: Atomic, Molecular and Optical Physics*, 49(15):152003, 2016.
- [79] Ming Gao, Yu-xi Liu, and Xiang-Bin Wang. Coupling Rydberg atoms to superconducting qubits via nanomechanical resonator. *Phys. Rev. A*, 83:022309, 2011.
- [80] F. Bariani, J. Otterbach, Huatang Tan, and P. Meystre. Single-atom quantum control of macroscopic mechanical oscillators. *Phys. Rev. A*, 89(1), 2014.
- [81] A. Sanz-Mora, A. Eisfeld, S. Wüster, and J.-M. Rost. Coupling of a nanomechanical oscillator and an atomic three-level medium. *Phys. Rev. A*, 93:023816, 2016.

- [82] A. Sanz-Mora, S. Wüster, and J.-M. Rost. On-chip quantum tomography of mechanical nanoscale oscillators with guided Rydberg atoms. *Phys. Rev. A*, 96:013855, 2017.
- [83] J. J. Balmer. Notiz über die spectrallinien des wasserstoffs. *Annalen der Physik*, 261(5):80–87, 1885.
- [84] Janne R Rydberg. Über den Bau der Linienspektren der chemischen Grundstoffe. *Zeitschrift für physikalische Chemie*, 5(1):227–232, 1890.
- [85] N. Bohr Dr. phil. I. on the constitution of atoms and molecules. *Philosophical Magazine*, 26(151):1–25, 1913.
- [86] E. Schrödinger. Quantisierung als Eigenwertproblem. *Annalen der Physik*, 384(4):361–376, 1926.
- [87] E. Schrödinger. Der stetige übergang von der mikro- zur makromechanik. *Naturwissenschaften*, 14(28):664–666, 1926.
- [88] W. Heisenberg. Über quantentheoretische Umdeutung kinematischer und mechanischer Beziehungen. *Zeitschrift für Physik*, 33(1):879–893, 1925.
- [89] M. Born, W. Heisenberg, and P. Jordan. Zur Quantenmechanik. ii. *Zeitschrift für Physik*, 35(8):557–615, 1926.
- [90] N. Bohr. Über die Serienspektren der Elemente. *Zeitschrift für Physik*, 2(5):423–469, 1920.
- [91] Francis M. Pipkin (eds.) P. Kienle (auth.), Daniel Kleppner. *Atomic Physics 7*. Springer US, 1 edition, 1981.
- [92] M. W. Horbatsch, E. A. Hessels, and M. Horbatsch. Classical calculation of the lifetimes and branching ratios for radiative decays of hydrogenic atoms. *Phys. Rev. A*, 71:020501, 2005.
- [93] Jean Pierre Briand (eds.) P. Armbruster (auth.). *Atoms in Unusual Situations*. Nato ASI Series 143. Springer US, 1 edition, 1986.
- [94] Serge Haroche and Jean-Michel Raimond. *Exploring the quantum: atoms, cavities, and photons*. Oxford university press, 2006.
- [95] J. M. Raimond, M. Brune, and S. Haroche. Manipulating quantum entanglement with atoms and photons in a cavity. *Rev. Mod. Phys.*, 73:565–582, 2001.
- [96] C.J. Joachain B.H. Bransden. *Physics of Atoms and Molecules*. Longman Publishing Group, 1983.

- [97] P. Goy, J. Liang, M. Gross, and S. Haroche. Quantum defects and specific-isotopic-shift measurements in ns and np highly excited states of lithium: Exchange effects between Rydberg and core electrons. *Phys. Rev. A*, 34:2889–2896, 1986.
- [98] Robert Löw, Hendrik Weimer, Johannes Nipper, Jonathan B Balewski, Björn Butscher, Hans Peter Büchler, and Tilman Pfau. An experimental and theoretical guide to strongly interacting Rydberg gases. *Journal of Physics B: Atomic, Molecular and Optical Physics*, 45(11):113001, 2012.
- [99] Vladimir S. Malinovsky Paul R. Berman. *Principles of Laser Spectroscopy and Quantum Optics*. Princeton University Press, 2010.
- [100] Gordon W. F. Drake. *Springer Handbook of Atomic, Molecular, and Optical Physics*. Springer, Berlin, 2nd edition, 2005.
- [101] Marlan O. Scully and M. Suhail Zubairy. *Quantum optics*. Cambridge University Press, Cambridge New York, 1997.
- [102] John David Jackson. *Classical electrodynamics*. Wiley, New York, NY, 3rd ed. edition, 1999.
- [103] Keith C. Schwab and Michael L. Roukes. Putting mechanics into quantum mechanics. *Physics Today*, 58(7):36–42, 2005.
- [104] Andrew Cleland. *Foundations of Nanomechanics : From Solid-State Theory to Device Applications*. Springer Berlin Heidelberg, 2003.
- [105] G. Milburn and M. Woolley. An introduction to quantum optomechanics. *Acta Physica Slovaca. Reviews and Tutorials*, 61(5), 2011.
- [106] A. J. Leggett. Macroscopic quantum systems and the quantum theory of measurement. *Progress of Theoretical Physics Supplement*, 69:80–100, 1980.
- [107] Richard Phillips Feynman, Fernando Bernardino Morinigo, and William G Wagner. *Lectures on Gravitation, 1962-63*. California Institute of Technology, 1971.
- [108] Kip Thorne and Roger Blanford. *Modern classical physics : optics, fluids, plasmas, elasticity, relativity, and statistical physics*. Princeton University Press, Princeton, New Jersey, 2017.
- [109] Silvan Schmid, Luis Guillermo Villanueva, and Michael Lee Roukes. *Fundamentals of Nanomechanical Resonators*. Springer Publishing Company, Incorporated, 1st edition, 2016.
- [110] L. D. Landau. *Mechanics*. Pergamon Press, Oxford New York, 1976.
- [111] Norbert Wiener. Generalized harmonic analysis. *Acta Math.*, 55:117–258, 1930.



- [112] A. A. Clerk, M. H. Devoret, S. M. Girvin, Florian Marquardt, and R. J. Schoelkopf. Introduction to quantum noise, measurement, and amplification. *Reviews of Modern Physics*, 82(2):1155–1208, 2010.
- [113] Michel Devoret, Benjamin Huard, Robert Schoelkopf, and Leticia F. Cugliandolo, editors. *Quantum Machines: Measurement and Control of Engineered Quantum Systems*. Oxford University Press, 2014.
- [114] Gerard J Bowen, Warwick P; Milburn. *Quantum optomechanics*. CRC Press, 2016.
- [115] Joseph G. Hoffman. The fluctuation dissipation theorem. *Physics Today*, 15(1):30–36, 1962.
- [116] R Kubo. The fluctuation-dissipation theorem. *Reports on Progress in Physics*, 29(1):255, 1966.
- [117] T. Dittrich, P. Hänggi, G.-L. Ingold, Bernhard Kramer, G. Schön, and Wilhelm Zwerger. *Quantum transport and dissipation*. Wiley-VCH, 1998.
- [118] Natsuki Hashitsume Ryogo Kubo, Morikazu Toda. *Statistical Physics II: Nonequilibrium Statistical Mechanics*. Springer Series in Solid-State Sciences 31. Springer-Verlag Berlin Heidelberg, 2 edition, 1991.
- [119] Herbert B. Callen and Theodore A. Welton. Irreversibility and generalized noise. *Phys. Rev.*, 83:34–40, 1951.
- [120] Massimiliano Esposito, Upendra Harbola, and Shaul Mukamel. Nonequilibrium fluctuations, fluctuation theorems, and counting statistics in quantum systems. *Rev. Mod. Phys.*, 81:1665–1702, 2009.
- [121] Michele Campisi, Peter Hänggi, and Peter Talkner. Colloquium: Quantum fluctuation relations: Foundations and applications. *Rev. Mod. Phys.*, 83:771–791, 2011.
- [122] Yanbei Chen. Macroscopic quantum mechanics: theory and experimental concepts of optomechanics. *Journal of Physics B: Atomic, Molecular and Optical Physics*, 46(10):104001, 2013.
- [123] Tofigh Heidarzadeh. *A history of physical theories of comets, from Aristotle to Whipple*. Springer, Dordrecht, 2008.
- [124] Albert Einstein. Über die Entwicklung unserer Anschauungen über das Wesen und die Konstitution der Strahlung. *Physikalische Blätter*, 25(9):386–391, 1969.
- [125] K. Karrai, I. Favero, and C. Metzger. Doppler optomechanics of a photonic crystal. *Phys. Rev. Lett.*, 100(24), 2008.
- [126] Peter Milonni and J. H. Eberly. *Lasers*. Wiley, New York, 1988.

- [127] Grynberg G. Cohen-Tannoudji C., Dupont-Ros J. *Photons & Atoms: Introduction to Quantum Electrodynamics*. Wiley, 1989.
- [128] Hermann A. Haus. *Waves and Fields in Optoelectronics*. Prentice Hall, ph edition, 1983.
- [129] C. K. Law. Interaction between a moving mirror and radiation pressure: A hamiltonian formulation. *Phys. Rev. A*, 51:2537–2541, 1995.
- [130] H. K. Cheung and C. K. Law. Nonadiabatic optomechanical hamiltonian of a moving dielectric membrane in a cavity. *Phys. Rev. A*, 84:023812, 2011.
- [131] Florian Marquardt, J. G. E. Harris, and S. M. Girvin. Dynamical multistability induced by radiation pressure in high-finesse micromechanical optical cavities. *Phys. Rev. Lett.*, 96:103901, 2006.
- [132] Constanze Metzger, Max Ludwig, Clemens Neuenhahn, Alexander Ortlieb, Ivan Favero, Khaled Karrai, and Florian Marquardt. Self-induced oscillations in an optomechanical system driven by bolometric backaction. *Phys. Rev. Lett.*, 101:133903, 2008.
- [133] Albert Schliesser. *Cavity Optomechanics and Optical Frequency Comb Generation with Silica Whispering-Gallery-Mode Microresonators*. PhD thesis, Ludwig-Maximilian University of Munich, 2009.
- [134] A. Schliesser, R. Rivière, G. Anetsberger, O. Arcizet, and T. J. Kippenberg. Resolved-sideband cooling of a micromechanical oscillator. *Nature Physics*, 4(5):415–419, 2008.
- [135] David J. Wineland and Wayne M. Itano. Laser cooling. *Physics Today*, 40(6):34–40, 1987.
- [136] C. Monroe, D. M. Meekhof, B. E. King, S. R. Jefferts, W. M. Itano, D. J. Wineland, and P. Gould. Resolved-sideband raman cooling of a bound atom to the 3d zero-point energy. *Phys. Rev. Lett.*, 75:4011–4014, 1995.
- [137] Florian Marquardt, Joe P. Chen, A. A. Clerk, and S. M. Girvin. Quantum theory of cavity-assisted sideband cooling of mechanical motion. *Phys. Rev. Lett.*, 99:093902, 2007.
- [138] Daniel De Zutter. Reflections from linearly vibrating objects: plane mirror at oblique incidence. *IEEE Transactions on Antennas and Propagation*, 30(5):898–903, 1982.
- [139] Jean Van Bladel and Daniel De Zutter. Reflections from linearly vibrating objects: Plane mirror at normal incidence. *IEEE Transactions on Antennas and Propagation*, 29(4):629–637, 1981.
- [140] Lukas Novotny and Bert Hecht. *Principles of nano-optics*. Cambridge university press, 2012.

- [141] J. E. Field, K. H. Hahn, and S. E. Harris. Observation of electromagnetically induced transparency in collisionally broadened lead vapor. *Phys. Rev. Lett.*, 67:3062–3065, 1991.
- [142] Stephen E. Harris. Electromagnetically induced transparency. *Phys. Today*, 50(7):36, 1997.
- [143] Gilbert Grynberg, Alain Aspect, Claude Fabre, and Cohen Tannoudji. *Introduction to quantum optics : from the semi-classical approach to quantized light*. Cambridge University Press, Cambridge, 2010.
- [144] Ugo Fano. On the absorption spectrum of noble gases at the arc spectrum limit. 2005.
- [145] M. D. Lukin. Colloquium: Trapping and manipulating photon states in atomic ensembles. *Rev. Mod. Phys.*, 75:457–472, 2003.
- [146] S. H. Autler and C. H. Townes. Stark effect in rapidly varying fields. *Phys. Rev.*, 100:703–722, 1955.
- [147] Petr M. Anisimov, Jonathan P. Dowling, and Barry C. Sanders. Objectively discerning autler-townes splitting from electromagnetically induced transparency. *Phys. Rev. Lett.*, 107:163604, 2011.
- [148] Tony Y. Abi-Salloum. Electromagnetically induced transparency and autler-townes splitting: Two similar but distinct phenomena in two categories of three-level atomic systems. *Phys. Rev. A*, 81:053836, 2010.
- [149] Harshawardhan Wanare. Multicolored coherent population trapping in a  $\Lambda$  system using phase modulated fields. *Phys. Rev. Lett.*, 96:183601, 2006.
- [150] Peng Li, Takashi Nakajima, and Xi-Jing Ning. Spectral properties of a v-type three-level atom driven by two bichromatic fields. *Phys. Rev. A*, 74:043408, 2006.
- [151] Yang Li-Jun, Zhao Min, Zhang Lian-Shui, Feng Xiao-Min, Li Xiao-Li, and Wei Chang-Jiang. Quantum coherence in  $\Lambda$ -three-level system driven by bichromatic coupling field. *Chin. Phys. B*, 19:084204, 2010.
- [152] Guo Hong-Ju, Niu Yue-Ping, Wang Li-Chun, Jin Shi-Qi, and Gong Shang-Qing. Trichromatic manipulation of kerr nonlinearity in a three-level  $\Lambda$  atomic system. *Chin. Phys. Lett.*, 25:3656, 2008.
- [153] Jiepeng Zhang, Jun Xu, Gessler Hernandez, X.M. Hu, and Yifu Zhu. Polychromatic-field-induced transparency and absorption in a three-level  $\Lambda$  system. *Phys. Rev. A*, 75:043810, 2007.
- [154] Y. R. Shen. *Principles Of Nonlinear Optics*. Wiley Classics Library. Wiley-Interscience, 2002.

- [155] Harshawardhan Wanare. Gain without population inversion in v-type systems driven by a frequency-modulated field. *Phys. Rev. A*, 65:033417, 2002.
- [156] T.J. Kippenberg and K.J. Vahala. Cavity opto-mechanics. *Opt. Express*, 15:17172, 2007.
- [157] I. Wilson-Rae, N. Nooshi, W. Zwerger, and T. J. Kippenberg. Theory of ground state cooling of a mechanical oscillator using dynamical backaction. *Phys. Rev. Lett.*, 99:093901, 2007.
- [158] P. H. Kim, B. D. Hauer, C. Doolin, F. Souris, and J. P. Davis. Approaching the standard quantum limit of mechanical torque sensing. *Nature Communications*, 7:13165, 2016.
- [159] P. H. Kim, C. Doolin, B. D. Hauer, A. J. R. MacDonald, M. R. Freeman, P. E. Barclay, and J. P. Davis. Nanoscale torsional optomechanics. *Applied Physics Letters*, 102(5), 2013.
- [160] T F Gallagher. *Rydberg Atoms*. Cambridge University Press, 1994.
- [161] T. Thiele, J. Deiglmayr, M. Stammeier, J.-A. Agner, H. Schmutz, F. Merkt, and A. Wallraff. Imaging electric fields in the vicinity of cryogenic surfaces using Rydberg atoms. *Phys. Rev. A*, 92:063425, 2015.
- [162] S. A. Basun, G. Cook, V. Yu. Reshetnyak, A. V. Glushchenko, and D. R. Evans. Dipole moment and spontaneous polarization of ferroelectric nanoparticles in a nonpolar fluid suspension. *Phys. Rev. B*, 84:024105, 2011.
- [163] J.C. Meyer, M. Paillet, and S. Roth. Single-molecule torsional pendulum. *Science*, 309(5740):1539–1541, 2005.
- [164] Marc Ganzhorn, Svetlana Klyatskaya, Mario Ruben, and Wolfgang Wernsdorfer. Strong spin–phonon coupling between a single-molecule magnet and a carbon nanotube nanoelectromechanical system. *Nature Nanotech*, 8(3):165–169, 2013.
- [165] V. B. Braginsky and F. Ya. Khalili. Quantum nondemolition measurements: the route from toys to tools. *Rev. Mod. Phys.*, 68:1–11, 1996.
- [166] Christine Guerlin, Julien Bernu, Samuel Deléglise, Clément Sayrin, Sébastien Gleyzes, Stefan Kuhr, Michel Brune, Jean-Michel Raimond, and Serge Haroche. Progressive field-state collapse and quantum non-demolition photon counting. *Nature*, 448(7156):889–893, 2007.
- [167] M. A. Beck, J. A. Isaacs, D. Booth, J. D. Pritchard, M. Saffman, and R. McDermott. Optimized coplanar waveguide resonators for a superconductor–atom interface. *Appl. Phys. Lett.*, 109(9):092602, 2016.

- [168] Natalia R. de Melo and Sandra S. Vianna. Frequency shift in three-photon resonant four-wave mixing by internal atom-field interaction. *Phys. Rev. A*, 92:053830, 2015.
- [169] Werner Vogel and Dirk-Gunnar Welsch. *Quantum optics*. John Wiley & Sons, 2006.
- [170] J. Dalibard, J.M. Raimond, and J. Zinn Justin, editors. *Fundamental Systems in Quantum Optics*. Elsevier Science & Technology, 1992.
- [171] J. Ishikawa, F. Riehle, J. Helmcke, and Ch. J. Bordé. Strong-field effects in coherent saturation spectroscopy of atomic beams. *Phys. Rev. A*, 49:4794–4825, 1994.
- [172] Seidel, D. and Muga, J. G. Ramsey interferometry with guided ultracold atoms. *Eur. Phys. J. D*, 41(1):71–75, 2007.
- [173] Bruce W Shore. Coherent manipulations of atoms using laser light. *Acta Phys. Slovaca*, 58(3):243–486, 2008.
- [174] Serge Haroche. Nobel lecture: Controlling photons in a box and exploring the quantum to classical boundary. *Rev. Mod. Phys.*, 85:1083–1102, 2013.
- [175] David J. Wineland. Nobel lecture: Superposition, entanglement, and raising schrödinger’s cat. *Rev. Mod. Phys.*, 85:1103–1114, 2013.
- [176] Vladimir B. Braginsky, Yuri I. Vorontsov, and Kip S. Thorne. Quantum nondemolition measurements. *Science*, 209(4456):547–557, 1980.
- [177] G. J. Milburn and D. F. Walls. Quantum nondemolition measurements via quadratic coupling. *Phys. Rev. A*, 28:2065–2070, 1983.
- [178] Vladimir Borisovich Braginskiĭ and Farid Ya Khalili. *Quantum measurement*. Cambridge University Press, 1995.
- [179] Norman F. Ramsey. A molecular beam resonance method with separated oscillating fields. *Phys. Rev.*, 78:695–699, 1950.
- [180] Todd A. Brun. A simple model of quantum trajectories. *American Journal of Physics*, 70(7):719–737, 2002.
- [181] Michael Nielsen and Isaac L. Chuang. *Quantum computation and quantum information*. Cambridge University Press, Cambridge New York, 2010.
- [182] Michel Bauer and Denis Bernard. Convergence of repeated quantum nondemolition measurements and wave-function collapse. *Phys. Rev. A*, 84:044103, 2011.
- [183] Michel Bauer, Tristan Benoist, and Denis Bernard. Repeated quantum non-demolition measurements: Convergence and continuous time limit. *Annales Henri Poincaré*, 14(4):639–679, 2013.

- [184] I. I. Beterov, I. I. Ryabtsev, D. B. Tretyakov, and V. M. Entin. Quasiclassical calculations of blackbody-radiation-induced depopulation rates and effective lifetimes of Rydberg  $ns$ ,  $np$ , and  $nd$  alkali-metal atoms with  $n \leq 80$ . *Phys. Rev. A*, 79:052504, 2009.
- [185] J. D. Carter and J. D. D. Martin. Coherent manipulation of cold Rydberg atoms near the surface of an atom chip. *Phys. Rev. A*, 88:043429, 2013.
- [186] Howard M Wiseman and Gerard J Milburn. *Quantum measurement and control*. Cambridge University Press, 2009.
- [187] Stephen D. Hogan. Rydberg-stark deceleration of atoms and molecules. *EPJ Techniques and Instrumentation*, 3(1):2, 2016.
- [188] P Lancuba and S D Hogan. Electrostatic trapping and in situ detection of Rydberg atoms above chip-based transmission lines. *Journal of Physics B: Atomic, Molecular and Optical Physics*, 49(7):074006, 2016.
- [189] Roy J. Glauber. Photon correlations. *Phys. Rev. Lett.*, 10:84–86, 1963.
- [190] Anatoli Polkovnikov. Phase space representation of quantum dynamics. *Annals of Physics*, 325(8):1790 – 1852, 2010.
- [191] M. Hillery, R.F. O’Connell, M.O. Scully, and E.P. Wigner. Distribution functions in physics: Fundamentals. *Physics Reports*, 106(3):121 – 167, 1984.
- [192] Ulf Leonhardt. *Measuring the quantum state of light*. Cambridge studies in modern optics. Cambridge University Press, 1 edition, 1997.
- [193] F. Strocchi. Complex coordinates and quantum mechanics. *Rev. Mod. Phys.*, 38:36–40, 1966.
- [194] R. Shankar. *Principles of Quantum Mechanics, 2nd Edition*. Plenum Press, 2nd edition, 2008.
- [195] E. Wigner. On the quantum correction for thermodynamic equilibrium. *Phys. Rev.*, 40:749–759, 1932.
- [196] Mark Keil, Omer Amit, Shuyu Zhou, David Groswasser, Yonathan Japha, and Ron Folman. Fifteen years of cold matter on the atom chip: promise, realizations, and prospects. *Journal of Modern Optics*, 63(18):1840–1885, 2016.
- [197] D. Hunger, S. Camerer, M. Korppi, A. Jöckel, T.W. Hänsch, and P. Treutlein. Coupling ultracold atoms to mechanical oscillators. *Comptes Rendus Physique*, 12(9):871 – 887, 2011.

- [198] Alexander Carmele, Berit Vogell, Kai Stannigel, and Peter Zoller. Opto-nanomechanics strongly coupled to a Rydberg superatom: coherent versus incoherent dynamics. *New Journal of Physics*, 16(6):063042, 2014.
- [199] I. Wilson-Rae. Intrinsic dissipation in nanomechanical resonators due to phonon tunneling. *Phys. Rev. B*, 77:245418, 2008.
- [200] A R Hall, S Paulson, T Cui, J P Lu, L-C Qin, and S Washburn. Torsional electromechanical systems based on carbon nanotubes. *Reports on Progress in Physics*, 75(11):116501, 2012.
- [201] Valentina Parigi, Erwan Bimbard, Jovica Stanojevic, Andrew J. Hilliard, Florence Nogrette, Rosa Tualle-Brouri, Alexei Ourjoumtsev, and Philippe Grangier. Observation and measurement of interaction-induced dispersive optical nonlinearities in an ensemble of cold Rydberg atoms. *Phys. Rev. Lett.*, 109:233602, 2012.
- [202] S Sevinçli, C Ates, T Pohl, H Schempp, C S Hofmann, G Günter, T Amthor, M Weidemüller, J D Pritchard, D Maxwell, A Gauguet, K J Weatherill, M P A Jones, and C S Adams. Quantum interference in interacting three-level Rydberg gases: coherent population trapping and electromagnetically induced transparency. *J. Phys. B*, 44:184018, 2011.
- [203] Inbal Friedler, David Petrosyan, Michael Fleischhauer, and Gershon Kurizki. Long-range interactions and entanglement of slow single-photon pulses. *Phys. Rev. A*, 72:043803, 2005.
- [204] A. K. Mohapatra, T. R. Jackson, and C. S. Adams. Coherent optical detection of highly excited rydberg states using electromagnetically induced transparency. *Phys. Rev. Lett.*, 98:113003, 2007.
- [205] S Mauger, J Millen, and M P A Jones. Spectroscopy of strontium Rydberg states using electromagnetically induced transparency. *J. Phys. B*, 40:F319, 2007.
- [206] A K Mohapatra, M G Bason, B Butscher, K J Weatherill, and C S Adams. A giant electro-optic effect using polarizable dark states. *Nature Physics*, 4:890, 2008.
- [207] H. Schempp, G. Günter, C. S. Hofmann, C. Giese, S. D. Saliba, B. D. DePaola, T. Amthor, M. Weidemüller, S. Sevinçli, and T. Pohl. Coherent population trapping with controlled interparticle interactions. *Phys. Rev. Lett.*, 104:173602, 2010.
- [208] Y. O. Dudin and A. Kuzmich. Strongly interacting Rydberg excitations of a cold atomic gas. *Science*, 336:887, 2012.
- [209] Thibault Peyronel, Ofer Firstenberg, Qi-Yu Liang, Sebastian Hofferberth, Alexey V. Gorshkov, Thomas Pohl, Mikhail D. Lukin, and Vladan Vuletić. Quantum nonlinear optics with single photons enabled by strongly interacting atoms. *Nature*, 488:57, 2012.

## References

- [210] S. Sevinçli, N. Henkel, C. Ates, and T. Pohl. Nonlocal nonlinear optics in cold Rydberg gases. *Phys. Rev. Lett.*, 107:153001, 2011.
- [211] Ali Asadian, Paul Erker, Marcus Huber, and Claude Klöckl. Heisenberg-weyl observables: Bloch vectors in phase space. *Phys. Rev. A*, 94:010301, 2016.
- [212] Alexander Eisfeld. Private communication.
- [213] Robert Johne. Private communication.
- [214] R W Boyd. *Nonlinear Optics*. Academic Press, 2003.
- [215] Peter Milonni. *Fast light, slow light, and left-handed light*. Institute of Physics, Bristol Philadelphia, 2005.
- [216] Peter Milonni. *Laser physics*. Wiley-Blackwell, Oxford, 2010.
- [217] Kristian Rymann Hansen. Standing Wave Electromagnetically Induced Transparency. Master's thesis, University of Aarhus, 2006.
- [218] Julius Stratton. *Electromagnetic theory*. IEEE Press, Piscataway, NJ, 2007.
- [219] L. D. Landau and E. M. Lifshitz. *The classical theory of fields*. Butterworth Heinemann, Oxford Boston, 2000.
- [220] Crispin Gardiner and Peter Zoller. *Quantum noise: a handbook of Markovian and non-Markovian quantum stochastic methods with applications to quantum optics*, volume 56. Springer Science & Business Media, 2004.



# Erklärung

Hiermit versichere ich, dass ich die vorliegende Arbeit ohne unzulässige Hilfe Dritter und ohne Benutzung anderer als der angegebenen Hilfsmittel angefertigt habe; die aus fremden Quellen direkt oder indirekt übernommenen Gedanken sind als solche kenntlich gemacht. Die Arbeit wurde bisher weder im Inland noch im Ausland in gleicher oder ähnlicher Form einer anderen Prüfungsbehörde vorgelegt.

Die Dissertation wurde am Max-Planck-Institut für Physik komplexer Systeme in der Abteilung „Endliche Systeme“ unter der wissenschaftlichen Betreuung von Herrn Prof. Dr. Jan-Michael Rost angefertigt. Es haben keine früheren erfolglosen Promotionsverfahren stattgefunden. Ich erkenne die Promotionsordnung der Fakultät Mathematik und Naturwissenschaften der Technischen Universität Dresden vom 23.02.2011 an.

Adrián Sanz Mora  
Dresden, January, 30, 2018